Characterizing novel genes involved in steroidogenesis during the larval development in *Drosophila melanogaster*

by

Song Wang

A thesis submitted in partial fulfillment of the requirements for the degree of

Doctor of Philosophy

in

Molecular Biology and Genetics

Department of Biological Sciences
University of Alberta

Abstract

The primary steroid hormone in *Drosophila melanogaster* is called ecdysone, which is synthesized in the larval prothoracic gland (PG) during developmental processes. Ecdysone biosynthesis is significantly up-regulated at the beginning of the third larval instar, resulting in a major ecdysone pulse that triggers metamorphosis. Cytochrome P450 enzymes (P450) require heme as a cofactor and play a key role in catalyzing the conversion from dietary cholesterol to ecdysone. Since heme needs iron to function, there has been a link between cellular heme/iron homeostasis and ecdysone biosynthesis in *Drosophila*.

My thesis focuses on two genes identified from two independent RNA interference (RNAi) screens carried out by previous lab members. The RNAi screens uncovered genes that may play essential roles in *Drosophila* development and heme biosynthesis. I will outline in two individual chapters how two genes of interest (RanBP3 and Su(var)2-10) impinge on ecdysone biosynthesis via different mechanisms.

RanBP3-depletion animals showed a late-larval lethality, and interestingly, a porphyria-like phenotype in the prothoracic gland. Porphyrias are a group of eight rare metabolic diseases induced by disrupted heme biosynthetic pathway. I showed that the *RanBP3* loss-of-function phenotype resulted from a disruption of heme biosynthesis and the accumulation of heme precursors. RanBP3 was further shown to play a vital role in the nuclear export of Iron-regulatory protein 1A (IRP1A), a central cellular iron sensor and regulator of iron homeostasis. I also examined how IRP1A is transported into the nucleus, which relies on an unusual mechanism mediated by a protein complex

formed by Ran and NTF2. Additionally, Chickadee (Chic) was shown to function as a negative regulator of IRP1A nuclear import. These findings provided molecular evidence for how IRP1A nucleocytoplasmic transport occurs in *Drosophila melanogaster*. RanBP3 was also characterized as a novel regulator of intracellular iron trafficking, which is critical for transporting cytosolic iron into the mitochondrion for heme biosynthesis and iron-sulfur cluster biogenesis.

The other gene that I investigated affects ecdysone biosynthesis via a different mechanism than *RanBP3*. S*uppressor of variegation 2-10* or *Su(var)2-10* encodes a protein inhibitor of activated STATs (PIAS) protein that regulates chromosome structure and function. Losing *Su(var)2-10* function in the prothoracic gland caused lethality and an overgrowth of the tissue, which suggests a feedback control mechanism to produce more ecdysone to sustain normal larval-to-pupal transition. I show that *Su(var)2-10* is required for the transcriptional regulation of *neverland* (*nvd*), which encodes an enzyme required for the conversion of dietary cholesterol to 7-dehydrocholesterol (7dC). Prior to this work, two transcription factors (TFs) were known to cooperatively regulate the *nvd* gene, Séance and Molting defective (Mld). Only the expression of *séance,* but not that of *mld*, was affected by *Su(var)2-10* loss-of-function in the PG cells. This finding established a regulatory network in which *nvd* transcription is controlled by a protein that functions upstream of a known transcription factor. Mass spectrometry analysis identified Histone H2A (His2A) as a Su(var)2-10-interacting protein. Knocking down *His2A* in the prothoracic gland down-regulated ecdysone biosynthetic gene transcription, suggesting that Su(var)2-10 may regulate *nvd* transcription via histone modification, presumably SUMOylation.

Preface

This thesis is an original work by Song Wang.

I have completed a manuscript corresponding to chapter 3, which we expect to submit for publication shortly. I carried out and analyzed most of the experiments. The mass spectrometry assay was conducted by Jack Moore at the Mass Spectrometry Facility in the Biochemistry Department at the University of Alberta. I wrote the manuscript, generated and revised figures with Dr. Kirst King-Jones' suggestion. I am responsible for all the figures and tables.

I also completed a second manuscript focusing on Su(var)2-10, which we expect to submit for publication next year. I performed and analyzed most of the experiment. Dr. Wen Liu helped with the RNA-sequencing analysis, whose name is listed as a co-author. The mass spectrometry analysis was done by Jack Moore. I wrote the manuscript, generated all the figures and tables with suggestions from Dr. Kirst King-Jones. I am responsible for all the figures and tables.

Acknowledgments

I want to begin by acknowledging Dr. Kirst King-Jones for accepting me into his lab and allowing me to pursue my degree by providing support and resources as much as he can. His pursuit of preciseness and perfection inspired me to become a better researcher. I would like to thank my committee members, Dr. Sarah Hughes and Dr. Enrico Scarpella, for always being supportive and encouraging. They provided great suggestions for my projects. I would also like to thank Dr. Jacob Berry for giving comments and great advice for my thesis.

I am grateful for all the help I got from all the previous and current lab members of the King-Jones lab. I would like to give special thanks to Dr. Wen Liu, a postdoctoral associate in our lab, for always being supportive and providing great ideas for my projects.

I would like to thank the Department of Biological Sciences GTA program, which has supported me during my Ph.D. work and department staff who always work behind the scenes but try their best to help every student. I would like to thank the Molecular Biology Service Unit (MBSU) team, Troy Locke, Cheryl Nargang, and Sophie Dang, for their generous help using their facilities. And lastly, I would like to thank myself for not giving up when there were troubles and difficulties in studies and life.

Table of Contents

List of Figures

List of Tables

Abbreviations

20E	20-hydroxyecdysone
7dC	7-dehydrocholesterol
ALA	aminolaevulinic acid
ALAD	ALA dehydratase
ALAS	ALA synthase
AGBE	*1,4-Alpha-Glucan Branching Enzyme* gene
aa	amino acid
BDSC	Bloomington *Drosophila* Stock Center
bp	base-pair
br	*broad* gene
BRGC	brain-ring gland complex
BPS	bathophenanthroline sulfate
BSA	bovine serum albumin
C	cholesterol
CA	corpus allatum
CC	corpora cardiacum
CRISPR	clustered regularly interspaced short palindromic repeats
Cas9	CRISPR-associated protein 9
chic	*chickadee* gene

cDNA	complementary DNA
co-IP	co-immunoprecipitation
ChIP	chromatin immunoprecipitation
Cpox	coproporphyrinogen oxidase
CT	threshold cycle
CUT & Tag	Cleavage Under Targets & Tagmentation
CRM1	chromosome maintenance protein 1
DNA	deoxyribonucleic acid
dib	*disembodied* gene
Dcytb	*Duodenal cytochrome b* gene
DMT1	Divalent metal-ion transporter 1
dPIAS	*Drosophila* Protein Inhibitor of Activated STAT
dmfrn	*Drosophila mitoferrin* gene
dU6:3	*Drosophila* U6:3 promoter
DEG	differentially expressed genes
E	α-ecdysone
EcR	*Ecdysone receptor* gene
E74	*Ecdysone-induced protein 74EF* gene
E75	*Ecdysone-induced protein 75B* gene
E93	*Ecdysone-induced protein 93F* gene

EGFP	enhanced green fluorescent protein
EDTA	ethylenediaminetetraacetic acid
ER	endoplasmic reticulum
ERp60	endoplasmic reticulum protein 60
FAC	ferric ammonium citrate
FB	fat body
FeCH	ferrochelatase
Fer1HCH	*Ferritin 1 Heavy Chain Homologue* gene
Fer2LCH	*Ferritin 2 Light Chain Homologue* gene
Ft	ferritin
Ferroportin	Fpn
gRNA	guide RNA
GOI	genes of interest
Gp93	glycoprotein 93
GS	GeneSwitch
G1	one generation on BPS
G2	two generations on BPS
hTfR	human transferrin receptor
hIRP1	human iron-regulatory protein 1
Hsp	heat shock protein

IR	RNA interference, RNAi
IRP	iron-regulatory protein
IRE	iron-responsive element
IP	immunoprecipitation
IF	immunofluorescence
ISC	iron-sulfur cluster
JAK	the Janus kinase
KD	knock-down
KO	knock-out
L1	first-instar larvae
L2	second-instar larvae
L3	third-instar larvae
MCF	mitochondrial carrier family
mRNA	messenger RNA
MCO	multi-copper oxidase
Mfrn	mitoferrin
MtFt	mitochondrial ferritin
mvl	*malvolio* gene
mld	*molting defective* gene
MS	mass spectrometry

Ntf-2	*Nuclear transport factor-2* gene
NPC	nuclear pore complex
NLS	nuclear localization signal
NES	nuclear export signal
nt	nucleotide
nvd	*neverland* gene
NGS	next generation sequencing
PIAS	Protein Inhibitor of Activated STAT
PBGD	porphobilinogen deaminase
PBGS	porphobilinogen synthase
PP	protoporphyrin IX
Ppox	*Protoporphyrinogen oxidase* gene
ppk20	*pickpocket 20* gene
phm	*phantom* gene
phm22	prothoracic gland-specific Gal4 driver
phmN1	a recombined prothoracic gland-specific Gal4 driver
P450	cytochrome P450 enzymes
PBS	phosphate buffered saline
PBST	0.3% Triton X-100 in phosphate buffered saline
PG	prothoracic gland

PCR	polymerase chain reaction
qPCR	quantitative real-time PCR
RNA	ribonucleic acid
rRNA	ribosomal RNA
RG	ring gland
RanGEF	Ran guanine nucleotide exchange factor
RanGAP	Ran GTPase activating protein
RanBP3	*Ran-binding protein 3* gene
RanBD1	Ran-binding domain 1
RIP	RNA-immunoprecipitation
RNAi	RNA interference
RT	room temperature
RPKM	reads per kilobase of transcript per million mapped reads
sad	*shadow* gene
spo	*spook* gene
spok	*spookier* gene
sro	*shroud* gene
Su(var)2-10	*Suppressor of variegation 2-10* gene
SUMO	small ubiquitin-like modifier
sdhB	*succinate dehydrogenase subunit B* gene

S2	*Drosophila* Schneider 2 cells
SG	salivary gland
shRNA	short-hairpin RNA
STAT	signal transducer and activator of transcription
SIM	SUMO-interacting motif
TIM2	T cell immunoglobulin and mucin domain protein 2
Tsf	Transferrin
TfR	Transferrin receptor
TF	transcription factor
Tub	*Tubulin* gene
UROS	uroporphyrinogen synthase
UROD	UROIII decarboxylase
usp	*ultraspiracle* gene
UTR	untranslated region
VDRC	Vienna *Drosophila* Resource center
WB	whole body
Znf	Zinc finger
ZnPP	Zinc protoporphyrin IX

Chapter 1 General introduction

1.1 The importance of studying steroid hormones

Steroid hormones are ancient signaling molecules that play crucial roles in many physiological processes in humans. For example, testosterone and estrogen are the main sex hormones contributing to sex development and growth [1]. Cortisol, one of the glucocorticoids, is made in the adrenal gland and is mainly related to the stress response [2, 3]. Additionally, many of the steroid hormones control immunity [4] and salt and water transport [5, 6]. Together, steroid hormones are linked to multiple cellular responses including development, stress response, and immunity. In my projects, I use the fruit fly *Drosophila melanogaster* as a model organism to characterize novel genes that are involved in the biosynthesis of the primary steroid hormone ecdysone in flies, which are released as pulses to direct all the developmental transitions, including larval molts and pupation [7]. Characterizing new factors that function in this process would allow us to better understand human diseases caused by abnormal steroid hormone signaling.

1.2 *Drosophila melanogaster*, a versatile model for biological and genetic studies

To study the molecular and genetic circuits that control fundamental biological processes in humans, we would need to rely on the use of animals to observe phenotypic results, which then help to determine strategies for treating human diseases. However, it is impossible to directly carry out biomedical research in humans due to experimental obstacles and, of course, ethical issues. An obvious avenue for modeling human diseases is to study pathogenic genes in the closely related mouse model using gene knock-out or gene editing techniques [8]. This approach is effective,

especially for diseases that have very similar phenotypes across species. However, in other cases, knocking out a gene or introducing mutations to genes that may trigger diseases in mice models are not necessarily as good as hoped for many reasons. For example, a mutation of interest might be strong enough to cause early embryonic lethality, excluding the analysis of later stages. And the greater gene redundancy in mice may mask the effect of mutations in single genes. Alternatively, researchers may search for help by using other model organisms, as both the invertebrates and vertebrates share similarities in their development, physiology, and behavior.

Drosophila melanogaster has been extensively used as one of the most effective tools for analyzing the function of human disease genes [9]. The fruit fly had not been well appreciated until Thomas Hunt Morgan used these little bugs to investigate the chromosomal theory of inheritance and subsequently identified the *white* eye pigment mutation at the turn of the last century [10]. After then, the primary approach in genetic studies using *Drosophila* for most of the time, has been forward genetics, where genes are discovered based on mutant phenotypes. However, for the current era, the primary goal is to understand the functions of newly discovered genes. This would require methods to specifically alter one gene's function when the sequence and position of the gene in the genome are known. The term "reverse genetics" has been used to describe this process. In general, reverse genetics can be sub-divided into two classes [11]. The first involves an indirect approach using a chemical or transposable element to introduce mutations in a specific gene of interest. In this case, the mutations are random but selected later for the gene of interest. The second approach directly targets the gene, in which the function of a particular gene is altered. It has always

been a challenge to disrupt targeted gene function. *Drosophila* researchers have only recently had access to those technologies, such as targeted gene replacement ("knock-in") and RNA interference (RNAi). Nevertheless, there have been many innovations developed that allow gene disruption without previous knowledge of mutant phenotype. Transgenes are generated by P-element insertions [12, 13] or site-directed transgenesis methods, for instance, FLP/FRT and φC31 recombination [14, 15]. Spatially restricted expression of transgenes in *Drosophila* is most widely accomplished by the yeast Gal4 protein and its target upstream activating sequences (GAL4/UAS system) [16, 17]. An increasingly popular approach that has been extensively used to introduce novel mutations into the fly genome is by CRISPR/Cas9 [18, 19]. A donor repair template is recruited to a precise genomic sequence to insert exogenous DNA mediated by homologous recombination. The other key advantage of using *Drosophila* to study both physiological and biological processes is that researchers can easily access a vast assortment of strains containing endogenous mutations collated in Flybase, including several independent fly stock centers worldwide.

From a practical point of view, *Drosophila* is easy and inexpensive to maintain in the lab. They have a relatively short life cycle of about ten days at 25°C. They also produce large numbers of externally laid embryos that can be genetically modified in numerous ways. Altogether, techniques, tools, screening ability, and most importantly, the conserved biology presented in *Drosophila* make it a versatile model organism for modeling human diseases [8, 20, 21].

1.3 Ecdysone controls developmental transitions in *Drosophila melanogaster*

The *Drosophila* life cycle is well-defined, which includes four main stages: embryo, larva, pupa, and adult fly [22]. A fertilized egg develops and hatch as larva in about one day at 25 ℃. The larva takes up nutrients from the *Drosophila* media and undergoes three molts until it pupates in about five days. Lastly, the late larva undergoes metamorphosis and develops into the adult fly in about four days. The developmental transitions of *Drosophila* involve several vital hormones and neuropeptides, including prothoracicotropic hormone (PTTH), juvenile hormone (JH), and ecdysone (E) [23, 24]. For the past few decades, PTTH was believed to act as the critical factor that determines the timing of developmental transitions. PTTH is a neuropeptide produced by two pairs of lateral neurosecretory cells in the insect brain, which integrates various environmental and developmental cues to determine the timing to progress into the next developmental stage [25-27]. Photoperiod cues have been identified as environmental inputs that affect ecdysone production based on physiological and molecular genetic studies [23, 26]. Only recently, the first loss-of-function analysis of PTTH was conducted in flies, where PTTH-producing neurons were genetically ablated [26]. Animals, as a result, showed significant delayed developmental progress. However, larvae lacking PTTH eventually pupated and eclosed with a bigger body size due to the prolonged larval feeding stage. This led to a revised understanding of insect endocrinology, where PTTH is not absolutely required for metamorphosis. Still, it has a more critical role in regulating the timing of metamorphosis and thereby controls the final body size of the animal [24].

The current view of insect endocrinology states that the steroid hormone ecdysone is the

master regulator of the insect developmental transitions, including embryogenesis, larval molting, and metamorphosis in general (Fig. 1.1a). During larval stages, α-ecdysone (E) is produced within the prothoracic gland (PG), an endocrine tissue that expresses genes that encode ecdysone biosynthetic enzymes. Once E is released into the hemolymph, E is further converted in peripheral tissues to biologically active ecdysteroids, of which 20-hydroxyecdysone (20E) is the best-studied. The binding of the primary molting hormone 20E to the EcR/Usp nuclear receptor heterodimer initiates gene expression cascades in target tissues [28-31], which ultimately leads to physiological, morphological, and behavioral changes associated with molting and metamorphosis. Extensive studies have been done to demonstrate the cascades that happen after the binding of ecdysone to its receptors. However, there are still several key questions remaining in understanding the biogenesis of ecdysone. For example, it is unknown what determines the distinct characteristics of each ecdysone pulse, since their amplitudes and lengths of effectiveness must be tightly controlled. Additionally, it is unclear how efficiently the hormone is converted to its biologically active form and how fast it is degraded. We will use *Drosophila* as a model organism to identify critical factors that may regulate ecdysone biosynthesis and model human diseases related to abnormal steroidogenesis.

1.4 Beyond steroids: Using the prothoracic gland as a model to study the dynamic cellular iron supply

The larval prothoracic gland (PG) is an endocrine tissue responsible for making ecdysone in

flies, which neighbors two other glands called the corpus allatum (CA) and the corpus cardiacum (CC) (Fig. 1.1b). Within the PG cells, dietary cholesterol and other suitable sterols are converted to the prohormone E by a series of enzymatic steps [24]. After release into the hemolymph, E is further converted in the target tissues to the biologically functional form 20-hydroxyecdysone (20E). To date, nine enzymes are documented to function in the ecdysone biosynthesis pathway (Table 1.1), in which seven of them are cytochrome P450 monooxygenases encoded by Halloween genes (Fig. 1.1c). Of note, *spook* (*spo*) and spookier (*spok*) encode two highly related and stage-specific cytochrome P450 enzymes for ecdysone biosynthesis in flies [32]. In addition to cytochrome P450 enzymes, the other two ecdysone biosynthetic enzymes are characterized as a Rieske electron oxygenase (Neverland) and a single short-chain dehydrogenase/reductase (Shroud) [33]. Neverland catalyzes the first enzymatic reaction in the ecdysone biosynthetic pathway that converts dietary cholesterol to 7-dehydrocholesterol (7DC). Following this conversion, our current understanding is limited until the step during which 5β-ketodiol is generated. This unknown stage is often referred to as the "black box". The only thing that appears to be sure is that Shroud, Spook/Spookier and Cyp6t3 act in the black box [34].

An interesting finding that we observe from the ecdysone biosynthetic pathway is that iron and heme are critical to the generation of ecdysone and, ultimately, crucial for development. As shown in the ecdysone biosynthetic pathway, all but one (Shroud) of these enzymes are iron-containing proteins. Neverland is an iron-sulfur cluster (ISC) protein, while cytochrome P450 enzymes require heme as a cofactor to exert their function. However, since both free iron and heme

are cytotoxic and only present in low concentrations, cells need to develop mechanisms to adjust intracellular iron levels as required. For instance, when animals need iron for pupation (due to the mass production of cytochrome P450 enzymes involved in the ecdysone peak), one plausible way PG cells could acquire iron is to mobilize iron that is stored in ferritin (an iron storage protein) or endocytose iron-bound proteins from the hemolymph. On the other hand, excess iron would be stored or excreted such that no cell damage can be caused.

The importance of using the prothoracic gland to study the dynamic iron supply has been understudied. It was only recently that our lab started to use the PG to examine the link between iron/heme and ecdysone production. Since the prothoracic gland has a much higher demand for iron as compared to two neighbouring glands (Fig. 1.1d), we hypothesize that the PG cell is a good model for characterizing novel regulators of cellular iron homeostasis.

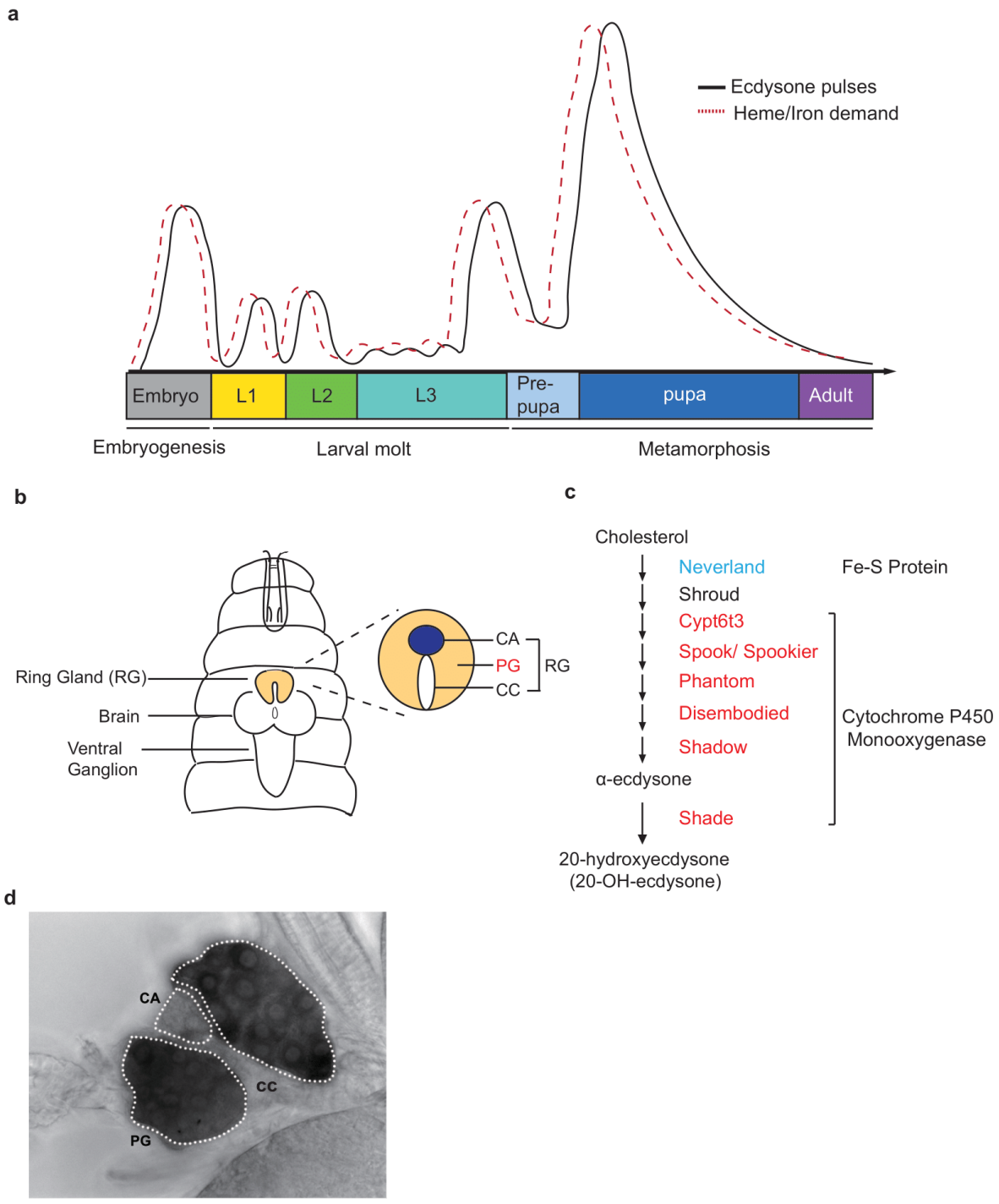

Figure 1.1 *Drosophila* prothoracic gland is a great model for studying ecdysone biosynthesis and the dynamic cellular iron supply.

(a) The main steroid hormone ecdysone is released in the form of pulses that direct all the developmental transitions in *Drosophila*, including embryogenesis, larval molting, pupation, and metamorphosis. (b) The larval prothoracic gland (PG) has two neighbouring glands, namely the corpus allatum (CA) and the corpus cardiacum (CC). They altogether make up a complex tissue known as the ring gland (RG). Several essential hormones and neuropeptides control developmental transitions in insects, including prothoracicotropic hormone (PTTH), juvenile hormone (JH), and ecdysone. Ecdysone has been identified as the master regulator of animal development. (c) The ecdysone biosynthetic pathway. Dietary cholesterol is converted to the functionally active form 20-hydroxyecdysone (20E) by a series of enzymes, most of which are cytochrome P450 monooxygenases (in red) encoded by Halloween genes. The first step is catalyzed by Neverland (in blue), an iron-containing oxygenase-like protein. (d) Ferric iron staining of the *Drosophila* prothoracic gland. The PG has a higher iron demand than the neighboring glands, providing an optimal model for studying cellular iron homeostasis.

Table 1.1 Ecdysone biosynthetic enzymes and enzymatic products.

Gene name	Enzyme name	Product
neverland (*nvd*)[a]	3-beta-hydroxy-delta(5)-steroid dehydrogenase	7-dehydrocholesterol
shroud (*sro*)	3-alpha-(17-beta)-hydroxysteroid dehydrogenase	unknown
Cyp6t3[b]	Encodes a cytochrome P45 enzyme	unknown
spookier (*spok*)[b]	Encodes a cytochrome P45 enzyme	5β-ketodiol
phantom (*phm*)[b]	Exhibits ecdysteroid 25-hydroxylase activity	3β, 5β-ketodiol
disembodied (*dib*)[b]	Exhibits ecdysteroid 22-hydroxylase activity	2-deoxyecdysone
shadow (*sad*)[b]	Exhibits ecdysteroid 2-hydroxylase activity	α-ecdysone (E)
shade (*shd*)[b]	Ecdysone 20-monooxygenase	20-hydroxyecdysone (20E)

[a] Gene encodes an iron-sulfur cluster protein

[b] Genes encode cytochrome P450 enzymes

1.5 Regulation of mammalian iron metabolism

Iron is essential for fundamental metabolic processes in nearly all living cells and organisms. Disruption of iron homeostasis, either by iron deficiency or iron overload, is detrimental and is an underlying condition found in some of the most common human diseases, for example, anemia and hereditary hemochromatosis [35, 36]. Mammalian iron metabolism is controlled by two key regulatory mechanisms [37], one that functions systemically coordinating the iron import and export via the hormone hepcidin and the iron exporter ferroprotein, and another that predominantly regulates iron metabolism gene expression post-transcriptionally through the binding of iron-regulatory proteins (IRPs) to cis-regulatory iron-responsive elements (IREs) in messenger RNAs (mRNAs). In this section, I will describe the main aspects of these two iron-regulatory systems.

1.5.1 Regulation of systemic iron homeostasis

The control of systemic iron levels occurs mainly through the regulation of iron acquisition and storage. In mammals, the dietary iron is first absorbed by duodenal enterocytes, and it is regulated through the expression of the intramembrane metal transporters Ferroportin (Fpn) and divalent metal transporter 1 (DMT1) in response to hepcidin, a liver-derived hormone that mainly functions in systemic iron regulation [37, 38]. The iron absorption is facilitated by duodenal cytochrome b (Dcytb), which reduces ferric iron such that ferrous iron can be transported through DMT1. Iron is released from enterocytes by ferroportin [39], but only after the ferrous iron is oxidated to ferric iron by the multicopper oxidase (MCO) Hephaestin [40]. Once iron has traversed

across the intestinal mucosa and entered the bloodstream, where it tightly binds to transferrin (Tsf), the Tsf-Fe(III) complex targets transferrin receptor 1 (TfR1) for internalization through forming clathrin-coated pits by receptor-mediated endocytosis [38, 41]. Transferrin-bound iron is then transported to tissues and cells (primarily reticulocytes), where it is incorporated into heme. Old erythrocytes are phagocytosed by macrophages, which degrade hemoglobin and recycle iron back into the plasma (~20-30 mg/day) [38], where it again binds transferrin. Iron is prone to be deposited in parenchymal tissues (such as the liver) in the form of non-transferrin-bound iron when iron absorbed or released into the plasma exceeds the loading capacity of transferrin. This frequently leads to iron overload symptoms [42-45], such as cirrhosis and cardiomyopathy.

1.5.2 Regulation of cellular iron homeostasis

Maintaining iron homeostasis by cells involves processes similar to those in systemic iron control, including regulating cellular iron uptake, utilization, and storage [37, 41, 46]. In addition, cellular iron trafficking also involves a process where mechanisms are required to control cellular iron excretion.

Like the systemic iron regulation where the plasma iron binds to transferrin and is absorbed via the high-affinity TfR1, transferrin-bound iron is also the primary iron source taken up by the cell. Humans and mice lacking transferrin expression will accumulate iron in nonhematopoietic tissues like the liver [37]. Disruption of TfR1 function in mice resulted in inefficient differentiation of erythroid, lymphoid, and neuroepithelial cells. However, this was not dispensable for the

development of tissues, suggesting some cells can still acquire iron independently of the transferrin cycle. For example, cells may take up iron in ferritin and heme. Serum ferritin enters cells via the Scara5 and TIM-2 receptors [47, 48], whereas specialized cells take up heme-bound iron via the SLC48A1 receptor [49]. Heme-bound iron can also be acquired indirectly by recycling heme moieties from dying red blood cells engulfed by macrophages via phagocytosis [50]. Taken together, cells can meet their iron needs via different uptake pathways.

Cellular iron that is not utilized directly for metalation reactions or exported is stored within the iron storage protein ferritin, which comprises 24 subunits of heavy and light chains [51]. The two ferritin subunits show both similarities and differences, which mainly lies in their expression characteristics. Both the heavy chain and light chain genes are ubiquitously expressed. However, their protein levels vary greatly depending on the cell type and whether or not they can respond to stimuli. The importance of having ferritin within the cell is that it provides a means to lock up excess iron in the inactive redox form to prevent iron-mediated cell and tissue damage. The mobilization of stored iron is under the control of the cellular iron regulation system. The third type of ferritin is present in mitochondria for protecting the organelle against iron-mediated toxicity. In contrast to its cytosolic counterpart, mitochondrial ferritin (MtFt) is not found ubiquitously, and the IRPs do not directly control its expression.

Cellular iron homeostasis is coordinately regulated post-transcriptionally by iron regulatory proteins IRP1 and IRP2 (also known as ACO1 and IREB2) [52]. Both proteins are RNA-binding proteins that bind to the conserved *cis*-regulatory hairpin structures known as iron-responsive

elements (IREs). A canonical IRE stem-loop contains a six-nucleotide loop, usually with the sequence CAGYGX, where Y presents U or C and X can be any residues except G [53]. The upper and lower stem sections are composed of complementary base pairs (N-N') and separated by an unpaired protruding C bulge (Fig. 1.2a). The high specificity and affinity of the IRP/IRE interaction are ensured by two spatially distant sites around the terminal loop and the C bulge of the IRE [54].

The binding of IRPs to IREs responds to cellular iron levels (Fig. 1.2b). IRP1 not only functions as an RNA-binding protein, but also as a cytosolic aconitase that catalyzes the switch between citrate and isocitrate. In iron-replete cells, IRP1 incorporates a 4Fe-4S cluster that causes a conformational change preventing IRE-binding. This form of IRP1 (holo-IRP1) instead acts as a cytosolic aconitase that interconverts the citrate and isocitrate. In iron-deficient cells, IRP1 loses the Fe-S cluster to become the apo-protein (apo-IRP1) and binds to IREs present in the untranslated regions (UTRs) of mRNAs encoded proteins involved in iron metabolism. Given that the Fe-S cluster is involved in the conformational change of IRP1, disruption of the ISC biogenesis pathway would stimulate the IRE-binding activity of IRP1 [55]. For the same reason, the ratio of holo- to apo-IRP1 depends primarily on mitochondrial iron availability and the efficiency of ISC biogenesis. Unlike IRP1, IRP2 is not bi-functional. Cellular iron level change can either promote IRP2 binding to IREs for cellular iron regulation when cellular iron level drops, or IRP2 interact with the FBXL5 (F-box and leucine-rich repeat protein 5) adaptor protein that recruits an SCF (SKP1-CUL1-F-box) E3 ligase complex, promoting IRP ubiquitination and subsequent degradation by the proteasome in iron-replete cells [56] (Fig. 1.2c). Genetic ablation of IRP1 and IRP2 in mice and subsequent

analyses have shown that IRP2 dominates iron metabolism in mammals, while IRP1 only contributes to basal level of cellular iron regulation in tissues with high expression levels of IRP1 [52].

One of the least understood aspects of cellular iron homeostasis is how iron is transported within cells. In the cytoplasm, iron is directly bound to specific proteins, but most iron is transported into the mitochondria, where it is utilized to generate heme and iron-sulfur cluster (ISC)-containing proteins involved in electron transport and oxidative phosphorylation [57]. Given that the mitochondrion has become a focal point of iron metabolism, the mechanism by which intracellular iron trafficking is regulated needs to be further investigated.

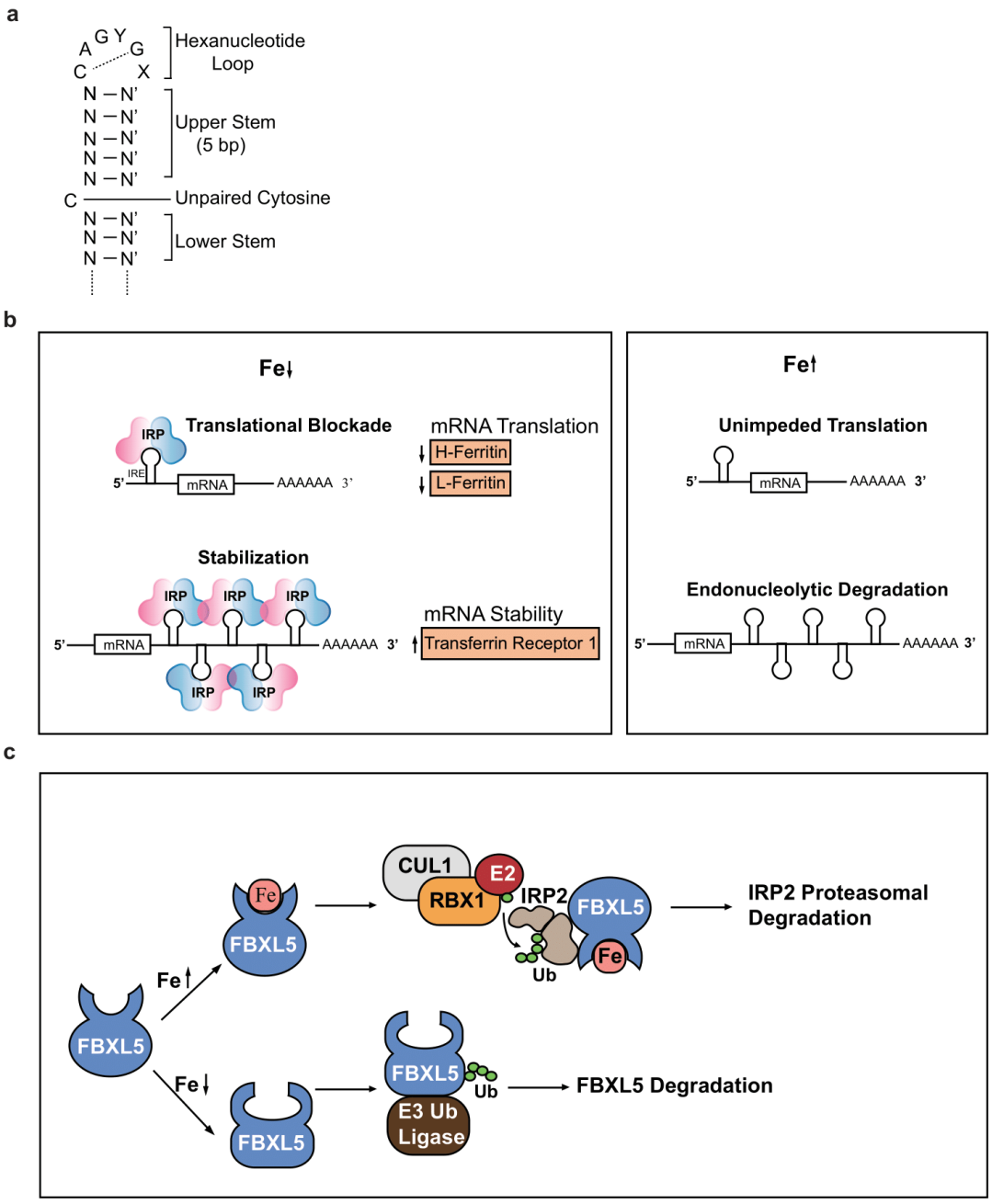

Figure 1.2 Vertebrate cellular iron regulation.

(a) A schematic demonstration of the stem-loop structure of a canonical iron-responsive element. The sequence and structure specificity of IREs are critical for the recognition by iron-regulatory

proteins (IRPs). (b) Vertebrates encode two Iron-Regulatory Proteins, namely IRP1 and IRP2. The regulation of cellular iron levels under iron depletion conditions is achieved by binding IRP to the Iron-Responsive Element (IRE), which further regulates iron metabolism gene expression. Depending on where the IRE is located, IRP either inhibits (5' UTR) or stimulates (3' UTR) the translation of corresponding mRNAs. (c) While IRP2 regulates cellular iron levels highlighting the same mechanism as IRP1 in iron depletion conditions, IRP2 degrades under iron-replete conditions.

1.6 Comparing cellular iron metabolism in *Drosophila* and mammals

Iron is essential for nearly all living organisms. Therefore, characterizing new players in simpler model organisms (e.g., through genetic screens) will significantly benefit our understanding of iron metabolism and iron-related pathogenesis in humans. Although sharing partially conserved regulatory mechanisms, iron regulation is not always the same among species. In insects, many aspects of iron metabolism remain poorly understood due to the absence of specific orthologous genes known to act in mammalian iron processes. For this reason, understanding the similarities and differences of iron metabolism between flies and mammals is of great importance to unravel the evolutionary biology of iron homeostasis. Ultimately, studying iron metabolism in invertebrates may also help develop new strategies to combat iron-related diseases. In this section, I will present a brief review on what we have known so far in *Drosophila* regarding cellular iron regulation, for instance, dietary iron absorption, iron transport and storage, and lastly, cellular iron regulation.

1.6.1 Dietary iron acquisition

Iron is absorbed by intestinal epithelia, followed by secretion into the circulatory system. The entire process can be divided into two steps: the dietary iron influx at the apical membrane and the dietary iron efflux at the basolateral membrane of intestinal epithelial cells [58]. In mammals, dietary ferric iron (Fe^{3+}) is reduced to ferrous iron (Fe^{2+}) by DcytB, a member of the cytochrome b561 family of plasma membrane reductase [59]. Then Fe^{2+} can traverse across the apical

membrane via the divalent metal transporter (DMT1 or NRAMP2). *Malvolio* (*Mvl*) encodes the DMT1 homolog in *Drosophila* and is predominantly expressed in the midgut, Malpighian tubes, the central nervous system, and plasmatocytes (a type of blood cell) [60]. *Mvl* mutants are iron-depleted in the midgut iron region (most likely the site where iron absorption occurs) [61]. *Mvl* mutants accumulate iron, which is rescued by midgut-specific *ferritin*-RNAi [62]. The *Drosophila* genome has two homologous genes of the mammalian *DcytB*, termed *CG1275* and *no extended memory* (*nemy*) [63]. However, genetic analysis shows that *nemy* appears to function in learning and memory [64], and it is thus unclear whether *nemy* has a role in iron absorption. *CG1275*, on the other hand, has not yet been studied to date.

Cellular iron efflux across the basolateral membrane of enterocytes in mammals requires the cooperation of ferroportin (Fpn), a multi-copper oxidase (MCO), and hephaestin (ceruloplasmin homolog expressed in the duodenum), which altogether oxidize Fe^{2+} to Fe^{3+} for loading into circulating serum transferrin (Tsf). Ferroportin is the only known mammalian iron transporter essential for transporting iron from one cell type to another [65]. Previous studies in different species, such as mice and zebrafish, have shown that the presence of Fpn is crucial for early development [66-68]. However, no known Fpn homolog has been reported in insects. Meanwhile, *Drosophila* encodes four multi-copper oxidases (MCO1, Straw, MCO3, and MCO4) [69]. Some MCO family members function as ferroxidases and as ascorbate oxidases and laccases [70]. MCO1 oxidizes ferrous iron and therefore has been proposed to be an intestinal ferroxidase essential for iron absorption. Knocking down *MCO1* results in a widespread lethality, suggesting that *MCO1*

may be critical for development in flies [69]. Disrupting *MCO3* function, in contrast, has a milder effect than *MCO1* in iron homeostasis [61]. *MCO3* mutants can rescue the depleted iron store of *Mvl* mutants. However, whether MCO3 has a ferroxidase activity needs to be confirmed via biochemical analysis. It should also be noted that MCO3 has no known orthologues outside of *Drosophilidae*. Lastly, *CG32557*, a gene annotated in 2017 as *MCO4*, was studied by an M. SC. student in our lab. In yeast, the gene is known as *fet3* and critical for high-affinity iron import [71]. Preliminary data based on RNA-Sequencing (RNA-Seq) suggest that *MCO4* is differentially expressed in response to changes in dietary iron levels.

1.6.2 Dietary iron transport and storage

In mammals, exported iron from enterocytes is mainly bound to transferrin and delivered to non-intestinal tissues through the transferrin 1 receptor-mediated endocytosis [46, 72, 73]. Various biochemical and genetic studies support the existence of transferrin-independent pathways for cellular iron uptake. In this section, I will briefly summarize the known functions of transferrin and ferritins in cellular iron transport and storage in flies.

Transferrin (Tsf) is a glycoprotein present in multicellular organisms with a high affinity for binding ferric iron at $K_d\ 10^{-23} M^{-1}$ [74]. The binding of iron to transferrin essentially limits the effects of iron to generate cytotoxic radicals. In mammals, *Tsf* mutations can lead to iron-overload disease [75]. The Tsf-Fe (III) complex in the plasma is transported into non-intestinal cells through binding to one of the two transferrin receptors (TfR1 and TfR2). While TfR1 is localized to cell membranes

in all living cells, TfR2 is primarily localized in the liver and binds iron with a much lower affinity than TfR1. Followed by the internalization of the Tsf-Fe (III)-TfR1 complex into cells, it localizes to an endosome that is acidified by an ATP-dependent proton pump that lowers the luminal pH to about 5.5. Acidification leads to a conformational change of the complex with the consequent release of iron. The endosomal Fe (III) is then converted into Fe (II) by STEAP3, a ferrireductase. However, *Drosophila* neither have transferrin receptors nor STEAP3 but encodes three transferrin homologs (Tsf1, Tsf2, and Tsf3). This suggests that there might be a different class of transferrin receptors or that iron is absorbed by an alternative transport mechanism [76].

Ferritins are highly stable, multi-subunit protein complexes with a capacity to bind ~4,500 iron atoms per molecule. While ferritins generally function in iron storage, their roles in iron metabolism vary depending on the species. Mammalian ferritin is predominantly cytosolic. By contrast, in most insects, including *Drosophila melanogaster*, ferritin is abundant in the hemolymph and found in the secretory pathway (ER, Golgi complexes, and secretory vesicles) [77, 78]. *Drosophila* encodes two types of ferritin: the testis-specific mitochondrial protein encoded by the *Ferritin-3-Heavy-Chain-Homolog* (*Fer3HCH*) gene [79], and the primary secretory type responsible for iron storage and cellular iron absorption encoded by the *Fer1HCH* and *Fer2LCH* genes. Each secretory ferritin molecule comprises 12 Fer1HCH and 12 Fer2LCH subunits, forming a hollow-sphere complex that stores up to 4,500 iron atoms [80]. The heavy chain homolog (H) subunit is required to oxidize ferrous iron to ferric iron. In contrast, the light chain homolog (L) subunit lacks the ferroxidase activity but promotes crystallization and stabilization of the iron core

[78, 81]. Midgut-specific knockdown of *ferritin* caused local iron accumulation but systemic iron deficiency and reduced survival, suggesting a critical role of ferritin in dietary iron absorption and transport [62]. To note, mammalian Tim2, Scara5, and TfR1 are three hypothesized ferritin receptors, but they do not have obvious orthologs in insect genomes. This raises the idea that insect ferritin may act as an iron transporter rather than an iron storage protein. Although some questions remain regarding where ferritin assembly and iron-loading occur, early electron microscopy studies indicate that iron-loaded ferritin occurs in the Golgi apparatus and the rough endoplasmic reticulum (RER) [82, 83]. Ferritin is also retained in the RER but not immediately secreted once assembled. As mentioned before, the *Drosophila* genome also reveals a third *ferritin* gene (*Fer3HCH*), identified initially as *CG4349*, located on the X chromosome [79]. *Fer3HCH* encodes a mitochondrial ferritin subunit that is similar to human mitochondrial ferritin (MtFt). In addition, *Fer3HCH* is predominantly expressed in male gonads. Unlike in humans and mice, mitochondrial ferritin is highly expressed in testis and expressed at low levels in other tissues. Since *Fer3HCH* overexpression does not affect levels of the other two ferritin subunits and does not change total iron levels in flies, mitochondrial ferritin may have little effect on iron metabolism but instead functions primarily to protect mitochondria from oxidative stress [79, 84].

1.6.3 Regulation of cellular iron homeostasis

Cellular iron levels are mainly controlled by the binding of iron-regulatory proteins to iron-responsive elements in mRNAs (IRP1/IRE system), which is a highly conserved system in both

vertebrates and *Drosophila.* Instead of having both IRP1 and IRP2, the *Drosophila* genome contains two IRP1-like proteins encoded by two different genes, *IRP1A* and *IRP1B* [85]. Of two duplicated cytosolic aconitases identified in *Drosophila*, only IRP1A acquires the IRE-binding activity and functions to regulate cellular iron levels via the IRP1/IRE system. In contrast, IRP1B has no RNA-binding activity and is predicted to only function as a cytosolic aconitase [85]. Like mammalian IRP1, IRP1A is bi-functional and can switch between an iron-sulfur protein with aconitase activity and an apoprotein that binds to IREs in response to cellular iron levels (Fig. 1.3). However, compared to about ten different genes (i.e., *ALAS2*, *ferritin H-* or *L-chain*, *TfR1*, *DMT1*) with canonical IREs identified in mammals [37], *Drosophila* IRP1A is only known to regulate mRNAs from two genes, *succinate dehydrogenase subunit B* (*SdhB*) and *Fer1HCH* [86-88]. Both *SdhB* and *Fer1HCH* possess 5'-IREs, resulting in a net outcome of increasing bioavailable intracellular iron levels via post-transcriptional regulation. There are two likely explanations for not finding other IRP1A-binding mRNAs, though not confirmed. First, insects may have adapted a new mechanism of iron regulation not restricted to the post-transcriptional IRP1/IRE system. Second, there might be non-canonical IREs (or simply IRP1A recognition sequences) that have not yet been characterized throughout the well-established genomes.

One should also consider currently unknown mechanisms that may regulate cellular iron homeostasis in *Drosophila*. For instance, ferritin is inducible in cells of the anterior midgut but is constitutively expressed in the iron region (a cluster of cells of the middle midgut) and is not detectable in the copper cells (a cluster of cells in between of the anterior midgut and the iron

region) [89, 90]. This result suggests that ferritin expression might be regulated differently even in the same tissue (like *Drosophila* midgut). In addition, our lab recently demonstrated that nuclear IRP1A also contributes to cellular iron regulation in *Drosophila* differently from the post-transcriptional regulation of cellular iron homeostasis via the IRP1/IRE system, which is to transcriptionally control the expression of specific iron-dependent genes during development [91]. PG-specific expression of $IRP1A^{3R3Q}$ (non-RNA-binding holoprotein) followed by RNA-seq and differential gene expression (DGE) analysis revealed a significant down-regulation of six out of seven Halloween genes and other genes involved in heme biosynthesis and ISC assembly. These results broadened our current understanding of iron biology by providing a new perspective of cellular iron regulation apart from the well-established IRP1/IRE system. Nevertheless, the nature of these non-canonical mechanisms and their physiological functions in the fruit fly are not well understood. Several questions still need to be answered. For instance, what is the mechanism by which IRP1A is transported across the nuclear membrane? What are the key factors involved in this process? Does vertebrate IRP1 have the same subcellular localization as *Drosophila* IRP1A and function similarly in cellular iron homeostasis? In this thesis, I will address some of these questions in detail.

In conclusion, although our knowledge of iron homeostasis in *Drosophila* is limited, with new studies from our lab and others exploring different aspects of iron metabolism in invertebrates, we anticipate making important contributions to iron biology.

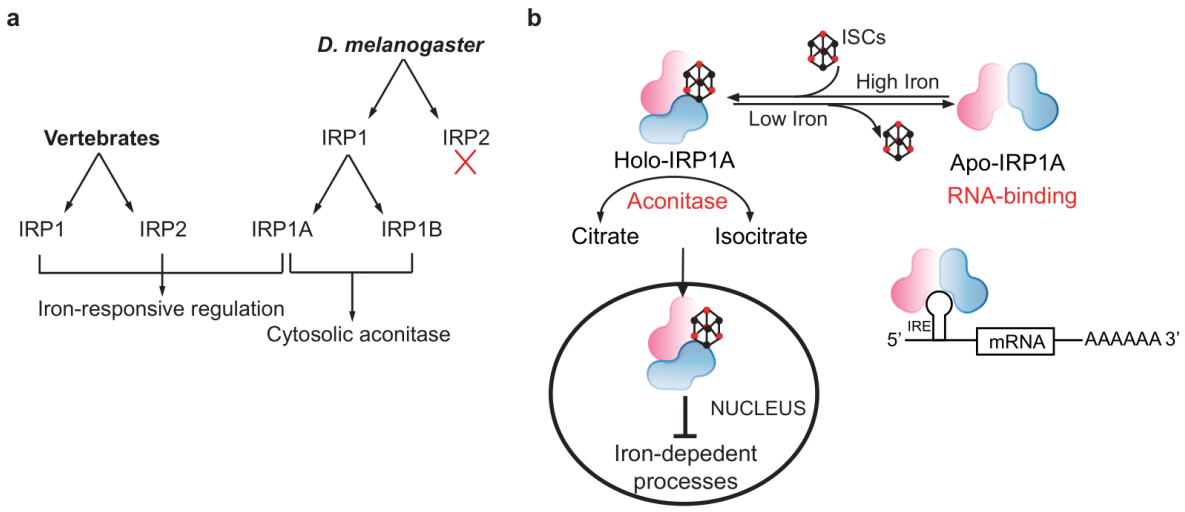

Figure 1.3 *Drosophila* cellular iron homeostasis is mainly regulated by IRP1A.

(a) Unlike vertebrates where both IRP1 and IRP2 are iron-responsive, *Drosophila* encodes two IRP1 proteins. IRP1B has been suggested to function as a cytosolic aconitase, whereas IRP1A is the primary regulator of cellular iron homeostasis in flies. (b) IRP1A registers cellular iron homeostasis via the IRP1A/IRE system, highlighting the same mechanism as in vertebrates. IRP1A has the ability to switch between the cytosolic aconitase form (holo-IRP1A) and the RNA-binding form (apo-IRP1A) in response to cellular iron levels. Under low iron conditions, IRP1A loses the iron-sulfur cluster (ISC) and binds to specific mRNAs that harbor IREs, which ultimately regulate the expression of iron metabolism genes. On the contrary, when cellular iron is replete, IRP1A acts as a cytosolic aconitase which catalyzes the interconversion between citrate and isocitrate. Holo-IRP1A is believed to accumulate in the nuclei of certain tissues, where it down-regulates iron-dependent processes when the cellular iron level drops.

1.7 Heme biosynthetic pathway and heme deficiency pathologies

As stated in section 1.4, seven out of nine enzymes involved in the ecdysone biosynthetic pathway are cytochrome P450 monooxygenases (which require heme as a cofactor), highlighting the importance of cellular iron and heme homeostasis for ecdysone biosynthesis and animal's development. Over decades, the heme biosynthesis pathway and intermediates have been studied in detail. And the heme biosynthetic pathway is highly conserved between vertebrates and *Drosophila*. Heme biosynthesis is accomplished in mitochondria and the cytosol by a series of enzymatic reactions. The entire pathway can be divided into four main stages: the synthesis of a single pyrrole, the assembly of the tetrapyrrole ring, modification of the side chains, and the incorporation of iron into the porphyrinogen ring (Fig. 1.4). Exposure to UV and air isomerizes the porphyrinogen rings (products of stage three) into auto-fluorescing porphyrins. An intriguing phenotype associated with this was noticed in *Drosophila* larvae with impaired heme production. The presence of red autofluorescence in the PG was noticed when RNAi larvae (*spz5, Updo*, *Ppox*, and *AGBE*) were exposed to UV [91]. In contrast, PG-specific *Alas*-RNAi failed to generate the red autofluorescence since the disruption of heme biosynthesis occurs prior to the formation of porphyrinogen ring. In humans, compromised heme biosynthesis by mutations affecting enzymatic activity or by environmental factors such as lead would cause pathway intermediates (excess of porphyrins or heme precursors) to be accumulated and appear in blood, urine, or feces, which confers to porphyria [92-94]. We thereby refer to the red autofluorescence observed in multiple

Drosophila RNAi lines as the "porphyria-like" phenotype. There are two simple explanations for the heme deficit. First, heme biosynthetic enzymes (Table 1.2) (i.e., *Updo* and *Ppox* loss-of-function) might be misregulated or have impaired functionality. Alternatively, it is also possible that the bioavailable iron levels are too low to be efficiently utilized by mitochondria for completing the last step in the heme biosynthesis. There has been evidence showing that *IRP1A* null mutants ($IRP1A^{KO}$) die in the early larval stage and display the porphyria-like phenotype, which can be rescued by iron feeding [91]. In addition, PG-specific *AGBE*-RNAi also shows the same porphyria-like phenotype. *AGBE* encodes a glycogen branching enzyme, which is critical for repairing IRP1A iron-sulfur clusters for its nuclear function of transcriptionally regulating iron-dependent gene expression.

Heme biosynthesis is also interconnected to iron-sulfur cluster (ISC) biogenesis, given that iron molecules are required for both biological processes (Fig.1.5). Mutants in the yeast ISC assembly machinery are defective in the last step of the heme biosynthetic pathway, in which porphyrin is converted to heme in the presence of iron [95]. In addition, the human aminolevulinic acid dehydratase (ALAD), which catalyzes the second step of heme biosynthesis, was identified as a Fe-S protein, therefore establishing a connection between these two iron-consuming pathways [96]. Taken together, identifying novel factors of heme biosynthesis will broaden our current knowledge on ecdysteroid production in flies.

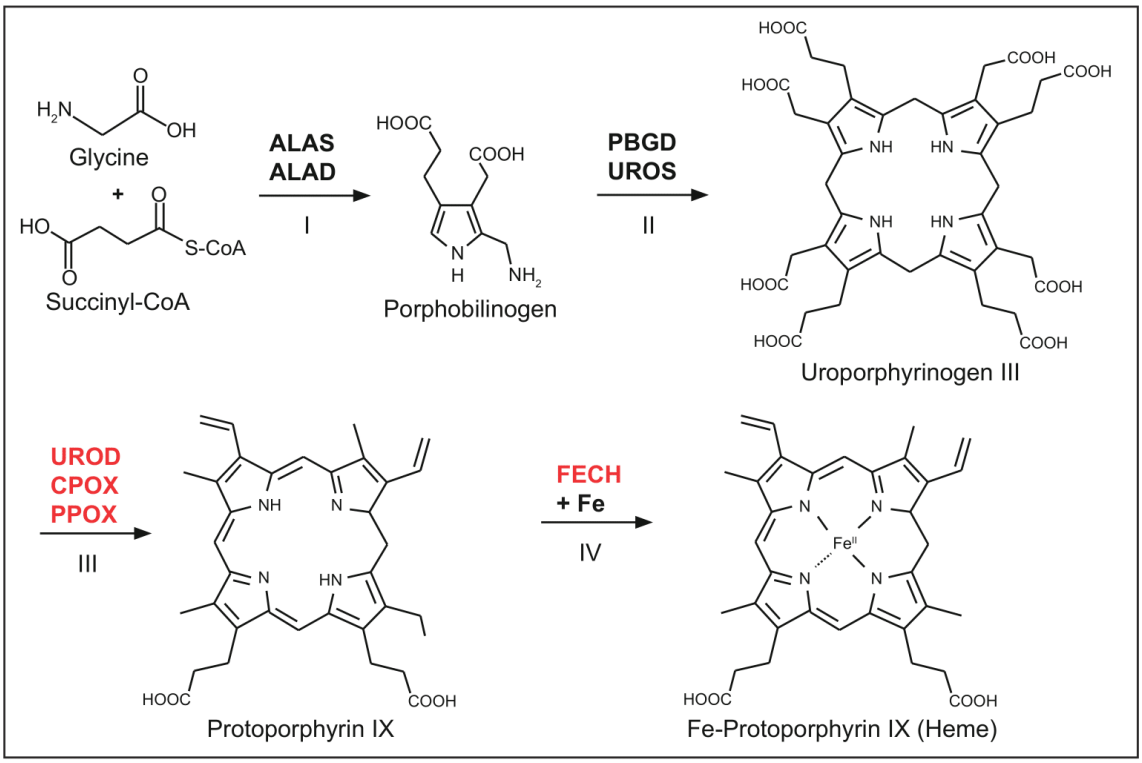

Figure 1.4 Heme biosynthetic pathway.

Heme biosynthesis is highly conserved between vertebrates and *Drosophila*, which constitutes four main stages: the synthesis of a single pyrrole (I), the assembly of the tetrapyrrole ring (II), modification of the side chains (III), and the incorporation of iron into the porphyrinogen ring (IV). Isomerized tetrapyrrole rings by air and UV light emit red autofluorescence. The heme moiety after the incorporation of iron is non-fluorescing. Interruption of the heme pathway, for example, by misregulating enzymatic activities of heme biosynthetic enzymes (red) or insufficient cellular iron supply to the mitochondria, would cause a porphyria-like phenotype in the prothoracic gland [91].

Table 1.2 List of heme biosynthetic pathway enzymes in vertebrates and *Drosophila.*

Step	Vertebrate name	Fly ortholog	Product
1	ALA Synthase (ALAS)[a]	*Alas*	Aminolevulinic acid (ALA)
2	ALA Dehydratase (ALAD)[a]	*Pbgs*	Porphobilinogen (PBG)
3	PBG Deaminase (PBGD)[b]	*l(3)02640*	Hydroxymethylbilane
4	UROIII Synthase (UROS)[b]	*CG1885*	Uroporphyrinogen III (UROIII)
5	UROIII Decarboxylase (UROD)[c]	*Updo*	Coproporphyrinogen III
6	Coproporphyrinogen III Oxidase (CPOX)[c]	*Coprox*	Protoporphyrinogen IX
7	Protoporphyrinogen IX Oxidase (PPOX)[c]	*Ppox*	Protoporphyrin IX
8	Ferrochelatase (FECH)[d]	*FeCH*	Heme

[a] Enzymes involved in the synthesis of a single pyrrole

[b] Enzymes involved in the assembly of tetrapyrrole ring

[c] Enzymes involved in the modification of the side chains

[d] Enzyme catalyzes the incorporation of iron into the porphyrinogen ring

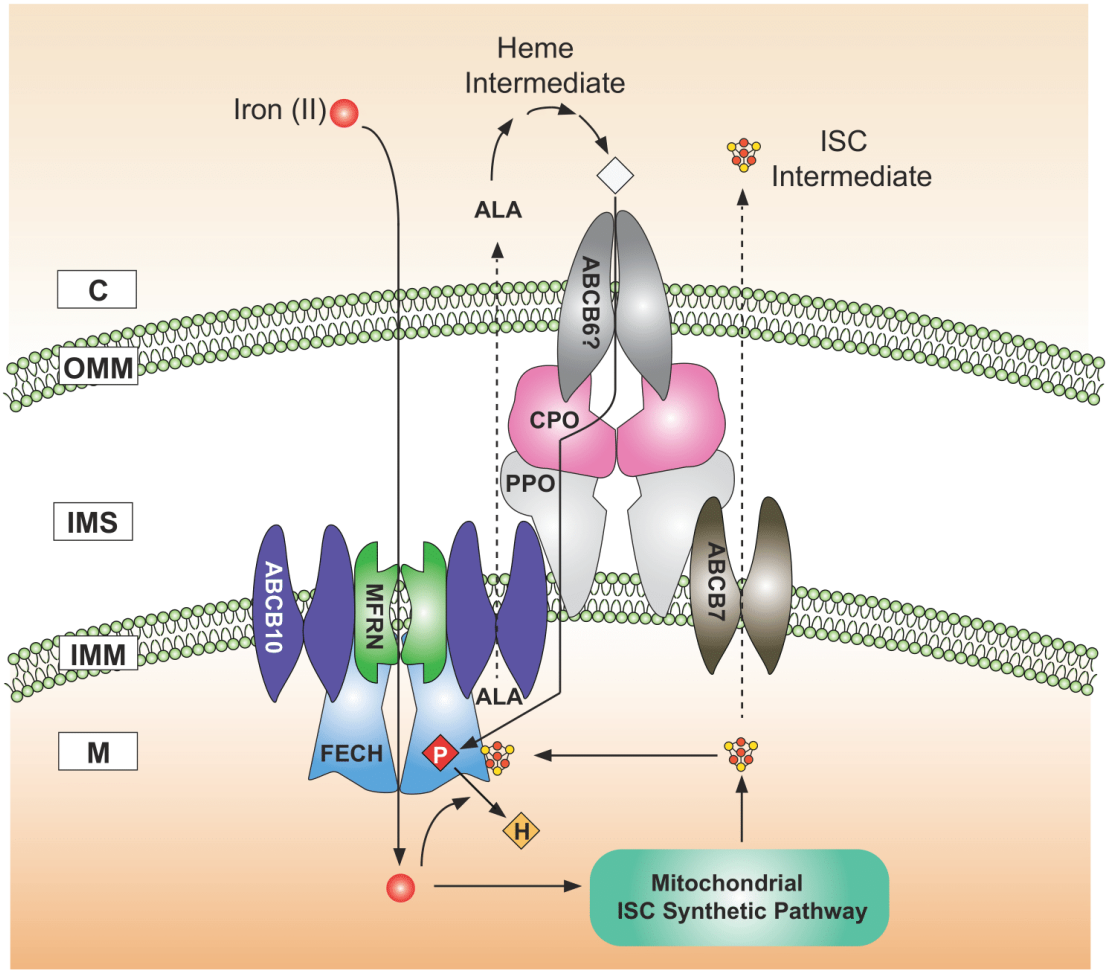

Figure 1.5 Iron is essential for both heme biosynthesis and ISC biogenesis.

Heme is converted from succinyl-CoA and glycine by eight enzymatic steps, in which FECH catalyzes the last step in the presence of iron. Cytosolic iron is transported into the mitochondrial matrix via MFRN to make iron-sulfur cluster (ISC) intermediates. Abbreviations: C, cytosol; OMM, outer mitochondrial membrane; IMS, inter-mitochondrial membrane space; IMM, inner mitochondrial membrane; M, mitochondrial matrix; H, heme; P, PPIX; MFRN, mitoferrin; CPOX, coproporphyrinogen III oxidase; PPOX, protoporphyrinogen III oxidase.

1.8 Thesis outline

My thesis focuses on two projects in which I characterize the roles of two genes acting in ecdysone biosynthesis during *Drosophila* larval development. The first project investigates the roles of RanBP3 in cellular iron regulation, which involves mechanisms to control cellular iron acquisition, cellular iron mobilization and the transport of cytosolic iron to the mitochondria for heme biosynthesis and ISC biogenesis. The second project's objective is to examine the roles of Su(var)2-10, originally identified as a Suppressor of position-effect variegation (PEV), in regulating ecdysone biosynthesis via *neverland* transcription.

1.8.1 Characterizing the roles of RanBP3 in cellular iron homeostasis

Drosophila Ran-binding protein 3 (RanBP3) was identified by two RNA interference (RNAi) screens to find novel regulators of heme biosynthesis and *Drosophila* development. PG-specific *RanBP3*-RNAi perturbed the larval development and induced the accumulation of protoporphyrin in the PG cells, evidenced by red autofluorescence observed under UV light. The porphyria-like phenotype was recapitulated when *RanBP3* was conditionally knocked out in PG cells using a *RanBP3* gRNA line crossed to transgenic line that expresses *Cas9* specifically in the PG. Interestingly, both the lethality and the porphyria-like phenotype were rescued by supplementing the diet with hemin (protoporphyrin IX-Fe^{3+}), but not elemental ferric iron (ferric ammonium citrate, FAC) in the *Drosophila* diet, suggesting that the elemental iron uptake pathway appears to be interrupted in *RanBP3*-depleted PG cells, whereas the heme-bound iron import pathway

remained intact and functional. The porphyria-like phenotype and the blocked larval-to-pupal transition were also complemented by expressing the transgenic *IRP1A*^{C450S} allele in the *RanBP3*-depleted PG cells. The single point mutation in the *IRP1A*^{C450S} allele abolishes the iron-sulfur cluster incorporation site, resulting in constitutively RNA-binding apo-IRP1A. Interestingly, apo-IRP1A was found to accumulate in the *RanBP3*-depleted PG cell nuclei. Subsequent experiments indicated that RanBP3 is a novel regulator of IRP1A for its nuclear export. The replenishment of cytosolic IRP1A is critical for cellular iron homeostasis via the binding of IRP1A to transcripts encoding genes with roles in iron metabolism. I also demonstrated how IRP1A is transported into the nucleus, which involves three essential proteins: Ran, NTF2 and Chickadee. Collectively, I provided molecular evidence showing the mechanism by which IRP1A is transported through the nuclear pore complex (NPC).

I also report that two endoplasmic reticulum (ER)-localized proteins could directly or indirectly interact with RanBP3. Interestingly, they both showed protein-protein interaction with the mitochondrial iron transporter protein, Mitoferrin (Mfrn) in *Drosophila* Schneider 2 (S2) cells, which suggested RanBP3 may also have a role in mediating the transport of cytoplasmic iron into the mitochondria for making iron-containing proteins, such as heme and iron-sulfur clusters.

1.8.2 Examining of the roles of Su(var)2-10 in ecdysone biosynthesis

The second project aimed to understand the mechanisms by which Su(var)2-10 regulates ecdysone biosynthesis during larval development in *Drosophila melanogaster*. Su(var)2-10 was

originally identified as a suppressor of PEV. PEV describes a situation where a euchromatic gene is positioned close to heterochromatin, i.e., due to a chromosomal rearrangement, resulting in the silencing of gene expression. *Drosophila* Su(var)2-10 has been reported to function as a SUMO E3 ligase that transfers the SUMO moiety to a lysine residue on the target protein. PG-specific *Su(var)2-10* knockdown induced a complete developmental arrest in the third-instar larval stage. In addition, *Su(var)2-10* loss-of-function in the PG cells resulted in enlarged ring glands compared to the wild-type control. Subsequent experiments implicated a role of Su(var)2-10 in ecdysone biosynthesis via regulating *nvd* transcription. Nvd catalyzes the conversion of dietary cholesterol to 7-dehydrocholesterol (7dC) in the PG cells; therefore, it is essential for ecdysone biosynthesis. Furthermore, I reported two independent mechanisms by which Su(var)2-10 regulates *nvd* transcription. First, Su(var)2-10 can transcriptionally regulate *séance*, which encodes one of the two known transcription factors of *nvd*. Second, histone H2A (His2A) was identified as a substrate of Su(var)2-10 in regulating *nvd* transcription. Su(var)2-10, as a SUMO E3 ligase, may SUMOylate His2A located at the *nvd* promoter to promote transcription.

Chapter 2 Materials and methods

2.1 *Drosophila* husbandry and fly media

Drosophila lines that were used in my projects will be specifically described in each chapter. In general, fly stocks were maintained at 18℃ on standard corn meal-based diet, whereas experimental flies were raised at 25℃ with humidity around 50-60%.

The development and lethal phenotypes were recorded when animals were supplied with manipulated diets, which were homemade by using the "Nutrifly" powder, a standard recipe provided by the Bloomington *Drosophila* Stock Center (BDSC) (https://bdsc.indiana.edu/information/supplies.html). Specifically, Nutrifly food was supplemented with different chemical compounds, which will be specified in each chapter. To make 100 ml food, 17.8 grams of Nutrifly powder was weighed and boiled in 100 mL autoclaved MiliQ water for at least 5 minutes (min). 450 μL propionic acid and optional chemical compounds (Table 2.1) at the desired concentration were added into the mixture when the temperature dropped to approximately 50-60℃. Food was mixed well and distributed into discs, vials, and bottles depending on the experimental purposes.

Table 2.1 Supplement concentrations used in survival rate studies.

Supplement	Solvent	Experimental purpose	Stock concentration	Final concentration
Cholesterol[a,b]	Ethanol	Sterol rescue	25 mg/mL	25 μg/mL
7-dehydrocholesterol (7dC)[b]	Ethanol	Sterol rescue	125 mg/mL	125 μg/mL
20-hydroxyecdysone (20E)[a,b]	Ethanol	Sterol rescue	250 mg/mL	250 μg/mL
Hemin[a]	NaOH	Iron manipulation	38 mM	1 mM
Zinc protoporphyrin IX (ZnPP)[a]	DMSO	Iron manipulation	50 mM	1 mM
Ferric ammonium citrate (FAC)[a]	Nuclease-free water	Iron manipulation	1 M	1 mM
Bathophenanthroline sulfate (BPS)[a]	Nuclease-free water	Iron manipulation	100 mM	100 μM

[a] Chemicals used in chapter 3

[b] Chemicals used in chapter 4

2.2 Survival rate analysis

Grape juice plates were used for embryo collection. For 100 ml grape juice mixture, 3 grams of agar was dissolved in 70 ml MiliQ water and proceeded to autoclave (solution A). For solution B, 0.5 g methylparaben was dissolved in 1 ml ethanol and added into 30 ml grape juice. The two solutions were mixed vigorously and distributed into Petri discs when the temperature dropped to about 50-60°C. Supplementation food concentrations are listed in Table 2.1.

At least 200 virgin females and 40 males (5 to 1 ratio) were used for each cross. Flies were allowed to mate in a small embryo collection cage at room temperature (RT) for one day. On the following day, flies were allowed to lay eggs for 3 hours to minimize the number of old embryos. Grape juice plates were replaced once per 1.5 hours. Newly deposited embryos were transferred with a paintbrush onto Petri discs containing the appropriate media type. Each replicate contained 50 embryos collected from the same cross on the same day. Embryos were allowed to develop at 25°C. Early third-instar larvae were gently transferred from the Petri dish into a vial containing the same food at 5 days after egg laying to quantify pupae numbers. The number of pupae and adults were quantified at 7 or 10 days after egg deposition based on the normal life cycle of flies. Three biological replicates were used for each food type for survival rate quantification. A two-tailed unpaired Student *t*-test was performed to show statistical difference of data from the same group or across groups.

Occasionally, a fourth replicate was set to record animals' development and to measure larval body length. The embryo collection process was the same as above. Images of the control and

experimental animals were taken on the fifth or tenth day after egg deposition. Body length was measured using ImageJ.

2.3 Ferric iron staining

This protocol was modified from Perl's staining for detecting iron in plants [61]. Late third-instar larvae were dissected for collecting brain-ring gland complexes (BRGCs) in 1x PBS. Samples were then fixed with 4% formaldehyde in PBS for 20 min at RT, followed by washing in 0.3% Triton-X100 in PBS for 3 x 5 min. To stain for elemental iron, samples were incubated in fresh staining solution (2% $K_4Fe(CN)_6$ + 2% HCl) at room temperature for 1 hour and briefly washed in PBST for 5x 2 min. Samples were then incubated in 0.01 NaN_3 / 0.3% H_2O_2 for 30 min at room temperature and washed 3 x 10 min in 0.1 M Phosphate buffer pH 7.0 (57.75mM Na_2HPO_4 and 42.25 mM NaH_2PO_4). Iron signals were enhanced by immersing samples in the fresh intensification buffer (0.1 M phosphate buffer pH 7.0 containing 0.00125% DAB and 0.0025% $CoCl_2$) for 10 min followed by 3x 10 min wash in 0.1M phosphate buffer pH 7.0. Images were taken using an epifluorescence camera (Nikon Digital Sight DS-U3).

2.4 Total RNA extraction and cDNA synthesis

2.4.1 RNA extraction from whole larvae sample

Ten late-instar stage larvae were collected into 200 µl TRIzol (ThermoFisher #15596026) and flash-frozen in liquid nitrogen. Samples were homogenized with pestles presoaked in 1% SDS.

Each RNA sample was brought to a final volume of 1 ml with TRIzol. Vortex vigorously to ensure complete homogenization. Samples were incubated at room temperature for 5 min, followed by adding 200 µl cold chloroform. Shake vigorously for 15 seconds. Samples were then incubated at RT for another 3 min, followed by centrifugation at 12,000 rpm at 4℃ for 15 min. After centrifugation, the upper colorless aqueous phase was transferred into a new microcentrifuge tube without any contamination of the interphase. 500 µl isopropanol was added, followed by inverting the tube five times. Samples were incubated at room temperature for 10 minutes followed by centrifugation at 12,000 rpm at 4℃ for 15 min. The supernatant was removed, and a pellet was left at the bottom. The pellet was air-dried at room temperature for 5 to 10 min followed by dissolving in 120 µl RNase-free water. Repeat the nucleic acid extraction process by adding 200 µl chloroform and vigorously shaking by hand for 15 seconds. Samples were incubated at room temperature for 3 minutes followed by centrifugation at 12,000 rpm at 4℃ for 15 min. Again, the upper aqueous phase was transferred into a new microcentrifuge tube. 10 µl 8 M LiCl was added and mixed well by inversion several times. To precipitate RNA, 300 µl 100% ethanol was added into the mixture followed by incubation on ice for 2 minutes or overnight at -20℃. Samples were centrifuged at 12,000 rpm at 4℃ for 30 minutes, and the supernatant was discarded. The pellet was washed with 1 ml 70% ethanol followed by centrifugation at 12,000 rpm at 4℃ for 5 min, and air-dried at RT. 10 µl RNase-free water was added to the pellet to dissolve the total RNA. The concentration was determined using the Qubit™ RNA HS Assay Kit (Invitrogen Q32852), whereas the RNA integrity was assessed using Agilent RNA 6000 Nanochip (RNA 6000 Nano kit) on a 2100 Bioanalyzer

instrument provided by the MBSU facility at the University of Alberta.

2.4.2 RNA extraction from ring gland samples

30 to 50 ring glands were dissected in cold PBS and transferred into an RNase-free microcentrifuge tube containing 150 µl TRIzol followed by flash-frozen in liquid nitrogen. Samples were kept at -80°C for long-term storage. To extract total RNA from the ring gland, samples were first homogenized with a pestle presoaked in 1% SDS. RNA was then extracted by phenol-chloroform separation, which was the same as whole larvae sample RNA extraction. The upper aqueous phase (contains both the DNA and RNA) was washed by adding an equal volume of 70% ethanol. The mixture was applied to the Qiagen RNeasy column (Qiagen #79254) to purify the total RNA following the manufacturer's instructions. The concentration of total RNA and the integrity were determined using Qubit™ RNA HS Assay Kit and Bioanalyzer instrument, respectively.

2.4.3 cDNA synthesis

1 µg extracted total RNA was reverse-transcribed to cDNA using the High-Capacity cDNA Reverse Transcription Kit (Applied Biosystems, ABI, Catalog number: 4368814) following manufacturer’s instructions. cDNA was then diluted 1:20 in PCR-grade water.

2.5 Quantitative real-time PCR (qPCR)

2.5.1 Primer validation

qPCR primers were designed using two cost-free online tools provided by Roche Life Science (https://lifescience.roche.com/en_ca/brands/universal-probe-library.html#assay-design-center) or NCBI Primer-BLAST (https://www.ncbi.nlm.nih.gov/tools/primer-blast/). All the primers used for the qPCR analyses are listed in Table 2.2.

The cDNA library reverse-transcribed from w^{1118} mRNA samples was serially diluted 1/4, 1/16, 1/64, 1/256, and 1/1024 using 20 µl cDNA (from the original or the previous dilution) and 60 µl PCR-grade water. Both the forward and reverse primers were added into a microcentrifuge tube at a final concentration of 3.2 µM. A master mix was prepared for each primer set to be tested, including 5 µl Luna® Universal qPCR Master Mix (NEB, M3003S) and 2.5 µl 3.2 µM primer mix. To set up the qPCR plate, 7.5 µL master mix was added into each well using an electronic pipette followed by adding 2.5 µl serially diluted cDNA template according to the map design. Each dilution was tested three times, therefore providing three replicates in total.

The reaction was examined on a QuantStudioTM 6 Flex Real-Time PCR System (ABI). Both the standard curve and the melting curve were analyzed. Two particular parameters were compared between the control and the experimental group for each primer set being analyzed. First, the standard curve slope for the gene of interest (GOI) should be as close as the slope of *RP49*, a commonly used housekeeping gene for *Drosophila* species. Second, the melting curve should only

generate a single peak, indicating that the primer binds to the template at a specific location. An optimal primer set that can be further used in the qPCR analysis should meet both criteria. A two-tailed unpaired Student *t*-test was performed for statistical analysis of data.

Table 2.2 Primer pairs used in qPCR analysis.

Target		Sequence (5' to 3')
Rp49	Forward	CGGATCGATATGCTAAGCTGT
Rp49	Reverse	CGACGCACTCTGTTGTCG
neverland (*nvd*)	Forward	CCCTCACCTAGGAGCCAACT
neverland (*nvd*)	Reverse	GGCATATAACACAGTCGTCAGC
shroud (*sro*)	Forward	CGAATCGCTGCACATGAC
shroud (*sro*)	Reverse	TAGGCCCTGCAGCAGTTTAG
spookier (*spok*)	Forward	GCGGTGATCGAAACAACTC
spookier (*spok*)	Reverse	CGAGCTAAATTTCTCCGCTTT
phantom (*phm*)	Forward	GGCATCATGGGTGGATTT
phantom (*phm*)	Reverse	CAAGGCCTTTAGCCAATCG
disembodied (*dib*)	Forward	GTGACCAAGGAGTTCATTAGATTTC
disembodied (*dib*)	Reverse	CCAAAGGTAAGCAAACAGGTTAAT
shadow (*sad*)	Forward	CAAGCGGATATTTGTAGACTTGG
shadow (*sad*)	Reverse	AAGCCCACTGACTGCTGAAT
Cyp6t3	Forward	GGTGTGTTTGGAGGCACTG
Cyp6t3	Reverse	GGTGCACTCTCTGTTGACGA
Alas	Forward	CCTGCTGAAGCGAGAAGG

Alas	Reverse	GAGGGTCTCCGATCTTAATGG
Pbgs	Forward	GAATCGCCTGAAGGAGCAC
Pbgs	Reverse	AAGAGCAGCACCGACGAC
l(3)02640	Forward	ATAGCCTCGCTTCCAAAGG
l(3)02640	Reverse	ACACCGTCAAATGGGGATAC
UROS	Forward	CCGATACGCTGCTATCCAAG
UROS	Reverse	CAGCGCGTCTCGTACACTT
Updo	Forward	GGACCGTCTCACAAAGAAGG
Updo	Reverse	AGTTCGCTCTGCTCCTTCAG
Coprox	Forward	CCAAGTGAAACAGGAGTGAGG
Coprox	Reverse	AGTCGGGATCCACTTGAGAA
Ppox	Forward	TTCACAGCAAGACCGAAAGC
Ppox	Reverse	CCGCTCAGCGAAACTGTAG
FeCH	Forward	AACACAAAGTTTTGCAGACTGG
FeCH	Reverse	ATCGCGGTCTTCGGTTTT
Ecdysone receptor (*EcR*)	Forward	TTAATTTGGTACCAGGATGG
Ecdysone receptor (*EcR*)	Reverse	TGTAAACGCTGGTAGACCTT
ultraspiracle (*usp*)	Forward	GCACTGCCGCCTGGAACA
ultraspiracle (*usp*)	Reverse	GGTAATGCGGAAGAGGAACA

Ecdysone-induced protein 74EF (*E74*)	Forward	GCGTCAGCTACGATCTCTCC
Ecdysone-induced protein 74EF (*E74*)	Reverse	GATCCTGGAGCAGTTTGAGG
Ecdysone-induced protein 75B (*E75*)	Forward	ACATTGTCGCCCAGAATAGG
Ecdysone-induced protein 75B (*E75*)	Reverse	GTCCTCCATGGACCACATCT
broad (*br*)	Forward	GATGTCAACTTCATGGACCT
broad (*br*)	Reverse	ATGGCTGTGTGTGTCCTC
Ecdysone-induced protein 93F (*E93*)	Forward	GAGTACAAGGTCAAGGAACG
Ecdysone-induced protein 93F (*E93*)	Reverse	GATTGTTTTGGTTCTTGAGG
embargoed (*emb*)	Forward	GATTAGCGAGGTGGAGGACG
embargoed (*emb*)	Reverse	CGGGGATACACTTGTTGCCT
Baz	Forward	GGCACCTATCAGCGGAATAA
Baz	Reverse	AAACTGGGCATTAGCACTGG
CG13559	Forward	ATCTGTCCAATGTGCCATGA

CG13559	Reverse	TGAAACAGTCGAGGATGCAG
TotA	Forward	TGAGGAACGGGAGAGTATCG
TotA	Reverse	GCCCTTCACACCTGGAGATA
CG13912	Forward	AAGCCGGAATACGATCACAG
CG13912	Reverse	GATACCGGAAACGCTGACTC
CG4804	Forward	TTCTTCAAAAGCTGCGCATA
CG4804	Reverse	CAGCTCGGAAGAATTTCTGG
CG9317	Forward	CCCCAATATGCGCTTAAAGA
CG9317	Reverse	CACAACAGCCGACAGAAAGA
socs36E	Forward	AAGTGCACACTGTCGAATGG
socs36E	Reverse	TTCCCCGTTTTCACGTTATC

2.5.2 qPCR reaction and fold change determination

The qPCR results shown in this thesis were analyzed using three biological replicates tested in triplicate unless specifically described. qPCR reactions were set up in the same manner as the primer validation. The reactions were then run using the comparative CT (ΔΔCT) mode with the following thermocycling parameters: Step 1: 95°C for 30 seconds (s); Step 2: 95°C for 15 s and Step 3: 60°C for 30 s. Steps two and three were performed for a total of 40 cycles.

After each run, CT (threshold cycle) values were determined for each biological sample with

each primer set. To utilize the ΔΔCT method for qPCR analysis, the relative expression level of the genes of interest (GOI) was first compared to that of the housekeeping gene (*Rp49*). Then, ΔΔCT was determined by using the ΔCT of the experimental condition, for instance, gene knockdown or supplementing the fly diet with a chemical compound, subtracting by the ΔCT of the control condition for every GOI. The average of ΔΔCT values was used to calculate the fold change (calculated as $2^{\wedge-\Delta\Delta CT}$) between the experimental and control conditions for GOI.

2.6 Cell culture and transfection

Drosophila Schneider 2 (S2) cells were maintained in the complete Schneider medium (ThermoFisher 21720001) containing 10% heat-inactivated FBS (Sigma 12103C) and Penicillin-Streptomycin (ThermoFisher 15140163) at a final concentration of 50 units penicillin G and 50 µg streptomycin sulfate per milliliter of medium. S2 cells were plated in a 35-mm well in 2 mL complete medium for each transfection, which should give an approximately 80% cell density within a field of view. In a microcentrifuge tube, 15 µg of recombinant plasmid was added into 36 µL 2M $CaCl_2$ and brought to a final volume of 300 µL (solution A). 300 µl 2 x HEPES-Buffered-Saline (50 mM HEPES, 1.5 mM Na2HPO4, 280 mM NaCl, pH 7.1) was added into a separate tube (solution B). Drop-wise add solution A to solution B with continuous vortex until solution A was depleted. This procedure was crucial for the efficiency of S2 cell transfection, which usually takes a few minutes. Continuous mixing ensures the production of a fine precipitate necessary for efficient transfection. The transfection reaction was incubated at room temperature for 30-40

minutes, then added to the cells with continuous swirling. Transfected cells were incubated at 28°C for 24 hours. One day post-transfection, the transfection reagent was removed and replaced by fresh, complete Schneider's *Drosophila* Medium. Cells were allowed to grow at 28°C for 24-48 hours, depending on target protein expression.

2.7 Immunofluorescence and microscopy

2.7.1 *Drosophila* tissue immunostaining

Brain-ring gland complexes (BRGCs) were collected from 40-42 hours third-instar larvae in cold PBS followed by fixation in 4% paraformaldehyde (PFA, ThermoFisher #28906) in PBS for 30 min at RT. Samples were then washed with 0.3% Triton X-100 in PBS (1x PBST) for 5 min and repeated twice, followed by blocking in 1% bovine serum albumin (BSA) in 1x PBST for 30 min. The primary antibody of choice was diluted in 1% BSA in 1:1000 and then applied to samples in a microcentrifuge tube at room temperature for 2 hours or overnight at 4℃ on a rotating platform. Samples were then washed with 1x PBST three times before applying the secondary antibody of choice diluted in 1% BSA (1: 10,000) for 1 hour at room temperature. Samples were then briefly washed in 1x PBST for 10 min and incubated with DAPI in PBS (1:50,000, Cell Signaling #4083) for 30 min at room temperature. Samples were thoroughly washed with 1xPBST for 3x 10 min followed by mounting in 1% glycerol in 1xPBST.

The following antibodies were used for immunofluorescence: a monoclonal mouse anti-Flag antibody (Cell Signaling #8146S), a monoclonal rabbit anti-Flag antibody (Cell Signaling

#14793S), a monoclonal rabbit anti-Myc antibody (Cell Signaling #2278S), a monoclonal rabbit anti-Myc antibody (Cell Signaling #2276S), a goat anti-rabbit IgG H&L (Alexa Fluor ®555, ab150078), a goat anti-mouse IgG H&L (Alexa Fluor ®555, ab150114), a goat anti-rabbit IgG H&L (Alexa Fluor ®488, ab150077), and a goat anti-mouse IgG H&L (Alexa Fluor ®488, ab150113). Antibodies used in my study are also listed in Table 2.3.

Table 2.3 List of antibodies in this study.

Antibody	Source	Manufacturer	Catalog #	Experiment	Dilution
Monoclonal anti-Flag	Rabbit	Cell Signaling	14793S	IF, IP	1:1000
				WB	1:2500
Monoclonal anti-Flag	Mouse	Cell Signaling	8146S	IF, IP	1:1000
				WB	1:2500
Monoclonal anti-Myc	Rabbit	Cell Signaling	2278S	IF, IP	1:1000
				WB	1:2500
Monoclonal anti-Myc	Mouse	Cell Signaling	2276S	IF, IP	1:1000
				WB	1:2500
Monoclonal anti-GFP	Mouse	Invitrogen	MA5-15256	IF, IP	1:1000
				WB	1:2500

Anti-rabbit IgG H&L (Alexa Fluor 555)	Goat	Abcam	150078	IF	1:20,000
Anti-mouse IgG H&L (Alexa Fluor 555)	Goat	Abcam	150114	IF	1:20,000
Anti-rabbit IgG H&L (Alexa Fluor 488)	Goat	Abcam	150077	IF	1:20,000
Anti-mouse IgG H&L (Alexa Fluor 488)	Goat	Abcam	150113	IF	1:20,000
Anti-rabbit IgG H&L HRP	Goat	Abcam	97051	WB	1:10,000
Anti-mouse IgG H&L HRP	Goat	Abcam	97023	WB	1:10,000

2.7.2 Immunostaining of *Drosophila* S2 cells

The staining procedure above was slightly modified for *Drosophila* S2 cell staining. First, cells were plated on a coverslip in a 35-mm well containing the complete Schneider medium with heat-inactivated FBS and antibiotics. This provided a layer allowing cells to grow on, which also eased the following staining steps. Second, all but one washing was done by immersing cells in PBS on the working bench without disruption. S2 cells were rinsed in 0.1% Triton X-100 in PBS

for 10 min after fixation in 4% PFA. The short time of permeabilization was essential for immunostaining. However, immersing cells in permeabilizing reagents for too long may result in the loss of protein contents. The rest of the staining remained the same as the tissue staining. The percentage of nuclear RanBP3 was quantified by comparing the area of DAPI signal (nucleus) and the whole cell region (nucleus and cytosol) using ImageJ [97].

2.7.3 Microscopy analyses

Images were acquired using an epifluorescence camera (Nikon Digital Sight DS-U3) and the Nikon Eclipse 80i Confocal C2 system. Images used for demonstration of the red autofluorescence in *Drosophila* PG were acquired by viewing slides with UV light (Lumen Dynamics, X-cite Series 120Q) or the red laser channel in the Nikon confocal system. Images used for immunostaining of *Drosophila* tissues or S2 cells were acquired by viewing slides with laser channels provided in the Nikon confocal system.

2.8 Co-immunoprecipitation (co-IP) and Western blotting

Transfected S2 cells were collected by centrifugation at 3,000 rpm for 2 min at 4°C. The cell pellet was washed in cold PBS three times for complete removal of cell culture media. Cold lysis buffer (50 mM Tris-HCl pH 7.5, 250 mM NaCl, 0.1% NP-40, 5 mM EDTA, 1x proteinase K inhibitor) was added to cells, followed by continuous mixing on ice for 30 min. For Western blotting of input samples, 200 µl lysis buffer was added into the collected cells. On the other hand, 400 µl lysis buffer was used for Co-IP samples for generating a better efficiency of protein binding

to antibody-conjugated beads. Lysed cells were centrifuged at 11,000 rpm for 30 min at 4°C. The supernatant was transferred to a new tube for later steps.

In co-immunoprecipitation (co-IP) experiments, Flag-tagged bait proteins were affinity-purified using M2 Flag agarose beads (Sigma-Aldrich # A2220). Myc-tagged proteins were pulled down by using Myc-Trap Agarose (Chromotek # yta-20) following instructions provided by the manufacturer. Cell lysates were added to the antibody-conjugated beads and incubated on a rotating platform overnight at 4°C. The protein-conjugated beads were washed with Wash Buffer #1 (25 mM Na-HEPES, pH 7.5, 75 mM NaCl, 0.5 mM EDTA, 0.1% Triton X-100, 5% glycerol) and wash buffer #2 (25 mM Na-HEPES, pH 7.5, 75 mM NaCl, 0.5 mM EDTA, 5% glycerol) for three times each. Flow-through was discarded after a short spin at 12,000 rpm. Proteins were eluted by adding 50 µl 1x Gel loading buffer (60 mM Tris-HCl pH 8.0, 2% SDS, 4 mM EDTA, 5% β-mercaptoethanol, 0.02% bromophenol blue, 10% glycerol) followed by boiling at 95°C for 5 mins.

To detect Flag-tagged proteins, monoclonal rabbit anti-Flag-tag antibodies were used at a 1: 2,500, followed by incubation with a goat anti-rabbit IgG H&L HRP secondary antibody (Abcam #97051) at a ratio of 1: 10,000. To detect Myc-tagged proteins, monoclonal mouse anti-Myc-tag antibodies were used at a concentration of 1: 2,500 in coupled with a goat anti-mouse IgG H&L HRP secondary antibody (Abcam #97023) at a ratio of 1:10,000. See Table 2.3 for antibody information. Blots were scanned with a ChemiDoc imaging system (Bio-Rad) provided by the Molecular Biology Service Unit (MBSU) at the University of Alberta.

2.9 Mass spectrometry (MS) analysis

Mass spectrometry analyses were conducted using *Drosophila* S2 cells. Cells were transfected with desired plasmids followed by standard protocols to pull down epitope-tagged proteins by co-IP (Chapter 2.8). Samples were then loaded on a 10% SDS-PAGE gel that was stained with Coomassie Blue. The gel was de-stained following standard procedures and submitted for MALDI-TOF MS analysis (carried out by the Alberta Proteomics and MS Facility, University of Alberta).

Chapter 3 RanBP3 is a novel regulator of heme and iron homeostasis in *Drosophila*

3.1 Introduction

3.1.1 Identification of *RanBP3*

Ran-binding protein 3 (*RanBP3*) was identified by two RNA interference (RNAi) screens (Fig. 3.1a) designed to find novel regulators of heme biosynthesis and *Drosophila* development. Dr. Qiuxiang Ou conducted the genome-wide RNAi screen for developmental defects in collaboration with two other labs. This allowed us to find genes that may play a vital role in producing the primary steroid hormone ecdysone [98]. In the secondary screen, Dr. Qiuxiang Ou further examined the ring gland morphology in about 800 lines that showed late larval lethality in the primary screen. The abnormal ring glands were categorized into two major groups (Table 3.1), the big and red ring glands and big but not red ring glands (Figure 3.1b). Knocking down *RanBP3* in the prothoracic gland induced a severe developmental defect, as well as big red auto-fluorescing ring glands. For this reason, *RanBP3* was considered a novel candidate gene for regulating heme and iron homeostasis in *Drosophila melanogaster. Su(var)2-10* was also identified from the same screen showing big but not red ring glands when the gene was knocked down in the PG cells, suggesting Su(var)2-10 may regulate ecdysone biosynthesis and animals' development via a different mechanism than RanBP3. For this reason, the focus of this chapter is to demonstrate roles of RanBP3 in ecdysone biosynthesis through regulating heme and iron homeostasis. Characterizing roles of Su(var)2-10 in ecdysone biosynthesis, on the other hand, will be the object of chapter 4.

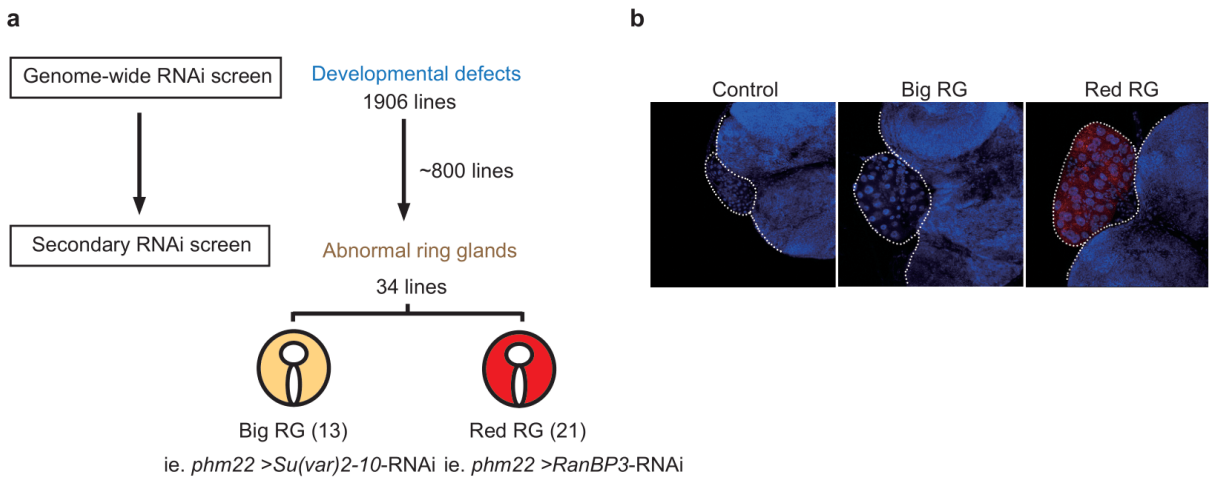

Figure 3.1 Identification of genes that are essential for heme biosynthesis.

(a) Given the role of the prothoracic gland (PG) in making the major growth hormone ecdysone in flies, two RNA interference (RNAi) screenings were conducted for identifying genes that have roles in development. The genome-wide RNAi screen, which was a collaborative effort with two other labs, found 1,906 lines[98] that showed developmental defects when the RNAi was triggered in the prothoracic gland using *phm22-Gal4*. The secondary RNAi screen, which was done in the King-Jones lab, identified 34 genes that displayed abnormal ring gland phenotype when knocked down specifically in the PG cells. (b) Confocal microscope images of dissected ring glands from 40-42 hours third-instar larvae showing the abnormal ring gland phenotype compared to the control. Big ring gland was dissected from *phm22>Su(var)2-10*-RNAi (v100813) animals; Red ring gland was dissected from *phm22>RanBP3*-RNAi (v104432) animals; Control ring gland was dissected from *phm22>*w^{1118} animals.

Table 3.1 Genes that show abnormal ring glands when knocked down in the PG.

CG Number	Name	Function	Phenotype
CG3260	*zfrp8*	Zinc-finger protein	Big red RG
CG8145	*séance*	Zinc-finger protein	Big red RG
CG5796	*Ppox*	Heme biosynthetic enzyme	Big red RG
CG9972	*spz5*	Growth factor	Big red RG
CG30493	*Coq9*	Ubiquitin biosynthesis	Big red RG
CG33138	*AGBE*	Glycogen biosynthesis	Big red RG
CG32843	*Dh31-R*	G protein-coupled receptor signaling	Big red RG
CG11771	*CG11771*	Peptide metabolic process and proteolysis	Big red RG
CG5910	*CG5910*	Protein kinase-like domain	Big red RG
CG34404	*CG34404*	Usher's syndrome protein 1	Big red RG
CG1818	*Updo*	Heme biosynthetic enzyme	Big red RG
CG7577	*Ppk20*	Sodium ion transport	Big red RG
CG17985	*CG17985*	Peptidoglycan-binding lysin subgroup	Big red RG
CG10531	*Cht9*	Glycoside hydrolase	Big red RG
CG10225	*RanBP3*	Negative regulator of STAT92E	Big red RG
CG13837	*CG13837*	Chitin metabolic pathway	Big red RG
CG11727	*Evi5*	RabGTPase GAP activity	Big red RG

CG2887	*CG2887*	DnaJ domain, chaperon binding	Big red RG
CG10704	*Toe*	Transcription repressor	Big red RG
CG13465	*CG13465*	Unknown	Big red RG
CG18497	*Spen*	Nucleic acid binding	Malformed RG
CG10335	*Pbgs*	Heme biosynthetic enzyme	Big RG
CG7955	*Abcb7*	Heme transporter	Big RG
CG12373	*mRpL18*	Mitochondrial structure protein	Big RG
CG8068	*Su(var)2-10*	Chromatin modifier	Big RG
CG14750	*Vps25*	A member of the ESCRT-II complexes	Big RG
CG7650	*CG7650*	Phototransduction	Big RG
CG10372	*Faf2*	Ubiquitin-dependent ERAD pathway	Big RG
CG10939	*CG10939*	Scaffold protein	Big RG
CG30410	*Rpi*	Age-dependent response to reactive oxygen species	Big RG
CG3017	*Alas*	Heme biosynthetic enzyme	Big RG
CG8211	*IntS2*	snRNA 3'-end processing; neurogenesis	Necrosis RG
CG6222	*su(sable)*	Suppressor of sable	RG with big cells

3.1.2 Molecular mechanism of nuclear protein import

Transport of macromolecules between the nucleus and the cytoplasm occurs predominantly through the nuclear pore complexes (NPCs), which are large proteinaceous channels that perforate the nuclear membrane [99]. Ions or metabolites diffuse freely between the nucleus and cytoplasm through NPCs, as do macromolecules smaller than ~5 nm or ~40 kDa in size. The directionality of the nucleocytoplasmic transport is determined by the Ran gradient across the nuclear membrane. Ran is a member of the Ras family of small GTPases and is crucial for directing nucleocytoplasmic trafficking of macromolecules [100-103]. Although Ran is found throughout a cell, it is predominantly localized in the nucleus in the RanGTP form. The strict compartmentalization of Ran is mainly defined by the Ran regulators, namely the Ran guanine nucleotide exchange factor (RanGEF) and the Ran GTPase-activating protein (RanGAP). Most nuclear Ran is GTP-bound because RanGEF is tethered to the DNA [104, 105]. Conversely, RanGAP is predominantly cytoplasmic, suggesting that the majority of cytoplasmic Ran is GDP-bound. The capability of Ran to shuttle across the nuclear membrane provides directionality to the transport processes. The nuclear import complexes usually form in the cytoplasm, constituting both the cargo and importins. Dissociation of nuclear import cargos occurs upon binding of RanGTP to the importin.

Protein cargo to be imported into the nucleus typically contain a Nuclear Localization Signal (NLS) that directs the nuclear import by binding to soluble transport receptors of the importin family of proteins. The nuclear import process is generally initiated by forming a ternary complex

with importin α, importin β1, and a cargo (Fig. 3.2). While importin β1 acts as a bridge connecting the complex to the NPC followed by the release of the cargo into the nucleus through the binding of Ran-GTP to importin β1, importin α serves as an adaptor that links the nuclear import cargo and importin β1, and more importantly, recognizes NLSs within the cargos [103, 106]. Classical NLSs contain consensus sequences that have been defined, consisting of a single (monopartite NLSs) or two (bipartite NLSs) clusters of basic amino acid residues [107]. To this date, there have been six classes of importin α-dependent NLSs [108] characterized that contain known consensus sequences (Table 3.2). Moreover, specific proteins may harbor signal patches, which are made up of amino acid residues that are distant to one another in the primary sequence, but come close to each other in the tertiary structure of the folded protein. Such signal sequences are difficult to predict compared to monopartite NLSs. It is also likely that a protein without a canonical NLS motif can be nuclear imported by binding to other proteins which nuclear import mechanism has been well characterized.

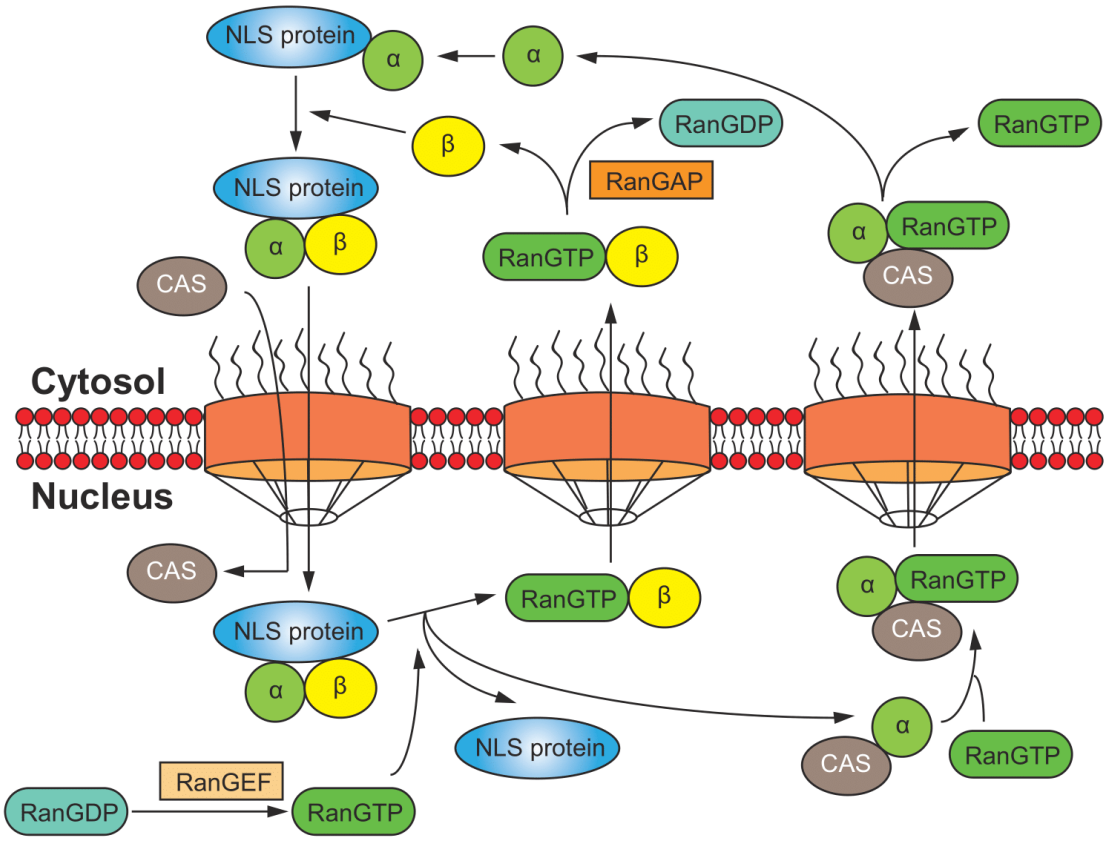

Figure 3.2 Canonical nuclear cargo import pathway.

Importin-α (α) recognizes proteins that contain a nuclear localization signal (NLS) and forms a complex. The complex then binds to importin-β (β), and is translocated through the nuclear pore complex (NPC) into the nucleus. In the nucleus, the high concentration of RanGTP is maintained by RanGEF. The NLS protein is disassociated from the nuclear import complex by RanGTP, while the RanGTP/importin-β complex is recycled back to the cytoplasm through the pore. Nuclear export of importin-α is by binding to both the nuclear export receptor CAS and RanGTP.

Table 3.2 Six classes of importin α-dependent NLSs.

NLS class	Consensus sequence[a]
Class 1	KR(K/R)R or K(K/R)RK
Class 2	(P/R)XXKR(ˆDE)(K/R)
Class 3	KRX(W/F/Y)XXAF
Class 4	(R/P)XXKR(K/R)(ˆDE)
Class 5	LGKR(K/R)(W/F/Y)
Class 6 (Bipartite)	$KRX_{10–12}K(KR)(KR)$ Or $KRX_{10–12}K(KR)X(K/R)$

[a] X, any amino acid; ˆDE, any amino acid except Asp or Glu. X_{10-12}, any 10-12 amino acids.

3.1.3 Nuclear import of Ran is mediated by the transport factor NTF2

The Ran gradient across the nuclear membrane is essential for transporting many proteins and nucleic acids in eukaryotes. Although Ran is small enough to be passively transported into the nucleus, the nuclear import efficiency by itself is considered far too low to sustain the requirement for shuffling of macromolecules through NPCs. Therefore, the cell provides the nuclear transport factor 2 (NTF2) to facilitate Ran transport [102]. In the cytosol, NTF2 acts as a dimer so that two RanGDP molecules can be translocated per cycle. This greatly increases the efficiency of Ran nuclear import. NTF2 also associates with nucleoporins such that it can move back and forth across the nuclear membrane. Once the import complex has entered the nucleus, nucleotide exchange of GDP for GTP catalyzed by RCC1 (the only RanGEF orthologue in *Drosophila*) will trigger the

release of Ran from NTF2. Ran can then cycle back to the cytoplasm where it is converted back to the GTP form by RanGAP, starting the cycle all over again.

Mutational analysis and the X-ray crystal structure of NTF2 revealed that NTF2 interacts with Ran and a subset of nucleoporins such as FxFG repeats at non-overlapping sites [109, 110]. The interaction between NTF2 and nucleoporins is more complex than the Ran-NTF2 association since NTF2 can interact with multiple FxFG repeats located at the internal surface of each NPC [111]. In addition, alternation of the affinity of NTF2 for FxFG nucleoporins could directly affect NTF2 binding to Ran. The tryptophan-7 (W7) residue is one of the potential sites for FxFG binding identified by crystal structure analysis of the rat NTF2 protein. The mutant W7A NTF2 protein, therefore, has a reduced affinity for FxFG nucleoporins. In contrast, the mammalian $NTF2^{N77Y}$ mutant has an increased affinity for nucleoporins. Overexpressing $NTF2^{N77Y}$ strongly blocked the nuclear protein import process, resulting in Ran being concentrated at the nuclear rim[110]. Another mammalian allele, *Ntf-2*^{D23A}, also exhibited a similar phenotype as the mutant $NTF2^{N77Y}$ protein binds to nucleoporins more efficiently and blocks nuclear protein import both *in vitro* and *in vivo*. Collectively, both $NTF2^{N77Y}$ and $NTF2^{D23A}$ are dominant negative mutants of NTF2 with increased binding activity to FxFG nucleoporins in mammals.

In *Drosophila*, NTF2 function is essential for animal development [112, 113]. The *Drosophila Ntf-2* gene was isolated from a P-element enhancer trap line *l(1)G0428* [112]. The P-element was mobilized, which generates several excision strains from the original *l(1)G0428* mutant allele. Depending on the allele, *Ntf-2* mutant animals die between the second larval instar and the pupal

stage. Homozygous *l(1)G0428* mutants die at the late larval stage and show reduced number of ommatidia in the eye. [112]. The eye phenotype in *Ntf-2* mutants is associated with the immune response since three NF-κB/Rel proteins Dorsal, Dif, and Relish, failed to target for nuclear import after infection. *chickadee* (*chic*), encoding *Drosophila* Profilin [114], was identified in a genetic screen for suppressors of *Ntf-2* [113]. $chic^{221}$ null mutant suppresses the small eye phenotype in various *Ntf-2* mutant alleles, therefore providing an interesting link between these two genes. However, whether the *Drosophila* NTF2 has other functions besides controlling eye development and immune response needs to be further investigated.

3.1.4 Mammalian RanBP3 is a cofactor that regulates nuclear export of proteins

Nuclear cargo export is mediated by the association of its nuclear export signal (NES) with chromosome maintenance protein 1 (CRM1) and RanGTP and subsequent transport through the NPC [115, 116]. After the exit from the nucleus, GTP hydrolysis by the RanGTP-activating protein (RanGAP) catalyzes the dissociation of CRM1 from the cargo, thereby the nuclear export cargo is released into the cytoplasm (Fig. 3.3). NES motifs for the transport receptor protein CRM1 are usually leucine-rich, with a consensus sequence of $HX_{2-3}HX_{2-3}HXH$, where H is a hydrophobic amino acid, such as leucine, isoleucine, methionine, phenylalanine, or valine, and X is any amino acid [117, 118]. Similar to nuclear cargo import, proteins exported via CRM1 may not contain a canonical NES, but instead, may have an altered or mismatched nuclear export sequence [119].

In fact, CRM1 usually uses cofactors, such as Ran-binding protein 3 (RanBP3), to facilitate

binding of nuclear export cargoes. Human RanBP3 was identified using the yeast two-hybrid system via Ran-mediated interaction with the nucleotide exchange factor RCC1 [120]. RanBP3 is essential for stabilizing the interaction between the nuclear export substrate and CRM1 [121]. RanBP3 also promotes the interaction between CRM1 and RCC1 in the presence of Ran. The binding of RanBP3 to RCC1 increased the catalytic activity of RCC1 toward Ran, and the stimulation was not affected in the presence of CRM1. A few nuclear export cargos of RanBP3 have been reported, for example, β-catenin [122] and Smad2 and Smad3 protein complex [123], which are key intracellular signal transducers for TGF-β signaling. Post-translational modifications have been shown to regulate the functions of regulators involved in the nuclear transport pathway. For instance, RCC1 is phosphorylated during mitosis by the Cdc2 kinase, which is essential for the proper positioning of RanGTP on mitotic chromosomes and spindle assembly in mammalian cells [124]. RanBP3 phosphorylation is also shown to regulate the Ran gradient by inhibiting the RCC1 activity [125]. However, whether phosphorylated RanBP3 could affect the nuclear export pathway in *Drosophila* is unknown and needs to be further investigated.

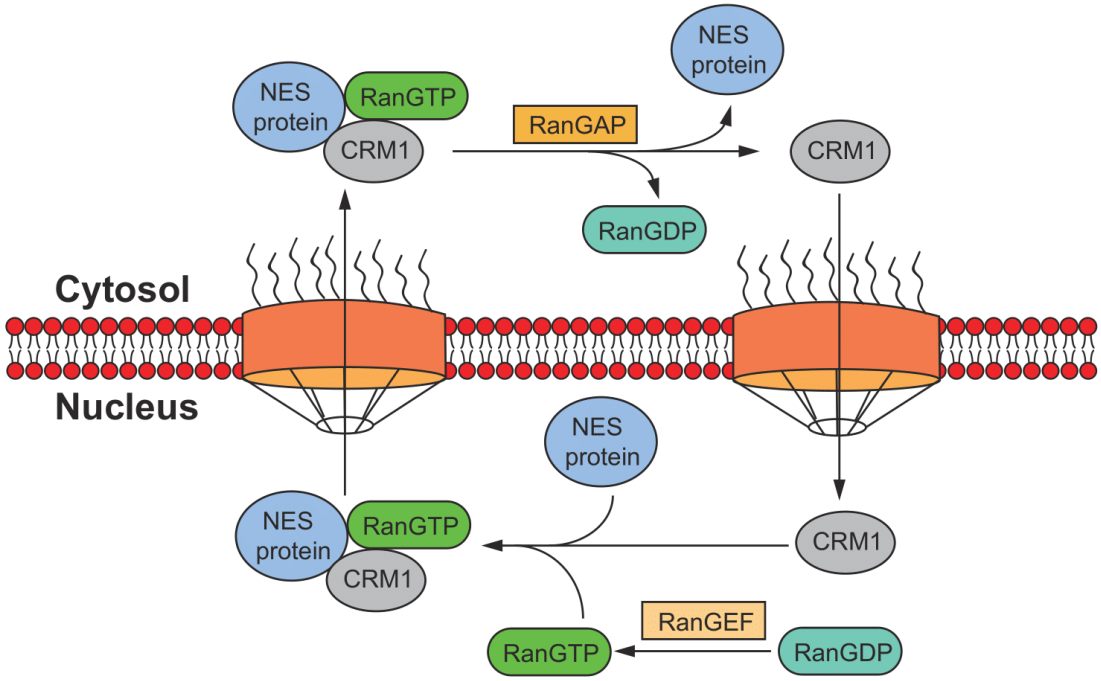

Figure 3.3 Canonical nuclear cargo export pathway.

Cargos that contain a nuclear export signal (NES) bind to CRM1 and RanGTP before they are exported out of the nucleus. The GTP hydrolysis in the cytosol is catalyzed by RanGAP, which promotes complex dissociation. CRM1 is recycled back to the nucleus where it binds to NES-containing protein cargo and RanGTP to start the nuclear export process over again.

3.1.5 Comparing *Drosophila* RanBP3 to its mammalian orthologs

Due to alternative splicing, *RanBP3* is transcribed into two unique mRNAs (*RanBP3-RA* and *RanBP3-RB*) (Fig. 3.4). Specifically, RanBP3b (isoform B) lacks a glutamic acid (E) which is present in isoform A. *Drosophila* RanBP3 protein sequence was aligned with both the human and mouse RanBP3 for comparing functional domains and motifs (Fig. 3.4c & 3.5). *Drosophila* RanBP3 contains all the functional domains and motifs, showing a 45% similarity to human and mouse RanBP3. Specifically, Ran-binding domain 1 (RanBD1) is the functional domain essential for recognizing nuclear export cargos [120]. The Phe-Gly sequence motif (FG motif) is commonly found in nuclear pore proteins and is vital to nuclear transport [126, 127]. In mammals, RanBP3 is localized to the nucleus due to the presence of N-terminal Nuclear Localization Signals (NLS). However, unlike the mammalian RanBP3, *Drosophila* RanBP3 does not have an N-terminal NLS sequence. Instead, I identified a putative NLS motif (designated as NLS*, RAQKRKYEEV) within the RanBD1 domain using the online prediction tool "cNLS Mapper" (http://nls-mapper.iab.keio.ac.jp/cgi-bin/NLS_Mapper_form.cgi).

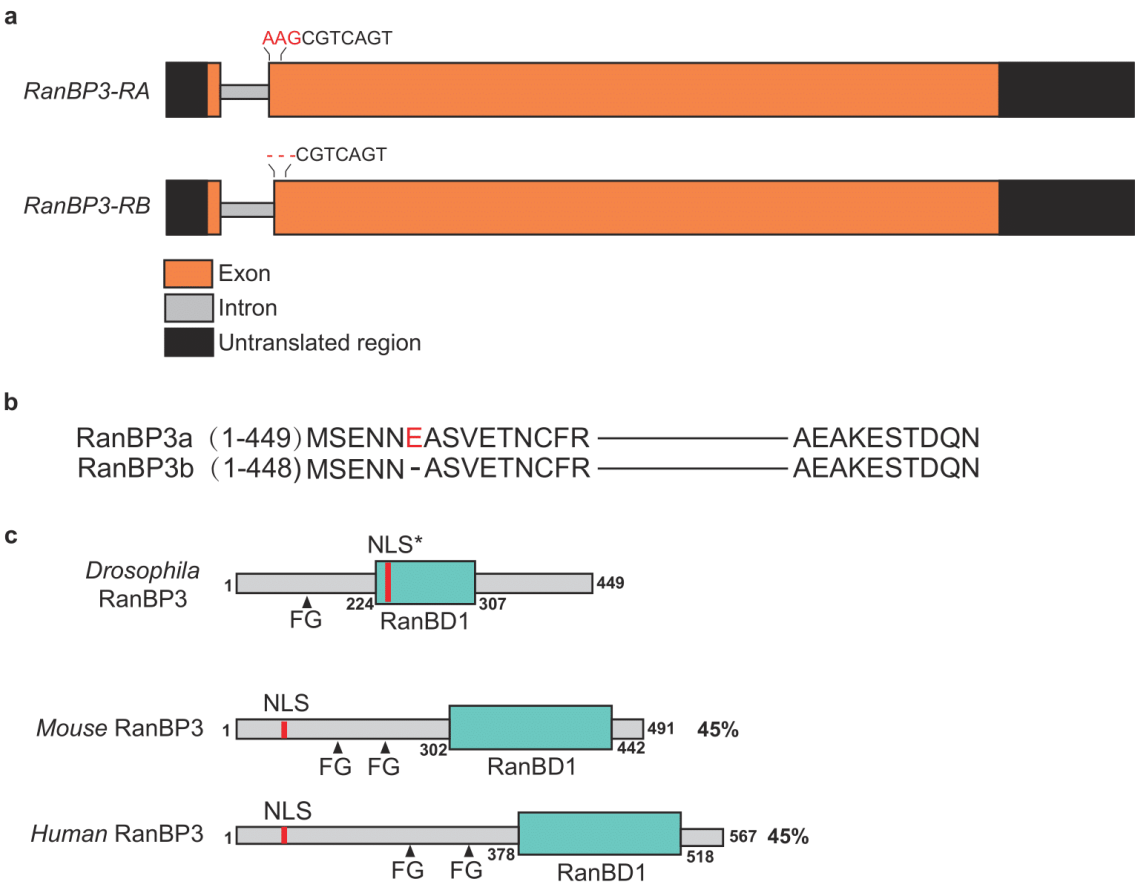

Figure 3.4 Schematic demonstration of the main functional domains of RanBP3.

(a) *Drosophila* RanBP3 has two alternatively spliced mRNAs that differ in three nucleotides. (b) Comparing the coding regions of RanBP3 isoform A and B. RanBP3a encodes a glutamic acid (E), which is absent from RanBP3b. (c) A comparison between the functional domains of mammalian and *Drosophila* RanBP3 proteins. *Drosophila* RanBP3 contains the same functional domain and motif as in mouse and human RanBP3. The Ran-binding domain (RanBD1) is involved in the binding of Ran, a Ras-related GTPase. The binding of RanBP3 to RanGTP increases the rate of

RanGAP-induced GTP hydrolysis. FxFG-type sequence motif is the characteristic of a subgroup of nucleoporins and was found in RanBP3 proteins. The FG tandem sequence repeats are based on hydrophobic Phe-rich cores separated by hydrophilic linkers, which are highly conserved and are based on FG, GLFG, or FxFG (where x is usually a small residue such as Ser, Gly, or Ala). The major difference between the *Drosophila* RanBP3 and mammalian RanBP3 proteins is that the nuclear localization signal (NLS*) that is predicted by "cNLS mapper" tool, is located in the RanBD1 domain within the fly ortholog. The numbers to the right of each protein represent the percent similarity of the entire protein sequence to that of the *Drosophila* RanBP3 protein.

Figure 3.5 Sequence alignment of *Drosophila* RanBP3 to mammalian counterpart proteins.

Fly RanBP3a sequence was compared to mouse and human RanBP3 proteins using the "Clustal

Omega" web tool. An asterisk indicates positions that have a single, fully conserved residue. A colon indicates conservation between groups of strongly similar properties. A period indicates conservation between amino acids with weakly similar properties. RanBD1 domain in *Drosophila* was highlighted in yellow, whereas mouse and human proteins were highlighted in green and light blue, respectively. FxFG motif was labeled pink, where x is usually a small residue such as Ser, Gly, or Ala. Nuclear localization signals (NLSs) in RanBP3 proteins were highlighted in purple.

3.1.6 Mitochondrial iron import and its role in *Drosophila melanogaster*

Essential steps in heme biosynthesis and iron-sulfur cluster (ISC) biogenesis occur in the mitochondria, making these organelles indispensable for cellular iron metabolism. In this section, I will briefly introduce key players and concepts involved in the transport of cytosolic iron into mitochondria.

Cytosolic iron may be imported into the mitochondria by one or more of the following mechanisms: (i) a “kiss-and-run” mechanism [128], which involves the direct contact of endosome with the mitochondrion; (ii) direct iron uptake from the labile iron pool (LIP) [129, 130]; (iii) the donation of cytosolic “chelator-inaccessible” iron to the mitochondrion by protein-protein interactions [131]. The only known mitochondrial iron transporter in eukaryotes is mitoferrin (Mfrn), which is a member of the mitochondrial carrier family (MCF). The metal traverses through both mitochondrial membranes to the matrix, where enzymes insert ferrous iron into intermediates,

such as protoporphyrin IX, to synthesize heme or other iron-containing proteins. Yeast *mfrn* orthologues, *MRS3* and *MRS4*, play essential roles in mitochondrial iron import [132]. Disruption of *MRS3* and *MRS4* causes defects in ISC biogenesis and cellular iron metabolism. Although not conserved in other MCF proteins, three highly conserved histidine residues located in regions of the transmembrane helices H1, H2 and H5, are important for *MRS3* function [133]. The zebrafish *mfrn* mutant is rescuable by murine *mfrn*, and zebrafish *mfrn* complements the yeast mutant [134], suggesting that the mitoferrin genes are highly conserved. In mammalian cells, *mfrn1* and *mfrn2* encode two highly similar proteins, which regulate mitochondrial iron levels [135]. Genetic analyses showed that expression of either mouse or zebrafish Mfrn1 could correct the hemoglobin deficiency in zebrafish *mfrn* mutants. However, the ectopic expression of Mfrn2 in cells that have low levels of Mfrn1 cannot support normal hemoglobinization. This could be possible because Mfrn2 does not accumulate in developing red blood cells or other cells, whereas Mfrn1 has a longer protein half-life and therefore accumulates in the mitochondria of developing red blood cells [135].

Drosophila mitoferrin (*dmfrn*) is orthologous to human *mfrn1* (*SLC25A37*). Overexpression of *dmfrn* in the *Drosophila* l(2)mbn cell line decreases cellular iron content by increasing *Fer1HCH* (*Ferritin heavy chain homologue*) transcript and protein levels [136]. P-element insertion in the 5' UTR of *dmfrn* confers $dmfrn^{SH115}$ mutants, resulting in male sterility [137]. Iron loading of $dmfrn^{SH115}$ flies is insufficient to provide enough iron for a low-affinity transporter to restore spermatogenesis. *Drosophila* mitoferrin is also implicated in a *Drosophila* model of Friedreich's ataxia (FRDA), the most common recessive ataxia in the Caucasian population [138]. Genetic

suppression of *dmfrn* counteracts the iron-loading effect induced by loss of frataxin function. Furthermore, *dmfrn* mutants show growth defects under low iron conditions, either by iron chelator BPS-mediated iron depletion or when ferritin function is partially compromised [139]. The mutant phenotype is partially rescued by increasing the 20-hydroxyecdysone (20E) concentrations in the diet, suggesting that sufficient mitochondrial iron supply is required for ecdysone biosynthesis in the prothoracic gland, as well as the normal development of the fruit fly.

3.1.7 ER-mitochondria contacts are required for cellular iron homeostasis

The compartmentalization of eukaryotic cells vastly increases the efficiency of biochemical reactions by concentrating biomolecules and confines toxic metabolites for protecting the rest of the cell. This also creates the need for communication between different organelles. The largest membrane system within a cell is the endoplasmic reticulum (ER). The ER is not an isolated structure. Instead, it has diverse contacts with many other cytosolic organelles, including the nucleus, mitochondria, Golgi, peroxisomes, endosomes, lysosomes, and lipid droplets [140, 141]. The ER provides a site for synthesizing both secreted and membrane-bound proteins and is responsible for their intracellular translocation. It is also a crucial site for storing Ca^{2+} and many biosynthetic enzymes involved in lipid metabolism. The best-characterized organelle contact sites are those between the ER and mitochondria. Contact sites are defined as regions where two membranes are closely apposed but not fused, and thus the organelles each maintain their identities. The protein complex that physically tethers the two organelles and creates a physical base for

communication is named the ER-mitochondria encounter structure (ERMES). Four core proteins constitute the ERMES, including the ER membrane protein maintenance of mitochondrial morphology protein 1 (Mmm1p), mitochondrial distribution and morphology protein 10 and 34 (Mdm10p and Mdm34p, both mitochondrial outer membrane proteins), and cytosolic protein Mdm12p [142]. ERMES-mediated ER-mitochondrial junction has been implicated in lipid exchange, protein import into the mitochondria, mitochondrial morphology and genome maintenance. Disruption of ERMEs induces iron deficiency and leads to iron accumulation in the cell and mitochondria [143]. Genetic ablation of the iron regulatory system exacerbates the respiration defect caused by ERMES deficiency. Altogether, the ER-mitochondrial junctions are essential for cellular iron homeostasis.

3.2 Modified materials and methods

3.2.1 *Drosophila* stocks and husbandry

The following *Drosophila* stocks were obtained from Bloomington *Drosophila* Stock Center (BDSC): w^{1118} (#3605), *Tubulin-Gal4/TM3, Ser.GFP* (#5138), *UAS-EGFP* (#5431), *Vas.Cas9* (#51323), $RanBP3^{TRiP.HMS02196}$ (#40948), $UAS\text{-}hTfR^{WT}.GFP$ (#36858). We obtained $UAS\text{-}RanBP3^{kk108741}$ (v104432) and $UAS\text{-}RanBP3^{GD6906}$ (v38363) from Vienna *Drosophila* Resource Center (VDRC). The *RanBP3-gRNA* line ($RanBP3^{gR}$) was generated to use in conjunction with Cas9 for tissue-specific gene editing. Transgenic flies were generated based on the ψC31 integrase method. $y^1w^*P[nos\text{-}PhiC31]X;\ P[\{carryP\}]\ attP40(II)$ and $y^1w^*P[nos\text{-}PhiC31]X;\ P[\{carryP\}]$

attP2(III) were gifts from BestGene Inc. *phm22-Gal4* was a kind gift from Dr. Michael O'Connor. Stocks were maintained on the standard agar cornmeal-based food at 25°C unless further specified.

3.2.2 Generation of CRISPR/Cas9 and transgenic fly lines

Two independent databases were used to find suitable target sites for the CRISPR/Cas9 gRNA construct, which are "DRSC find CRISPRs" from Harvard Medical School (https://www.flyrnai.org/crispr/) and "CRISPR Optimal Target Finder" from University of Wisconsin (http://tools.flycrispr.molbio.wisc.edu/targetFinder/index.php). gRNA target sites were PCR-amplified from the genome of *Vas.Cas9* (Bloomington #51323) flies and verified by sequencing. Two gRNA target sites were cloned into the pCFD5 (Addgene #73914) vector to make the recombinant plasmid. A total of 100 ng gRNA construct containing two gRNA target sites was injected into *Vas.Cas9* germline cells followed by screening for the marker. The injection was performed by GenetiVision Corporation following standard procedures.

To make transgenic *RanBP3* lines, *RanBP3* isoform A CDS was PCR-amplified from the *RanBP3* cDNA clone (LD02979) obtained from *Drosophila* Genomics Resource Center. While the 3xFlag tag was amplified from pAFW, the 2xHA tag was acquired from the pAHW vector. More information about these two vectors is available at: https://emb.carnegiescience.edu/drosophila-gateway-vector-collection. The *RanBP3* CDS and epitope tag sequence were recombined into the pUASTattB vector (GenBank EF362409). The final recombination construct was injected into y^1*w*P[{nos-PhiC31/int.NLS}]X; P[{carryP}] attP2(III)* (#25710). Embryo injection was

performed at the University of Alberta following standard procedures[144]. Approximately 300-500 embryos were injected per construct. Surviving adults were backcrossed to w^{1118} and used to generate independent lines.

3.2.3 Generating constructs for S2 cell transfection

cDNA clones of *RanBP3* (LD02979), *Ran* (LD32416), *Ntf-2* (GM08921), *chickadee* (LD19369), *CRM1* (LD45806), *RCC1* (LD22520) and *IRP1A* (LD36361) were obtained from *Drosophila* Genomics Resource Center (DGRC). cDNA sequences of *EGFP*, *Gp93*, *ERp60*, *Mfrn*, and *Fer1HCH* were obtained by PCR amplification using a reverse-transcribed cDNA library from w^{1118} whole larvae. The cDNA was subcloned into the pAFW plasmid that carries the 3xFlag epitope tag to generate plasmids encoding N-terminal tagged proteins. Similarly, pAMW and pAHW vectors were used to make N-terminal 6xMyc and 3xHA tagged proteins, respectively. Detailed information about the vector collection is available at https://emb.carnegiescience.edu/drosophila-gateway-vector-collection. The generation of C-terminal tagged recombinant plasmids took a few more steps: First, two EGFP recombinant plasmids carrying either C-terminal 3xFlag (designated as EGFP-3CF) or 4xMyc tag (designated as EGFP-4CM) were made by inserting the *EGFP* cDNA into the Ac5-STABLE2-Neo (Addgene # 32426) backbone amplified by PCR. Next, the whole plasmid backbone that carries either C-terminal 3xFlag or 4xMyc tag was amplified using PCR. Lastly, the cDNA fragment with a short overlap region with the backbone was recombined with the plasmid backbone in a Gibson assembly

reaction. All the PCR products were purified by using the QIAquick Gel Extraction Kit (Qiagen #28704) following standard procedures.

Mutations were introduced using the robust Q5 high-fidelity DNA polymerase (NEB, M0491S) and custom mutagenic primers. For substitution mutations, desired nucleotide changes were placed in the center of the forward primer, including at least ten complementary nucleotides on the 3'-side of the mutation. The reverse primer went in the opposite direction so that the 5'-ends of the two primers could anneal back-to-back. Deletion mutations were created by designing standard, non-mutagenic forward and reverse primers that flank the region targeted for deletion. Small insertions (less than or equal to 6 nucleotides) were incorporated into the 5'-end of the forward primer, while the reverse primer was annealed back-to-back with the 5'-end of the overlap region of the forward primer. Upon the PCR fragments were obtained, the blunt end fragment was re-ligated using T4 polynucleotide kinase (NEB M0201S) and T4 DNA ligase (NEB M0202S). The template plasmid leftover was removed by adding the DpnI restriction enzyme (ThermoFisher FD1703) in the same ligation reaction. The newly generated recombinant mutant plasmid was transformed into *E. coli* competent cells followed by plasmid extraction and DNA sequencing. A list of constructs made for transfection of S2 cells is shown in Table 3.3. Primer sequences are provided in Table 3.4.

Table 3.3 A list of plasmids used for S2 cell transfection in chapter 3.

Plasmid name	Features
Ac5-STABL2-Neo	Vector used to generate plasmids encoding C-terminal epitope-tagged proteins
pAFW	Vector used to generate plasmids encoding N-terminal Flag-tagged proteins
pAMW	Vector used to generate plasmids encoding N-terminal Myc-tagged proteins
EGFP-3CF	Expresses C-terminal 3xFlag-tagged EGFP
EGFP-4CM	Expresses C-terminal 4xMyc-tagged EGFP
Ac5-RanBP3a-4CM	Expresses C-terminal 4xMyc-tagged RanBP3 isoform a
Ac5-RanBP3b-4CM	Expresses C-terminal 4xMyc-tagged RanBP3 isoform b
Ac5-RanBP3a-3CF	Expresses C-terminal 3xFlag-tagged RanBP3 isoform a
Ac5-RanBP3b-3CF	Expresses C-terminal 3xFlag-tagged RanBP3 isoform b
Ac5-RanBP3a-ΔNLS-4CM	Expresses C-terminal 4xMyc-tagged RanBP3 isoform a without the nuclear localization signal (NLS)
Ac5-RanBP3b-ΔNLS-4CM	Expresses C-terminal 4xMyc-tagged RanBP3 isoform b without the nuclear localization signal (NLS)
Ac5-RanBP3a-ΔRBD-4CM	Expresses C-terminal 4xMyc-tagged RanBP3 isoform a

	without the Ran-binding domain 1 (RBD)
Ac5-RanBP3b-ΔRBD-4CM	Expresses C-terminal 4xMyc-tagged RanBP3 isoform b without the Ran-binding domain 1 (RBD)
Ac5-RanBP3a^{TripleE}-4CM	Expresses C-terminal 4xMyc-tagged RanBP3 isoform a that contains an "NEA to EEE" amino acid change.
Ac5-RanBP3a$^{\Delta RBD\text{-}TripleE}$-4CM	Expresses C-terminal 4xMyc-tagged RanBP3 isoform a that deletes the Ran-binding domain 1 (RBD) and contains the "NEA to EEE" amino acid change.
pAFW-Ran	Expresses N-terminal 3xFlag-tagged Ran
pAMW-Ran	Expresses N-terminal 6xMyc-tagged Ran
pAMW-NTF2	Expresses N-terminal 6xMyc-tagged NTF2
pAMW-NTF2^{D23A}	Expresses N-terminal 6xMyc-tagged NTF2 that harbors an aspartic acid (D) to alanine (A) change at residue 23.
pAMW-NTF2^{D81A}	Expresses N-terminal 6xMyc-tagged NTF2 that harbors an aspartic acid (D) to alanine (A) change at residue 81.
pAMW-NTF2^{2D2A}	Expresses N-terminal 6xMyc-tagged NTF2 that harbors both D23A and D81A mutations.
pAFW-IRP1A^{WT}	Expresses N-terminal 3xFlag-tagged wild-type IRP1A
pAFW-IRP1A^{C450S}	Expresses N-terminal 3xFlag-tagged IRP1A^{C450S} that is

	constitutively RNA-binding
pAFW-IRP1A^{3R3Q}	Expresses N-terminal 3xFlag-tagged IRP1A^{3R3Q} that abolishes the RNA-binding ability
pAMW-IRP1A^{WT}	Expresses N-terminal 6xMyc-tagged wild-type IRP1A
pAMW-IRP1A^{C450S}	Expresses N-terminal 6xMyc -tagged IRP1A^{C450S} that is constitutively RNA-binding
pAMW-IRP1A^{3R3Q}	Expresses N-terminal 6xMyc-tagged IRP1A^{3R3Q} that abolishes the RNA-binding ability
Ac5-Chic-3CF	Expresses C-terminal 3xFlag-tagged Chickadee
Ac5-Chic-4CM	Expresses C-terminal 4xMyc-tagged Chickadee
Ac5-RCC1-4CM	Expresses C-terminal 4xMyc-tagged RCC1
Ac5-CRM1-3CF	Expresses C-terminal 3xFlag-tagged CRM1
Ac5-Gp93-3CF	Expresses C-terminal 3xFlag-tagged glycoprotein 93
Ac5-Gp93$^{\Delta SS}$-3CF	Expresses C-terminal 3xFlag-tagged Gp93 without the secretion signal (SS)
Ac5-Gp93$^{\Delta HATPase}$-3CF	Expresses C-terminal 3xFlag-tagged Gp93 in which the HATPase domain is removed
Ac5-Gp93$^{\Delta Hsp90}$-3CF	Expresses C-terminal 3xFlag-tagged Gp93 in which the Hsp90 domain is removed

Ac5-ERp60-4CM	Expresses C-terminal 4xMyc-tagged ERp60
Ac5-Mfrn-3CF	Expresses C-terminal 3xFlag-tagged mitoferrin
Ac5-Mfrn-4CM	Expresses C-terminal 4xMyc-tagged mitoferrin
Ac5-Fer1HCH-4CM	Expresses C-terminal 4xMyc-tagged ferritin 1 heavy chain homologue

Table 3.4 Primers used to generate constructs in chapter 3.

Primer name	**Sequence (5' to 3')**
Generation of *RanBP3* somatic CRISPR gRNA line	
RanBP3 gRNA FP	TTCGATTCCCGGCCGATGCACTTAAGGGGCGACTCGCGC GGTTTTAGAGCTAGAAATAGC
RanBP3 gRNA RP	CTATTTCTAGCTCTAAAACTTAGTCGTAGGGACTTTTGGT GCACCAGCCGGGAATCGAAC
Generation of N-terminal epitope-tagged protein backbones	
pAFW BB attB1 F	AATGCAGGCAACTCGTGAAAGGTAGGCGGATC
pAFW attB1 R	AGCCTGCTTTTTTGTACAAACTTGATACCGGTGCTTGTCA TCGTCATCC
pAFW attB2 F	GCCCAGCTTTCTTGTACAAAGTGGGGACGTAAGCTAGCA GGATCTTTGTGAAG
pAMW BB attB1 F	TCACATGTTCTTTCC TGCGTTATC
pAMW attB1 R	AGCCTGCTTTTTTGTACAAACTTGATACCGGTGATTCAAG TCCTC
pAMW BB attB2 F	GCCCAGCTTTCTTGTACAAAGTGGGGACGTAAGCTAGCA GGATC
pAMW attB2 R	GGAAAGAACATGTGAGCAAAAG
Generation of C-terminal epitope-tagged protein backbones	
3Flag BB1 F	GGAATTCGAGCGGGCCACCATGGCC
3Flag BB2 R	GGCGACTACAAAGACCATGACGGTG
4Myc BB1 F	CACATTTCCCCGAAAAGTGCCACCTGACGTCTAAGAA
4Myc BB1 R	GGCCATGGTGGCGAATTCCACCACACTGG
4Myc BB2 F	ATCAGAAGCTCCGCCACCATGGAGCAAAAGC
4Myc BB2 R	GCACTTTTCGGGGAAATGTGCGCGGAACCCCTATTTG

Generation of cDNA fragments	
attB1 IRP1A F	CAAAAAAGCAGGCTTCCGGCTCCG
attB2 IRP1A R	AGAAAGCTGGGCTAATCCAGCATTTTGCG
IRP1A C450S SDM F	ATCACCTCGAGCACGAACACTTC
IRP1A C450S SDM R	GGCGGCAATCACAAAGATC
IRP1A R549Q SDM F	CGGGCAATCAGAATTTCGAG
IRP1AR549Q SDM R	ACAGGACGCCACAGCAAAC
IRP1A R554Q SDM F	ATACTAGGGCCAATTATCTGGCCAG
IRP1AR554Q SDM R	TGGGATGGATCTGACCCTC
IRP1A R793Q SDM F	TGGCAGCTCACAGGATTGGGCCGCCAAG
IRP1AR793Q SDM R	CTGCCGTAGTCCTTGCCTAC
attB1 RanBP3 F	TCAAGTTTGTACAAAAAAGCAGGCTTCTGAAAATAATGAAGCGTCAGTCGAAACTAACTG
attB2 RanBP3 R	CCCACTTTGTACAAGAAAGCTGGGTTTAATTCTGATCGGTTGACTCCTTGGC
EGFP C uni F	GCCACCATGGCCATGGTGAGCAAGGGCGAG
EGFP C 4Myc R	GGCGGAGCTTCTGATCTTGTACAGCTCGTCCATG
EGFP C 3Flag R	TGGTCTTTGTAGTCGCCCTTGTACAGCTCGTCCATG
RanBP3 PA F	GCCACCATGGCCATGTCTGAAAATAATGAAGCGTCAGTCG
RanBP3 PB F	GCCACCATGGCCATGTCTGAAAATAATGCGTCAGTCG
RanBP3 C-4MYC R	TGGCGGAGCTTCTGATATTCTGATCGGTTGACTCCTTGG
RanBP3 C-3Flag R	CATGGTCTTTGTAGTCGCCATTCTGATCGGTTGACTCCTTGG
RanBP3 SDM ΔNLS F	GAGACCTTCACCGGCGAGGAGGAC
RanBP3SDM ΔNLS R	GCTCTCCTCATACTCCCGGGCCAC

RanBP3 SDM ΔRBD F	GTGGCGGAGCGAGCCAGCCAAAAGTC
RanBP3 SDM ΔRBD R	CCGGGCCACATCCGTCAGGCTC
RanBP3 SDM TripleE F	CTGAAAATGAAGAAGAGTCAGTCGAAACTAACTG
RanBP3 SDM TripleE R	ACATGGCCATGGTGGCGAATTC
attB1 Ran F	TCAAGTTTGTACAAAAAAGCAGGCTATGGCTCAGGAAGGTCAGGATATACC
attB2 Ran R	ACTTTGTACAAGAAAGCTGGGCTTATAGCTCCTCGTCCTCGTCGG
attB1 NTF2 F	CAAAAAAGCAGGCTATGTCGCTGAATCCGCAGTACG
attB2 NTF2 R	AGAAAGCTGGGCTAGGCAGAGTTGTGGATGTTGAGACG
NTF2 SDM D23A F	ATGCGATATTCGATGCCCCGGCGAATCG
NTF2 SDM D23A R	AGTACTGCTGCACAAATCCCTTGCCAATG
NTF2 SDM D81A F	AGCCAACTTTCGCTGGCGGAGTTCTGATC
NTF2 SDM D81A R	GCGAGTCCACTGTGGTTATCACTCTGG
Chic C-3Flag F	CGCCACCATGGCCATGAGCTGGCAAGATTATGTGGACAAC
Chic C-3Flag R	TGGTCTTTGTAGTCGCCGTACCCGCAAGTAATCAGATAATCTCCAAG
Chic C-4Myc R	TGGCGGAGCTTCTGATGTACCCGCAAGTAATCAGATAATCTCC
CRM1 C-3Flag F	CGCCACCATGGCCATGGCGACAATGTTGACATCG
CRM1 C-3Flag R	TGGTCTTTGTAGTCGCCTTCGTCCTGCATATCCTCG
RCC1 C-4Myc F	CGCCACCATGGCCATGCCGCGCAGAAAGGC
RCC1 C-4Myc R	GGCGGAGCTTCTGATTGTCTTTTTACCGCCCCGCTTG
Gp93 C-3Flag F	CGCCACCATGGCCATGAAGTACTTTTTGCTGGTGGGCCTG
Gp93 C-3Flag R	TGGTCTTTGTAGTCGCCCAGCTCGTCGTGCTGCTG

Gp93 SDM ΔSS F	GATGACGAGGCCGCCACAACGGAG
Gp93 SDM ΔHATpase F	GCCCAGGACTTCCTGGAGG
Gp93 SDM ΔHATpase R	GCGGTAAAGCGAGTTGATAATCAGC
Gp93 SDM ΔHsp90 F	GGCAGCCAGGAGAGCGGCAAC
Gp93 SDM ΔHsp90 R	CTGGGCTTCTTCCTTCAGATACAGCGAGATCACGGATC
ERp60 C-4Myc F	CGCCACCATGGCCATGATGTGGCGCCTTGCTG
ERp60 C-4Myc R	TGGCGGAGCTTCTGATGAGCTCGGTCTTCTTGGGCTTG
Mfrn uni F	CGCCACCATGGCCATGAACATCGACGACTACGAATCG
Mfrn C-4Myc R	GGCGGAGCTTCTGATCGTGCTGAAGCCCCGCTC
Mfrn C-3Flag R	TGGTCTTTGTAGTCGCCCGTGCTGAAGCCCCGCTC
Fer1HCH uni F	CGCCACCATGGCCATGGTGAAACTAATTGCTAGCCTGCTC
Fer1HCH C-4Myc R	TGGCGGAGCTTCTGATCAGGGTCTTGTCGAACAGGAAC

3.3 Results

3.3.1 Losing *RanBP3* function blocked larval development and induced a porphyria-like phenotype in the *Drosophila* PG

Knocking down *RanBP3* ubiquitously by crossing the *RanBP3*-RNAi (v104432, designated as $RanBP3^{IR}$) with the ubiquitous *Tubulin-Gal4* driver (*Tub-Gal4*) completely blocked the larval-to-pupal transition (Fig. 3.6a). The resulting animals kept feeding and eventually died as third-instar larvae (Fig. 3.6b). This result suggested that RanBP3 is required for normal larval development in flies. A weak red-autofluorescence was also observed in PG cells of these ubiquitously *RanBP3* loss-of-function animals when larvae were exposed under UV light (Fig. 3.6c). Interestingly, knocking down *RanBP3* specifically in PG cells by using the *phm22-Gal4* driver induced a much stronger porphyria-like phenotype compared to the ubiquitous knockdown (Fig. 3.6c). However, only one out of four RNAi lines examined (Fig. 3.7a) induced both the lethality and the red auto-fluorescing ring gland phenotype. To examine if the *RanBP3*-RNAi phenotypes were induced by off-target effects, I sought to validate the RNAi phenotype using an independent loss-of-function approach. To do so, I generated a *RanBP3* gRNA line ($RanBP3^{gR}$ flies), therefore, would express two gRNAs that target the second exon of *RanBP3* mRNA under the control of a ubiquitous promoter *U6:3* (Fig. 3.7b). Crossing $RanBP3^{gR}$ flies to flies expressing PG-specific Cas9 (Spok-Cas9) should impair RanBP3 function only in PG cells but not anywhere else. This approach allows a fast examination of loss-of-function phenotypes in multiple tissues if

different tissue-specific Cas9 lines are used. As a result, the red auto-fluorescence was recapitulated in PG cells of *Spok-Cas9*; *RanBP3*^{gR} larvae (Fig. 3.6d). However, it should be noted that the conditional *RanBP3* knockout PG cells showed a weaker porphyria-like phenotype compared to the RNAi line (Fig. 3.6e). It is plausible that the weaker phenotype was resulted from a low gene editing efficiency induced by inefficient cleavage of double-stranded DNA by Cas9. To test the genome editing efficiency of CRISPR/Cas9, I extracted genomic DNA from dissected ring glands of *PG-Cas9*> *RanBP3*^{gR} larvae, followed by cloning and sequencing to see if CRISPR/Cas9 induced gene editing as I expected, and what kind of mutations this CRISPR line had caused (Fig. 3.8a). It turned out that the majority of the sequenced PG cells had small indels less than ten base pairs (bp) (Fig. 3.8b). Occasionally, small inserts were found in the target gRNA site. This result was consistent with the previous idea explaining the weak phenotype induced by the conditional CRISPR/Cas9 approach. Nevertheless, I verified that the porphyria-like phenotype induced by PG-specific *RanBP3*-RNAi was not caused by an off-target effect but only by losing *RanBP3* function in the prothoracic gland, consistent with the previous idea that *RanBP3* might be a novel regulator of heme biosynthesis.

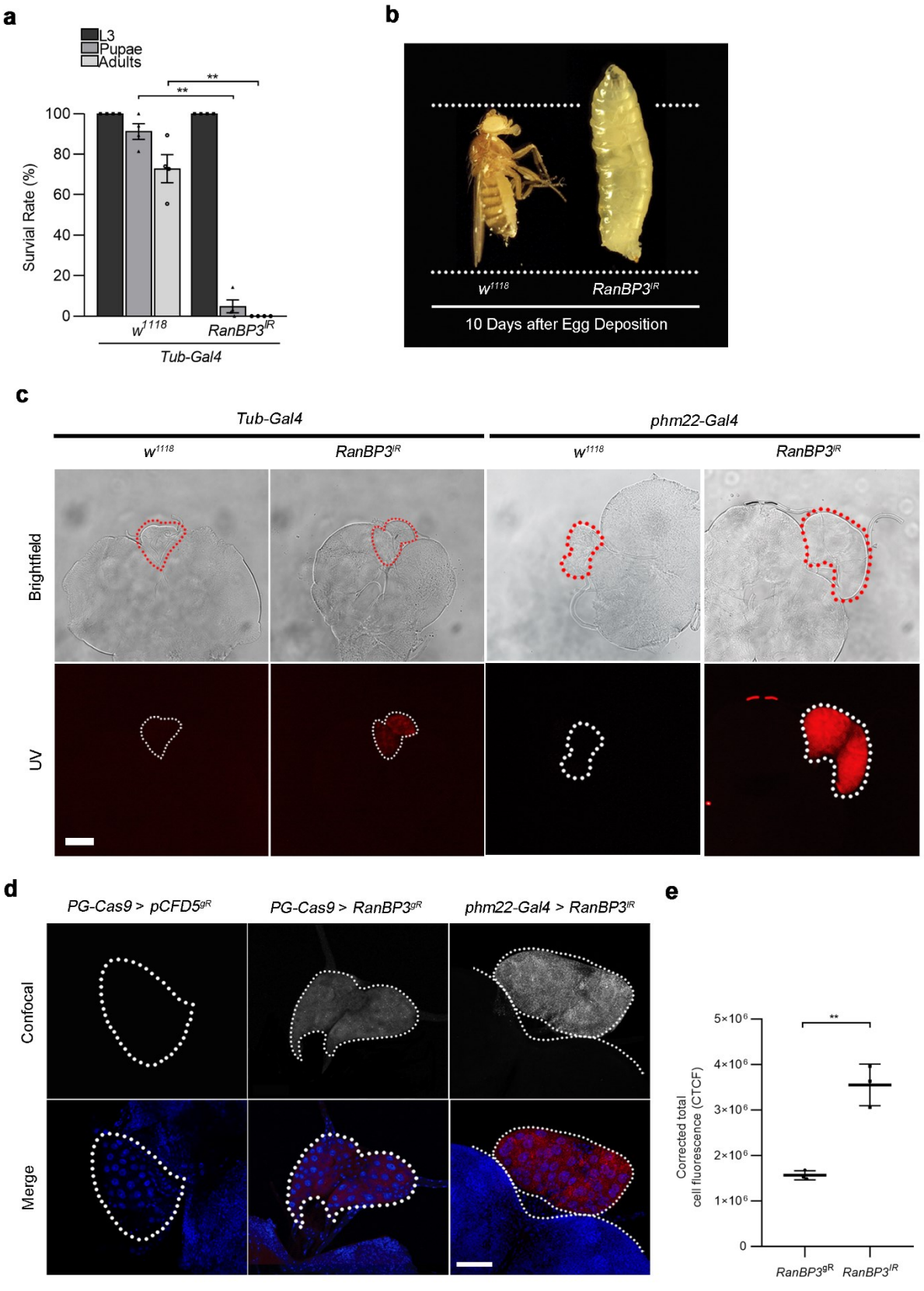
a
L3
Pupae
Adults
**
**
Survial Rate (%)
100
80
60
40
20
0
w1118
RanBP3IR
Tub-Gal4
b
w1118
RanBP3IR
10 Days after Egg Deposition
c
Tub-Gal4
phm22-Gal4
w1118
RanBP3IR
w1118
RanBP3IR
Brightfield
UV
d
PG-Cas9 > pCFD5gR
PG-Cas9 > RanBP3gR
phm22-Gal4 > RanBP3IR
Confocal
Merge
e
**
Corrected total cell fluorescence (CTCF)
5×10^6
4×10^6
3×10^6
2×10^6
1×10^6
0
RanBP3gR
RanBP3IR

Figure 3.6 *RanBP3* depletion blocked larval development and induced a porphyria-like phenotype in PG cells.

(a) Survival of *RanBP3* ubiquitous knockdown animals. *Tubulin-Gal4* (*Tub-Gal4*) was used to drive *RanBP3*-RNAi (VDRC v104432, designated as $RanBP3^{IR}$) expression in the whole body. Error bars represent standard deviation. ***$p < 0.001$, **$p < 0.01$, *$p < 0.05$. (b) Development of *Tub-Gal4>*$RanBP3^{IR}$ animals ten days after egg deposition. (c) Confocal microscope image of *RanBP3* loss-of-function ring glands dissected from 40-42 hours third-instar larvae. *Tub-Gal4* was used to induce transgene expression in the whole body, whereas *phm22-Gal4* was a PG-specific driver. (d) Confocal microscope image of dissected ring glands from conditional *RanBP3* knockout animals. The *RanBP3* gRNA line ($RanBP3^{gR}$) was crossed to a PG-specific Cas9 line (Spok-Cas9) to induce tissue-specific gene knockout. *pCFD5* was used as a control which contains no target sequence but only an empty vector used to generate the *RanBP3* gRNA construct. (e) Quantification of fluorescence intensity within the *RanBP3* conditional knockout ring gland using ImageJ.

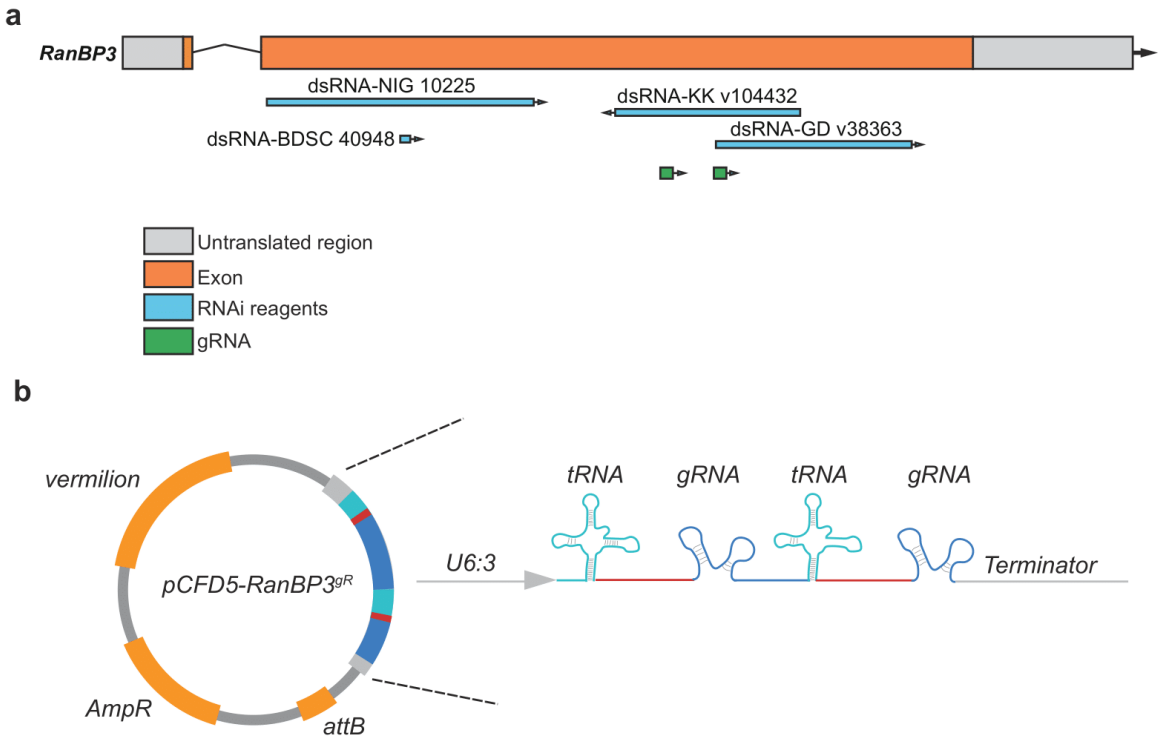

Figure 3.7 Schematic demonstration of two loss-of-function approaches used to verify *RanBP3*-RNAi phenotype.

(a) Double-stranded RNA (dsRNA)-mediated RNAi (blue) targets *RanBP3* transcript in exon two. A total of four RNAi lines (VDRC KK & GD lines; BDSC 40948; NIG 10225) were used to examine loss-of-*RanBP3* phenotypes. Only VDRC KK line (v104432) caused both lethality and the porphyria-like ring gland phenotype. *RanBP3* gRNA line (green) also targets exon two and overlaps with the target sites of both KK and GD lines. (b) Demonstration of the recombinant plasmid for *RanBP3* gRNA line.

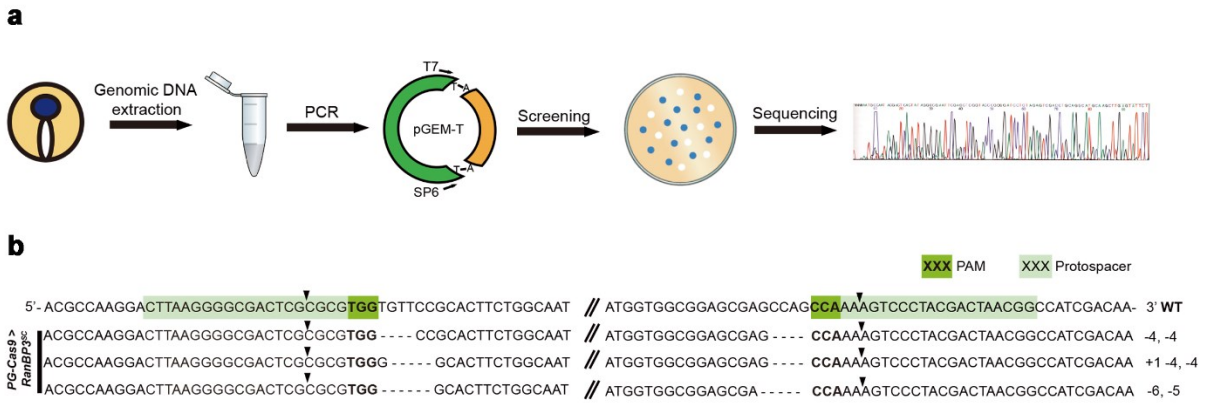

Figure 3.8 Verifying gene-editing efficiency via sequencing.

(a) Ring glands were dissected from *PG-Cas9 > RanBP3*^{gR} larvae. The gene region where two gRNA target sites were located was amplified by PCR followed by recombination into the pGEM-T vector and sequencing. (b) Sequences of *RanBP3* loci from dissected ring glands of *PG-Cas9>RanBP3*^{gR} animals.

3.3.2 Establishing the link between RanBP3 and heme/iron homeostasis

Disruption of *RanBP3* function ubiquitously blocked the larval-to-pupal transition, resulting in larvae that arrested in the third-instar larval stage. I reasoned that the developmental defect of these *RanBP3* loss-of-function animals may most likely due to insufficient levels of the steroid hormone ecdysone. Since the porphyria-like phenotype was strengthened when I switched to *phm22-Gal4* driver, I further hypothesized that RanBP3 may have a novel role in heme biosynthesis in flies. This is likely true because iron is a part of heme, and heme is a cofactor of cytochrome P450 enzymes that catalyze most reactions of the ecdysone biosynthetic pathway (Fig. 1.1c). To test this hypothesis, I supplemented the *Drosophila* media with either cholesterol or 20-hydroxyecdysone (20E) to see whether dietary sterol feeding can rescue the *RanBP3*-RNAi phenotype. As a result, I found that only the biologically active form of ecdysone, the steroid hormone 20E, could significantly rescue animals' survival rate, measured as the percentage of *RanBP3* loss-of-function animals that reach the pupal stage (Fig. 3.9). This result was consistent with the notion that ecdysone titers were reduced due to the lack of *RanBP3* function in the PG. In contrast, supplementing fly media with dietary cholesterol, the precursor of the ecdysone biosynthetic pathway, was ineffective to produce a rescue effect. Collectively, these results suggested that dietary cholesterol can be efficiently acquired by *RanBP3*-depletion PG cells, whereas one or more following ecdysone biosynthetic steps were blocked such that insufficient amount of ecdysone can be produced to support normal larval development.

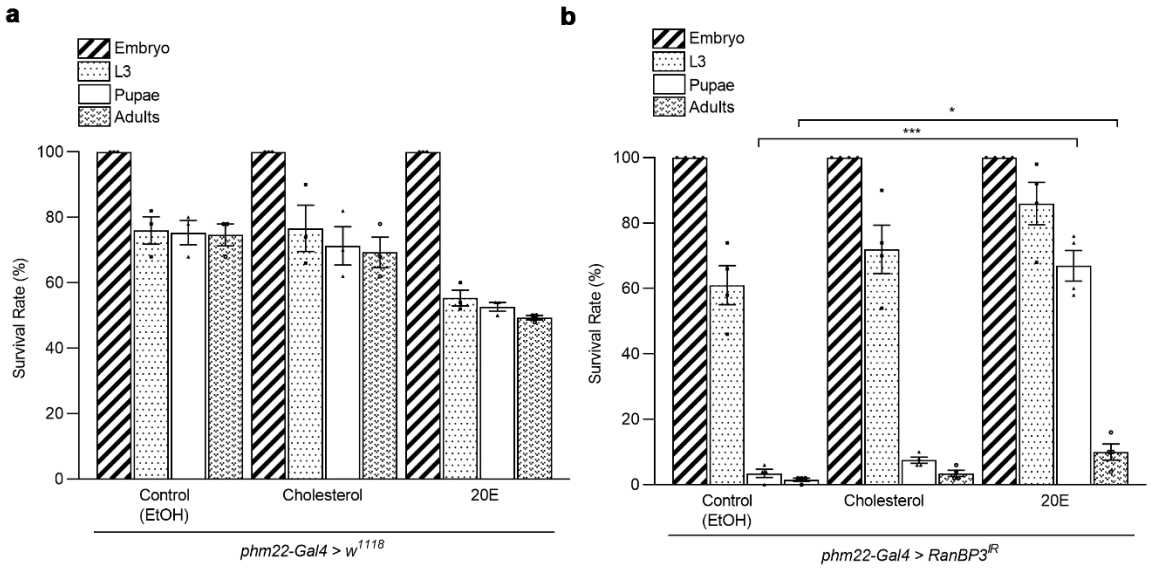

Figure 3.9 Sterol rescue of PG-specific *RanBP3* loss-of-function and control animals.

(a) Survival of w^{1118} animals supplemented with cholesterol, 20-hydroxyecdysone (20E), or control food. *phm22-Gal4* was used to induce transgene expression specifically in the prothoracic gland. Error bars represent standard deviation. (b) Survival of *RanBP3* loss-of-function animals supplemented with sterols. Error bars represent standard deviation. ***$p < 0.001$, **$p < 0.01$, *$p < 0.05$.

The synthesis of the steroid hormone ecdysone requires substantial amounts of iron to make heme that equip ecdysone biosynthetic enzymes as a cofactor. The notice of red autofluorescence in the PG when exposed *RanBP3* loss-of-function under UV light implicated that RanBP3 is a novel regulator of heme biosynthesis in flies. Two potential scenarios may cause the porphyria-like phenotype in these animals. First, it is likely that enzymatic activities of proteins that catalyze the conversion from succinyl-CoA and glycine to heme are affected. Therefore, the accumulation of heme precursors could result in the red autofluorescence in cells that have an impaired heme biosynthetic pathway. Alternatively, it is also possible that an insufficient cellular iron supply or interrupted intracellular iron trafficking can induce the same phenotype in the PG cells since iron must be safely delivered into the mitochondria to complete the last step of heme biosynthesis (via ferrochelatase = FeCH). To test which scenario is true for PG-specific *RanBP3*-RNAi animals, I reared *phm22>RanBP3*^{IR} animals on fly media supplemented with hemin (ferric iron-protoporphyrin IX), while using ZnPP (zinc- protoporphyrin IX) as a control. Interestingly, hemin partially rescued both the developmental defect and the accumulation of protoporphyrin induced by *RanBP3* loss-of-function in the PG cells (Fig. 3.10). In stark contrast, while ZnPP supplementation successfully rescued the porphyria-like phenotype in *Ppox*-RNAi animals, it did not rescue the red autofluorescence in *RanBP3* loss-of-function PG cells. Overall, hemin but not ZnPP rescued *RanBP3* loss-of-function phenotypes, suggesting a lack of bioavailable iron that can be utilized by mitochondria to make heme.

Since it was the iron in the heme that rescued the porphyria-like phenotype and the lethality

in *phm22>RanBP3*^{IR} animals, I next sought to examine whether supplementing elemental iron, in the form of ferric ammonium citrate (FAC), could rescue *RanBP3* loss-of-function phenotypes. Surprisingly, when I used FAC instead of hemin as an iron source in fly media, I did not see a rescue of the lethality induced by PG-specific depletion of *RanBP3* (Fig. 3.11a). *phm22>RanBP3*^{IR} animals reared on iron-rich (FAC-supplemented) diet or iron-depletion diet mediated by the iron chelator bathophenanthroline sulfate (BPS) both showed similar survival compared to control animals reared on normal fly media. In contrast, *IRP1A* knockout (*IRP1A*^{KO}) mutants generated by CRISPR/Cas9 that died as first-instar or second-instar larvae, can develop into phenotypically normal adults when reared animals on iron-rich media supplemented with FAC, showing normal developmental progress [91]. This result was unexpected but exciting, since it suggested a few things. First, cellular iron levels can be restored by different iron sources. The hemin uptake pathway must remain intact and work independently of the elemental iron acquisition pathway to fully rescue the loss-of-function phenotype induced by low levels of RanBP3 in the PG. Second, since IRP1A, as the major sensor and regulator of cellular iron homeostasis, can only mobilize cellular bioavailable iron to be utilized for heme biosynthesis, the rescue effect of elemental iron would be relatively limiting if the uptake pathway was blocked at the beginning. Thus, I reasoned that RanBP3 may have a role to regulate elemental iron uptake in flies.

In vertebrates, serum iron is delivered to transferrin proteins in the circulatory system, followed by internalization by transferrin receptor (TfR)-mediated endocytosis. *Drosophila* encodes three transferrin proteins (Tsf1, Tsf2, and Tsf3). Only Tsf1 was suggested to resemble

human transferrin 1 in cellular iron regulation functionally [145]. However, no transferrin receptor (TfR) has been identified in *Drosophila*, which raised some difficulties to analyze further if *RanBP3* has a role in regulating cellular iron uptake via the transferrin iron pathway. There is a transgenic *human transferrin receptor* (*hTfR*) allele available at the Bloomington center. And I wanted to know whether this transgene can be expressed in the PG and where the protein was localized. Therefore, I expressed the transgenic *hTfR* allele in the PG and found that hTfR mostly localized to the membrane of PG cells (Fig. 3.11b), consistent with the subcellular localization of hTfR in vertebrates. Then, I examined whether expressing this transgenic allele can complement the iron deficit phenotype induced by *RanBP3* loss-of-function. As a result, both the blocked larval-to-pupal transition and the porphyria-like phenotype induced by loss of *RanBP3* function were partially rescued by hTfR overexpression (Fig. 3.11c, d). With hTfR overexpressed, ~70% of *RanBP3*-RNAi animals can now survive to the pupal stage compared to only 20% in the RNAi control. The red auto-fluorescence was also greatly diminished. To test the validity of this transgenic allele, I used *pickpocket 20* (*ppk20*), another potential novel regulator of heme biosynthesis identified by our lab, as a positive control. Similar to what occurred in *RanBP3*-RNAi animals, expressing *hTfR* allele was effective to rescue both the larval lethality and the porphyria-like phenotype of *ppk20*-RNAi animals. However, unlike *RanBP3*-RNAi, *ppk20*-RNAi animals co-expressing hTfR in the PG cells showed a significant increase in the number of adults (Fig. 3.11c). On the other hand, the developmental delay of *evi5*-RNAi animals was not able to be rescued by overexpressing hTfR in the PG (not shown). Since evi5 has been studied by Dr. Sattar

Soltani in our lab, as a candidate gene functioning in the vesicular iron trafficking pathway in flies, I concluded that the rescue effect of hTfR in *RanBP3*-RNAi PG cells was specific. It is most likely that hTfR plays an evolutionarily conserved role in the cellular iron uptake pathway, through binding to transferrin-iron (III) complex followed by endocytosis. *Drosophila* may encode another protein that substitutes the function of TfR to modulate transferrin-iron uptake, though not identified yet. On the other hand, *Drosophila* ferritin has been suggested to play an important role in dietary iron absorption since midgut-specific *ferritin*-RNAi induced an iron accumulation in the gut but systemic iron deficiency [62]. Since most ferritins in insects are plasma but not cytosol, this raised another possibility explaining why a transferrin receptor has not been identified in flies. It is reasonable that the ferritin-mediated iron uptake pathway works to replace the transferrin-iron intake in *Drosophila* and insects.

Taken together, my preliminary results suggested that *RanBP3* has a role to regulate elemental iron uptake.

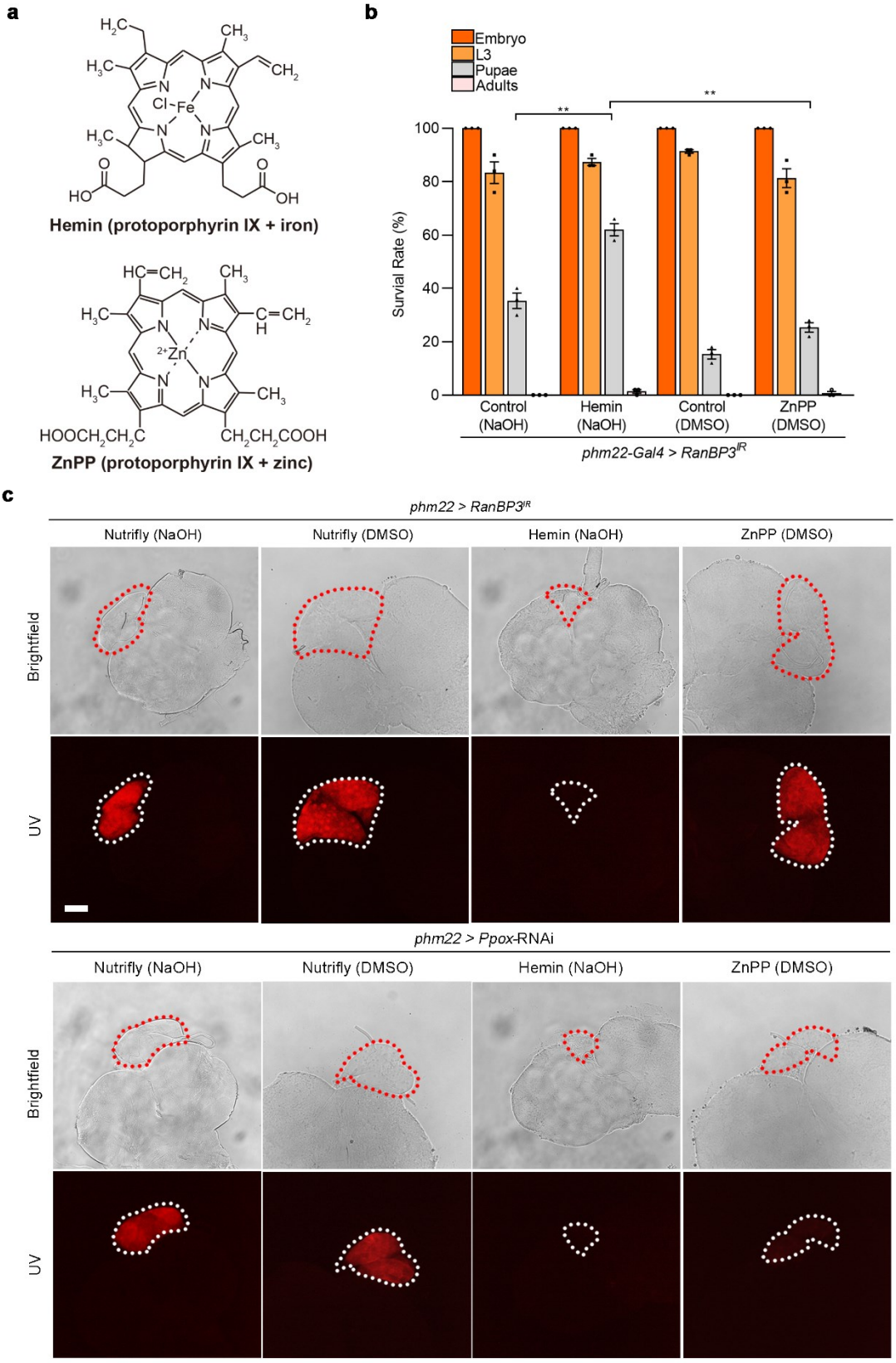
a
Hemin (protoporphyrin IX + iron)
ZnPP (protoporphyrin IX + zinc)
b
Embryo
L3
Pupae
Adults
Survial Rate (%)
Control (NaOH)
Hemin (NaOH)
Control (DMSO)
ZnPP (DMSO)
phm22-Gal4 > RanBP3IR
c
phm22 > RanBP3IR
Nutrifly (NaOH)
Nutrifly (DMSO)
Hemin (NaOH)
ZnPP (DMSO)
Brightfield
UV
phm22 > Ppox-RNAi

Figure 3.10 Hemin supplementation partially rescued the lethality and the porphyria-like phenotype of *RanBP3* loss-of-function animals.

(a) Schematic demonstration of hemin and zinc protoporphyrin IX (ZnPP). (b) Survival of *phm22>RanBP3*-RNAi animals supplemented with hemin, ZnPP, and control food. Error bars represent standard deviation. ***$p < 0.001$, **$p < 0.01$, *$p < 0.05$. (c) Dissected ring glands exposed under the UV light. *Ppox* encodes an enzyme that functions in the heme biosynthetic pathway. Loss-of-*Ppox* induced a porphyria-like phenotype, similar to *RanBP3*, which can be rescued by hemin and ZnPP supplementation. *Ppox*-RNAi was used as a control to show the effectiveness of ZnPP in this experiment. Scale bar = 250 μm.

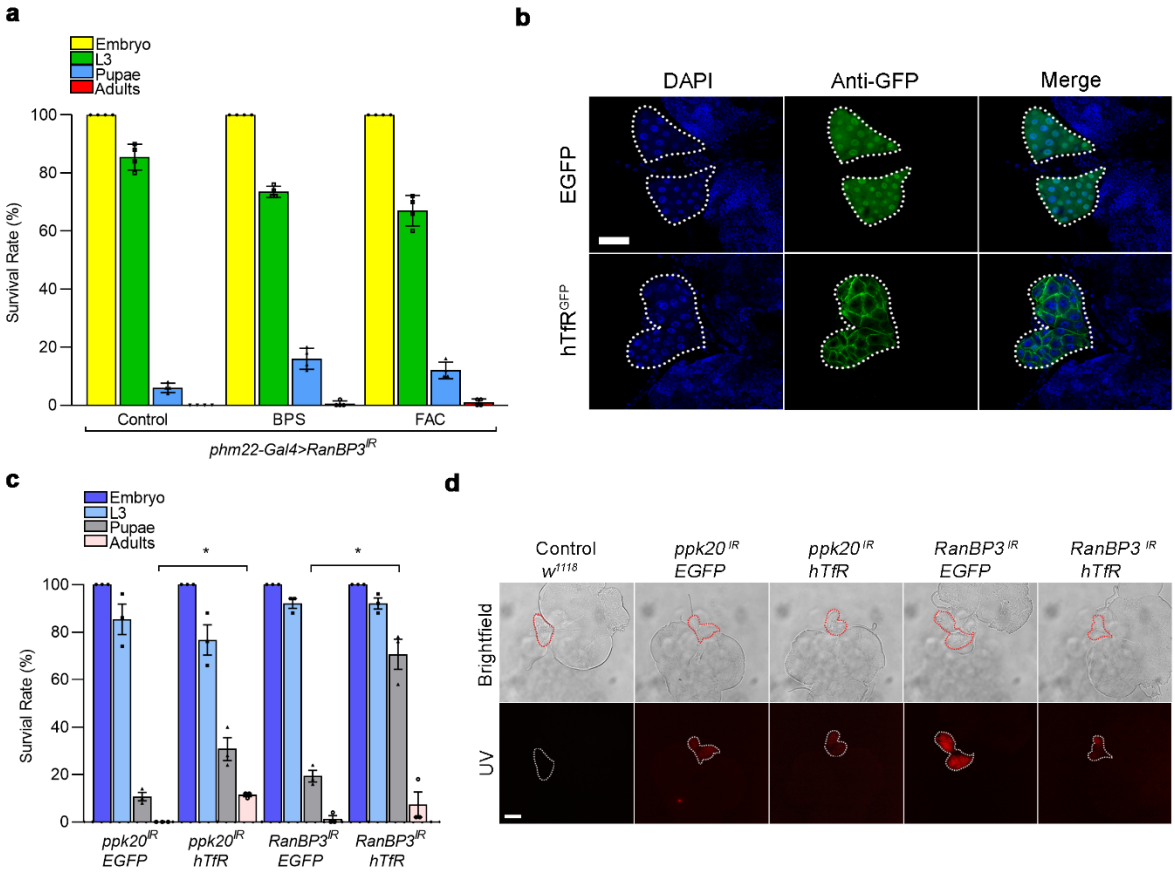

Figure 3.11 Ectopic expression of the transgenic *hTfR* allele in *RanBP3*-depletion PG cells.

(a) Iron manipulation of *phm22>RanBP3*^{IR} animals followed by survival quantification. Error bars represent standard deviation. FAC: ferric iron ammonium; BPS: bathophenanthroline sulfate. (b) Expressing the *hTfR*^{GFP} allele in the prothoracic gland using *phm22* driver. EGFP was used as a control to show protein with both nuclear and cytosolic localization. Scale bar = 500 μm. (c) Survival quantification of *RanBP3* loss-of-function animals co-expressing hTfR in the PG cells. *Pickpocket 20 (ppk20)*, similar to *RanBP3*, was also identified as a potential heme regulator. *Ppk20* loss-of-function animals can also be rescued by the ectopic expression of hTfR in the PG cells. *p < 0.05. (d) UV exposure of dissected ring glands from 40-42 hour third-instar larvae with either

EGFP or hTfR overexpressed in the prothoracic gland.

3.3.3 Subcellular localization of RanBP3 in *Drosophila*

As stated in section 3.1.5, *Drosophila* RanBP3 has the same functional domains and motifs as mammals (Fig. 3.4c), suggesting RanBP3 in the fruit fly might play a conserved role in regulating the nucleocytoplasmic transport of macromolecules. However, since the predicted NLS motif in the *Drosophila* RanBP3 protein is localized within the RanBD1 domain compared to an NLS motif localized at the N-terminal end of the mammalian counterparts, I first sought to examine the subcellular localization of RanBP3 *in vitro* and *in vivo*.

I first examined the subcellular localization of wild-type RanBP3 and mutant RanBP3 proteins using *the Drosophila* Schneider 2 (S2) cell line. Cultured *Drosophila* cell lines are popular model systems for cell biological and functional genomic studies [146, 147]. S2 cells are the most commonly used *Drosophila* cell line because they are easy to maintain in the lab. More importantly, they take up large DNA molecules, which is beneficial for *in vitro* studies that require transfection. Being isolated from late embryonic stage *Drosophila* embryos, S2 cells are roughly spherical and about 15–20 um in diameter. To study the localization of wild-type RanBP3 in S2 cells, I generated two plasmids encoding C-terminal Myc-tagged RanBP3 isoforms, which were designated as RanBP3a^{M} and RanBP3b^{M}, respectively (Fig. 3.12). The expression of RanBP3 proteins in S2 cells was driven by the ubiquitous *Actin 5C* promoter.

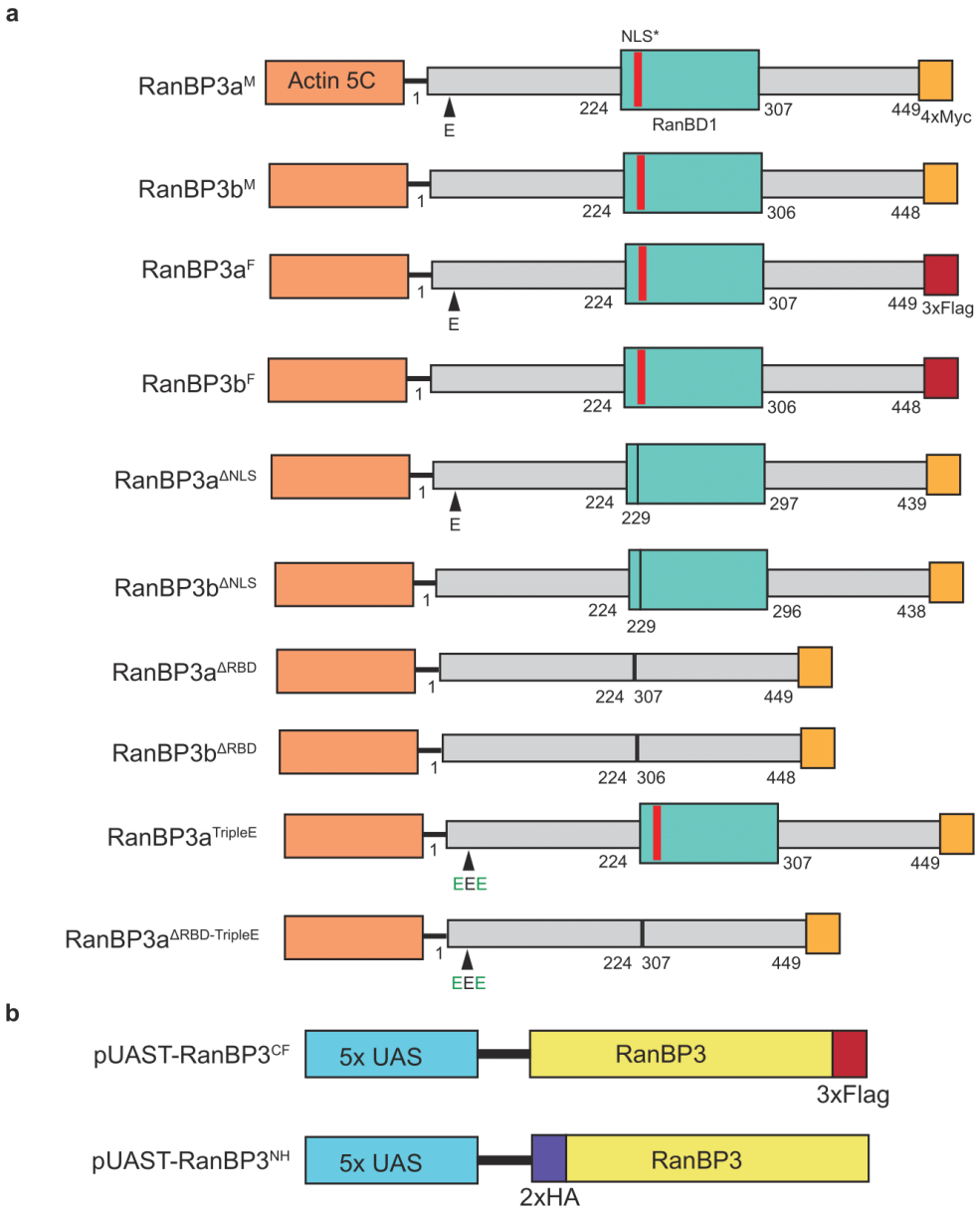

Figure 3.12 Plasmids that I generated to examine the subcellular localization of RanBP3.

(a) Plasmids used for *Drosophila* S2 cell transfections. *Actin-5C* promoter was used to drive the expression of plasmids in S2 cells. 4xMyc tag or 3xFlag tag was added to in frame with the *RanBP3* CDS, respectively. (b) Recombinant plasmids used for making transgenic *RanBP3* flies. CF: C-terminal Flag; NH: N-terminal HA.

Although RanBP3a and RanBP3b differ by one amino acid, both protein isoforms showed predominantly nuclear localization in *Drosophila* S2 cells (Fig. 3.13a). Interestingly, I noticed that RanBP3a showed strong overlap with DAPI signals that correspond to the inner nucleus region (nucleolus) in a cell, and the outer shell of the nucleus (nuclear membrane). In contrast, RanBP3b was found to have a more significant portion localized to the cytosol compared to RanBP3a. Consistent with this notion, RanBP3a has a higher percentage of nuclear proteins (% nuclear) than RanBP3b in transfected S2 cells quantified with ImageJ (Fig. 3.13d). I then made two mutant constructs in which the *Drosophila* RanBP3 NLS motif was removed entirely by site-directed mutagenesis (SDM). RanBP3 mutants generated in this way (RanBP3a$^{\Delta NLS}$ and RanBP3b$^{\Delta NLS}$) both showed noticeable cytosolic localization (Fig. 3.13b). However, RanBP3b$^{\Delta NLS}$ displayed a "donut" shape localization characterized by a void (weak signal) in the center of the nucleus and strong signals at the nuclear membrane (indicated by an arrow in Fig. 3.13b). The translocation of mutant RanBP3a and RanBP3b proteins from the nucleus to the cytosol suggested that the predicted NLS motif was valid to drive the expression of RanBP3 protein in the nucleus. The retention of RanBP3b$^{\Delta NLS}$ on the nuclear membrane may suggest the existence of an unusual NLS motif that current tools cannot predict. This might be true because mammalian RanBP3 possesses an unusual NLS motif at the N-terminal region of the protein that shows preferential binding to importin-α3 [148]. This unusual NLS does not fall into any of the six classes of importin α-dependent NLSs (Table 3.2).

To examine whether RanBP3b contains an unusual NLS motif like its mammalian

counterparts, I generated two plasmids encoding mutant RanBP3 proteins without the RanBD1 functional domains (designated as ΔRBD). Removing the RanBD1 domain would result in a complete loss of the NLS motif. Therefore, a cytosolic localization of RanBP3$^{\Delta RBD}$ protein isoforms was expected. As a result, only RanBP3a$^{\Delta RBD}$ showed the “donut” shape localization of the protein (Fig. 3.13b), suggesting a translocation of RanBP3 protein from the inner side of the nucleus to the outer membrane and the cytosol in S2 cells. In stark contrast, RanBP3b$^{\Delta RBD}$ was completely trapped in the nucleus showing a colocalization with the nucleoli (Fig. 3.13b & d). These results suggested that the three-nucleotide difference in RanBP3 isoforms might be important for determining the subcellular localization of RanBP3 in S2 cells. One possibility is that a non-canonical NLS motif is present only in RanBP3b near the glutamic acid (E) location. The key to validate this idea was to replace the asparagine (N) and the alanine (A) at both sides of the "E" in RanBP3 isoform A with other non-essential residues (such as E), such that these missense mutations would cause a similar effect in RanBP3 isoform B (Fig. 3.12). To test this idea, I introduced two missense mutations in the plasmid that encodes the RanBP3a without the RanBD1 domain (designated as RanBP3a$^{\Delta RBD\text{-}TripleE}$). Specifically, I replaced the adjacent amino acids (N and A) nearby E using SDM in RanBP3a and RanBP3a$^{\Delta RBD}$. The mutant plasmids were named as RanBP3a^{TripleE} and RanBP3a$^{\Delta RBD\text{-}TripleE}$, respectively. If the amino acids adjacent to E were crucial for the nuclear localization of RanBP3, I would expect these missense mutations to cause a complete cytosolic localization of RanBP3a$^{\Delta RBD\text{-}TripleE}$. In contrast, the control mutant RanBP3a^{TripleE} should remain in the nucleus due to the presence of the NLS motif located in the

RanBD1 functional domain. As a result, RanBP3a^{TripleE} was primarily found in the nucleolus and at the nuclear membrane (Fig. 3.13c). In stark contrast, RanBP3a$^{\Delta RBD\text{-}TripleE}$ was found accumulated at the nuclear membrane and cytosol, resulting in the "donut" shape localization of the mutant protein. However, there seemed to have little difference between the expression of RanBP3a$^{\Delta RBD}$ (Fig. 3.13b) and RanBP3a$^{\Delta RBD\text{-}TripleE}$ (Fig. 3.13c), suggesting that mutating the sequence of *RanBP3b* cDNA does not affect the function of this unusual NLS motif to direct the protein into the nucleus. Instead, it is more likely that this unusual NLS motif would form a "signal patch" connect the downstream NLS motif in the RanBD1 domain to cooperatively regulate RanBP3 nuclear import.

Since there were no tagged *RanBP3* lines available for studying the subcellular localization of RanBP3 in flies, I generated two plasmids encoding either C-terminal Flag-tagged RanBP3 or N-terminal HA-tagged RanBP3 proteins (Fig. 3.12). The plasmid was injected into embryos of *y^{1}w*P[nos-PhiC31]X; P[{carryP}] attP2(III)* animals that encode the site-specific ψC31 integrase, the enzyme that catalyzes the genome integration reaction into the *attP* site in the *Drosophila* genome[14]. Followed by embryo injection and screening, I managed to create two *RanBP3* transgenic lines, designated as *RanBP3^{CF}* and *RanBP3^{NH}*, respectively. Upon the expression of RanBP3 in whole larvae using the ubiquitous *Tub-Gal4* driver, I examined RanBP3 protein localization in multiple tissues dissected from late instar stage *Tub-Gal4>RanBP3^{CF}* and *Tub-Gal4>RanBP3^{NH}* animals (Fig. 3.14). Interestingly, RanBP3 seemed to have tissue-specific subcellular localizations in flies. For example, in both the prothoracic gland (PG) and salivary gland

(SG), I found RanBP3 in both the nucleus and the cytosol. In contrast, RanBP3 was predominantly cytoplasmic in the foregut (FG) and fat body (FB) cells. The tissue-specific localization of RanBP3 suggested that *Drosophila* RanBP3 may have tissue-specific functions in flies. Like in mammals where RanBP3 is predominantly nuclear, nuclear RanBP3 may most likely regulate nuclear protein export through NPCs. On the other hand, the cytosolic function of RanBP3 has been unevaluated, which awaits to be further investigated. I will show my initial results to characterize roles of cytosolic RanBP3 in regulating intracellular iron trafficking in section 3.3.8.

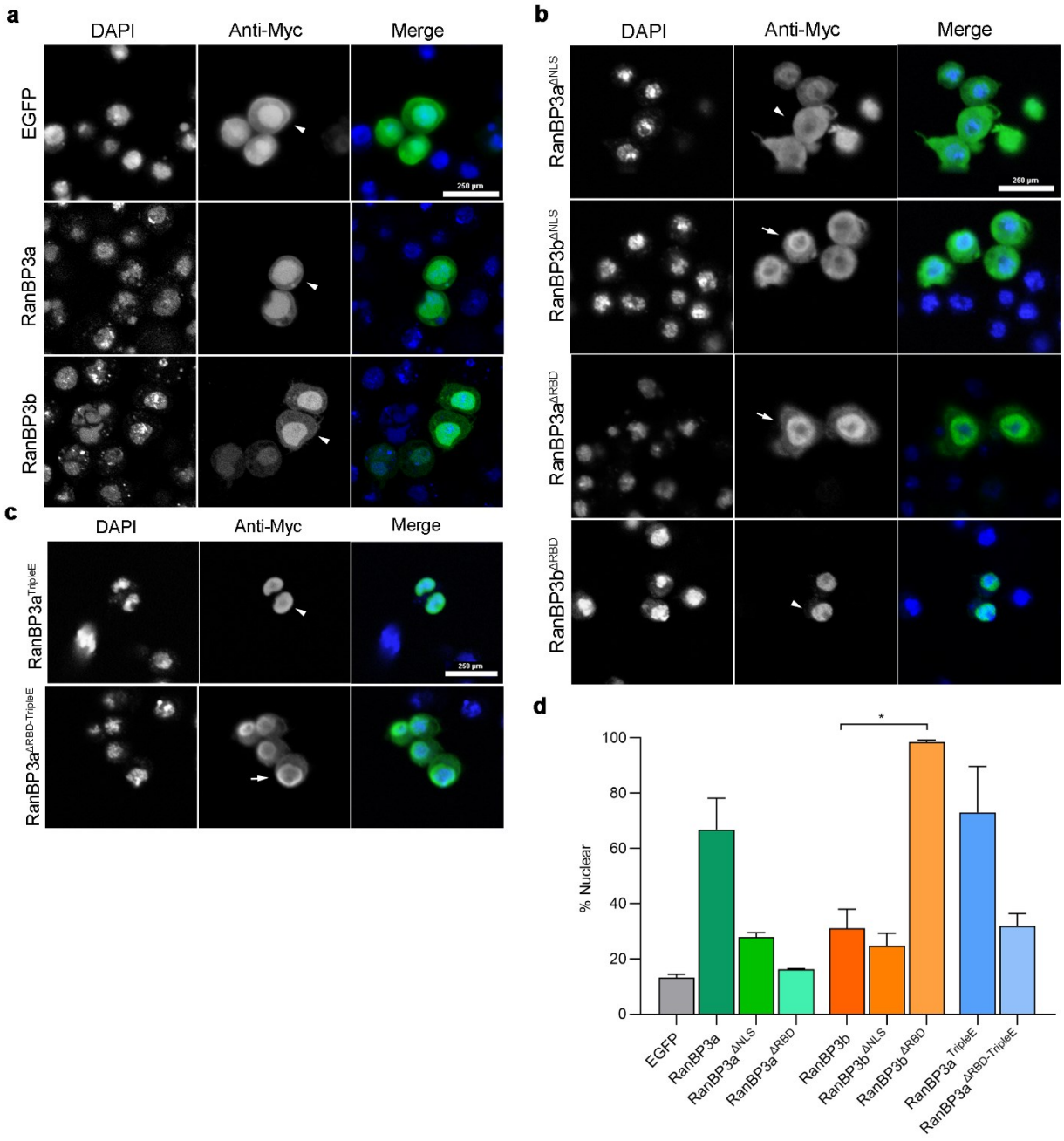

Figure 3.13 Expressing wild type and mutant *RanBP3* transgenes in *Drosophila* S2 cells.

(a) Transfection of S2 cells with plasmids encoding two RanBP3 isoforms followed by immunostaining via anti-Myc antibodies and confocal microscopy. Myc-tagged EGFP was used as a control. Scale bar = 250 µm. Representative cells are indicated as arrow heads. (b) Examining

the subcellular localization of RanBP3 proteins without the nuclear localization signal (NLS) or Ran-binding domain (RBD). Scale bar = 250 μm. Arrows indicate cells with a “donut” shape localization of RanBP3 proteins. (c) Transfection of S2 cells with plasmids encoding a substitution mutation that differs in RanBP3 isoforms. Scale bar = 250 μm. Arrows indicate cells with a “donut” shape localization of RanBP3 proteins. (d) Quantification of the percentage of nuclear EGFP and RanBP3 protein variants using ImageJ.

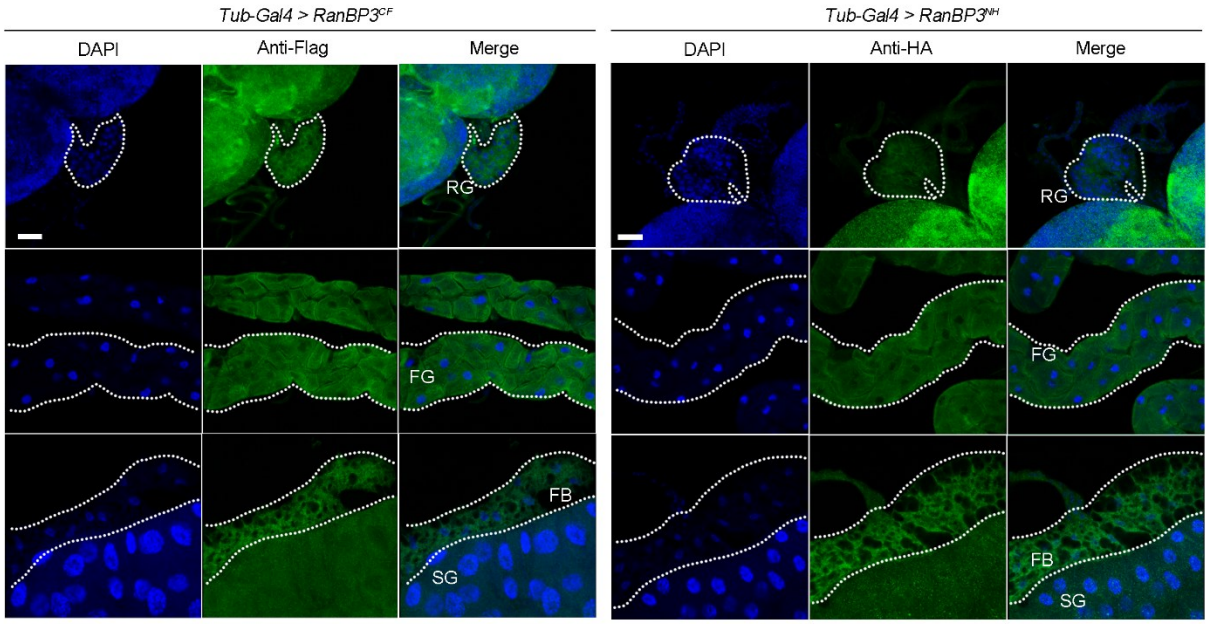

Figure 3.14 Overexpressing transgenic *RanBP3* alleles in multiple *Drosophila* tissues.

Tub-Gal4 was used to drive transgene expression ubiquitously in flies. Two transgenic *RanBP3* alleles were examined, which encode RanBP3 proteins with either C-terminal Flag tag ($RanBP3^{CF}$) or N-terminal HA tag ($RanBP3^{NH}$). RG: ring gland; FG: foregut; SG: salivary gland; FB: fat body. Scale bar = 250 μm.

3.3.4 Overexpressing IRP1A genetically rescued *RanBP3* loss-of-function phenotypes

As shown in section 3.3.2, I established a likely link between RanBP3 and cellular iron homeostasis, which suggests that low cellular iron levels are the most likely cause for the red auto-fluorescence in *RanBP3*-depleted PG cells. Therefore, the next question was what could be the cause of these presumed low iron levels in PG cells. The central cytosolic iron sensor and regulator in both vertebrates and *Drosophila* is Iron-regulatory protein 1 (IRP1), which controls cellular iron homeostasis in response to cellular iron levels. In flies, there are two IRP1 proteins. However, only IRP1A, but not IRP1B, can switch between the aconitase form (holo-IRP1A) and the RNA-binding form (apo-IRP1A), which is the same mechanism utilized by vertebrate IRP1 [41, 58, 85, 149]. Taking this into consideration, I sought to examine whether losing *RanBP3* function in the PG cells would affect IRP1A function in regulating cellular iron homeostasis. To test this, I expressed IRP1A and IRP1A variants in *RanBP3* loss-of-function PG cells using transgenic *IRP1A* alleles. Essentially, the single point mutation in $IRP1A^{C450S}$ (cysteine to serine) impairs the incorporation of the Fe-S cluster, resulting in a protein that constitutively binds to RNA (apo-IRP1A) [91]. In contrast, three-point mutations in $IRP1A^{3R3Q}$ (arginine to glutamine) altogether abolishes the RNA-binding site, encoding the non-RNA-binding IRP1A. Remarkably, only when the RNA-binding IRP1A was expressed in the *RanBP3*-RNAi PG cells, the porphyria ring gland phenotype was completely rescued (Fig. 3.15a). In contrast, overexpression of the $IRP1A^{3R3Q}$ allele had the opposite effect, making the accumulation of the protoporphyrin visible even without the UV light

(Fig. 3.15b). Meanwhile, the survival rate of *RanBP3* loss-of-function animals with RNA-binding IRP1A co-expressed in the PG cells was significantly increased and approached similar levels as the control group where IRP1A^{C450S} was co-expressed with EGFP (Fig. 3.15c). Consistent with this result, the ectopic expression of wild-type IRP1A can only partially rescue the porphyria-like phenotype, but not the lethality induced by *RanBP3* loss-of-function. The partial rescue makes sense because the transgenic *IRP1A*^{WT} allele encodes both the holo- and apo-IRP1A, which might not be present in equal amounts under normal iron conditions. On the other hand, expressing the non-RNA-binding form encoded by the transgenic *IRP1A*^{3R3Q} allele was ineffective to rescue the larval lethality induced by *RanBP3* loss-of-function, leading to almost zero percent of animals that grew into the adulthood. Collectively, these results strongly implicated that RanBP3 is critical for cellular iron homeostasis via sustaining the appropriate levels of RNA-binding IRP1A in the cytoplasm.

Drosophila IRP1A is a bi-functional protein that switches between the aconitase holo-form and the RNA-binding apo-form in response to cellular iron levels. Work from our lab suggests that IRP1A can enter nuclei of PG cells to down-regulate expression of genes that are linked to iron-dependent processes, such as genes that are tied to steroid production [91]. In the prothoracic gland and fat body, IRP1A predominantly localizes in the nucleus, whereas in salivary gland cells, IRP1A is cytoplasmic. These results made me wonder whether RanBP3 could regulate the nucleocytoplasmic transport of IRP1A since mammalian RanBP3 has been suggested to function as a cofactor in the nuclear export pathway. To test this, I examined the IRP1A subcellular

localization in *RanBP3* loss-of-function PG cells via immunostaining. Strikingly, RNA-binding IRP1A encoded by the *IRP1A*^{C450S} transgene accumulated in the nucleus upon the induction of *RanBP3*-RNAi in the prothoracic gland (Fig. 3.16). In contrast, knocking down *RanBP3* did not affect the localization of non-RNA-binding IRP1A encoded by the transgenic *IRP1A*^{3R3Q} allele that much. These results implicated that RanBP3 might play a critical role in regulating the nuclear export of IRP1A. The reason why IRP1A^{C450S} can get into the nucleus is likely because the single point mutation was not necessarily to completely abolish the Fe-S cluster binding activity, but instead, strongly reduced the binding efficiency of the IRP1A mutant to Fe-S clusters. As such, that small portion of IRP1A can still incorporate Fe-S clusters followed by nuclear import. However, with lacked RanBP3 function in the nucleus, nuclear IRP1A would be trapped in the nucleus, ultimately resulting in low levels of RNA-binding IRP1A in the cytosol to post-transcriptionally regulate expression of iron metabolism genes.

Altogether, I found RanBP3 may play an essential role in cellular iron homeostasis via regulating the nuclear export of IRP1A.

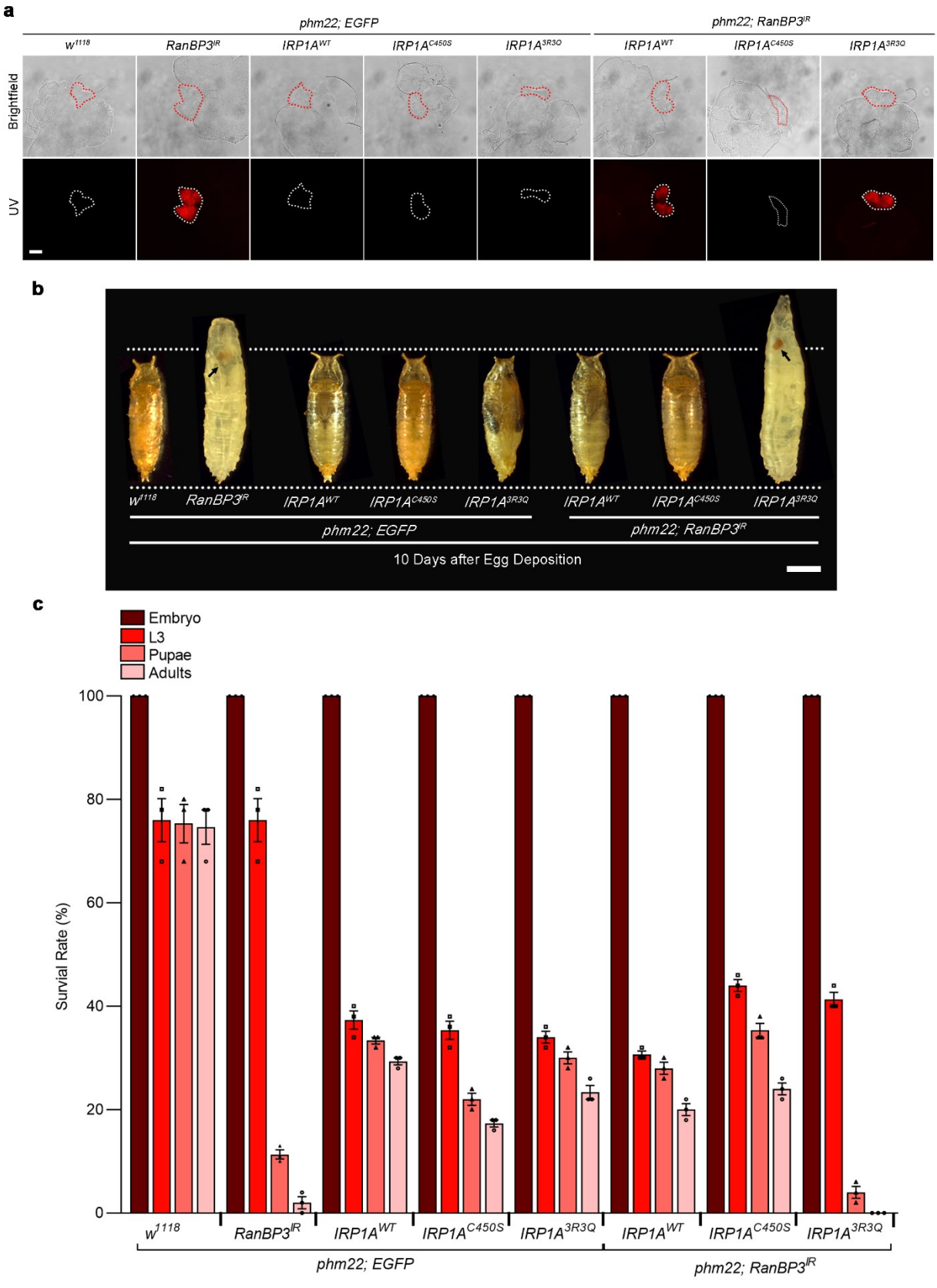
a
phm22; EGFP
phm22; RanBP3IR
w1118
RanBP3IR
IRP1AWT
IRP1AC450S
IRP1A3R3Q
IRP1AWT
IRP1AC450S
IRP1A3R3Q
Brightfield
UV
b
w1118
RanBP3IR
IRP1AWT
IRP1AC450S
IRP1A3R3Q
IRP1AWT
IRP1AC450S
IRP1A3R3Q
phm22; EGFP
phm22; RanBP3IR
10 Days after Egg Deposition
c
Embryo
L3
Pupae
Adults
Survial Rate (%)
100
80
60
40
20
0
w1118
RanBP3IR
IRP1AWT
IRP1AC450S
IRP1A3R3Q
IRP1AWT
IRP1AC450S
IRP1A3R3Q
phm22; EGFP
phm22; RanBP3IR

Figure 3.15 Rescue studies via the expression of transgenic *IRP1A* alleles in *phm22>RanBP3^{IR}* animals.

(a) UV exposure of dissected ring glands from 40-42 hours third-instar larvae overexpressing I *RanBP3* loss-of-function animals with or without IRP1A alleles co-expressed in PG cells. Error bars represent standard variation. (b) Development of *RanBP3* loss-of-function animals co-expressing *IRP1A* transgenic allele in PG cells. Arrows indicate the accumulation of protoporphyrin in PG cells. (c) Survival of *RanBP3*-RNAi animals co-expressing IRP1A proteins. Error bars represent standard deviation.

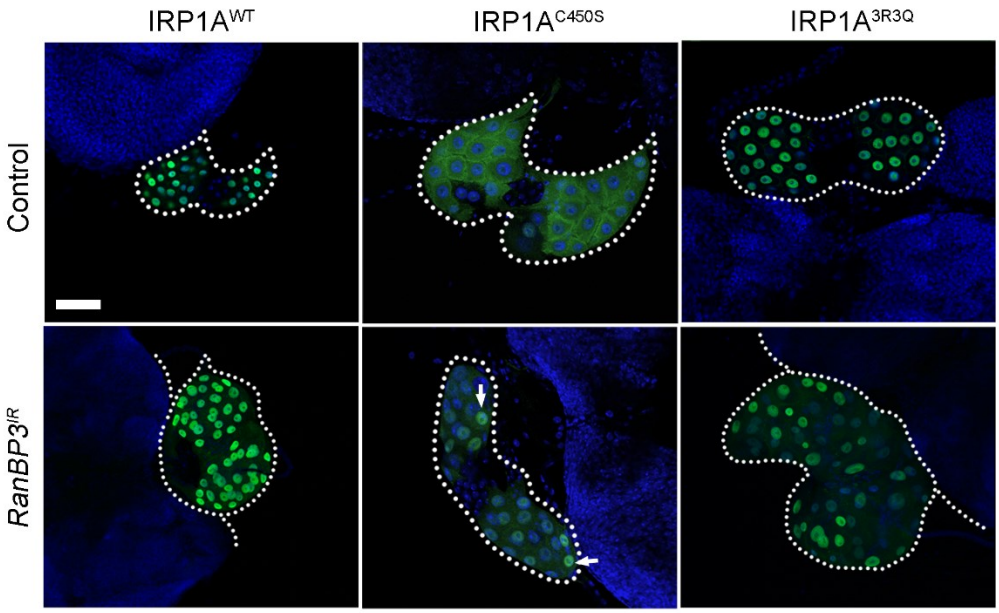

Figure 3.16 Knocking down *RanBP3* in the PG accumulated IRP1A in the PG cell nuclei.

Transgenic *IRP1A* alleles, including $IRP1A^{WT}$, $IRP1A^{C450S}$, and $IRP1A^{3R3Q}$, were ectopically expressed in *RanBP3* loss-of-function or control PG cells followed by immunostaining via anti-Flag antibodies. Green signals represent immunostaining of IRP1A proteins via anti-Flag antibodies. Blue signals represent DAPI staining. Arrows indicate IRP1A accumulation in *RanBP3*-depletion PG nuclei.

3.3.5 The nuclear import of IRP1A is mediated by Ran and NTF2

The finding that IRP1A can localize to the nuclei was exciting, and challenged the existing decades-old paradigm. Essentially, IRP1A was believed to function only in the cytosol, either as an aconitase or an mRNA-binding protein. One possible explanation for not detecting nuclear IRP1A is that mammalian cells usually have smaller nuclei than PG cells. A much larger nucleus would allow the visualization of nuclear proteins via immunohistochemistry. In addition, many studies on vertebrate IRP1 have been conducted in just two types of cell cultures [150, 151]. Since we found that nuclear IRP1A is cell-type specific [91], it is conceivable that the subcellular distribution of vertebrate IRP1 follows a similar pattern. Therefore, it is quite possible that a nuclear function of IRP1 in vertebrates has been overlooked. The study in both *Drosophila* tissues and *Drosophila* S2 cells for understanding the mechanism of IRP1A transported across the nuclear membrane would provide further clues as to whether this mechanism may also exist in vertebrates.

Drosophila IRP1A does not have a recognizable nuclear localization signal (NLS) as many nuclear proteins do, which raised an interesting question: how is a protein without a known NLS, like IRP1A, is recognized by importins and transported into the nucleus? There are two possible explanations for this. First, IRP1A may carry an unusual NLS motif that prediction tools have not well characterized. For instance, signal patches, which are composed of at least two distinct regions of the protein, are difficult to identify. Or it is possible that IRP1A can physically interact with a protein or a set of proteins whose nuclear import pathway has been well examined. A previous lab

member, Dr. Nhan Huynh, conducted a mass spectrometry assay (MS) where he identified putative IRP1A interacting proteins using three transgenic *IRP1A* alleles encoding wild-type, apo-IRP1A, and holo-IRP1A proteins (Appendix A.1). From the list of proteins identified from the MS, three proteins caught my attention for several reasons: the small GTPase Ran, the nuclear transport factor 2 (NTF2), and Chickadee (Chic). First of all, it has been previously shown that the nuclear import of Ran is mediated by NTF2, which permits the rapid entry of Ran into the nucleus where the GTP-GDP exchange is mediated by RanGEF [152]. The interaction between NTF2 and Ran is required to concentrate Ran in the nucleus and consequently for protein transport between the nucleus and the cytoplasm [110]. Secondly, the severe eye phenotype caused by the reduction of *Drosophila* NTF2 is suppressed by loss of function mutations in *chic*, therefore providing a genetic interaction between these two proteins[113]. Last but not least, the mouse *Profilin 2* (*Pfn2*, equivalent to *chic* in *Drosophila*) mRNA encodes an actin-binding protein, but importantly, it is a novel IRP-interacting transcript due to the presence of a non-canonical IRE in the transcript. Thus, Pfn2, and potentially its *Drosophila* homolog Chic, appear to have unidentified roles in iron metabolism[153].

Since there were no transgenic epitope tagged lines of *Ran*, *Ntf-2*, or *chic* to validate the MS result, I adopted the cell culture approach to examine protein-protein interactions. Plasmids applicable for transfection were generated via PCR and verified by sequencing. To begin with, I examined the subcellular localization of proteins that I would further use in co-immunoprecipitation (co-IP) and Western blotting. As expected, both Ran and NTF2 showed predominantly nuclear localization in S2 cells (Fig. 3.17a), consistent with the idea that NTF2

mainly functions as a nuclear import receptor of Ran. The protein-protein interaction was then verified via co-IP and Western blotting (Fig. 3. 17b). Similarly, I examined the subcellular localization of IRP1A and IRP1A variants in S2 cells using the same approach. Both the subcellular localization of wild-type IRP1A encoded by $IRP1A^{WT}$ cDNA and the RNA-binding IRP1A encoded by $IRP1A^{C450S}$ cDNA were consistent with previous results in the PG (Fig. 3.17c). Unexpectedly, the subcellular localization of the non-RNA-binding IRP1A, encoded by $IRP1A^{3R3Q}$ cDNA in S2 cells was slightly different than in the PG. While $IRP1A^{3R3Q}$ showed both nuclear and cytoplasmic localization in S2 cells, $IRP1A^{3R3Q}$ was found predominantly in the nucleus in PG cells (Fig. 3.16). Since *Drosophila* S2 cells are embryonic stage cells, it makes sense that some genes (i.e., *IRP1A*) show differential expression at different developmental stages. Nevertheless, I examined whether IRP1A can physically interact with Ran and NTF2 in S2 cells via co-IP. As a result, IRP1A was able to interact with both Ran and NTF2, but not the negative control EGFP in S2 cells (Fig. 3.17d), consistent with the MS result. Collectively, my experiments showed that the nuclear import of IRP1A was mediated by Ran and NTF2 proteins via protein binding.

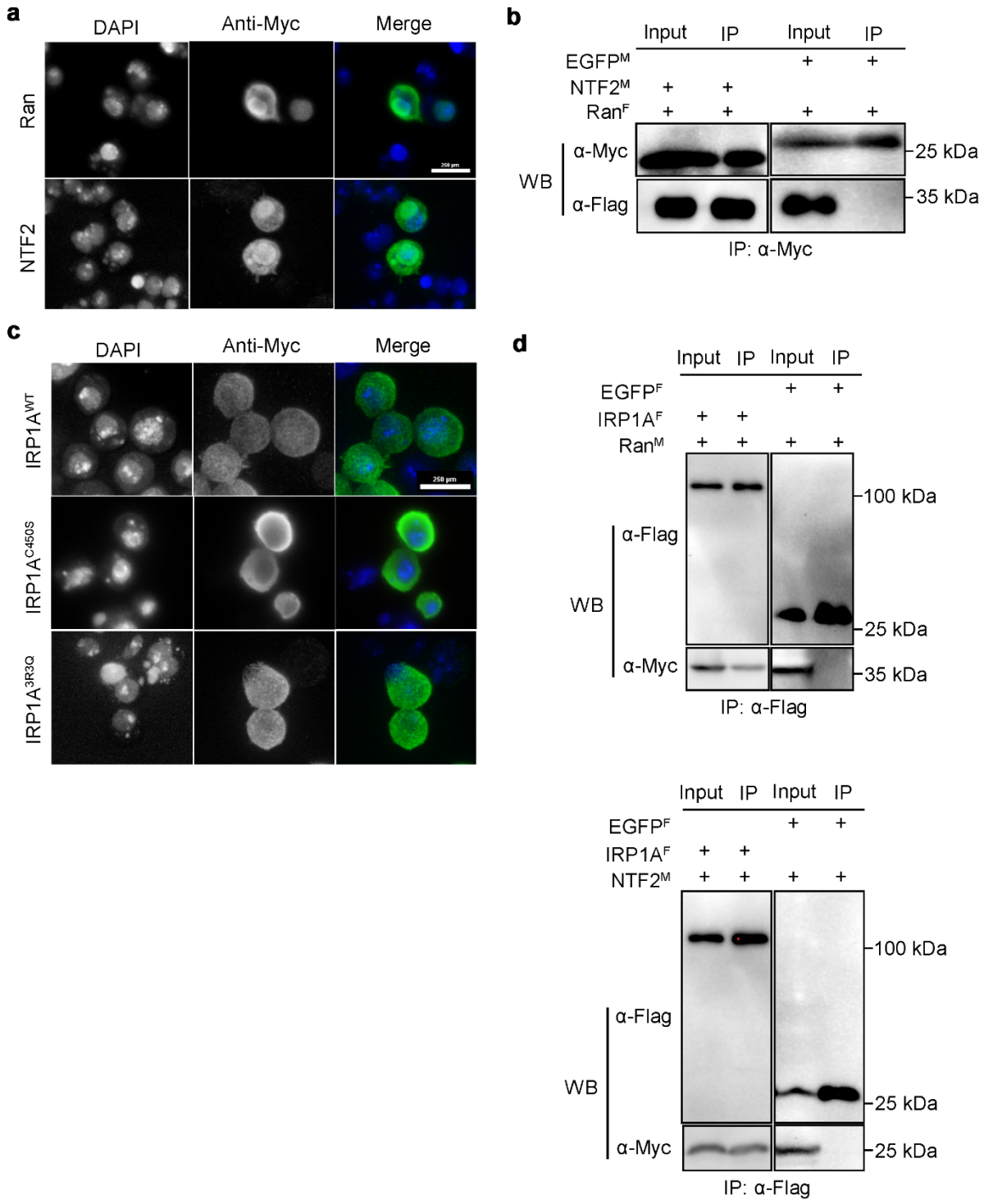

Figure 3.17 IRP1A nuclear import is mediated by Ran and NTF2.

(a) Subcellular localization of Ran and NTF2 in *Drosophila* S2 cells. Scale bar = 250 μm. (b) Co-

transfection of S2 cells with plasmids encoding Myc-tagged NTF2, Myc-tagged EGFP, and Flag-tagged Ran followed by co-IP via anti-Myc antibodies and Western blotting. EGFP was used as a control. (c) Examining IRP1A and IRP1A variant subcellular localization in S2 cells. Scale bar = 250 μm. (d) Verifying protein-protein interactions between IRP1A and Ran, IRP1A and NTF2 using *Drosophila* S2 cells.

Mutational analysis of the NTF2 protein was also conducted based on a previous study showing the interaction between RanGDP and NTF2 might involve complementation of positively charged residues on Ran by the negatively charged cluster surrounding NTF2 (i.e., E42K, D92/94N, H66A, etc.) [109]. Since mammalian D23A and N77Y mutants exhibit the dominant-negative phenotype of NTF2 thus inhibiting the nuclear import of NLS-mediated nuclear cargos [110], I generated three recombinant plasmids (*Ntf-2*^{D23A}, *Ntf-2*^{D81A} and *Ntf-2*^{2D2A}) encoding the equivalent counterparts compatible for S2 cell transfection. Surprisingly, NTF2^{2D2A}, which harbors two single point mutations (D23A and D81A), showed an exclusive nucleolus localization, whereas the other two NTF2 mutants (NTF2^{D23A} and NTF2^{D81A}) were found accumulated at the nuclear membrane leaving a void in the center of the nucleus (Fig. 3.18a). Since NTF2 plays such an essential role in mediating the nuclear import of Ran and nuclear cargos, I then examined whether expressing the NTF2^{2D2A} double mutant can alter the subcellular localization of Ran and IRP1A in S2 cells. As a result, overexpressing NTF2^{2D2A} accumulated Ran in the nucleus (Fig. 3.18b). In contrast, expressing wild-type *Ntf-2* or the other two *Ntf-2* transgenes did not affect the normal distribution of Ran, which showed both nuclear and cytosolic localization in S2 cells. I reasoned that the nuclear retention of Ran may most likely result in malfunctional nuclear transport of IRP1A and other target proteins by affecting the steep Ran gradient across the nuclear membrane. Consistent with this notion, I found that expressing the *Ntf-2*^{2D2A} transgene trapped holo-IRP1A in the nuclei (Fig. 3.18c). In addition, wild-type IRP1A with a predominantly cytosolic localization failed to interact with NTF2^{2D2A} that was found accumulated in the nucleus (Fig. 3.18d). These results suggested

that the double point mutations in *Ntf-2*^{2D2A} cDNA may most likely induce a conformational change of the protein that renders a higher binding affinity of NTF2 and its target proteins to nucleoporins, which ultimately results in the accumulation of the nuclear import complex composed of NTF2, Ran and IRP1A in the nucleus.

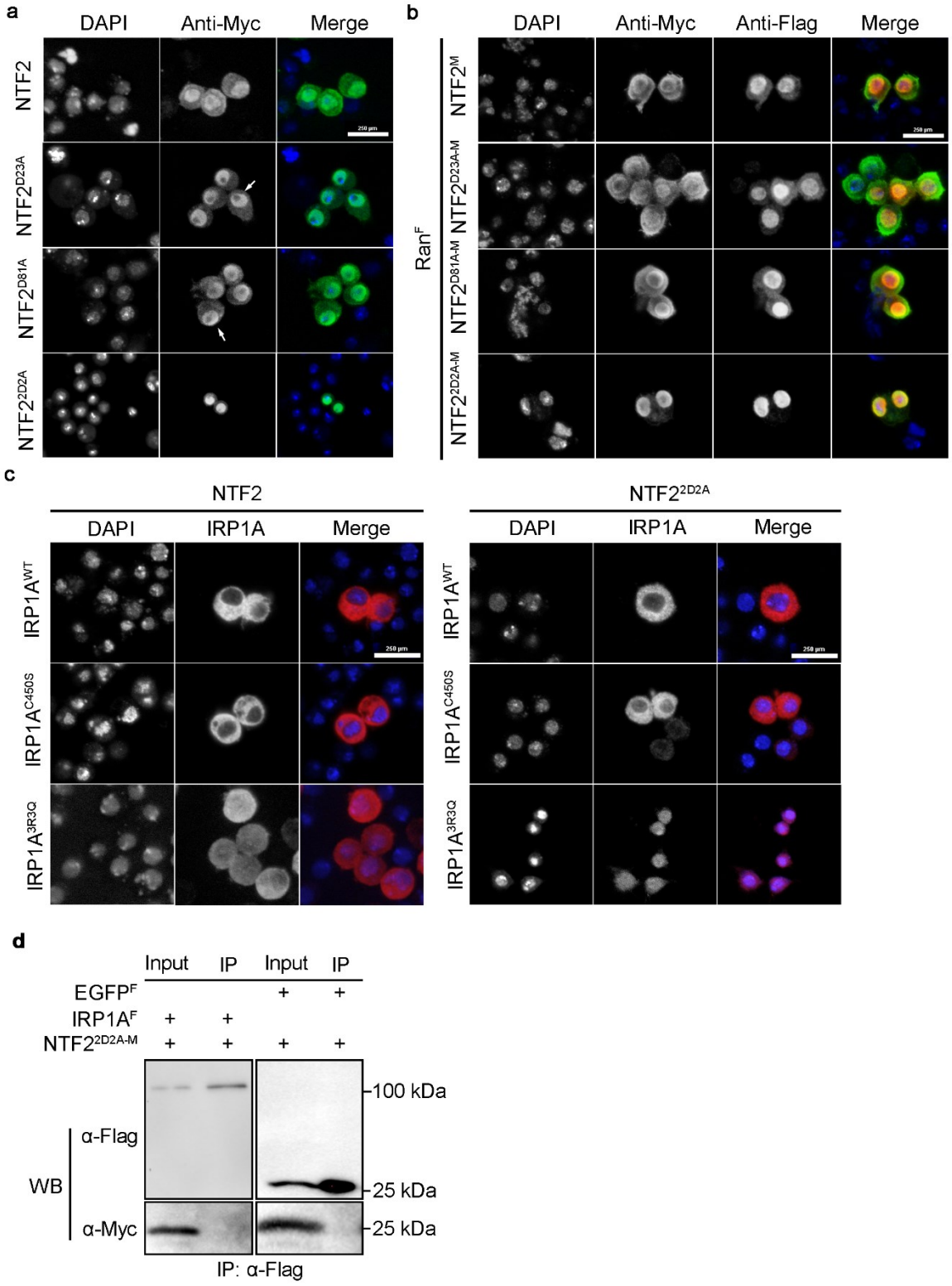

Figure 3.18 NTF2 mutational analysis.

(a) Overexpressing wild-type and mutant *Ntf-2* cDNAs in *Drosophila* S2 cells. Scale bar = 250 μm. Arrows indicate representative cells with a void staining in the center of the nucleus. (b) Co-transfection of S2 cells with plasmids encoding Flag-tagged Ran and Myc-tagged NTF2 proteins followed by immunostaining and microscopy. Scale bar = 250 μm. (c) Co-expressing Flag-tagged IRP1A variants and Myc-tagged $NTF2^{2D2A}$ in S2 cells. Scale bar = 250 μm. Red signals represent anti-Flag staining of IRP1A proteins. Blue signals represent DAPI staining. (d) Co-transfection of S2 cells with plasmids encoding Flag-tagged IRP1A, Flag-tagged EGFP and Myc-tagged $NTF2^{2D2A}$ mutant followed by immunoprecipitation and Western blotting. EGFP was used as a control.

3.3.6 Chickadee negatively regulated IRP1A nuclear import

Besides Ran and NTF2, Chickadee (Chic) was also identified by IRP1A MS as a candidate protein that may interact with *Drosophila* IRP1A. *chic* encodes an actin monomer-binding protein that is orthologous to the human profilin family member 4 (PFN4). Profilin family proteins have been suggested to regulate cellular iron homeostasis, given that non-canonical IREs were identified in the mouse *Pfn2* transcript [153]. In the MS data, IRP1A and Chic showed protein-protein interactions (PPIs) in both the third third-instar larvae raised on regular fly media and iron-depletion media induced by the iron chelator bathophenanthroline sulfate (BPS) (Appendix A1). Since BPS-mediated iron chelation in fly media promotes the conversion of holo-IRP1A to apo-

IRP1A for binding iron metabolism transcripts to upregulate cellular iron levels, we would expect higher levels of RNA-binding IRP1A in the *IRP1A*^{WT} animals reared on BPS-supplemented food. The MS data also revealed a strong PPI between Chic and IRP1A^{WT} in larvae raised on BPS-supplemented food for two consecutive generations, which made me reason that Chic may suppress IRP1A nuclear import by keeping RNA-binding IRP1A in the cytosol under low iron conditions.

To test whether Chic inhibits IRP1A nuclear import via protein binding, wild-type IRP1A and Chic were co-expressed in *Drosophila* S2 cells followed by co-IP via anti-Flag antibodies and Western blotting. Consistent with the IRP1A MS data, Chic showed a strong protein-protein interaction with IRP1A (Fig. 3.19a). Meanwhile, IRP1A did not interact with the Flag-tagged EGFP control. Based on my previous finding, holo-IRP1A targets NTF2 and Ran for its nuclear import. This led me to think that Chic may directly bind to holo-IRP1A such that the physical interaction between these two proteins would retain IRP1A in the cytosol, resulting in lower efficiency of IRP1A nuclear import. However, the strong PPI between Chic and IRP1A protein identified in transgenic *IRP1A*^{WT} larvae reared on BPS-supplemented food seemed to suggest the opposite: given that BPS chelates cellular iron which subsequently results in the switch of holo-IRP1A to apo-IRP1A, Chic may trap cytosolic IRP1A in the RNA-binding form via protein binding. To find out which scenario is occurring, I overexpressed Chic in S2 cells co-expressing IRP1A variant proteins. While the *IRP1A*^{C450S} cDNA encodes constitutively RNA-binding apo-IRP1A, the *IRP1A*^{3R3Q} cDNA results in non-RNA-binding IRP1A with a strongly reduced RNA-binding activity. Subsequent co-IP and Western blotting results showed that Chic specifically interacted

with RNA-binding IRP1A encoded by *IRP1A*^{C450S} cDNA but not with non-RNA-binding IRP1A encoded by *IRP1A*^{3R3Q} cDNA (Fig. 3.19b). This result was consistent with the previous IRP1A MS data, where Chic exhibited extensive protein interactions with IRP1A in larvae reared on iron-deprivation media.

I then sought to examine how Chic might be involved in regulating IRP1A nuclear import in iron-replete cells. As suggested by the previous study, Chic might function as a negative regulator of NTF2 in flies [113]. Thus, I reasoned that Chic may regulate IRP1A nuclear import via NTF2, given that NTF2 is a central regulator of IRP1A nuclear import. To test this idea, I co-expressed *Ntf-2* and *chic* cDNA in S2 cells, where I found that overexpressing Chic induced an accumulation of NTF2 in the cytosol (Fig. 3.19c). In contrast, NTF2 in control cells was found in both the nucleus and the cytosol. In addition, Chic showed a specific PPI with NTF2 in S2 cells (Fig. 3.19d). These results verified the previous notion that Chic is a suppressor of NTF2. Next, I wondered what could be the consequence of such inhibitory role of Chic on NTF2 in cellular iron homeostasis. Whether or not Chic negatively regulates IRP1A nuclear import via NTF2? Since holo-IRP1A is both required for the aconitase activity and the nuclear entry, I expressed *chic* cDNA in S2 cells co-expressing IRP1A^{3R3Q} to see whether the subcellular localization of IRP1A can be altered. In the control group, IRP1A^{3R3Q} was found in both the nucleus and cytosol with a predominantly nuclear localization in S2 cells (Fig. 3.19e). Overexpressing *chic* cDNA resulted in an accumulation of IRP1A in the cytosol, suggesting that Chic may function to inhibit IRP1A nuclear import. However, it should be noted that Chic physically interacted with RNA-binding IRP1A (Fig. 3.19b), but not

non-RNA-binding IRP1A. Thus, the sequestration of IRP1A in the cytosol by expressing Chic may not be due to direct protein binding of Chic and IRP1A^{3R3Q}, but rather more likely by an indirect regulatory mechanism, presumably through affecting NTF2 function in nuclear import. That being said, it is most likely that Chic first accumulates NTF2 in the cytosol, followed by the trap of holo-IRP1A in the cytosol.

Taken together, I provided molecular evidence showing Chic physically interacted with RNA-binding IRP1A in *Drosophila* S2 cells. Chickadee is a negative regulator of IRP1A nuclear import. In iron-depletion cells, Chic would preferentially bind to RNA-binding IRP1A. As such, less IRP1A can be converted to the holo-form followed by nuclear entry. In iron-replete cells, Chic strongly sequesters NTF2 and IRP1A in the cytosol, forming an inhibitory complex to inhibit IRP1A nuclear import. Furthermore, my results further emphasized the role of NTF2 in the regulation of IRP1A nuclear import. It implicated that only when NTF2 is expressed at an appropriate level across the nuclear membrane may the nuclear import of cargos be achieved.

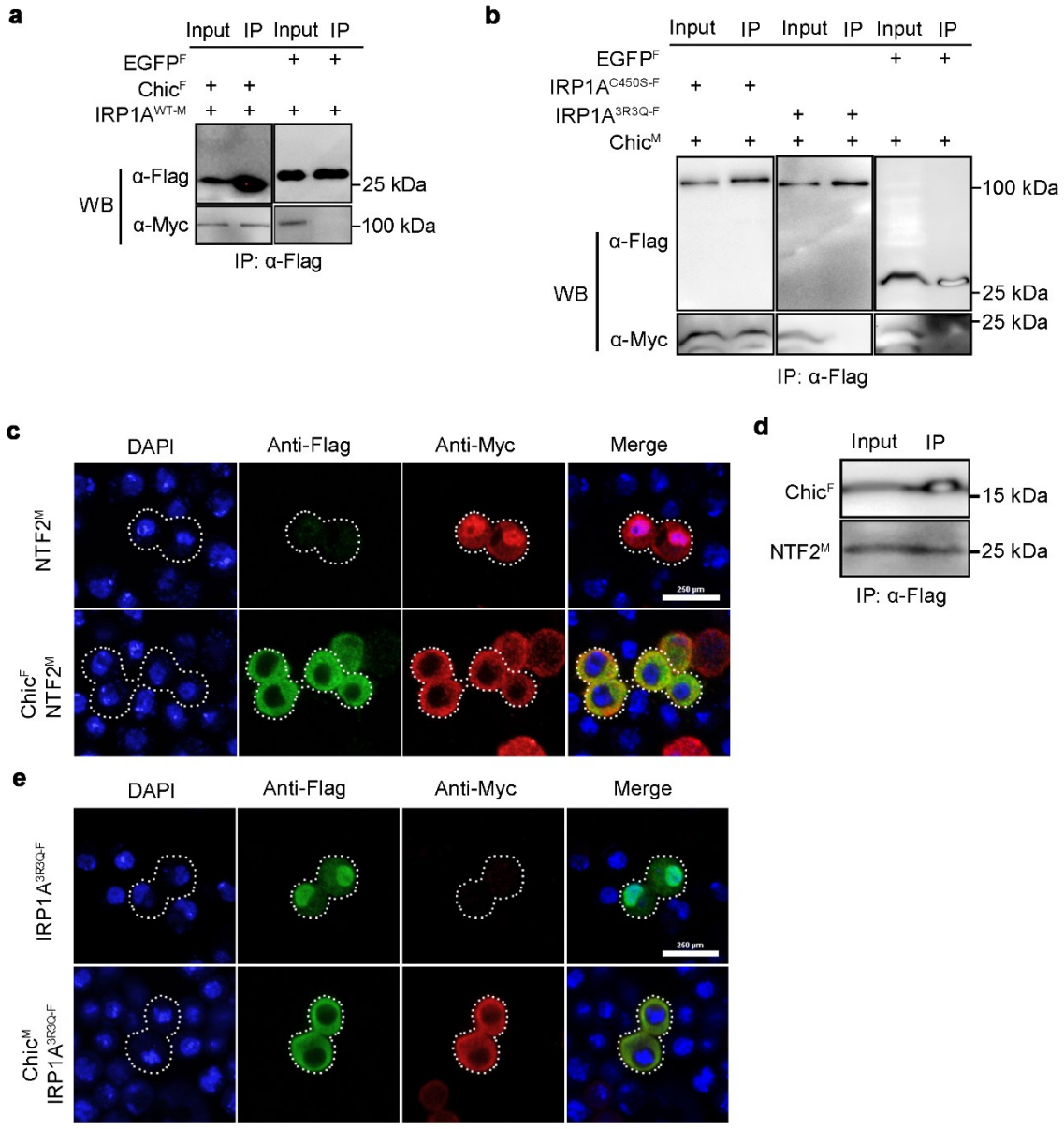

Figure 3.19 IRP1A nuclear import is suppressed by Chic overexpression.

(a) Co-transfection of S2 cells with plasmids encoding Flag-tagged Chic, Flag-tagged EGFP, and Myc-tagged IRP1A followed by immunoprecipitation via anti-Flag antibodies and Western blotting. EGFP was used as a control. (b) Transfection of S2 cells with plasmids encoding IRP1A variants and Chic followed by immunoprecipitation and Western blotting. (c) Co-expressing Chic in S2 cells with NTF2 protein for examining whether Chic has a role in regulating NTF2 subcellular

localization. Scale bar = 250 μm. (d) Co-transfection of S2 cells with plasmids encoding Flag-tagged Chic and Myc-tagged NTF2 followed by co-IP via anti-Flag antibodies and Western blotting. (e) Examining subcellular localization of IRP1A^{3R3Q} in S2 cells co-expressing Chic. Scale bar = 250 μm.

3.3.7 RanBP3 is required for nuclear export of IRP1A

As previously stated, *Drosophila RanBP3* encodes a protein that harbors the same functional domains and motifs as vertebrates (Fig. 3.4). Therefore, fly RanBP3 most likely also plays roles in regulating the nuclear export of macromolecules. Consistent with this idea, IRP1A, the central regulator of cellular iron homeostasis, appears to be one of the key candidates for RanBP3 mediated export. Losing *RanBP3* function in the PG resulted in the accumulation of IRP1A in the nucleus (Fig. 3.16). A few interesting questions were raised which need to be further studied. For example, mammalian RanBP3 functions as a cofactor of nuclear protein export by binding to key components in the pathway, such as CRM1 and RCC1. Does *Drosophila* RanBP3 have the same interactions with these proteins? What is the mechanism by which IRP1A is transported back to the cytosol? How is RanBP3 involved in the process? Lastly, since I have shown that holo-IRP1A but not apo-IRP1A is delivered into the nucleus via the Ran/NTF2 complex (Fig. 3.18 & Fig. 3.19), is there any molecular evidence showing which form of IRP1A (holo- or apo-IRP1A) can be recognized by the "nuclear export machinery" mediated by RanBP3?

To answer these questions, I adopted the cell culture approach since many of the genes/proteins that I am studying lack a corresponding transgenic line to produce tagged proteins *in vivo*. First, I examined the subcellular localization of CRM1 and RCC1, the only *Drosophila* ortholog of RanGEF, in S2 cells. Both proteins were found in the nucleus and the cytosol (Fig. 3.20a). Then, protein-protein interactions were examined via co-immunoprecipitation (co-IP) and Western blotting. Consistent with findings in vertebrates, CRM1 presented a strong interaction with RCC1 in S2 cells (Fig. 3.20b), therefore constituting a nuclear export complex essential for recognizing and delivering nuclear protein via NPCs. Meanwhile, RanBP3 also interacted with RCC1 and CRM1 in S2 cells (Fig. 3.20b), which most likely contributes to a stimulated export by enhancing the affinity of CRM1 for RanGTP and cargo proteins[154]. Therefore, *Drosophila* RanBP3 is similar to human and mouse counterpart proteins not only restricted to their sequence identities but also because they all promote nuclear protein export in a similar way to promote nuclear cargo loading efficiency.

My previous experiment has shown that *RanBP3* loss-of-function caused an accumulation of IRP1A in the PG cell nuclei (Fig. 3.16). However, the question raised by this finding was whether there was any molecular evidence showing that apo-IRP1A, but not holo-IRP1A, is targeted for nuclear export. Since IRP1A has no canonical nuclear export signal (NES) as most nuclear proteins do, I hypothesized that a "chaperon" protein would exist in the IRP1A nuclear export pathway to deliver the cargo (IRP1A) to the nuclear export complex composed of CRM1 and RCC1. Given that RanBP3 has been shown to associate both components in the nuclear export complex, I

wondered if RanBP3 could be the candidate protein that connects IRP1A and the CRM1/RCC1 complex. To test this idea, I co-transfected S2 cells with plasmids encoding RanBP3 and wild-type IRP1A, followed by co-IP and Western blotting. Interestingly, a band indicating protein-protein interaction between RanBP3 and IRP1A was observed (Fig. 3.20c), verifying the aforementioned idea that IRP1A is a target protein of RanBP3 for nuclear export. Then, I examined which form of IRP1A can interact with RanBP3 in S2 cells by co-transfection. Interestingly, RanBP3 was found to only interact with apo-IRP1A encoded by $IRP1A^{C450S}$, while no interaction was identified between RanBP3 and the non-RNA-binding form of IRP1A encoded by $IRP1A^{3R3Q}$ (Fig. 3.20d). These results altogether implicated that RanBP3 is essential for the nuclear export of IRP1A in *Drosophila* S2 cells, most likely by functioning as a cofactor to recognize and deliver IRP1A to the nuclear export complex constituted of CRM1 and RCC1. In addition, consistent with the finding where I showed that apo-IRP1A was trapped in the *RanBP3* loss-of-function PG cells, I provided molecular evidence showing RanBP3 only targets apo-IRP1A, but not holo-IRP1A, for nuclear export.

Taken together, I established a model demonstrating the mechanism by which IRP1A is transported across the nuclear membrane in *Drosophila* S2 cells. Specifically, the nuclear import of IRP1A is mediated by the nuclear import complex formed by Ran and NTF2. Chic is a negative regulator of IRP1A nuclear import by trapping NTF2 in the cytosol. Since the binding of IRP1A to mRNA transcripts occurs in the cytosol, nuclear-localized IRP1A needs to be transported back to the cytosol to function in the IRP1/IRE system. I identified RanBP3 as a novel regulator of IRP1A

nuclear export, which serves as a cofactor for CRM1-mediated nuclear export and function as a chaperon protein in delivering IRP1A to the nuclear export complex (Fig. 3.21).

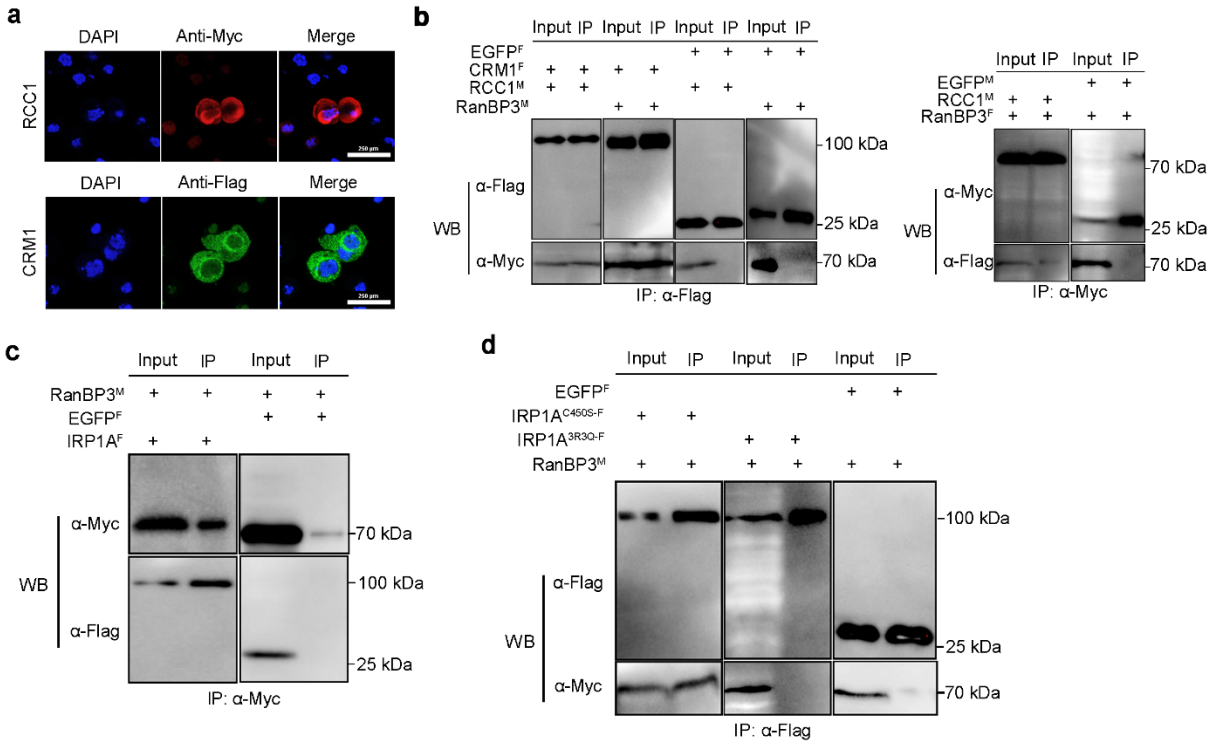

Figure 3.20 RanBP3 is a cofactor that regulates IRP1A nuclear export.

(a) Expressing RCC1 and CRM1 proteins in S2 cells followed by immunostaining and microscopy to examine protein subcellular localization. Scale bar = 250 μm. (b) Detecting protein-protein interactions via immunoprecipitation and Western blotting. EGFP was used as a control to test if there were any non-specific protein binding. (c) Co-transfection of S2 cells with plasmids encoding Myc-tagged RanBP3, Flag-tagged EGFP, and Flag-tagged IRP1A followed by immunoprecipitation via anti-Myc antibodies and Western blotting. (d) Examining the protein-protein interactions between IRP1A variant proteins and RanBP3 via immunoprecipitation and Western blotting.

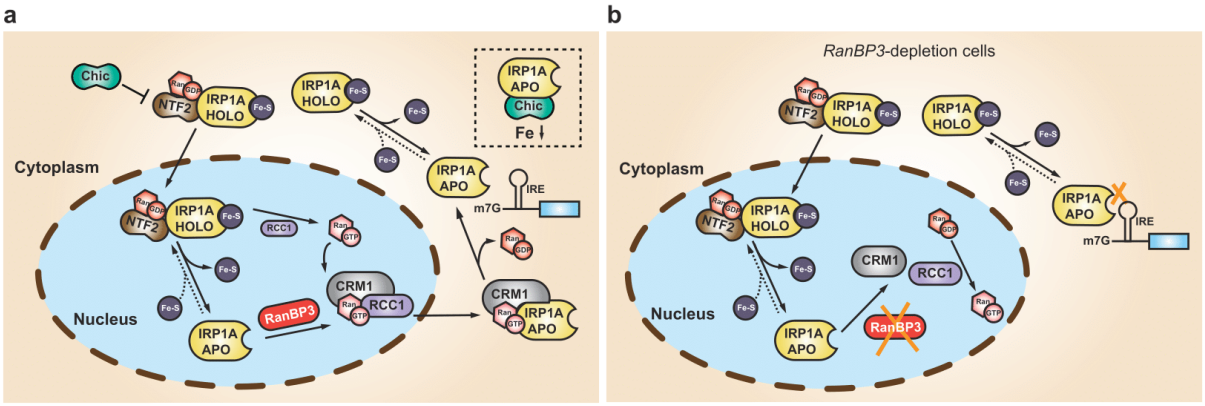

Figure 3.21 A model of IRP1A nucleocytoplasmic transport in *Drosophila* S2 cells.

(a) IRP1A interconverts between the apo- and holo-form in both the cytosol and the nucleus. Holo-IRP1A is transported into the nucleus by binding to the Ran/NTF2 complex. Chickadee negatively regulates IRP1A nuclear import by presenting interactions with NTF2, the central regulator of IRP1A nuclear import (in iron-replete cells), or RNA-binding IRP1A (in iron-deprived cells). Such interactions subsequently suppress IRP1A nuclear entry. In the nucleus, the GDP-GTP exchange factor (RCC1) catalyzes the disassociation of holo-IRP1A and NTF2 from the nuclear import complex. RanBP3 physically interacts with apo-IRP1A, followed by delivering IRP1A to the nuclear export complex formed by CRM1 and RCC1. In the cytosol, GTP hydrolysis of RanGTP to RanGDP dissociates IRP1A from the complex to replenish cytosolic RNA-binding IRP1A. (b) In *RanBP3*-depletion cells, the nuclear export of apo-IRP1A would be strongly reduced due to the lack of RanBP3 function in the nucleus. This subsequently results in low levels of cytosolic IRP1A that binds iron-responsive elements (IREs) located in untranslated regions (UTR) of specific mRNAs acting in cellular iron metabolism.

3.3.8 RanBP3 regulates intracellular iron trafficking via Gp93 and ERp60

In section 3.3.2, I have shown that the lethality and the porphyria-like phenotype in *phm22>RanBP3^{IR}* animals can be partially rescued by rearing animals on hemin-supplemented fly media or ectopically expressing *hTfR* allele to increase cellular iron import, which provided an interesting link of RanBP3 to cellular iron acquisition and regulation. In section 3.3.3, I demonstrated that both *Drosophila* RanBP3 isoforms accumulated in the nucleus, but with a small portion localized to the cytosol (Fig. 3.13). The cytosolic localization of RanBP3 proteins suggested a possibility that RanBP3 may have novel roles in addition to regulating nuclear protein export. In this section, I will further expand the topic by introducing a novel function of RanBP3 to regulate intracellular iron transport from the cytosol to the mitochondria via *Drosophila* mitoferrin (Mfrn).

Intracellular iron is incorporated into prosthetic groups, for example, heme and iron-sulfur clusters that function in a multitude of biochemical processes. Although functionally distinct, assembly of both iron cofactors requires mitochondrial iron assimilation to deliver iron into the organelle [155]. In vertebrates, iron is imported into mitochondria via two transporters: mitoferrin-1 (Mfrn1) and mitoferrin-2 (Mfrn2), which showed spatially differentiated distribution pattern [134, 135]. While *mfrn2* is ubiquitously expressed, *mfrn1* is only found in differentiating erythroid cells. Although the loss of *mfrn1* in zebrafish and mice disrupts both the heme and ISC synthesis, none of them develop porphyria [134, 156]. This could be possible because, in the absence of Mfrn1-

mediated mitochondrial iron import, IRP1 protects against porphyria by binding to the 5' IREs located in *Alas2*, which encodes the enzyme that catalyzes the first step in the heme biosynthetic pathway [157]. The binding of IRP1 to 5'-UTR IREs inhibits the translation of ALAS to lower the demand for heme biosynthesis. As demonstrated in section 3.3.2, *RanBP3* loss-of-function cannot be rescued by elemental iron supplementation. In contrast, *IRP1A* knockout animals are rescuable by dietary supplementation of FAC as an iron source [91]. This raised the possibility that RanBP3 might have a role in transporting cytosolic iron into the mitochondria for efficient heme biosynthesis and ISC biogenesis. Since this hypothesis might involve a novel function for RanBP3 in regulating cellular iron homeostasis independent of IRP1A function, I conducted a MALDI-TOF-based mass spectrometry assay to identify tentative RanBP3-interacting proteins using *Drosophila* S2 cells.

As introduced in section 3.3.3, *RanBP3* encodes two spliced isoforms that differ in one amino acid at the beginning of exon 2 (Fig. 3.4). Preliminary data showed that this one-amino acid difference in the polypeptide sequence might be related to the different subcellular localizations of RanBP3 (Fig. 3.13). To characterize the roles of RanBP3, I examined the interactome of both isoforms via mass spectrometry (Fig. 3.22a). While a total of 48 proteins (co-immunoprecipitated proteins found in controls were excluded) were identified as potential interactors of RanBP3a (Table 3.5), only six tentative RanBP3 interactors were identified using RanBP3b as the bait (Table 3.6). Only three candidate proteins were found as the overlap between the two data sets. One of the overlapping proteins was RanBP3 itself, while the other two were CG18501 and Glycoprotein 93

(Gp93). Gp93 seemed to be a possible candidate involved in regulating cellular iron homeostasis for a few reasons. First, *Gp93* encodes a heat shock protein Hsp90 family member involved in midgut development [158]. Gp93 is found in both the extracellular space and in the endomembrane system [159, 160]. The differential expression pattern may most likely be due to the presence of a signal peptide (predicted by SAM: SignalIP) located at the N-terminal of this protein. Furthermore, *Gp93* mutants display a significant growth defect showing the third-instar larval arrest [158], which recapitulates what I saw in the *RanBP3* loss-of-function animals. A previous case study showed that seven patients with erythropoietic protoporphyria (EPP) had aberrant transcripts identified in *mfrn1* exons and splice junctions, which led to the sequestration of Mfrn1 in the cytosol by colocalizing with Hsp90 [161]. Lastly, the genomic loci of *Gp93* and *Drosophila mitoferrin* (*dmfrn*) are close, with a less than one-kilo base pair (bp) distance between each other (Fig. 3.23a), suggesting a potential genetic interaction of these two genes, for example, to coordinately regulate intracellular iron transport.

To examine the putative link between RanBP3 and Gp93, I first examined whether the protein-protein interaction between RanBP3 and Gp93 identified by MS can be verified. I generated a plasmid encoding the C-terminal Flag-tagged Gp93, as well as two mutant constructs, where I deleted functional domains of Gp93 using site-directed mutagenesis (Fig. 3.23b, c). The HATPase domain is found in many proteins that show ATP-binding activity, such as heat shock protein HSP90 family proteins. The Heat shock protein Hsp90 family (Hsp90_fam) domain is a common feature identified in heat shock proteins that act to maintain proper protein folding within the cell

[162]. Mutant plasmids that lack either of these two functional domains were designated as $Gp93^{\Delta HATPase}$ and $Gp93^{\Delta Hsp90}$, respectively. Following co-IP and Western blotting, neither of the mutants, but the wild-type protein, showed a protein-protein interaction with RanBP3 (Fig. 3.22b). This result suggested that both the HATPase and the Hsp90 domain are essential for a complete Gp93 function. Since SAM: SignalP identified a signal peptide at the amino acid 1 to 20 in the coding sequence of Gp93 protein, I then made a third mutant construct, $Gp93^{\Delta SS}$ (Fig. 3.23c), where I removed the signal peptide and compared protein subcellular localization to that of the wild-type protein. Interestingly, $Gp93^{\Delta SS}$ showed no significant difference to the wild-type Gp93 (Fig. 3.22c). Both proteins showed a punctate distribution pattern in S2 cells, suggesting that the protein may most likely localize to the endomembrane system rather than be secreted into the extracellular matrix.

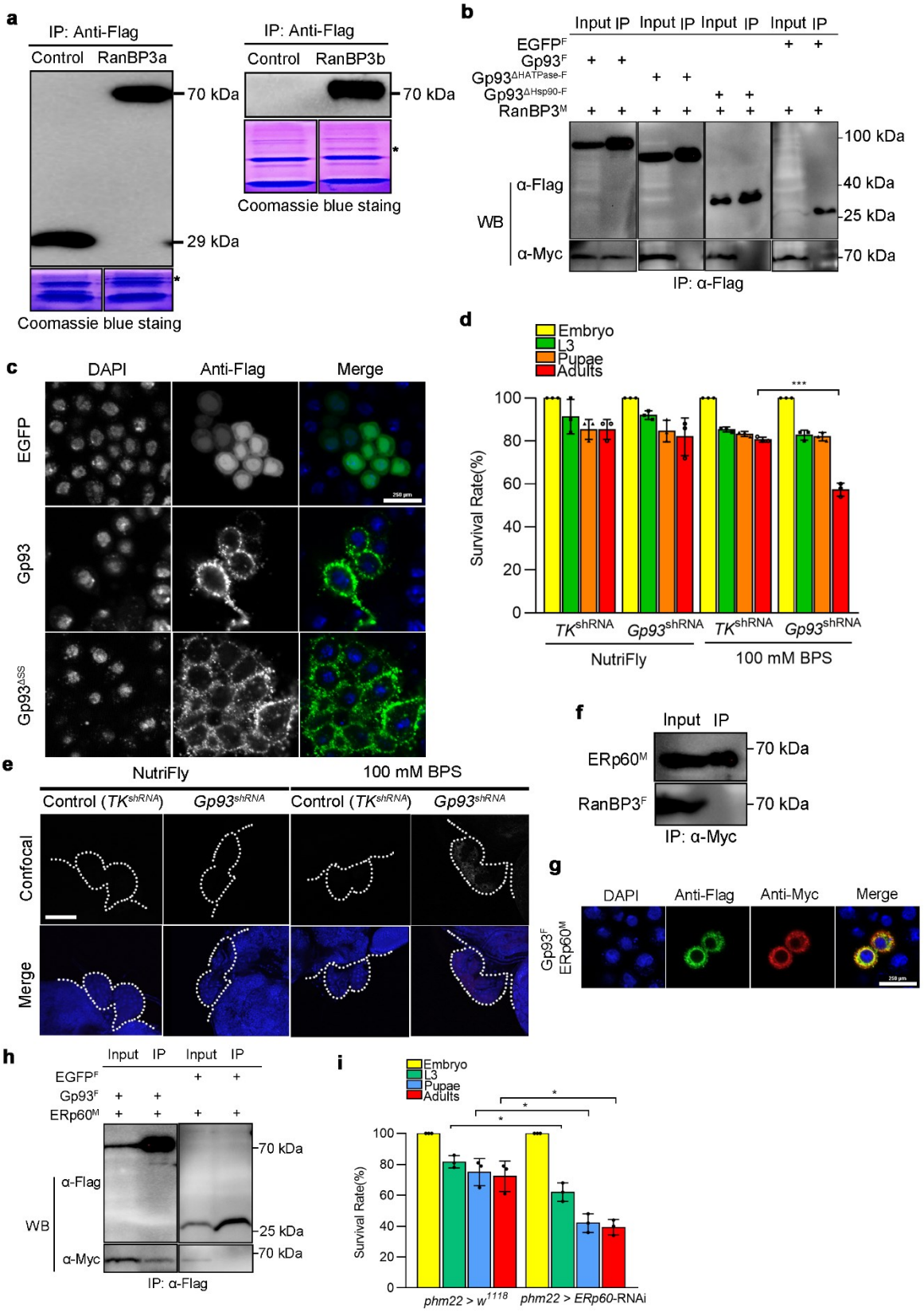
a
IP: Anti-Flag
Control RanBP3a
70 kDa
29 kDa
Coomassie blue staing
IP: Anti-Flag
Control RanBP3b
70 kDa
Coomassie blue staing
b
Input IP Input IP Input IP Input IP
EGFP^F
Gp93^F
Gp93^ΔHATPase-F
Gp93^ΔHsp90-F
RanBP3^M
100 kDa
40 kDa
25 kDa
70 kDa
WB
α-Flag
α-Myc
IP: α-Flag
c
DAPI
Anti-Flag
Merge
EGFP
Gp93
Gp93^ΔSS
d
Embryo
L3
Pupae
Adults
Survival Rate(%)
TK^shRNA
Gp93^shRNA
TK^shRNA
Gp93^shRNA
NutriFly
100 mM BPS
e
NutriFly
100 mM BPS
Control (TK^shRNA)
Gp93^shRNA
Control (TK^shRNA)
Gp93^shRNA
Confocal
Merge
f
Input IP
ERp60^M
RanBP3^F
70 kDa
70 kDa
IP: α-Myc
g
DAPI
Anti-Flag
Anti-Myc
Merge
Gp93^F
ERp60^M
h
Input IP Input IP
EGFP^F
Gp93^F
ERp60^M
70 kDa
25 kDa
70 kDa
WB
α-Flag
α-Myc
IP: α-Flag
i
Embryo
L3
Pupae
Adults
Survival Rate(%)
phm22 > w^1118
phm22 > ERp60-RNAi

Figure 3.22 RanBP3 interacts with Gp93 and ERp60 in S2 cells.

(a) Mass spectrometry using *Drosophila* S2 cells. Flag-tagged EGFP was used as a control for RanBP3a, whereas the pAFW (empty vector) was used as the control for RanBP3b. Asterisks represent enriched RanBP3 proteins visualized by Coomassie blue staining. (b) Co-transfection of S2 cells with plasmids encoding Flag-tagged Gp93 and Myc-tagged RanBP3 proteins followed by immunoprecipitation via anti-Flag antibodies and Western blotting. Flag-tagged EGFP was used as a control. (c) Subcellular localization of Gp93 and Gp93 mutant without the secretion signal in S2 cells. Scale bar = 250 μm. (d) The survival rate of *Gp93* loss-of-function animals supplemented with normal diet and BPS-mediated iron deprivation diet. Error bars represent standard deviation. *p<0.05, **p<0.01, ***p<0.001. (e) Confocal microscopy of dissected ring glands from 40-42 hours third-instar larvae raised on the normal or low-iron diet. Scale bar = 500 μm. Signals of confocal microscope images on the top row represent red auto-fluorescence in grey scale for easier visualization. Blue signals on the bottom row represent DAPI staining. (f) Co-transfection of S2 cells with plasmids encoding Myc-tagged ERp60 and Flag-tagged RanBP3 followed by immunoprecipitation via Myc antibodies and Western blotting. (g) Co-transfection of S2 cells with plasmids encoding Flag-tagged Gp93 and Myc-tagged ERp60 followed by immunostaining and microscopy. Scale bar = 250 μm. (h) Co-transfection of S2 cells with plasmids encoding Flag-tagged Gp93 and Myc-tagged ERp60 followed by immunoprecipitation via anti-Flag antibodies and Western blotting. (i) Survival quantification of *phm22>ERp60*-RNAi and *phm22>ERp60*-RNAi animals. Error bars represent standard deviation. *p<0.05, **p<0.01, ***p<0.001.

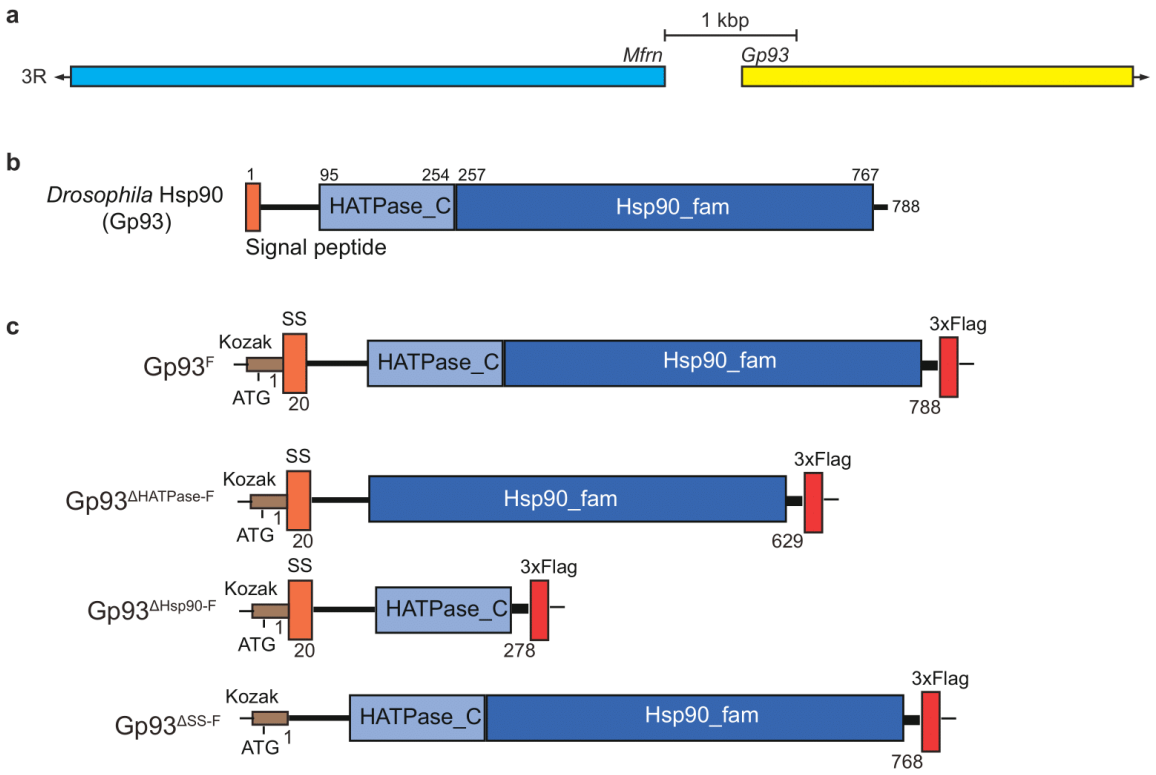

Figure 3.23 Schematic demonstration of Gp93 functional domains.

(a) Genetic locus of *Gp93* in the *Drosophila* genome. *Mitoferrin (Mfrn)* is located less than one-kilo base pair (kbp) apart. (b) Schematic demonstration of the functional domains and motifs in Gp93. A signal peptide has been reported in Gp93, located at the beginning of the coding region. HATPase domain is found in many proteins that show ATP-binding activity. Hsp90 chaperones are unique in their ability to regulate a specific subset of cellular signaling proteins that have been implicated in disease processes. (c) Plasmids encoding C-terminal Flag-tagged Gp93 and Gp93 mutants.

Table 3.5 Tentative RanBP3 isoform A-interacting proteins identified via MS.

Accession	Protein encoded	Score	# Proteins
A0A0B4KGQ0	RanBP3 isoform A[a]	224.50	2
Q9VC93	Dis3	30.42	1
Q9VK19	Ski6	19.65	1
P09180	RpL4 PE	12.68	1
P08928	Lam	12.65	1
Q9VMM3	CG7239	10.98	1
P39018	RpS19a	10.94	1
Q9VKJ4	Csl4	9.75	1
Q9W1B9	RpL12	9.25	1
Q9V3Q4	Jafrac2	8.56	1
P08570	RpLP1	8.30	1
Q9VNE9	RpL13A	8.02	1
Q24208	eIF-2gamma	7.88	1
P41042	RpS4	7.37	1
Q9VFF3	Rrp6	7.20	1
Q9VXL4	Rrp47	6.97	1
Q95RJ9	ebi	6.53	1
P41374	eIF-2alpha	6.42	1
Q9VPK3	CG18501[a]	6.01	2
Q9VAY2	Gp93[a]	5.66	1
Q29QQ9	Rrp42	5.54	1
Q9VTP4	RpL10Ab	5.47	1
Q9VN50	eIF3-S5-1	5.43	1
Q9V9W2	RpL6	5.30	2
P41093	RpL18A	5.18	1
P20240	Ote	4.97	1
P41092	RpL27A	4.88	1
O61231	RpL10	4.87	1
X2JC80	Sta	4.77	2
Q9W5N2	RpL38	4.75	1
Q9V426	vig	4.60	1
Q9VFV9	Droj2	4.51	1
Q9V455	Kap-alpha3	4.41	1
Q9W4M9	Nsun2	4.26	1
O96827	Ef1beta	4.23	1

P13060	EF2	3.92	1
Q3YMU0	ERp60	3.85	1
A0A0B4LGB7	SERCA	3.84	2
P41126	RpL13	3.76	1
P14130	RpS14a	3.73	1
P46223	RpL7A	3.45	1
P46222	RpL11	3.34	1
Q9VS34	RpL18	3.31	1
P50882	RpL9	2.06	1
Q9VFT4	rin	2.05	1
O18640	Rack1	1.87	1
Q76NQ0	CG33303	1.82	1
A0A0B4JD24	CG17002	0.00	3

[a]Proteins that were also identified from RanBP3 isoform B mass spectrometry.

Table 3.6 Tentative RanBP3 isoform B-interacting proteins identified via MS.

Accession	Protein encoded	Score	# Proteins
A0A0B4KGQ0	RanBP3 isoform B[a]	46.61	2
Q8IPX7	Rrp40	15.21	1
Q9VAY2	Gp93[a]	8.1	1
P17704	RpS17	7.84	1
P29845	Hsc70-5	7.36	1
Q9VPK3	CG18501[a]	7.14	2

[a]Proteins that were also identified from RanBP3 isoform A mass spectrometry.

Gp93 function is essential for normal growth of *Drosophila*. P-element excision from the P{EPgy2}*Gp93*^{EY06213} allele results in *Gp93* loss-of-function mutants, which died as third instar larvae [158]. However, no evidence indicates that Gp93 is directly linked to ecdysone biosynthesis in the prothoracic gland. To test whether Gp93 is involved in ecdysteroidogenesis, I disrupted the gene function by using the short-hairpin-mediated RNA interference (shRNA) coupled with the PG driver *phm22-Gal4*. As a control, *TK*^{shRNA} that carries the empty vector used to generate the shRNA lines was crossed to *phm22-Gal4*. As a result, knocking down *Gp93* in PG cells did not affect the development of animals reared on normal fly media (Fig. 3.22d). However, iron deprivation via supplementing the fly media with BPS (an iron chelator) significantly decreased the number of *Gp93*^{shRNA} animals that developed to adults. In addition, iron chelation also induced a weak but discernible red auto-fluorescence in the PG when *Gp93*^{shRNA} third-instar larvae were exposed under UV light (Fig. 3.22e). These results were consistent with the previous notion that Gp93 might have a role in cellular iron metabolism, presumably cellular iron trafficking. And the reason why I did not observe a strong porphyria-like phenotype was possibly because Gp93 might require a partner protein for fulfilling its role in cellular iron homeostasis. Intrigued by this possibility, I looked back to RanBP3 MS data. I found endoplasmic reticulum protein 60 (ERp60), identified as a potential RanBP3 isoform A-interacting protein, may work cooperatively with Gp93 in cellular iron regulation. Surprisingly, RanBP3 failed to interact with ERp60 when I attempted to validate this interaction in S2 cells, which was unexpected (Fig. 3.22f). However, since both ERp60 and Gp93 localized to the endomembrane system and showed a significant co-localization in S2 cells (Fig.

3.22g), I reasoned that ERp60 might be associated with Gp93 such that both proteins were found presenting protein-protein interaction with RanBP3. Consistent with this idea, a PPI was found between ERp60 and Gp93 in S2 cells, explaining why ERp60 was identified as a RanBP3-interacting protein in the MS assay (Fig 3.22h). In addition, losing *ERp60* function in the PG also suppressed the development of animals compared to the control (Fig. 3.22i).

Then, I sought to examine the function of the Gp93/ERp60 complex in regulating intracellular iron trafficking. As mentioned above, the *Gp93* gene lies physically close to the *dmfrn* gene, with less than one kbp separating the two. In addition, Mfrn, when expressed in S2 cells, showed a similar punctuate expression pattern to Gp93 (Fig. 3.24a), which suggested a potential link between these two proteins. To test this idea, I co-expressed Mfrn and Gp93/ERp60 in S2 cells to examine whether these proteins would co-localize. As a result, these three protein signals showed only limited portion that overlapped with each other (Fig. 3.24b), which made sense because ER is a membrane tissue spread out within the cell, therefore creating some junctions with other organelles, like mitochondria. Consistent with this idea, I found that Gp93 and ERp60 can physically interact with Mfrn in S2 cells (Fig. 3.24c), providing an interesting link between the Gp93/ERp60 complex and the regulation of intracellular iron transport via Mfrn. Further evidence was shown by co-transfection of S2 cells with plasmids encoding Mfrn and Gp93$^{\Delta HATPase}$ or Gp93$^{\Delta Hsp90}$ followed by immunostaining and co-IP. Neither Gp93$^{\Delta HATPase}$ nor Gp93$^{\Delta Hsp90}$ co-localized with Mfrn in S2 cells (Fig. 3.24d). In addition, none of these two Gp93 mutants can interact with Mfrn (Fig. 3.24e). Collectively, these results suggested that both the HATPase and Hsp90 domains were essential for

binding Mfrn in S2 cells. Moreover, these results showed that mitoferrin, an iron transporter targeting the mitochondrion for delivering cytosolic iron, can interact and most likely be modified by proteins that localize to the ER membrane. It could be possible that Gp93, as a heat shock family protein, can modulate mitoferrin function in different ways. For instance, it might prevent protein aggregation and degradation, keep the protein in a conformation that permits activation, etc.

Lastly, given that Gp93 has been reported to display a protein-protein interaction with ferritin 1 heavy chain homolog [163], I wondered if the same interaction is valid in S2 cells. To test this, I generated a plasmid to express Fer1HCH in S2 cells and verified physical interactions via co-IP and Western blotting (Fig. 3.25). The interaction caught in S2 cells between Gp93 and Fer1HCH suggested that ferritin might be another target protein whose function can be modulated by the Gp93/ERp60 complex.

Taken together, I proposed a model where I showed that RanBP3 plays multiple roles in *Drosophila* cellular iron regulation (Fig. 3.26). First, losing *RanBP3* function in the PG interrupts the Tsf-Fe (III) uptake pathway, in which the *Drosophila* homolog of the human TfR1 needs to be further characterized. Second, RanBP3 is essential for cellular iron regulation by functioning as a cofactor for IRP1A nuclear export. The mechanism by which IRP1A is transported across the nuclear membrane has been previously demonstrated (section 3.3.5 to 3.3.7). Last but not least, RanBP3 may also have a role to regulate intracellular iron transport from the cytosol to the mitochondria. An ER-mitochondria link was established via the protein-protein interactions between Gp93/ERp60 complex and mitoferrin, the only *Drosophila* homolog of mammalian

MFRN1/MFRN2. In addition, Gp93 also displayed a physical interaction with Fer1HCH in *Drosophila* S2 cells. Since Gp93 is a heat shock family protein, I reasoned that the central role of the Gp93/ERp60 complex might be to modulate the protein function of these cellular iron transporters such that intracellular iron can be effectively transported into the mitochondria to make heme and ISCs.

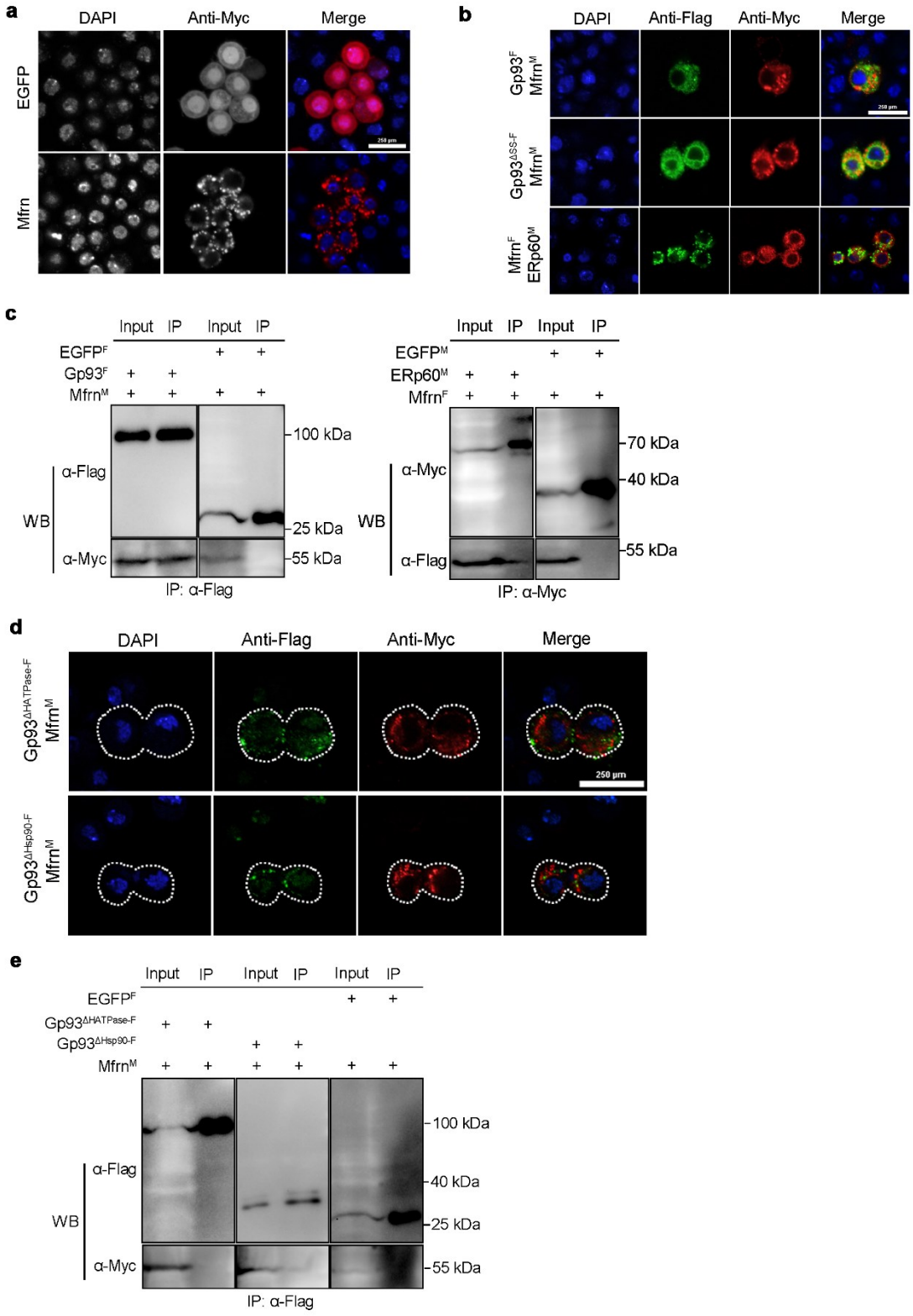
a
DAPI
Anti-Myc
Merge
EGFP
Mfrn
b
DAPI
Anti-Flag
Anti-Myc
Merge
Gp93F MfrnM
Gp93ΔSS-F MfrnM
MfrnF ERp60M
c
Input IP Input IP
EGFPF
Gp93F
MfrnM
100 kDa
25 kDa
55 kDa
α-Flag
α-Myc
WB
IP: α-Flag
EGFPM
ERp60M
MfrnF
70 kDa
40 kDa
55 kDa
α-Myc
α-Flag
WB
IP: α-Myc
d
DAPI
Anti-Flag
Anti-Myc
Merge
Gp93ΔHATPase-F MfrnM
Gp93ΔHsp90-F MfrnM
250 μm
e
Input IP Input IP Input IP
EGFPF
Gp93ΔHATPase-F
Gp93ΔHsp90-F
MfrnM
100 kDa
40 kDa
25 kDa
55 kDa
α-Flag
α-Myc
WB
IP: α-Flag

Figure 3.24 Gp93/ERp60 complex interacts with mitoferrin in S2 cells.

(a) Examining mitoferrin (Mfrn) subcellular localization in S2 cells. Scale bar = 250 μm. (b) Co-transfection of S2 cells with plasmids encoding Gp93 or ERp60, and Mfrn followed by immunostaining and microscopy. Scale bar = 250 μm. (c) Examining whether Gp93/ERp60 complex displays protein-protein interactions with Mfrn in S2 cells via co-IP and Western blotting. (d) Co-transfection of S2 cells with plasmids encoding Mfrn and mutant Gp93 proteins followed by examining co-localization of proteins via immunostaining. Scale bar = 250 μm. (e) Co-transfection of S2 cells with plasmids encoding Flag-tagged Gp93 mutants and Myc-tagged Mfrn followed by immunoprecipitation via anti-Flag antibodies and Western blotting.

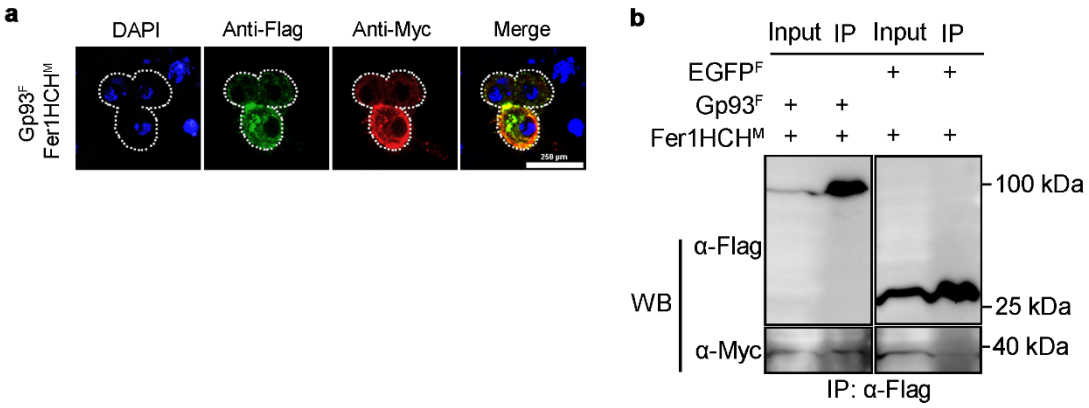

Figure 3.25 Verifying the physical interaction between Gp93 and Fer1HCH in S2 cells.

(a) Co-expressing Gp93 and Fer1HCH in S2 cells followed by immunostaining and microscopy. Scale bar = 250 μm. (b) Co-transfection of S2 cells with plasmids encoding Flag-tagged Gp93, Flag-tagged EGFP, and Myc-tagged Fer1HCH followed by immunoprecipitation via anti-Flag antibodies and Western blotting.

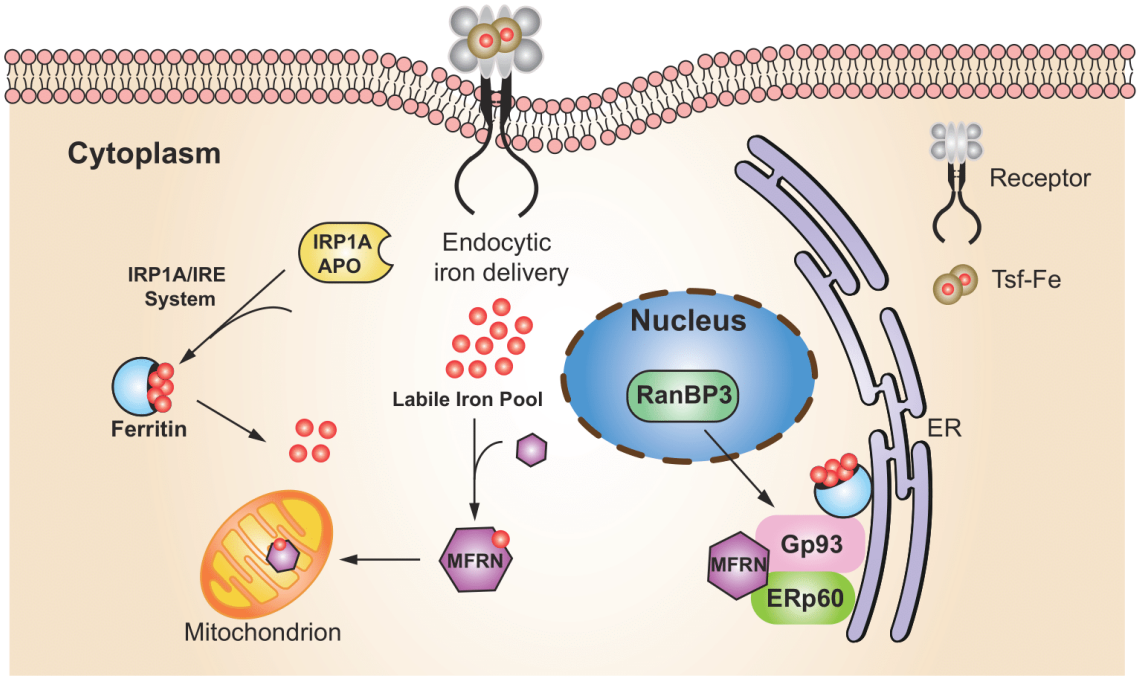

Figure 3.26 A model for RanBP3 in cellular iron regulation.

Cellular iron is acquired via different pathways. In *Drosophila*, transferrin-bound iron may most likely be absorbed via binding to an unknown receptor protein located on the cell membrane, highlighting the same mechanism by which human TfR1-mediated iron import via endocytosis. RanBP3 sustains cytosolic levels of RNA-binding IRP1A, which regulates cellular iron homeostasis via the IRP1A/IRE system. Two ER-bound proteins, namely Gp93 and ERp60, physically interact with mitoferrin and ferritin 1 heavy chain homolog, which might be essential for transporting cytosolic iron into the mitochondrion for iron-dependent biological processes, such as heme biosynthesis and iron-sulfur cluster biogenesis.

3.3.9 Expressing the transgenic *IRP1B* allele in *RanBP3* loss-of-function PG cells

Mammalian iron homeostasis is primarily regulated through the post-transcriptional control of gene expression by IRP proteins (IRP1 and IRP2) binding to specific mRNA transcripts that contain IREs. However, the *Drosophila* genome encodes two IRP1-like proteins (IRP1A and IRP1B) but lacks an IRP2 ortholog. Of the two IRP1 proteins in *Drosophila*, only IRP1A is believed to act in cellular iron homeostasis by binding to IREs [85]. IRP1B, on the other hand, has been suggested to function as an aconitase in flies. From an evolutionary point of view, this could be caused by a duplication of the ancient cytosolic aconitase in insects, with one variant acquiring the IRE-binding activity [85]. Consistent with this finding, losing *IRP1B* function in the prothoracic gland, either by RNA interference or genetic ablation via CRISPR/Cas9, did not show any obvious phenotype [91]. In contrast, *IRP1A* loss-of-function animals displayed significant larval lethality, which was rescued by iron supplementation. These results collectively suggest that IRP1A, but not IRP1B, is the central regulator of cellular iron homeostasis in *Drosophila*.

The subcellular localization of IRP1A and IRP1B showed both similarities and differences. Specifically, the expression of the tagged transgenes showed that both IRP1A and IRP1B were enriched in PG nuclei [91]. Expressing the single-point mutation variants $IRP1A^{C450S}$ or $IRP1B^{C447S}$ (which is predicted to abolish Fe-S binding in IRP1B) resulted in predominantly cytosolic accumulation of either protein. Since we know that IRP1A is expected to have a conformational change from the holo- to apo-form under iron-depletion conditions, one would reason that this

could result in an accumulation of IRP1A in the cytosol. While one generation of iron deprivation on BPS-supplemented food is sufficient for IRP1A to become entirely cytoplasmic in fat body cells, IRP1B does not show the same behavior and remains nuclear after three generations of iron depletion [91]. These results raised some interesting questions: If IRP1B only functions as a cytosolic aconitase in flies, why does it enter the nucleus, even when the cellular iron level drops? And what caused the different subcellular localization of IRP1A and IRP1B and the difference between tissues? Is RanBP3 involved in regulating IRP1B nuclear export, similar to what it does for IRP1A?

As demonstrated in section 3.3.4, losing *RanBP3* function in PG cells resulted in an accumulation of IRP1A in the nucleus, which suggested a role of RanBP3 in regulating IRP1A nuclear export. In addition, the expression of the transgenic $IRP1A^{C450S}$ allele rescued the porphyria-like phenotype induced by *RanBP3* loss-of-function. This led me to think whether expressing the transgenic $IRP1B^{C447S}$ allele would behave the same in *RanBP3*-depletion PG cells since the single point mutation in the $IRP1B^{C447S}$ allele was predicted to abolish the Fe-S binding activity, similar to the $IRP1A^{C450S}$ allele. To test this, I knocked down *RanBP3* in PG cells that co-expressed transgenic *IRP1B* alleles. While the single-point mutation is predicted to abolish the Fe-S binding activity in $IRP1B^{C447S}$, three-point mutations in $IRP1B^{3R3Q}$ altogether result in no RNA-binding activity of the protein [91]. Interestingly, expression of the transgenic $IRP1B^{WT}$ or $IRP1B^{3R3Q}$ allele did not rescue the accumulation of porphyrins in the *RanBP3*-RNAi PG cells (Fig. 3.27a), whereas the porphyria-like phenotype was rescued by expressing the $IRP1B^{C447S}$ allele. This

result suggested that IRP1B^{C447S} may function the same as IRP1A^{C450S} to regulate cellular iron homeostasis via binding to specific mRNAs that harbor IREs. Given that the binding of IRP1A to the transcripts of *Fer1HCH* and *SdhB* can only explain certain aspects of cellular iron homeostasis, IRP1 proteins in *Drosophila*, including both IRP1A and IRP1B, might have novel target transcripts containing non-canonical IREs. Further work, such as a ChIP-Seq analysis, should be conducted to identify more transcripts whose gene expression is under the control of the post-transcriptional regulation via the IRP1/IRE system.

Next, I examined the subcellular localization of IRP1B proteins in *RanBP3* loss-of-function PG cells. Both IRP1B^{WT} and IRP1B^{3R3Q} were found to have nuclear and cytosolic localization, whereas IRP1B^{C447S} was found to be accumulated predominantly in the cytosol (Fig. 3.27b). Interestingly, upon the introduction of *RanBP3*-RNAi, the nuclear signal of both IRP1B^{WT} and IRP1B^{3R3Q} proteins were significantly decreased, suggesting that RanBP3 might have a role in keeping IRP1B in PG cell nuclei. In agreement with this idea, since IRP1B^{C447S} was exclusively cytosolic, losing *RanBP3* function cannot alter the subcellular localization of IRP1B^{C447S} like what it does with the other IRP1B proteins. This result was opposite to what I have shown previously regarding the role of RanBP3 in promoting the nuclear export of IRP1A (Fig. 3.16). However, it should be noted that the accumulation of IRP1B in the nucleus did not increase the survival rate of *RanBP3*-RNAi animals (Fig. 3.27c) and seemed to have no effect on rescuing the porphyria-like phenotype of *RanBP3*-RNAi animals (Fig. 3.27a). Collectively, these results suggested that IRP1B may have a minor role in cellular iron regulation by binding to specific mRNAs that harbor non-

canonical IREs. Future work should focus on identifying novel transcripts that contain IRP1A and IRP1B binding sites in *Drosophila* genome.

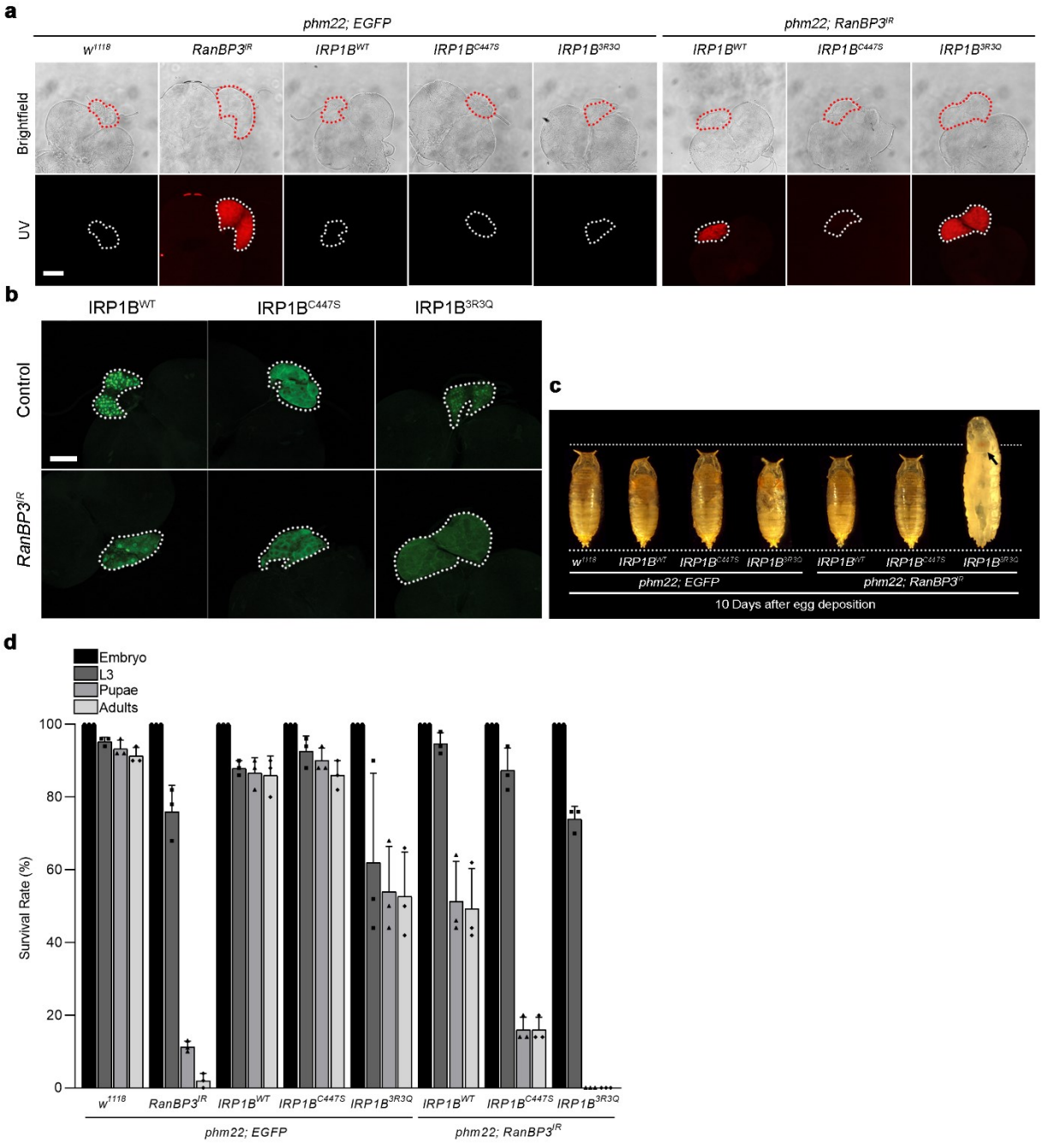

Figure 3.27 Expressing transgenic *IRP1B* alleles in *RanBP3* loss-of-function PG cells.

(a) UV exposure of dissected ring glands from 40-42 hours third-instar larvae expressing transgenic *IRP1B* alleles. Scale bar = 250 μm. (b) Subcellular localization of IRP1B and IRP1B variant proteins when knocking down *RanBP3* in the PG. Scale bar = 250 μm. (c) Development of animals

overexpressing IRP1B proteins in *RanBP3* loss-of-function PG cells. Arrow indicates PG cells that accumulated protoporphyrin. (d) Survival rate quantification of animals overexpressing IRP1B and IRP1B variants in control or *RanBP3*-depletion PG cells. Error bars represent standard deviation.

3.4 Discussion and future directions

3.4.1 The nuclear localization of IRP1A is supported by molecular and genetic evidence

IRP1A, as the central regulator of cellular iron homeostasis, has been reported by our lab to localize in the nuclei of both fat body and PG cells [91]. Strikingly, one generation of BPS (iron chelator) supplementation in *Drosophila* media was sufficient to induce a complete translocation of IRP1A from the nucleus to the cytosol, suggesting that IRP1A can shuttle across the nuclear membrane in response to cellular iron levels [91]. Additional evidence showing IRP1A can localize to the nucleus in flies was provided by both the transcriptome analysis of transgenic *IRP1A* alleles in the PG, and the interactome of $IRP1A^{3F}$ encoded by a Flag-tagged *IRP1A* CRISPR knock-in allele [91]. Specifically, nuclear IRP1A responds to high iron demand, and is required for downregulating the expression of genes acting in iron-dependent processes, such as steroidogenesis and heme/iron homeostasis. My study followed up on these studies where I identified several key factors for IRP1A nuclear import. The absence of a known NLS sequence led me to find Ran and NTF2 from the transgenic *IRP1A* allele mass spectrometry assay, which functions as a nuclear import complex to transport IRP1A into the nucleus. Chickadee (Chic) also displayed an interaction

with IRP1A, for which I then provided data showing that it acts as a novel negative regulator of IRP1A nuclear import. I also found that only holo-IRP1A with no RNA-binding activity can be transported into the nucleus, which provided strict compartmentalization of the IRP1A proteins across the nuclear membrane that carries out different cellular functions. My work was mainly based on *Drosophila* S2 cells, given the constraint of not having transgenic lines. For this reason, efforts should be made to establish both the transgenic lines and endogenous knock-in lines in the future for continuing the *in vivo* studies of the IRP1A nuclear import. Besides, since it has been long believed that vertebrate IRP1 is exclusively cytosolic, it would be interesting to know whether human IRP1 (hIRP1) has a nuclear localization in *Drosophila* S2 cells. And if so, whether Ran and NTF2 mediate the nuclear import of hIRP1 by the same mechanism as in *Drosophila*. To solve these questions, I would make a series of plasmids that enable the expression of human orthologs in S2 cells under the control of *actin* promoter, followed by verifying protein-protein interactions via co-IP and Western blotting.

3.4.2 RanBP3 is essential for the RNA-binding activity of apo-IRP1A

The ectopic expression of the transgenic *IRP1A*^{C450S} allele in *RanBP3* loss-of-function PG cells completely restored the ring gland function to synthesize heme for sustaining cytochrome P450 enzymes that catalyze enzymatic steps in ecdysone production (Fig. 3.15). This result suggested an important role for RanBP3 in regulating cellular iron homeostasis via maintaining an appropriate level of cytosolic IRP1A for RNA-binding. Similarly, the mechanism by which

RanBP3 regulates the subcellular localization of IRP1A was examined in the *Drosophila* S2 cell line. I first verified the conservative nuclear export pathway of CRM1 and RCC1 via co-IP followed by Western blotting. In addition, RanBP3 showed protein associations with both CRM1 and RCC1 in S2 cells, consistent with the idea that RanBP3 may function as a cofactor by promoting the catalytic activity of RCC1, which is essential for nuclear cargo export. Although it is more likely that RanBP3 is a general regulator of nuclear export, IRP1A was identified as one of the candidate proteins whose nuclear export was mediated by RanBP3 via the classic CRM1-mediated nuclear export machinery. More importantly, mutational studies of IRP1A revealed that only apo-IRP1A could target the nuclear export pathway. At the same time, holo-IRP1A would go through the conversion to become apo-IRP1A in the nucleus to be transported back to the cytosol.

3.4.3 Cellular iron homeostasis is regulated by both cytosolic and nuclear IRP1A

Wild-type IRP1A was found to be predominantly nuclear, whereas IRP1A^{C450S} (constitutively RNA-binding) was exclusively cytosolic in the prothoracic gland (Fig. 3.16). The subcellular localization of IRP1A is also tissue-specific [91], suggesting that the nucleocytoplasmic transport of IRP1A might also rely on different cofactors that are expressed differentially in various types of cells. One interesting question raised from this was to understand the importance of nuclear-localized IRP1A in cellular iron homeostasis. Since the IRP1/IRE system registered by apo-IRP1A has been well-established in both vertebrates and *Drosophila*, how would these two regulatory mechanisms be controlled by apo- and holo-IRP1A differ and potentially work cooperatively

within a cell?

The intriguing finding that holo-IRP1 (IRP1A^{3R3Q} and IRP1B^{3R3Q}) localized to the nucleus implicated that holo-IRP1 proteins may have additional roles in the nucleus that contribute to tissue-specific cellular iron homeostasis in *Drosophila*. Both IRP1A^{3R3Q} and IRP1B^{3R3Q} interact with different subsets of histone proteins, which were identified by mass spectrometry using transgenic alleles [91]. Consistent with this finding, genome-wide transcript profiling of ring glands that expressed nuclear-localized IRP1 proteins (no RNA-binding activity) showed strong enrichment of transcripts involved in iron-dependent processes, most notably those involved in steroid hormone biosynthesis. In contrast, IRP1A^{C450S} (constitutively RNA-binding) had little influence on changing the expression of the same genes. These results suggested that IRP1 proteins have different subcellular roles. While apo-IRP1A works post-transcriptionally to regulate the expression of genes via binding to mRNA transcripts, holo-IRP1A mainly function to alter the expression of genes involved in iron-dependent processes.

Next, it would be interesting to know whether a cell chooses which conformational form of IRP1A is used to regulate cellular iron homeostasis. It is possible that the tissue-specific subcellular localization of IRP1A would be important in determining which regulatory system to initiate to respond to the acute drop of cellular iron levels. For example, IRP1A is predominantly nuclear in the prothoracic gland but mostly cytosolic in the salivary gland. Therefore, holo-IRP1A may instantly work to down-regulate the expression of genes involved in iron-dependent processes within PG cells. At the same time, apo-IRP1A might respond to the drop of cellular iron levels

faster than holo-IRP1A in the salivary gland. Eventually, both holo-IRP1A and apo-IRP1A would work cooperatively to up-regulate bioavailable cellular iron levels for sustaining the need to produce iron-containing proteins.

3.4.4 Characterizing novel roles of RanBP3 in cellular iron homeostasis

The mass spectrometry results revealed Glycoprotein 93 (Gp93, Hsp90) as a key candidate protein, showing protein-protein interaction with RanBP3 in S2 cells. Losing *Gp93* function in the PG could not induce a severe lethality or the porphyria-like phenotype. This finding suggested that Gp93, by itself, was not sufficient to cause iron deficiency, but only in the presence of a cofactor protein. The cofactor was later found out to be another ER protein, called ERp60. Both Gp93 and ERp60 were found to have physical interactions with Mitoferrin, the only ortholog of vertebrate MFRN1/2 in *Drosophila*. In addition, Ferritin 1 Heavy Chain Homolog (Fer1HCH) was shown to interact with Gp93 both *in vivo* and *in vitro*. The binding of Gp93/ERp60 to iron transporter proteins may be of great importance in modifying the protein function, such that cytosolic bioavailable iron can be transported into the mitochondria for both heme and iron-sulfur cluster biogenesis. However, it is still unknown what exact role Gp93 and ERp60 complex may play *in vivo*. Hsp90 family proteins are unique in their ability to regulate a specific subset of cellular signaling proteins that have been implicated in disease processes. To follow up on this, a *Gp93* transgenic line carrying an epitope tag can be generated and further used for MS analysis to target specific proteins involved in the regulation of cellular iron homeostasis. Besides, it would be

essential to know what type of ATP-dependent cellular process Gp93 may have an impact on Mitoferrin and ferritin, respectively. These include, for example, prevention of protein aggregation, protein degradation, and maintenance of signaling proteins in a conformation that permits activation.

Lastly, overexpression of the *hTfR* allele significantly rescued the lethality and the porphyria-like phenotype induced by *RanBP3* loss-of-function. This finding suggested that the transferrin-bound iron uptake pathway is conserved in *Drosophila*. Since flies lack a TfR1 ortholog, the function of TfR1 might be substituted by an unknown fly protein that needs to be identified. Since the *Drosophila* genome encodes three transferrin proteins (Tsf1, Tsf2, and Tsf3), one can generate transgenic lines producing tagged Tsf proteins, and use MS to identify candidate receptor proteins. Besides, cellular iron may also be acquired from other ways. Ferritin might work as a vital iron transporter in *Drosophila*, which delivers iron independent of a receptor protein, compensating cellular iron uptake differently than transferrin.

3.4.5 What is the role of IRP1B in *Drosophila melanogaster*?

Mammalian cellular iron homeostasis is mainly regulated by the post-transcriptional control of gene expression by binding iron-regulatory proteins (IRP1 and IRP2) to iron-responsive elements (IREs) located in the untranslated regions of specific mRNA transcripts. The most distinguishable difference between IRP1 and IRP2 is an extra 73-amino-acid segment in IRP2, which has no aconitase activity [164-166]. Extensive analyses of knock-out mice led to a common

conclusion that IRP2, but not IRP1, dominates mammalian cellular iron metabolism [52]. The mRNA levels of IRP1 and IRP2 examined by *in situ* hybridization, and the protein levels examined by Western blotting both suggest that IRP1 and IRP2 have different expression patterns among cell types within specific tissues. While IRP1 is predominantly expressed in the kidney, liver, and brown fat, the highest expression of IRP2 is found in the forebrain and cerebellum.

In contrast to vertebrates, two IRP1-like proteins (IRP1A and IRP1B) are expressed in *Drosophila,* displaying 86% identity and 93% similarity to each other [85, 167]. Comparative sequence analysis and mutational analysis revealed that IRP1A and IRP1B are both homologs of vertebrate IRP1. Although both proteins possess aconitase activity, only IRP1A can bind to IREs. On the other hand, IRP2-type proteins, as known from mammalian cells, have not been identified in *Drosophila*.

Therefore, the question remains: Why does the *Drosophila* genome encode two IRP1 homologs, with only one capable of regulating cellular iron homeostasis via the IRP1/IRE system? It is most likely IRP1A and IRP1B were generated by gene duplication and subsequent divergence. Enzymes that function in iron metabolism and redox reactions are required in more than one subcellular compartment. For example, cytosolic aconitase can be further divided into two groups. One that interconverts citrate and isocitrate in the cytoplasm, whereas the other type would be located in the mitochondrion for the same process. It should be noted that information that determines the subcellular localization of proteins is usually contained in signal sequences at the N-terminus, which can be easily changed by either alternative splicing of mRNAs or gene

duplication that allows targeting of proteins of similar function to different subcellular compartments. One of the advantages of having two copies in the genome would be providing a chance for independent evolution by acquiring new mutations and molecular adaptations. Since IRP1A and IRP1B are 78 and 79% similar to human IRP1 based on sequence alignment at the protein level, three-dimensional models of *Drosophila* IRP1 based on the solved structure of human IRP1 can therefore be established. This showed that *Drosophila* IRP1A and IRP1B have an almost identical core structure to human IRP1, including three arginine residues implicated in IRE binding [85]. The only main differences between these two homologs are only found on the external surfaces of the protein, which may most likely affect the IRE binding ability. Interestingly, a few differences with respect to protein expression were identified when applying the substitution mutations that can induce both the conformational and functional changes of IRP1A proteins to *IRP1B* cDNA. Overexpressing the transgenic $IRP1B^{C447S}$ allele in the *RanBP3* loss-of-function PG cells partially rescued the accumulation of protoporphyrinogen (Fig. 3.27). Taking the impact of losing *RanBP3* function on IRP1A into consideration, no significant conclusion could be drawn regarding whether $IRP1B^{C447S}$ has a positive role in compensating the heme deficiency. Additionally, the survival of transgenic $IRP1B^{C447S}$ animals with *RanBP3* depletion in PG cells was significantly decreased, with only ~11% of the RNAi animals surviving to adulthood instead of 77% in control without *RanBP3* knock-down in the presence of $IRP1B^{C447S}$. Again, this could be induced by affecting IRP1A function in the PG. However, the finding that knocking down *RanBP3* in PG cells did not change the predominant cytosolic localization of $IRP1B^{C447S}$, suggesting that it is

essential to have appropriate levels of cytosolic IRP1A and IRP1B in position for an efficient IRP1/IRE system to work.

Taken together, although IRP1B has been suggested to only function as an aconitase for the interconversion of citrate and isocitrate in the cytosol, which has no direct link to cellular iron regulation in *Drosophila*, my preliminary data shows that there might be conservative sites in IRP1B that contribute to its protein structure and ability to bind mRNAs that harbor non-canonical IREs, such that the binding of IRP1B to IREs would work highlighting the same mechanism as IRP1A for cellular iron homeostasis. Though not verified, it is possible that IRP1B may acquire the function to regulate cellular iron homeostasis via the IRP1/IRE system if specific mutations were introduced.

3.4.6 To examine the roles of three proteins in the MS data that were unique to RanBP3b

As shown in Table 3.5 and Table 3.6, a total of 48 proteins were identified via MS, showing potential binding activities to RanBP3a. In contrast, only six proteins were identified as tentative interacting proteins to RanBP3b. Since only a few proteins were identified and three of them were unique to RanBP3b, these three proteins might regulate completely different biological processes in *Drosophila* than RanBP3a. An overview of the molecular functions and phenotype associated with PG-specific loss-of-function is shown in Table 3.7. Only PG-specific *Rrp40*-RNAi showed a late larval lethality, while the RNAi lines of the other two genes either showed no significant effect on animals' survival rate (*Hsc70-5*) or were not examined. To follow up on this preliminary

screening, I would first get RNAi lines for *RpS17* since it is still unknown whether losing *RpS17* in the PG induced a developmental defect of the animals or not. If there were a lethality observed, I would next validate the MS result of RanBP3b by making plasmids that encode tagged Rrp40 and RpS17, followed by co-IP and Western blot. For genes that encode proteins showing positive protein-protein interactions with RanBP3b, I will then perform an MS analysis to identify tentative interacting proteins to get an overview of what signaling pathways and molecular functions of these proteins might be involved in.

Table 3.7 Genes that encode proteins showing tentative interactions uniquely to RanBP3b.

Gene name	CG number	Gene summary[a]	Phenotype[b]
Rrp40	CG31938	*Rrp40* encodes a protein involved in gene expression regulation	L3 arrest
RpS17	CG3922	*RpS17* encodes an essential component of the ribosomal 40S subunit	NA
Hsc70-5	CG8542	ATP binding activity; ATP hydrolysis activity; Misfold protein binding activity	NOP

[a]Gene summary resource: FlyBase Gene Snapshot

[b]Survival analysis of *phm22*>RNAi animals reared on standard Nutrifly fly diet were examined by KKJ lab, Rewitz lab and O'Connor lab. Abbreviations: L3: third-instar; NA: not available; NOP: no phenotype.

Chapter 4 Examining roles of Su(var)2-10 in ecdysone biosynthesis

4.1 Introduction

4.1.1 Identification of Su(var)2-10 and its role in the position effect of variegation

Su(var)2-10 (*CG8068*) was identified as one of the genes showing both developmental defect and the abnormal RG phenotype when the gene was knocked down in PG cells using RNAi (Fig. 3.1). Unlike *RanBP3* loss-of-function animals, losing *Su(var)2-10* function did not cause an accumulation of protoporphyrin but instead caused enlarged non-autofluorescing ring glands. This finding suggested that *Su(var)2-10* may function differently than *RanBP3* in regulating steroid production and animals' development.

The *Drosophila* Su(var)2-10 was initially identified as a Suppressor of Position-Effect Variegation (PEV) [168]. PEV describes a mosaic pattern of expression when a chromosomal rearrangement occurs, placing a gene that resides in euchromatin next to a breakpoint in heterochromatin (For review, see [169-171]). A classic example of such a PEV is the insertion of the *white* gene into the vicinity of pericentric heterochromatin in *Drosophila,* resulting in the *white* mottled 4b (*white*^{m4b}) allele (Fig. 4.1). The *white* gene is located in euchromatin at the distal end of the X chromosome, which encodes a protein required for the red-eye pigmentation in wild-type flies [171, 172]. Upon rearrangement, eyes of w^{m4b} flies display variegated red and white patches caused by random silencing of the *white* gene, which is then clonally inherited. Patterns of variegated expression, for example, the number of pigmented cells and the size of pigmented patches, can be modified by many factors. Temperature of development and the amount of

heterochromatin within the genome are two first identified factors that affect the extent of variegation [173]. The PEV phenotype can also be regulated by genetic factors. Two major classes of genes were identified by chemical mutagenesis of the w^{m4b} indicator strain that displayed red/white pigment distribution [174], namely *Suppressors of variegation* or *Su(var)* and *Enhancers of variegation* or *E(var)*. As the name implies, *Su(var)* mutations weaken the establishment and maintenance of the heterochromatin (loss of silencing), whereas *E(var)* mutations diminish euchromatin and allow the expansion of heterochromatin (increase of silencing). Approximately 150 loci have been identified from such screens in *Drosophila,* of which the molecular identities of around 60 *Su(var)* and 25 *E(var)* genes are known to date in the fruit fly [175]. The naming of these genes is based on the chromosome where the mutation is located, the gene number, and the number of the allele. *Su(var)2-10* symbolizes the tenth gene identified on the second *Drosophila* chromosome.

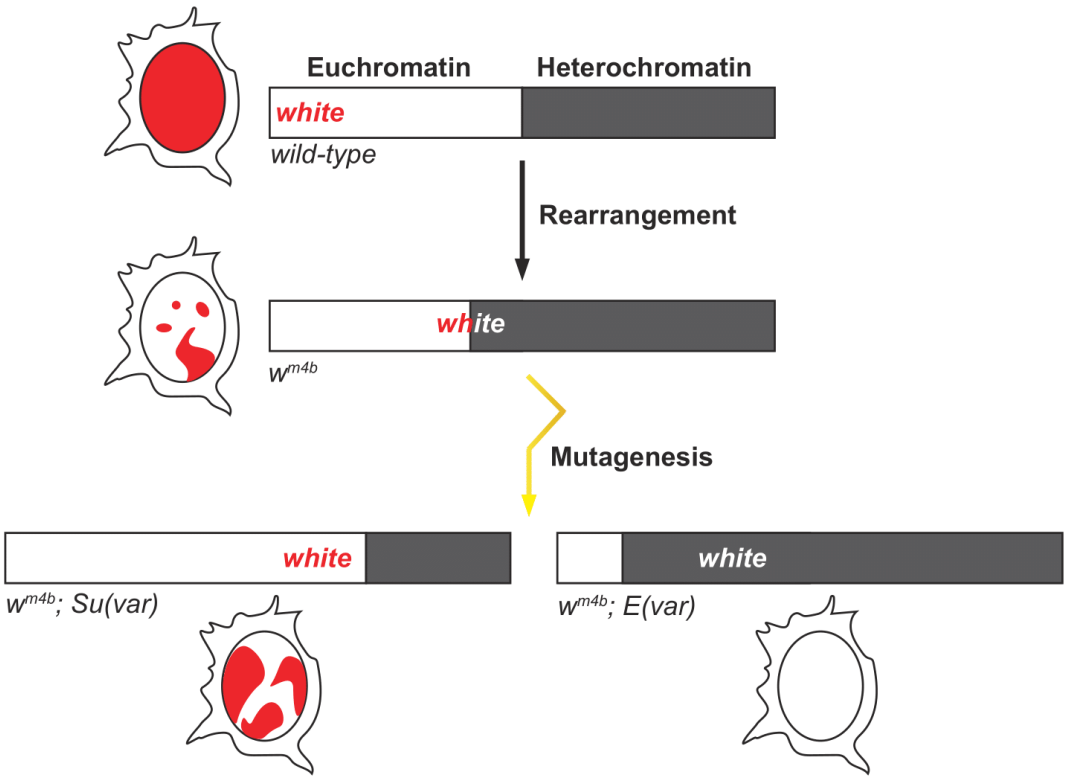

Figure 4.1 PEV of the *Drosophila white* gene.

A classic example of the Position Effect Variegation (PEV) in *Drosophila* is the eye color pigmentation via the *white* gene. The *white* gene is localized on euchromatin at the distal end of the X chromosome. Flies with the wild-type *white* gene would show red eyes. Individuals display red and white patches in the eye after rearrangement of the gene (as shown in the w^{m4b} mutant). Two classes of genes were identified, followed by applying mutagenesis on the w^{m4b} mutant, namely *Suppressor of variegation* or *Su(var)* and *Enhancers of variegation* or *E(var)*. The *Su(var)* mutants tend to have a greater red pigment area than the control, whereas *E(var)* mutants might have a completely white-eye phenotype.

4.1.2 *Su(var)2-10* encodes a PIAS homolog and is essential for *Drosophila* development

Drosophila Su(var)2-10, also known as *Zimp* and *dPIAS*, encodes a Protein Inhibitor of Activated STAT (PIAS) family protein similar to mouse Miz1 and PIAS3 [176]. The most striking similarity between the proteins of this family is in a domain predicted to form a single zinc finger (Znf). Znf motifs are among the most abundant protein motifs, presented in an estimated 1% of mammalian genes [177]. Znf motifs were initially identified as a DNA-binding domain. However, some of them are involved in protein-protein interactions. Three spliced forms were detected in a cDNA library screen and on an RNA blot of *Su(var)2-10* [176]. The longest transcript, known as *zimp-1*, is only detected in the embryonic stage, whereas two other transcripts (*zimp-2* and *zimp-3*) are detected in adult mRNA. Two unique proteins are encoded by the *Su(var)2-10* gene, of 554 and 522 amino acids, respectively. *Zimp-1* encodes the 554 -aa protein (Zimp-A), using the translational start site in exon 2c and the stop codon in exon 7d. In contrast, *zimp-2* and *zimp-3* use the stop codon in exon 7b, resulting in a shorter protein (Zimp-B) sharing most of the coding region identical to *zimp-1*.

Zinc finger domains are relatively small protein motifs that contain multiple finger-like protrusions that make tandem contacts with their target molecules [178-182]. There are many superfamilies of Znf motifs, which vary in both sequence and structure. In addition, the binding modes of different types of zinc fingers can also be very different. For example, the classical C2H2 zinc finger binds to DNA, RNA and proteins, whereas the nuclear hormone receptor only binds to

DNA [181]. As a result of the versatility in binding modes, Znf-containing proteins may have evolved specialized functions for carrying out different cellular processes. Of note, *Drosophila* Su(var)2-10 is predicted to harbor a “RING-type” zinc finger motif (also known as C3HC4-type) by the Pfam HMM tool, which might bind proteins via ubiquitin ligation [181, 183].

Functional annotation of Su(var)2-10 protein showed two common domains that appear in all the Su(var)2-10 isoforms, which are: the SAP domain that is located at the N-terminal from amino acid 2 to 36 (essential for DNA-binding), and the Znf domain from amino acid 325 to 367 (Fig. 4.2). The previous study has provided a comprehensive classification of each zinc finger structure into one of eight groups defined based on the structural properties in the vicinity of the zinc-binding site [184]. The Znf identified in Su(var)2-10 protein was classified into the RING finger-like group, consisting of a conserved 40-60 residue cysteine-rich domain capable of binding to two zinc ions. The "RING" finger is also termed as C3HC4 zinc-finger. Similar domains are also found in many proteins from invertebrates, such as *Caenorhabditis elegans, Saccharomyces cerevisiae*, and *Arabidopsis thaliana* [185].

Drosophila Su(var)2-10 is essential for viability. Deletion or *P*-element insertion of the gene is lethal [176]. Mutations in the *Su(var)2-10* gene cause severe chromosome inheritance defects, ultimately leading to the failure of growth [168]. Meanwhile, diverse phenotypes demonstrated by *Su(var)2-10* mutants also suggest that the gene plays multiple roles in a cell for various biological processes. For example, mutants have condensation defects during metaphase in embryos and neuroblasts and interphase polytene cells [168]. The melanotic tumors in mutant larvae implicated

a role of *Su(var)2-10* in the canonical JAK/STAT signaling pathway. *Su(var)2-10* may also be involved in telomere function and nuclear organization, which was demonstrated by various defects identified in telomere clustering and telomere-lamina associations [168].

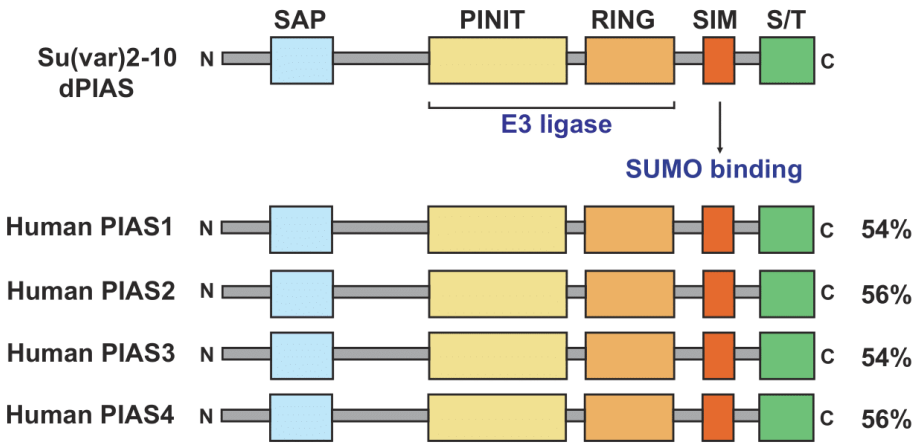

Figure 4.2 Schematic demonstration of functional domains in PIAS family proteins.

Su(var)2-10 encodes a PIAS protein (dPIAS or Zimp) in flies, which shows about 54-56% similarities to its human counterparts. Three out of five functional domains/motifs of these PIAS proteins are associated with their role in the SUMO conjugation pathway. Abbreviations: SAP: N-terminal scaffold attachment factor-A/B; PINIT: Pro-Ile-Asn-Ile-Thr motif; RING: Ring-finger-like zinc-binding domain; SIM: SUMO-interacting motif; S/T: Serine/threonine-rich C-terminal region.

4.1.3 Su(var)2-10 negatively regulates the *Drosophila* JAK/STAT pathway

The transduction of information from the outside of a cell to produce a specific response is essential for development, homeostasis and cell survival and is mediated by a small number of signal transduction cascades. The Janus kinase (JAK)-Signal Transducer and Activator of Transcription (STAT) pathway (JAK/STAT) was first identified in mammals as a signaling mechanism central to hematopoiesis and has since been shown to exert a wide range of pleiotropic effects on multiple development processes [186-188]. The canonical model for JAK/STAT signaling has been well-characterized in mammals, including a wide range of extracellular ligands and transmembrane receptors, four Janus kinases (JAKs), and seven genes coding for signal transducers and activators of transcription (STATs). The binding of the extracellular ligand to the transmembrane receptor results in the activation of the receptor-associated JAKs, which then phosphorylate themselves and their associated receptors to provide the binding sites for the SH2 domains STATs. The activated STATs form homo- and heterodimers and translocate to the nucleus, bind to a palindromic DNA recognition sequence, and activate the transcription of pathway target genes. The JAK/STAT signal transduction pathway has been conserved throughout evolution such that functional homologs of components are also present in flies. The pathway in *Drosophila melanogaster* represents a much simpler and genetically tractable system with which it can be studied (Fig. 4.3).

Genetic analysis in *Drosophila* has identified all the core components of the JAK/STAT

pathway (Fig. 4.3a), which include: three ligands named unpaired (UPD1, UPD2 and UPD3) [189]; a transmembrane receptor called Domeless (DOME); a JAK kinase known as Hopscotch (HOP); and a transcription factor called STAT92E [190-192]. Mutational analyses of these components have revealed several interesting developmental roles (Fig. 4.3b). Hop can be subdivided into seven JAK-homology (JH) domains. Mutations in the JH domain, such as Hop^{Tum-1} and Hop^{T42}, have been suggested to function as two hyperactive mutations [193]. *STAT92E* was named based on the gene is located at chromosome band 92E. The gene encodes a 761 amino acids protein sharing 37% identity to STAT5. Several domains conserved in STATs can also be recognized in STAT92E, including a DNA-binding domain in the central region, an SH2 domain, and a critical tyrosine residue at 711, which is phosphorylated by Hop and required for DNA-binding activity [194]. ΔNSTAT92E, a truncated protein that lacks the N-terminal 133 amino acids, negatively regulates JAK/STAT signaling based on genetic analysis [195].

Given the multiple roles of JAK/STAT signaling and the potential developmental consequences, it is not surprising that numerous regulatory mechanisms exist to control it. The regulators can be broadly grouped into positive and negative classes (For review, see [191, 196]). The SOCS (suppressors of cytokine signaling) genes are the best-characterized negative JAK/STAT pathway regulators. Three SOCS-like genes (*socs36E, socs44A,* and *socs16D*) have been identified in *Drosophila* by sequence homology. PIAS (protein inhibitors of activated STAT) proteins represent another well-characterized group of regulators that negatively regulates the JAK/STAT pathway. *Drosophila* Su(var)2-10 was identified by sequence homology as the single PIAS

homolog, which physically interacts with STAT92E to induce protein degradation via SUMOylation [191, 197, 198]. Despite extensive studies in characterizing the JAK/STAT signaling components and their functioning, whether the JAK/STAT pathway is linked to *Drosophila* development by regulating ecdysone biosynthesis is unknown and needs further investigation.

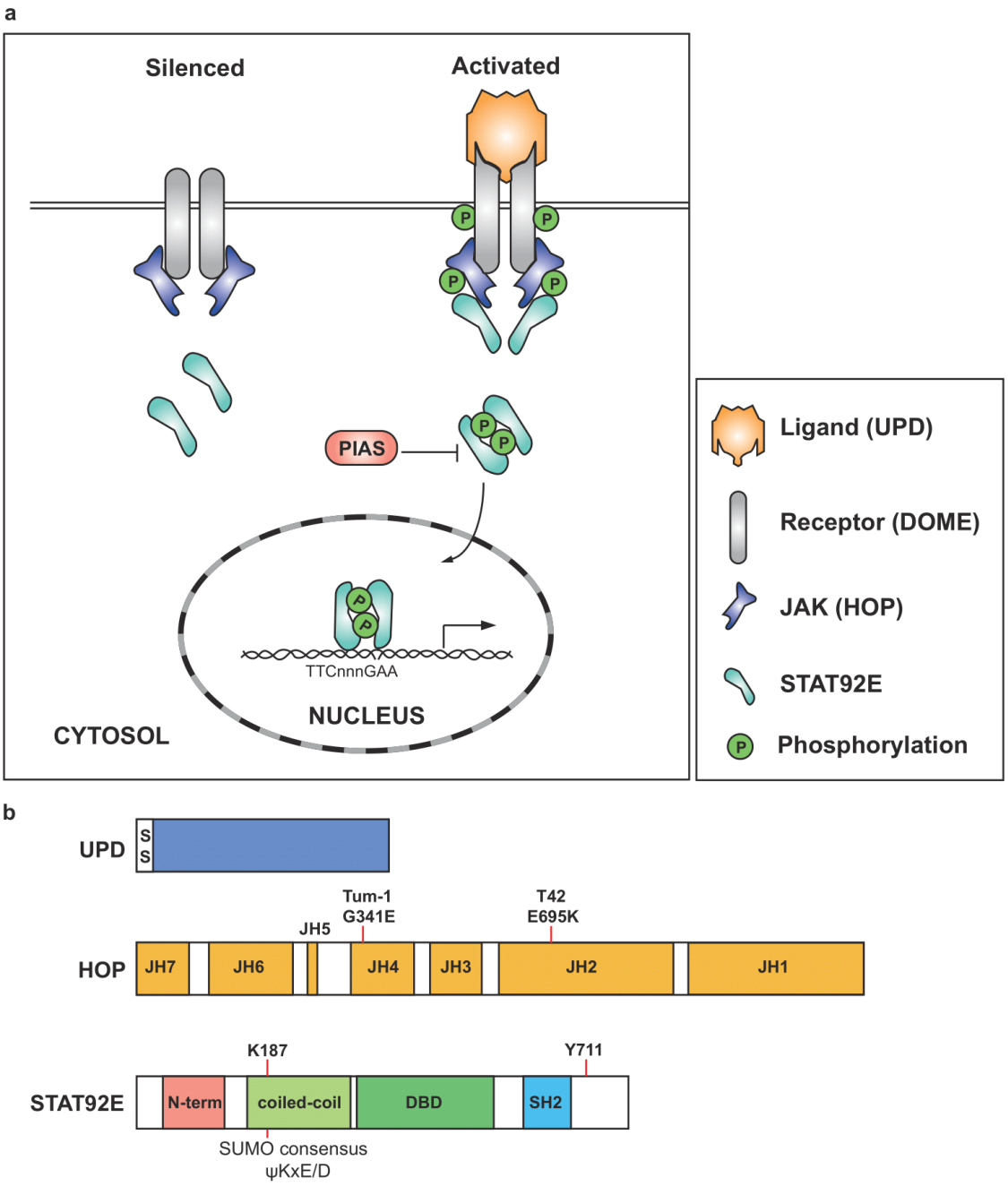

Figure 4.3 Canonical JAK/STAT signaling in *Drosophila melanogaster.*

(a) A model of JAK/STAT pathway activation. Pre-dimerized receptors (grey) and Janus kinases (JAKs) are activated, followed by ligand-binding. Upon phosphorylation of the JAKs and the receptors, a docking site for the STATs, which constitutively shuttles between the nucleus and the

cytosol, is generated, allowing for the recruitment of cytosolic STATs to the active complex. Phosphorylation further leads to the dimerization of the STATs, which translocate to the nucleus and bind to a palindromic DNA sequence in the promoters of target genes to activate their transcription. The names of the core pathway components in *Drosophila* are provided in the key. (b) Schematic structure of UPD (ligand), HOP (JAK), and STAT92E (Transcription factor). The conserved Jak-Homology (JH) domains are defined. Two hyperactive mutations $Hop^{Tum\text{-}l}$ and Hop^{T42}, are also shown. Abbreviations: SS, signal sequence; N-term, N-terminal domain; DBD, DNA-binding domain; SH2, Src-Homology 2 domain; Y711, a critical tyrosine residue that can be phosphorylated by Hop.

4.1.4 Su(var)2-10 acts as an E3 ligase in the SUMOylation pathway in *Drosophila*

A major theme of gene regulation lies in identifying proteins responsible for DNA packaging and understanding how regulation of these proteins modulates the functional accessibility of DNA during gene expression. Of all the gene regulation mechanisms, recent genome-wide proteomic and genetic studies have linked modification by the small ubiquitin-related modifier (SUMO), a ~12 kDa peptide, to many biological processes, including DNA replication and repair, chromosome segregation, transcriptional activation/repression, etc. [199]. As a critical post-translational protein modification, SUMOylation targets proteins by multiple mechanisms, for example, as a signal to facilitate protein-protein interactions on chromatin, altering protein subcellular localization, affecting protein stability and their enzymatic activities. SUMOylation involves a series of enzyme cascades and is mechanistically very similar to ubiquitylation (Fig. 4.4). The SUMOylation pathway is conserved in all eukaryotic organisms and is a reversible cycle consisting of E1-activating enzymes, E2-conjugating enzymes and E3 ligases, and SUMO cleaving proteases [200, 201]. SUMO is activated by the specific activity of E1, which is a heterodimer comprising SAE1/Aos1 and SAE2/Uba2 proteins [202]. Subsequently, SUMO is transferred to the E2-conjugating enzyme Ubc9. The last step involves the E3 ubiquitin protein ligases that promote the transfer of ubiquitin from the E2 enzyme to the ε-amino group of the target lysine residue in the substrate. The E3 ubiquitin protein ligases are mainly responsible for the substrate specificity of ubiquitination [176].

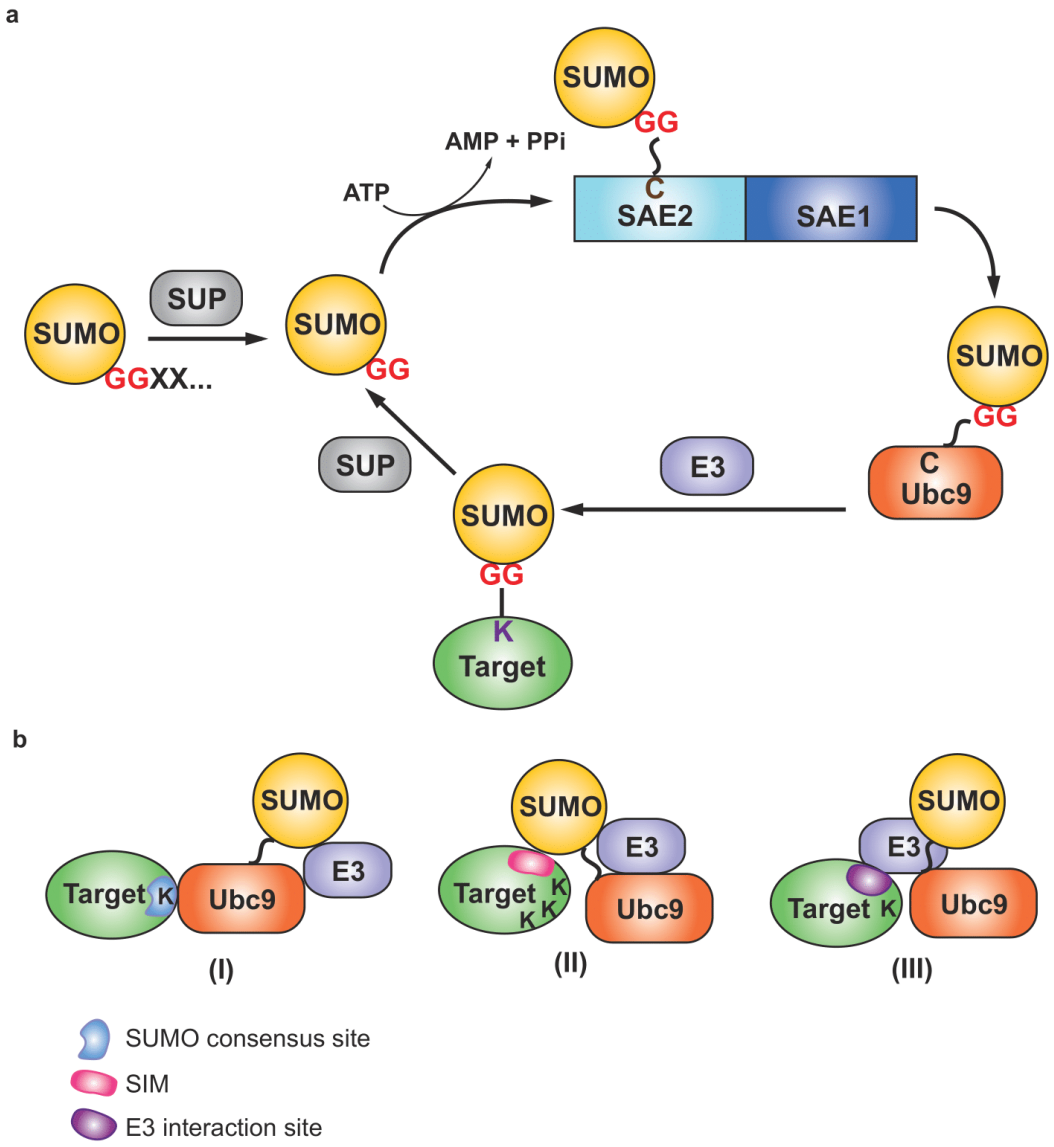

Figure 4.4 SUMOylation pathway.

(a) The reversible SUMOylation cycle consists of four steps. The nascent SUMO is proteolytically cleaved to expose its glycine-glycine (GG) motif before getting into the cycle. The cleavage is catalyzed by SUMO-specific proteases (SUPs) of the Ulp/SENP family. The mature SUMO is

activated by E1 heterodimer SAE1/SAE2 (SUMO-activating enzyme subunit 1 and 2) in the presence of ATP, resulting in a thioester bond between the C-terminal glycine and the cysteine of SAE2. SUMO is then transferred to the catalytic cysteine of the E2 enzyme Ubc9. Ubc9 catalyzes the formation of an isopeptide bond between the glycine residue of SUMO and the lysine (K) residue in the substrate, usually together with a SUMO E3 ligase. Finally, SUMO is released by SUP for subsequent cycles. (b) Mechanisms of the acceptor lysine (K) selection. For SUMOylation to work, the acceptor lysine must gain access to the Ubc9-SUMO thioester bond. Three distinct mechanisms can determine the process. (I) Consensus site SUMOylation: the acceptor lysine is embedded in a short motif directly recognized by Ubc9. (II) SIM-dependent SUMOylation: The interaction between the SUMO interaction motif (SIM) and SUMO recruits the Ubc9-SUMO thioester, allowing the nearby lysine residues to be modified. (III) E3 ligase-dependent SUMOylation: SUMO E3 ligase directly binds the target at a specific lysine residue.

The SUMO conjugation pathway is less redundant in invertebrates. For example, while four SUMO variants are present in vertebrates, *Drosophila* expresses only one vertebrate SUMO homolog, known as Smt3. Interestingly, Smt3 is required for ecdysone biosynthesis and is essential for the developmental transition from larval to the pupal stage in flies [203]. *smt3* knockdown in the prothoracic gland phenocopies *Su(var)2-10* loss-of-function animals, suggesting a possible link between SUMOylation and the ecdysteroid synthesis. Other orthologous genes of the vertebrate SUMOylation pathway, such as Ulp1, Aos1, Uba2 and Lesswright (Lwr), were also identified in *Drosophila* [204]. Two E3 ligases were identified in *Drosophila* based on sequence homology with their vertebrate homologs. Specifically, Tonalli (Tna) is the orthologue of human Zimp7 and Zimp10, while Su(var)2-10, also known as dPIAS, is orthologous to human PIAS1. The *tna* gene encodes at least two proteins ($TnaA_{130}$ and $TnaA_{123}$) throughout development [205, 206]. Genetic analysis shows that 65% of tna^{1}/tna^{5} animals reach the third-instar larval stage but never eclosed as adults [206]. TnaA signals are mostly detected at discrete sites on polytene salivary gland chromosomes of late larvae, suggesting that TnaA is required for regulating homeotic gene expression during development [205]. The other putative E3 ligase described in *Drosophila* is Su(var)2-10. In mammals, PIAS1 interferes with the promoter-binding activity of tyrosine-phosphorylated STAT1 via SUMOylation [207]. The most conserved part in PIAS family proteins is the central zinc finger RING-type domain (Fig. 4.2). Functional analysis also shows that the PINIT domain is specific for PIAS proteins and promotes SUMO binding.

A large number of proteins have been identified as SUMO substrates in vertebrates and

Drosophila. However, predicting the biological impact of SUMOylation on these targets is difficult. Some evidence suggests that SUMOylation in *Drosophila* links various cellular processes, such as cell survival and proliferation, cellular trafficking, enhancement of transcriptional activation or transcriptional repression, and chromatin regulation. First of all, components of the SUMOylation pathway are expressed in proliferative tissues, such as undifferentiated cells of imaginal discs or the gonads [208, 209], providing solid evidence that SUMOylation is associated with the survival and proliferation of cells. Besides, Su(var)2-10, as an E3 ligase in SUMOylation, is essential for both transcriptional inhibition of STAT92E [197] and chromosomal stabilization and maintenance [168]. Taken together, the post-translational modification implemented by SUMOylation is a "fine-tuning" mechanism to regulate multiple proteins in a variety of signaling pathways.

4.1.5 Cooperative control of *neverland* transcription by Séance and Molting defective

neverland (*nvd*) encodes an oxygenase-like protein with a Rieske electron carrier domain, which is explicitly expressed in tissues that synthesize ecdysone, such as the prothoracic gland [210]. *nvd* loss-of-function flies show a developmental defect, which is rescued by supplementing either 20-hydroxyecdysone (20E), the biologically functional ecdysone, or the precursor 7-dehydrocholesterol (7dC). Neverland proteins from the silkworm *Bombyx mori* and the fruit fly *Drosophila melanogaster* contain a Rieke [2Fe-2S] center binding motif (C-X-H-X_{16-17}-C-X_2-H) that is known to function as an electron acceptor and is involved in electron transfer to other proteins. Additionally, the Nvd family proteins also contain a highly conserved C-terminal region

(E/D-X_3-D-X_2-H-X_4-H) that shows non-heme iron-binding activity, which is thought to be involved in oxygen binding.

Two transcription factors, Séance and Molting defective (Mld), cooperatively control *neverland* transcription in *Drosophila* [211]. Loss-of-function animals of *séance* and *mld* can be genetically rescued by transgenic expression of *nvd* in the PG. Interestingly, unlike *nvd*, which is specifically expressed in the prothoracic gland for ecdysone biosynthesis, both *séance* and *mld* are highly expressed in non-PG tissues. This raises an interesting question: why is *nvd* not expressed in non-PG tissues where the corresponding transcription factors are present? A straightforward explanation is that *neverland* transcription requires the proper function of *séance* and *molting defective* and other cofactors that are only highly expressed in PG cells. The other possibility is that there are co-existing and most likely repressive mechanisms to turn off *neverland* transcription in non-PG tissues to suppress ecdysone biosynthesis. *neverland* is located in the pericentromeric region of the third chromosome in the fly genome, which forms constitutive heterochromosome. For this reason, one may argue that perhaps there is an uncharacterized mechanism by which the chromosome state of *nvd* is repressed such that *nvd* transcription is maintained at a relatively low level in non-PG tissues. In general, heterochromatin silencing involves various types of post-translational modifications (PTMs), such as global hypoacetylation and trimethylation of histone H3 on lysine 9 (a repressive mark) [173, 212]. Whether PTMs modulate the expression of *nvd* and its transcription factors need to be further investigated. Lastly, *séance* and *mld* are not found in any species thus far investigated other than the *Drosophilidae*. In contrast, almost all insect genomes

examined so far contain a single copy of *nvd*, suggesting that there might be other mechanisms for regulating *nvd* transcription in species where Séance and Mld are absent.

4.1.6 Regulation of nucleosome dynamics by histone modifications

In eukaryotes, DNA is organized together with histones and non-histone proteins into chromatin, with the nucleosome as its monomeric subunit, a particle in which ~146 bp of DNA are wrapped in a left-handed superhelix around an octamer of core histones, consisting of two molecules each of H2A, H2B, H3 and H4 [213]. The chromatin organization ultimately dictates every cellular process requiring DNA access, including transcription, replication and repair. The properties of nucleosomes can be altered by different means, such as replacing core histones with specialized histone variants, repositioning or eviction of histones from DNA by ATP-dependent chromatin remodeling enzymes, and covalent modification of histones [214]. There have been >100 histone modifications described, ranging from the well-known types, such as lysine acetylation, lysine methylation, and serine/threonine phosphorylation [215], to more exotic modifications, such as histone SUMOylation [216, 217] and crotonylation [218].

All histones can be post-translationally modified, which most often occur on the histone tails. These covalently modified histone proteins dictate chromatin structure and, more importantly, gene expression profiles, which usually start with stimulation of euchromatin by the delivery of chromatin-modifying enzymes recruited to target sites sequence-specific DNA-binding transcription factors. Histone modifications can be divided into two classes at the transcriptional

level, one that correlates with activation and one that correlates with repression. Generally speaking, active genes typically contain high levels of lysine acetylation on the H3 and H4 tails (H3/H4 acetylation), trimethylation of H3 lysine 4 (H3K4me3), trimethylation of H3 lysine 79 (H3K79me3), ubiquitylation of H2B (H2BK120ub1), and trimethylation of H3 lysine 36 (H3K36me3) (this marks active genes, but is technically a repressive mark) [215, 219]. On the other hand, marks that are associated with repressed genes include, for example, trimethylation of H3 lysine 27 (H3K27me3), ubiquitylation of H2A on lysine 119 (H2AK119ub1), and trimethylation of H3 lysine 9 (H3K9me3). It should be noted that a hallmark of active genes, for instance, H3K36me3, can play a repressive role in transcription [220].

One particular post-translational modification that I would like to introduce here is histone SUMOylation, given that Su(var)2-10 is a SUMO E3 ligase in the same pathway. SUMOylation of proteins exhibits various effects, including changes in cellular localization or stability, modulation of protein-protein or protein-DNA interaction, and antagonizing other lysine modifications such as ubiquitylation, etc. [221-223]. Nevertheless, SUMOylation of transcriptional activators is primarily involved in transcriptional repression. This covalent modification was found in all four histone proteins that constitute nucleosome with specific sites of SUMOylation identified in histones H2A, H2B, and H4 of *Saccharomyces cerevisiae* [216]. While a SUMOylation site at the C-terminal K126 of histone H2A exists, the substitution of this site (H2A K126R) did not change H2A SUMOylation levels compared to the wild type. In contrast, SUMOylation sites of H2B and H4 are both located in the N-terminal regions. Importantly, histone SUMOylation negatively regulates

transcription in *S. cerevisiae* by a potential block to activating modifications, for instance, histone acetylation and ubiquitylation.

Given a large number of histone modifications, there might be numerous combinations of modifications that provide crosstalk between these marks. Such crosstalk may occur in *cis* between modifications located on the same histone tail or in *trans* either on neighboring histones within the same nucleosome or on neighboring nucleosomes in a chromatin domain [219]. In the past decade, there has been progress made, such as chromatin immunoprecipitation coupled with high-throughput sequencing (ChIP-seq) for identifying both the distribution and localization of histone marks associated with genome-wide gene expression. Mass spectrometry also enables mapping known histone marks at the level of a single histone tail using epitope tag labeling. Further efforts should be made to decipher the complex network of histone modifications by identifying combinatorial histone marks and looking for novel chromatin modifiers that read and rewrite the histone modifications such that gene expression states can be switched.

4.2 Modified materials and methods

4.2.1 *Drosophila* strains and husbandry

We obtained the following stocks from the Bloomington *Drosophila* Stock Center (BDSC): w^{1118} (#3605), *UAS-CG8068*$^{TRiP.\ JF03384}$ (#29448), *UAS-CG8068*$^{TRiP.\ HMS00705}$*/TM3, Sb1* (#32915), *UAS-CG8068*$^{TRiP.HMJ21959}$ (#58067), *PBac{Su(var)2-10-GFP.FPTB} VK00037* (#64795). *UAS-CG8068*^{KK108790} (v100813) and *UAS-SUMO*^{KK101786} (v105980) were obtained from Vienna

Drosophila Resource Center (VDRC). The *phm22-GAL4* and *phmN1-GAL4* were kind gifts from Dr. Michael O'Connor and used to drive transgene expression in the prothoracic gland. *UAS-nvd-Bm [WT]* and *séance-V5/Cyo; mld/TM6* were kind gifts from Dr. Ryusuke Niwa. *Drosophila melanogaster* flies were reared on the standard agar cornmeal-based food at 25℃ unless further specified.

4.2.2 Generation of S2 cell constructs

Su(var)2-10 cDNA clone (RE73180) was obtained from the *Drosophila* Genomics Resource Center. The CDS region of *Su(var)2-10* was then subcloned into the pAFW vector for expressing N-terminal 3xFlag-tagged Su(var)2-10 protein. For *His2A* construct, the coding sequence was PCR-amplified from the cDNA library that reverse-transcribed from w^{1118} total larval mRNA. The CDS was then recombined into the backbone acquired from the EGFP-4CM plasmid via the Gibson assembly. Point mutation was introduced by site-directed mutagenesis. See Table 4.1 for a list of plasmids generated for S2 cells transfection. Primers for the generation of plasmids are listed in Table 4.2.

Table 4.1 A list of plasmids used for S2 cell transfection in chapter 4.

Plasmid name	Features
pAFW	Vector used to generate plasmids encoding N-terminal 3xFlag-tagged proteins
Ac5-STABLE2-neo	Vector used to generate plasmids encoding C-terminal 4xMyc-tagged proteins
EGFP-4CM	Expresses C-terminal 4xMyc-tagged EGFP
pAFW-Su(var)2-10	Expresses N-terminal 3xFlag-tagged Su(var)2-10
Ac5-His2A-4CM	Expresses C-terminal 4xMyc-tagged His2A
Ac5-His2A^{K119A}-4CM	Expresses C-terminal 4xMyc-tagged His2A mutant that carries a lysine to alanine change at residue 119

Table 4.2 Primers used to generate constructs in chapter 4.

Primer name	Sequence (5' to 3')
Su(var)2-10 NF FP	TTGTACAAAAAAGCAGGCTATGCGAAAGACCCGCTCTCAG
Su(var)2-10 NF RP	GTACAAGAAAGCTGGGCCTAGCCGACGTTTGGGCGCCTTG
EGFP 4CM EGFP FP	ATGGTGAGCAAGGGCGAGGAG
EGFP 4CM BB2 RP	GCACTTTTCGGGGAAATGTGCGCGGAACCCCTATTTG
His2A C-Myc FP	CGCCACCATGGCCATGTCTGGACGTGGAAAAGGTG
His2A C-Myc RP	GCCCTTGCTCACCATGGCCTTCTTCTCGGTCTTCTTGG
His2A SDM K119A FP	CTGTTCTGTTGCCCAAG GCG ACCGAGAAGAAG
His2A SDM K119A RP	CCTGTATATTAGGCAACACGCCACCTTGTGCAATTGTG

4.2.3 RNA-Sequencing (RNA-Seq)

Animals were reared on standard Nutrifly media (https://bdsc.indiana.edu/information/supplies.html). For a single biological replicate, 30-50 ring glands were dissected in cold PBS and transferred to Trizol (ThermoFisher #15596026). Samples were flash-frozen in liquid nitrogen and stored at -80℃ for long-term use. RNA was carefully extracted using the RNeasy kit (Qiagen #74106), followed by examining the RNA integrity on Bioanalyzer using the Agilent RNA 600 nano kit (#5067-1511). For library generation, a total of 4 ng total RNA from each sample was used based on the Ovation SoLo RNA-Seq System (0502). The Ovation SoLo RNA-Seq System provides a solution for a range of low input as little as 500 cells or 10 pg-10 ng of total RNA. The use of "AnyDeplete" technology provided targeted depletion of ribosomal RNAs (rRNAs), resulting in a significant reduction in sequencing reads derived from rRNAs for more efficient readouts.

Additional equipment, reagents, and labware were required but not provided in the Ovation SoLo RNA-Seq kit to generate a strand-specific library for RNA-Seq. This includes, for example, thermal cycler, Qubit fluorometer, Agencourt RNAClean XP Beads (Beckman Coulter, #A63987), EvaGreen (Biotium #31000), magnetic stand for 0.2 ml thin-wall PCR plates, NEBNext® Library Quant Kit for Illumina (NEB, #E7630S), etc.

Total RNA from each biological replicate was extracted from *Drosophila* ring gland cells. The RNA-seq cDNA library was then generated following standard procedures provided by the

manufacturer. Specifically, 4 ng of total RNA from each sample was used as input for cDNA library preparation, which was categorized into the following stages: DNase treatment and primer annealing, first strand cDNA synthesis, cDNA processing, second strand synthesis, end repair, adaptor ligation and purification, library amplification step I and purification, AnyDeplete, library amplification step II and purification. The number of amplification cycles used in library amplification step I was determined empirically by qPCR. The amplification curves were displayed as log fluorescence vs. cycle number, and the number should be within the exponential phase of the amplification. To conduct the quantitative analysis of RNA-Seq libraries, library samples were analyzed using the NEBNext® Library Quant Kit for Illumina. Each library sample was serial diluted to 1:1000, 1:10,000, and 100,000. In each 384 well, 8 µl master mix (containing master mix, primer mix, and low ROX) was added, followed by adding 2 µl DNA samples (DNA standards, no template control, or diluted library) using an electronic pipettor. qPCR assay was run following the cycling conditions listed as below: 95℃-1 min; 35 cycles (95℃-15 s, 63℃-45 s). Ct values were recorded and used to calculate the final concentrations of each library sample using the NEB qPCR web tool (https://nebiocalculator.neb.com/#!/qPCRlibQnt). cDNA Library concentrations should be no less than 3 nM and no more than 100 nM with a total of 25 µl for an efficient readout for the NovaSeq sequencing platform (The McGill University and Génome Québec Innovation Centre). See Appendix A2 & A3 for library concentrations measured by NEBNext® Library Quant Kit for Illumina coupled with qPCR.

The differentially expressed genes among samples were acquired by computational analysis

began with raw RNA-Seq reads in FASTQ format. In short, the raw data were first aligned to the reference genome of *Drosophila melanogaster.* The short reads were then assembled into transcripts using reference transcript annotation. Next, the expression level of each gene was estimated by counting the number of total reads that aligned to the full-length transcript. To accurately estimate gene expression, read counts were normalized to reads per kilobase of exon model per million mapped reads (RPKM) to correct systematic variability, such as library fragment size, sequence composition bias, and read depth [224, 225]. The RPKM was then used to analyze the fold change and statistical significance of each gene.

For RNA-Seq result analysis, raw reads acquired after sequencing were mapped to *Drosophila* reference transcriptome using Arraystar 4.0, followed by calculation of RPKM values to represent relative abundance of the transcripts. Relative fold change of expression was determined by comparing the RPKMs between the experimental groups (*Su(var)2-10*-RNAi and *smt3*-RNAi) to the control groups (w^{1118}). RNA-Seq data was then analyzed using Microsoft Access and Microsoft Excel to find DEGs under certain filtering conditions. Transcripts with an RPKM less than 1 were discarded. Gene ontology analysis was performed with DAVID [226, 227] and the OmicShare tools, a free online platform for data analysis (www.omicshare.com/tools).

4.3 Results

4.3.1 Loss of *Su(var)2-10* in PG cells blocked animal development

Knocking down *Su(var)2-10* in PG cells using *Su(var)2-10*-RNAi (VDRC KK, v100813)

completely blocked the larval-to-pupal transitions in animals (Fig. 4.5), suggesting that *Su(var)2-10* is an essential gene for *Drosophila* development. In addition, nearly all the arrested L3 larvae had enlarged ring glands compared to control animals, which might be caused by feedback control of not having enough ecdysone in those *Su(var)2-10* loss-of-function PG cells for directing the developmental transition. Since the ring gland did not show the red auto-fluorescence seen in *RanBP3* loss-of-function animals, I reasoned that *Su(var)2-10* might regulate ecdysone biosynthesis via a different mechanism than *RanBP3*.

The *phmN1* line was recombined between the second chromosome *phm22-Gal4* and the third chromosome *UAS-Mcd8::GFP* (BDSC #5137), which ectopically expresses GFP on the PG cell membrane. Thus, I switched from *phm22* to *phmN1* driver to see whether or not the PG size could be altered by PG-specific *Su(var)2-10* loss-of-function. I examined a total of four *Su(var)2-10* RNAi lines by crossing them with *phmN1-Gal4*, respectively, followed by survival rate quantification and ring gland morphology observation. Three out of four lines (except RNAi 4) targeted the *Su(var)2-10* locus in the genome at different sites without any overlap (Fig. 4.6a). As a result, all the *Su(var)2-10* loss-of-function animals showed the same developmental defect (not shown), as well as enlarged ring glands (Fig. 4.6b), consistent with the earlier notion that *Su(var)2-10* is essential for viability. Collectively, loss-of-function analyses showed that *Su(var)2-10* is critical for the larval-to-pupal transition in *Drosophila*, most likely by affecting the PG function to synthesize ecdysone. Since all the RNAi lines mentioned above showed the comparable phenotype, I decided to use the VDRC KK line (v100813, designated as *Su(var)2-10*^{IR}) hereafter for all the

following experiments unless specifically described.

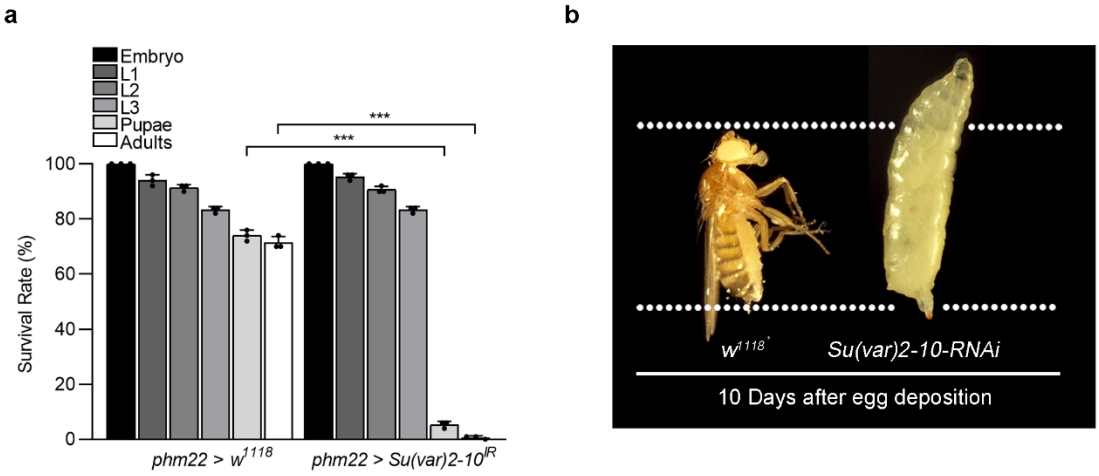

Figure 4.5 Losing *Su(var)2-10* function in PG cells caused a severe developmental defect.

(a) Survival of PG> *Su(var)2-10*-RNAi animals compared to the control. Error bars represent standard deviation. *P<0.05, **P<0.01, ***P<0.001. (b) Development of PG-specific *Su(var)2-10* loss-of-function animals compared to the control ten days after egg deposition.

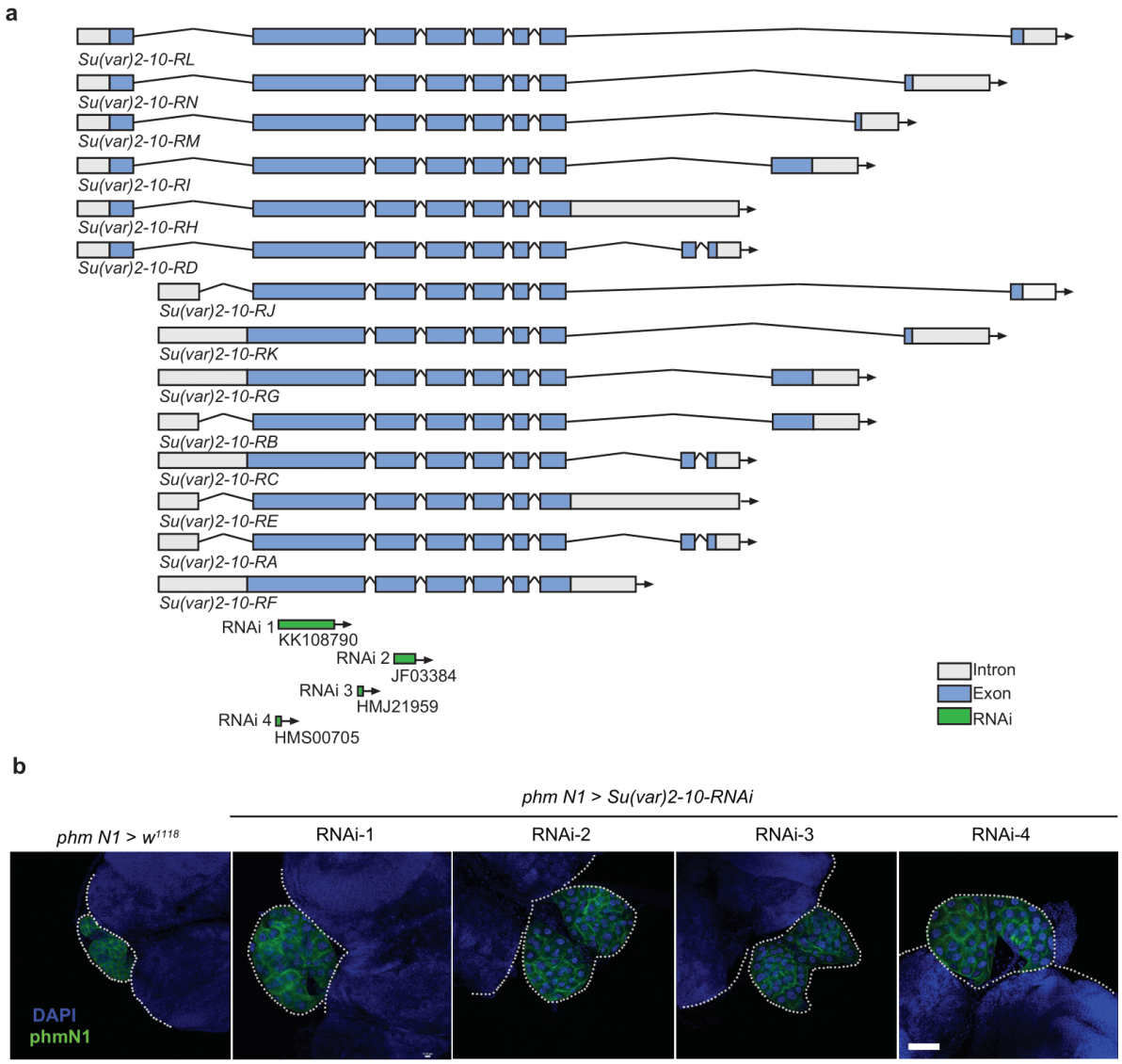

Figure 4.6 Verification of *Su(var)2-10* loss-of-function phenotype using RNAi lines targeting different sites in the genome.

(a) *Su(var)2-10* is alternatively spliced into 14 different transcripts and encodes at least four unique proteins. However, the double-stranded RNA mediated interference lines target consensus regions in the *Su(var)2-10* mRNA. However, three out of four lines have non-overlapping target sites. (b) Confocal microscopy of dissected ring glands collected from 40-42 hours third-instar larvae in

which *Su(var)2-10* was knocked down using *phmN1-Gal4* driver. The green signal represents GFP protein expression originated from the transgenic *UAS-mCD8-GFP* line. Scale bar = 500 μm.

4.3.2 Melanotic tumors were found in *Su(var)2-10* trans-heterozygotes

Mutant *Su(var)2-10*$^{[1]}$ (#6236) allele yields a leucine-to-methionine change in amino acid 327, whereas the *Su(var)2-10*$^{[2]}$ (#6235) mutant harbors a tryptophan-to-STOP change in amino acid 260 (Fig. 4.7a). A previous study has shown that chromosome structures of the *Su(var)2-10*$^{[1]}$*/Su(var)2-10*$^{[2]}$ trans-heterozygotes were grossly abnormal in both males and females [168]. One interesting finding was that the development of *Su(var)2-10*$^{[1]}$*/Su(var)2-10*$^{[2]}$ trans-heterozygous animals was blocked at the late larval or early pupal stage (not shown), similar to what I found in the *phmN1>Su(var)2-10*-RNAi animals (Fig. 4.6b). Interestingly, melanotic tumors were found on the cuticle of mutant larvae (3-15%), which phenocopied *Hop* hypermorphs (*Hop*$^{Tum-1}$ and *Hop*^{T42}), in which the JAK/STAT signaling was hyperactivated [228] (Fig. 4.7). These observations implicated that Su(var)2-10 may have a potential link with the canonical JAK/STAT pathway, a major driver in hematopoietic tumor formation (Fig. 4.3). Mis-regulation of Su(var)2-10 function in the prothoracic gland may stimulate the JAK/STAT pathway, subsequently leading to tumor growth.

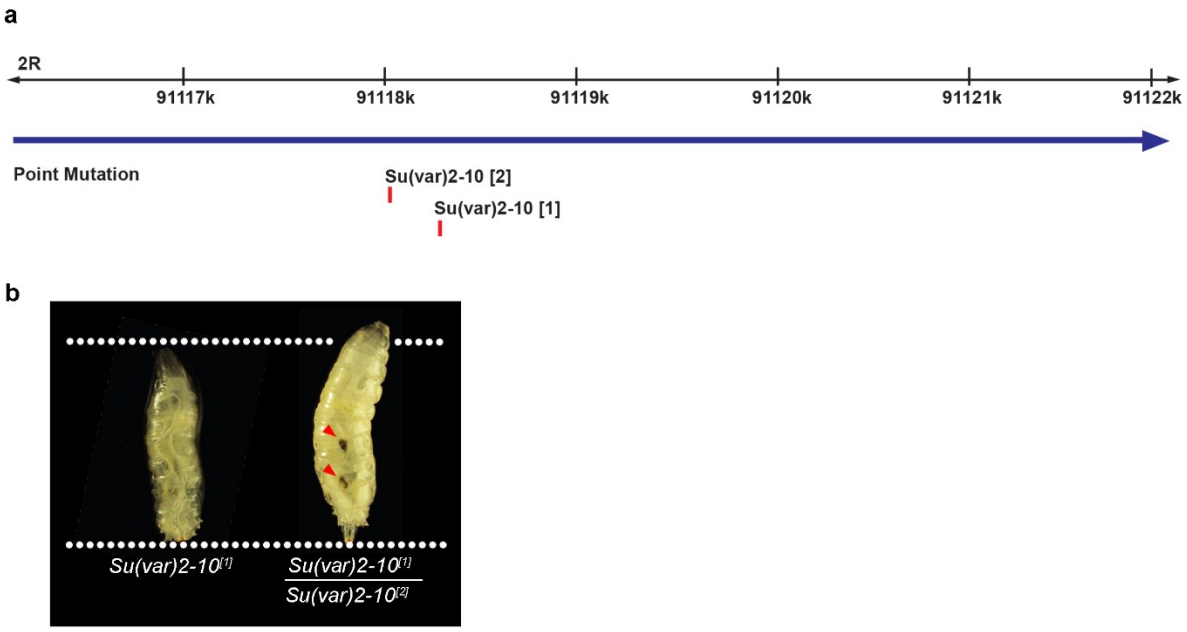

Figure 4.7 *Su(var)2-10* trans-heterozygotes developed melanotic tumors.

(a) Schematic demonstration of the genetic loci of *Su(var)2-10* mutations in the *Drosophila* genome. Both mutations were point mutations resulting in a change of amino acid. (b) The trans-heterozygous mutant of *Su(var)2-10* showed a block in metamorphic development, and importantly, the mutants also developed melanotic tumors on the cuticle (red arrow heads).

Su(var)2-10 encodes a PIAS family protein that negatively regulates the JAK/STAT pathway via SUMOylating the only homolog of STAT (STAT92E) in flies [197, 198]. STAT92E can be phosphorylated on a critical tyrosine residue (Y711) [229], which has been suggested to be essential for the nucleocytoplasmic transport of the protein followed by the subsequent activation of responsive gene expression (Fig. 4.3). A SUMOylation site on STAT92E was also identified in *Drosophila* S2 cells. The lysine residue at amino acid 187 within a consensus sequence ψ-K-X-D/E, where ψ indicates a hydrophobic amino acid and X indicates any amino acid would undergo SUMOylation when key components of the modification are all present [198]. SUMOylation of Lys187 may either interrupt the protein binding activity of STAT92E and its transcriptional coregulators or affect downstream target gene expression by recruiting histone deacetylases to promoter regions.

If *Su(var)2-10* controls ecdysone biosynthesis and larval development through modulating the gene expression in response to the canonical JAK/STAT signaling, I would expect to see similar phenotypes (lethality and enlarged ring glands) in *STAT92E* gain-of-function animals since PIAS is a negative regulator of the JAK/STAT pathway. To my surprise, no significant phenotype was observed in the $STAT92E^{EY10528}$ hypermorphic animals (#20181). One possibility is that although the transgenic insert carried by the transposable element (TE) in $STAT92E^{EY10528}$ [12, 13] strengthens the expression of the gene, the effect might not be strong enough to cause a noticeable phenotype. To address whether *Su(var)2-10* has a role in the canonical JAK/STAT pathway, I examined relative mRNA expression of a multitude of genes that are differentially regulated by

activation of JAK/STAT signaling using BRGC samples dissected from *phm22>Su(var)2-10^{IR}* and *phm22>Su(var)2-10^{TRiP29448}* third-instar larvae, respectively. Of note, *Baz*, *CG13912* and *CG9317* are among those differentially expressed genes showing a significant down-regulation upon the stimulation of Upd. At the same time, *CG13559*, *TotA*, *CG4804* and *socs36E* are significantly up-regulated when JAK/STAT signaling is activated [230]. Interestingly, mRNA expression of *CG13559* was significantly up-regulated in *phm22>Su(var)2-10^{TRiP29448}* brain-ring gland complex, but not in BRGCs collected from *phm22>Su(var)2-10^{IR}* (Fig. 4.8). Unexpectedly, the transcript of *CG9317* was also increased in BRGCs collected from *phm22>Su(var)2-10^{IR}* animals. In addition, the transcription level of other genes remained unchanged. Overall, five out of seven JAK/STAT signaling target genes showed no significant change with respect to their transcription levels upon the expression of *Su(var)2-10*-RNAi in the PG, suggesting that the canonical JAK/STAT pathway may most likely remain intact when knocking down *Su(var)2-10* in PG cells. The loss-of-function phenotypes were not a direct output of disrupting the JAK/STAT pathway in flies.

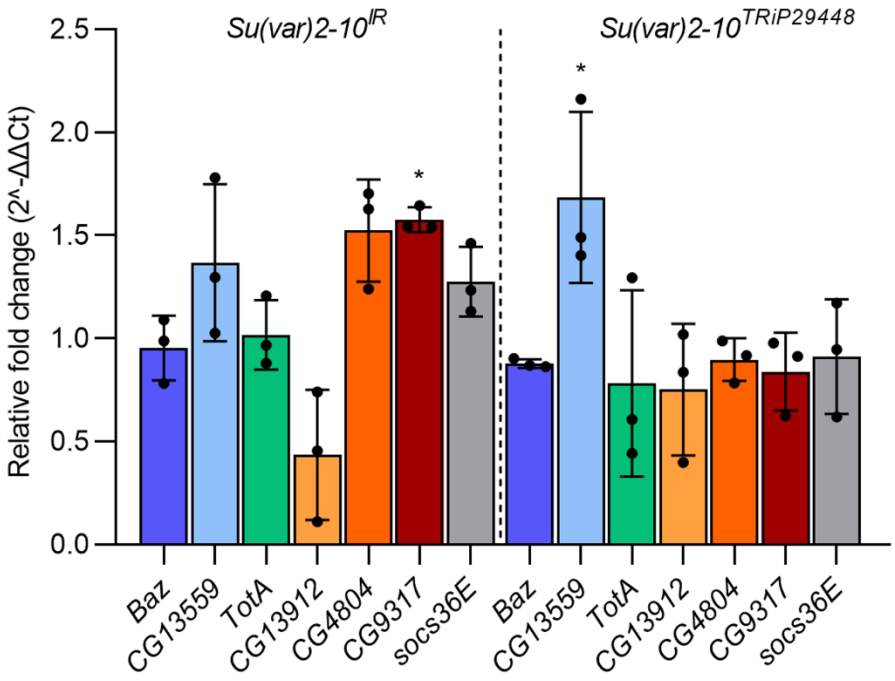

Figure 4.8 qPCR for genes in response to JAK/STAT signaling.

Brain-ring gland complexes were collected from 40-42 hours *phm22 > Su(var)2-10^{IR}* and *phm22 > Su(var)2-10^{TRiP29448}* third-instar larvae. Total RNA was extracted followed by cDNA synthesis and quantification of mRNA transcription of JAK/STAT signaling targets by qPCR. *phm22 > w^{1118}* animals were used as a control. Transcription of target genes was analyzed by using the ΔΔCt method.

4.3.3 *Su(var)2-10* is involved in ecdysone biosynthesis via regulating *nvd* transcription

To address the question of why losing *Su(var)2-10* function in the prothoracic gland blocked larval development, *phm22>Su(var)2-10^{IR}* animals were reared on *Drosophila* diets supplemented with different types of sterols (Table 2.1). Cholesterol is the building block of 20-hydroxyecdysone (20E), the biologically active form of ecdysone that triggers each developmental transition through binding to ecdysone receptors (the EcR/Usp heterodimer) [30, 31]. 7-dehydrocholesterol (7dC) was also included in this experiment. Unlike other intermediates generated in the ecdysone biosynthetic pathway, 7dC is converted from dietary cholesterol by an iron-sulfur cluster protein called Neverland (Nvd) [210] (Table 1.1). Interestingly, the larval lethality of *phm22>Su(var)2-10^{IR}* animals was significantly rescued by supplementing these sterols in *Drosophila* diets (Fig. 4.9a). However, 7dC supplementation showed an optimal effect to rescue *Su(var)2-10* loss-of-function phenotype and was significantly more effective than the other added sterols. Specifically, around 70% of *phm22>Su(var)2-10^{IR}* animals could survive to adulthood after 7dC supplementation compared to almost zero adults in the control groups. Meanwhile, both cholesterol and 20E showed a partial rescue regarding animals' survival rate, where only ~5% of animals can get into adulthood. The enlarged ring glands in the *phm22>Su(var)2-10^{IR}* animals were also rescued to a similar size compared with *phm22>w^{1118}* animals after supplementing sterols into *Drosophila* diets (Fig. 4.9b). However, it seemed that sterol feeding caused a reduced body length of *phm22>Su(var)2-10^{IR}* animals, although the difference was not statistically significant during

the late-larval stage (Fig. 4.9c). I also measured the mRNA expression of genes in the 20E signaling pathway using *Su(var)2-10* loss-of-function brain-ring gland complexes (BRGCs), including ecdysone receptor (*EcR*) [30], *ultraspiracle* (*usp*) [231], *Ecdysone-induced protein 74EF* (*E74*) [232], *Ecdysone-induced protein 75B* (*E75*) [233], *Ecdysone-induced protein 93F* (*E93*) [234], and *broad* (*br*) [235]. I found a significant down-regulation of transcription levels of *EcR* (the receptor gene) and *br* (an early response gene inducible by ecdysone), suggesting that Su(var)2-10 is required for ecdysone production that takes place in the prothoracic gland (Fig. 4.9c). More importantly, since dietary supplementation of 7dC in *the Drosophila* diet rescued *phm22>Su(var)2-10^{IR}* animals' survival, I reasoned that Su(var)2-10 might be of critical importance for the first step in the ecdysone biosynthetic pathway, where the cholesterol is converted to 7dC in the presence of Nvd.

Since not all the intermediates in the ecdysone biosynthetic pathway can be examined due to the presence of the "black box" (uncharacterized conversion steps between 7dC and 5β-ketodiol in the ecdysone biosynthetic pathway) [236], I quantified the mRNA expression of ecdysone biosynthetic genes in *phm22>Su(var)2-10^{IR}* PG cells and compared it to the control (*phm22>w^{1118}*). Of all the genes examined, only *nvd* transcription was dramatically down-regulated. In contrast, transcription of the remaining Halloween genes that encode cytochrome P450 enzymes, such as *phm, dib,* and *sad*, were all up-regulated (Fig. 4.10a). In addition, *Su(var)2-10*-depleted PG nuclei was found bigger than the control nuclei (Fig. 4.10b). Of note, the *Drosophila* prothoracic gland undergoes endoreplication, where multiple copies of the diploid genome are present by DNA

replication without cell division [237]. It has been shown that a pause in the endocycle could induce a block of larval development by a reduction of ecdysone biosynthesis [238]. One possible explanation for observing the enlarged PG cell nuclei in *Su(var)2-10*-RNAi animals was that there might be a feedback mechanism to up-regulate transcription of Halloween genes, such as *phm, dib* and *sad*, in order to compensate for the decrease of ecdysone levels in the PG. To confirm the qPCR result where I found *Su(var)2-10* loss-of-function induced a significant down-regulation of *nvd* transcription, I overexpressed a *nvd* cDNA originated from the silkworm *Bombyx mori* (designated as *nvd-Bombyx*). *nvd-Bombyx* has been previously described to rescue the block of larval development of *nvd*-RNAi animals in the fruit fly [239]. Overexpressing *nvd* cDNA in PG cells significantly rescued both the survival rate and the enlarged ring gland phenotype induced by loss-of-*Su(var)2-10* function (Fig. 4.10c, d). Taken together, these results suggested that Su(var)2-10 is essential for *neverland* transcription, which ultimately regulates ecdysone biosynthesis and *Drosophila* development.

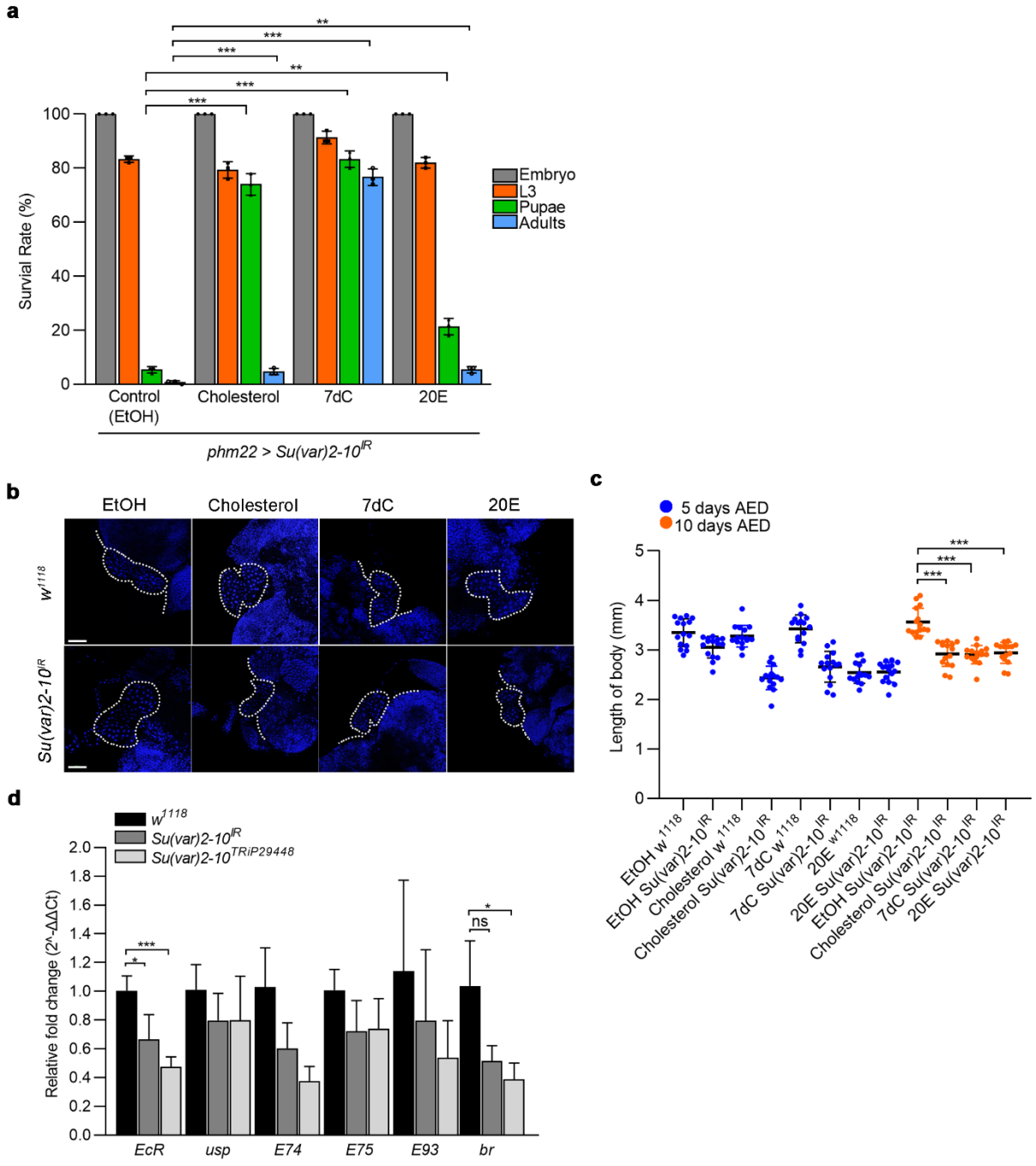

Figure 4.9 Su(var)2-10 is essential for ecdysone biosynthesis in flies.

(a) Survival rate studies of *Su(var)2-10* loss-of-function animals raised on supplementation diets. *phm22-Gal4* was used as a driver to direct transgene expression in the prothoracic gland. 7-

dehydrocholesterol (7dC) is an intermediate product after the first step, whereas 20-hydroxyecdysone (20E) is the biologically active growth hormone converted from dietary cholesterol. *Su(var)2-10*^{IR} stands for the VDRC KK line (v100813). Error bars represent standard deviation. *P<0.05, **P<0.01, ***P<0.001. (b) Confocal microscopy of dissected ring glands from 40-42 hours third-instar larvae. Scale bar = 250 μm. (c) Body length quantification of *phm22>Su(var)2-10*^{IR} and *phm22>w*^{1118} animals reared on sterol-supplemented *Drosophila* diets five and ten days after egg deposition. (d) Relative mRNA expression of genes in *Su(var)2-10* loss-of-function brain-ring gland complexes (BRGCs). Two RNAi lines were examined, and the qPCR results were analyzed using the ΔΔCt method.

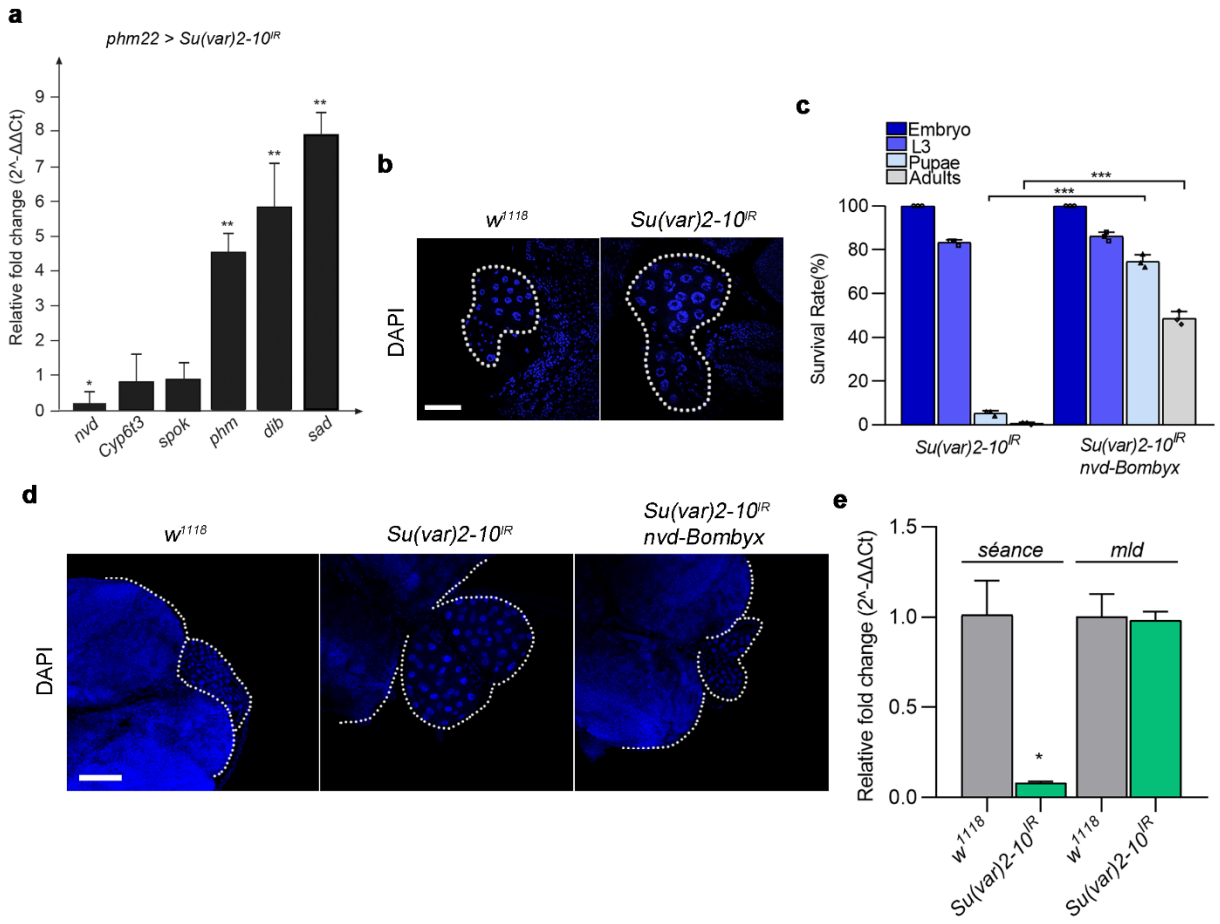

Figure 4.10 Su(var)2-10 regulates *nvd* transcription via Séance.

(a) Measuring mRNA expression of ecdysone biosynthetic genes in *phm22>Su(var)2-10^{IR}* PG cells compared to the control. qPCR results were analyzed using the ΔΔCt method and normalized to the *w^{1118}* control. Error bars represent standard deviation. *P<0.05, **P<0.01, ***P<0.001. (b) Confocal microscopy of dissected ring glands from *phm22>Su(var)2-10^{IR}* and *phm22>w^{1118}* larvae. Scale bar = 500 μm. (c) Survival of *phm22>Su(var)2-10^{IR}* animals that overexpressing *nvd* cDNA. Error bars represent standard deviation. *P<0.05, **P<0.01, ***P<0.001. (d) Confocal microscopy of dissected ring glands from 40-42 hours third-instar larvae co-expressing *nvd* cDNA. Scale bar = 250 μm. (e) Relative fold change of *séance* and *molting defective* (*mld*) mRNA expression in

phm22>Su(var)2-10^{IR} brain-ring gland complexes. Error bars represent standard deviation. Asterisk indicates a P-value < 0.05 based on the student's t-test.

4.3.4 *Su(var)2-10* depletion in the PG down-regulated *séance* transcription

Previous studies have shown that *neverland* transcription is coordinately regulated by two known transcription factors (TFs): Séance and Molting defective (Mld). Mld not only activates *nvd* transcription in cooperation with *séance* but also regulates *spook*ier (*spok*) transcription in collaboration with Ouija board (Ouib) [211]. However, there has been no direct link between Su(var)2-10 and any of these known TFs for the regulation of *nvd* transcription. To examine whether *Su(var)2-10* regulates *neverland* transcription via one or more of the established pathways, I performed a qPCR experiment to measure the mRNA expression levels of these two genes in loss-of-function *Su(var)2-10* BRGCs compared to the control. I found that only *séance*, but not *mld*, showed a significant down-regulation in *Su(var)2-10*-depleted PG cells using the *phm22-Gal4* driver in combination with the *Su(var)2-10^{IR}* RNAi line (Fig. 4.10e). This was consistent with the finding that only *nvd* transcription, but not other Halloween genes, particularly *spok*, were significantly down-regulated. Collectively, Su(var)2-10 plays a critical regulatory role in *neverland* transcription. The finding that *séance* was transcriptionally controlled by Su(var)2-10 was exciting, which showed an intriguing example of a protein regulating transcription factor activity to express the target gene.

4.3.5 His2A may function as a cofactor of Su(var)2-10 in regulating *nvd* transcription

To further characterize the roles of Su(var)2-10 in regulating *nvd* transcription, I wanted to know which proteins were able to physically interact with Su(var)2-10. *Su(var)2-10*$^{GFP.FPTB}$ (#64795) expresses GFP- and Flag-tagged Su(var)2-10 protein. Immunostaining via anti-GFP antibodies of ring glands dissected from third-instar larvae of this line showed predominantly nuclear localization of Su(var)2-10 (Fig. 4.11a). However, the protein was not detectable via Western blotting using anti-GFP antibodies. A simple explanation for not detecting the protein via Western blotting was that this *Su(var)2-10*^{GFP} allele was a transposable element insertion that represented an endogenous expression of the protein. Therefore, the protein levels were too low to be detected. Alternatively, I used *Drosophila* S2 cells to identify Su(var)2-10-interacting proteins. Consistent with the subcellular localization in PG cells, Su(var)2-10 accumulated in S2 cell nuclei (Fig. 4.11b). To pull down Su(var)2-10 proteins, S2 cells were transfected with a plasmid encoding 3xFlag-tagged Su(var)2-10. Cells were then lysed and run on SDS-PAGE gel followed by Coomassie blue staining for mass spectrometry analysis (Fig. 4.11c). Only three candidate proteins were enriched in MS samples (Table 4.3). Among these three candidates, I reasoned that the interaction between Su(var)2-10 and Histone 2A (His2A) family proteins might provide great insights into the mechanism by which Su(var)2-10 regulates *neverland* transcription. The reason that I thought His2A might play a critical role in this process was because His2A was only identified by Su(var)2-10 MS, but not in the other two independent MS experiments (pAFW control and

RanBP3 isoform B) conducted in the same batch as Su(var)2-10 MS. The enrichment of His2A proteins in the Su(var)2-10 MS sample was more likely specific and did not randomly occur.

His2A family of proteins are highly evolutionarily conserved in flies. H2A, H2B, H3 and H4 constitute "canonical" nucleosomes that are structural components of chromatins. The *Drosophila* genome encodes a total of 17 copies of His2A proteins identical to each other (Fig. 4.11d). Given that His2A proteins play such a fundamental role in genome organization and the control of gene expression, it was not surprising that knocking down *His2A* (*CG31618*) in the prothoracic gland blocked the larval development (Fig. 4.11e). Whether His2A plays a role in ecdysone biosynthesis needs to be further investigated.

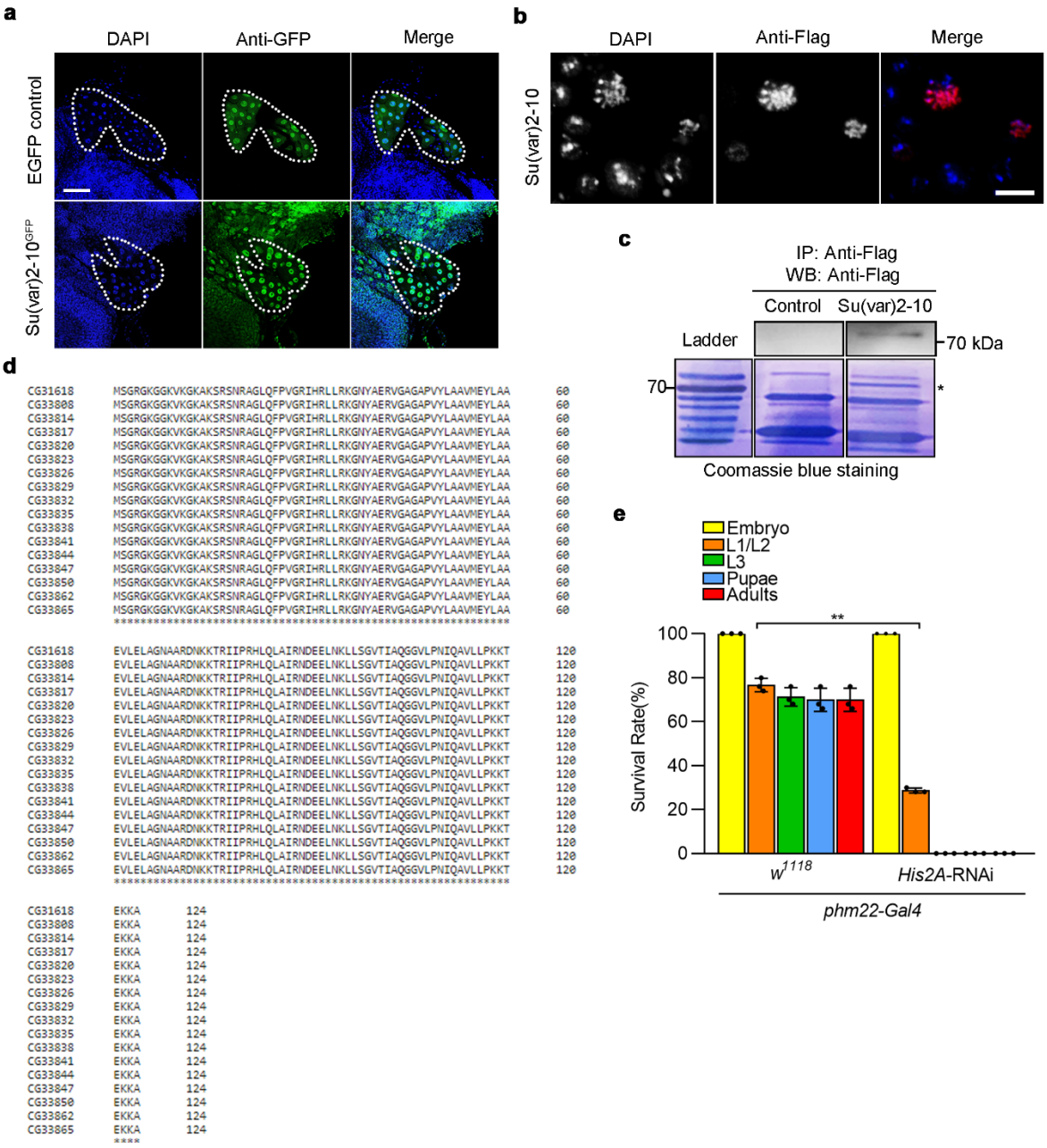

Figure 4.11 His2A was identified as a Su(var)2-10-interacting protein in S2 cells.

(a) Immunostaining of dissected ring glands via GFP antibodies. *phm22>EGFP* animals were used as a control. Scale bar = 250 μm. (b) Transfection of *Drosophila* S2 cells with a plasmid encoding Flag-tagged Su(var)2-10 followed by immunostaining and microscopy analysis. Scale bar = 250 μm. (c) Coomassie blue staining and Western blotting of Su(var)2-10-enriched protein samples.

The gel was later submitted for MALDI-TOF-based mass spectrometry analysis to identify Su(var)2-10-interacting proteins. Cells that were transfected with the pAFW plasmid were used as the control. pAFW is an empty vector carrying no insertion genes but a 3xFlag epitope tag. (d) Sequence alignment of *Drosophila* His2A family proteins. An asterisk indicates positions that have a single, fully conserved residue. (e) Survival of *phm22>His2A*-RNAi animals using *phm22>w*^{1118} animals as the control. Error bars represent standard deviation. *P<0.05, **P<0.01, ***P<0.001.

Table 4.3 Tentative Su(var)2-10-interacting proteins identified by mass spectrometry.

Protein encoded[a]	**CG number**	**Score**	**# Proteins**	**Phenotype**[b]	**Reference**[c]
Suppressor of variegation 2-10	CG8068	192.49	14	L3 arrest	O' Connor
Tubulin beta-1 chain (β-tubulin)	CG9277	18.23	5	NOP	O' Connor
Elongation factor 1-alpha 1 (Ef1alpha48D)	CG8280	6.96	1	L3 arrest	Rewitz
Histone 2A (His2A)	CG31618	6.4	2	L1 arrest	Rewitz

[a] Proteins that showed tentative protein-protein interactions with Su(var)2-10 in *Drosophila* S2 cells (control was excluded).

[b] Animal's development was evaluated after knocking down the gene in the prothoracic gland via crossing with UAS-driven RNAi line. NOP: no phenotype.

[c] The genome-wide RNAi screening was conducted by our lab and two others led by Dr. Michael O'Connor and Dr. Kim Rewitz. Results are shared as a valuable repertoire among three labs.

To establish the link between His2A and Su(var)2-10, I did a series of *in vitro* analyses using the *Drosophila* S2 cell line. To begin with, I made a plasmid encoding C-terminal Myc-tagged His2A protein in S2 cells. Transfection of S2 cells with this plasmid showed that His2A is predominantly nuclear (Fig. 4.12a). As expected, the subcellular localization of His2A overlapped extensively with the DAPI signal, consistent with the role of His2A in the form of nucleosomes. I then co-transfected S2 cells with plasmids encoding Flag-tagged Su(var)2-10 and Myc-tagged His2A to see whether these two proteins could co-localize in the cell. Since both proteins were located in the nucleus, the signals for Su(var)2-10 and His2A overlapped greatly in S2 cells (Fig. 4.12b). Lastly, I verified the protein-protein interaction between these two proteins via co-immunoprecipitation (co-IP) and Western blotting (Fig. 4.12c). Since the loss-of-function phenotype induced by knocking down *His2A* in PG cells using the *phm22* driver was too strong and not beneficial for the subsequent studies, I then used a conditional Gal4 driver allowing the transgene expression in a temporally controlled manner [240]. The induction of the UAS-driven transgene was triggered on the presence of the activator RU486 (mifepristone) at two time points during *Drosophila* development: at the beginning of the embryonic stage (zero hour after egg deposition), or at the onset of the second-instar larval stage (48 hour after egg deposition). Upon feeding RU486 to animals, I noticed a milder but significant developmental defect in *His2A* loss-of-function animals (Fig. 4.12d). However, the ring glands of *His2A* loss-of-function animals were smaller than the control (Fig. 4.12e). Because the smaller size makes it difficult to dissect these

ring glands directly, I instead collected brain-ring gland complexes (BRGCs) from these animals and measured the mRNA expression of ecdysone biosynthetic genes via qPCR. Remarkably, three out of five genes showed a significant down-regulation at the transcriptional level in response to the loss of *His2A* function in the PG (Fig. 4.12f). Among these ecdysone biosynthetic genes, *neverland*, *spookier* and *phantom* showed significant down-regulation, while others remained unchanged. This result suggested that although His2A has a pivotal effect in controlling gene expression in a broad spectrum, only the transcription of specific genes in the ecdysone biosynthetic pathway was affected. Collectively, His2A was identified as a Su(var)2-10-interacting protein in S2 cells. Losing *His2A* function blocked developmental transitions such that most animals were found arrested in the early larval stage. Importantly, His2A may function as the substrate for Su(var)2-10 in regulating *nvd* transcription in ecdysone biosynthesis.

Taken together, current evidence suggests that Su(var)2-10 regulates *neverland* transcription via two pathways. First, Su(var)2-10 might directly affect *nvd* transcription through a post-translational modification of His2A proteins located at *the nvd* promoter region. Second, Su(var)2-10 regulates *séance* transcription specifically in the prothoracic gland, modulating *nvd* transcription. Since the transcription level of *séance* in *His2A* loss-of-function BRGCs showed no statistical difference compared to the control (Fig. 4.12g), I concluded that these two control mechanisms of *neverland* transcription were most likely independent to each other.

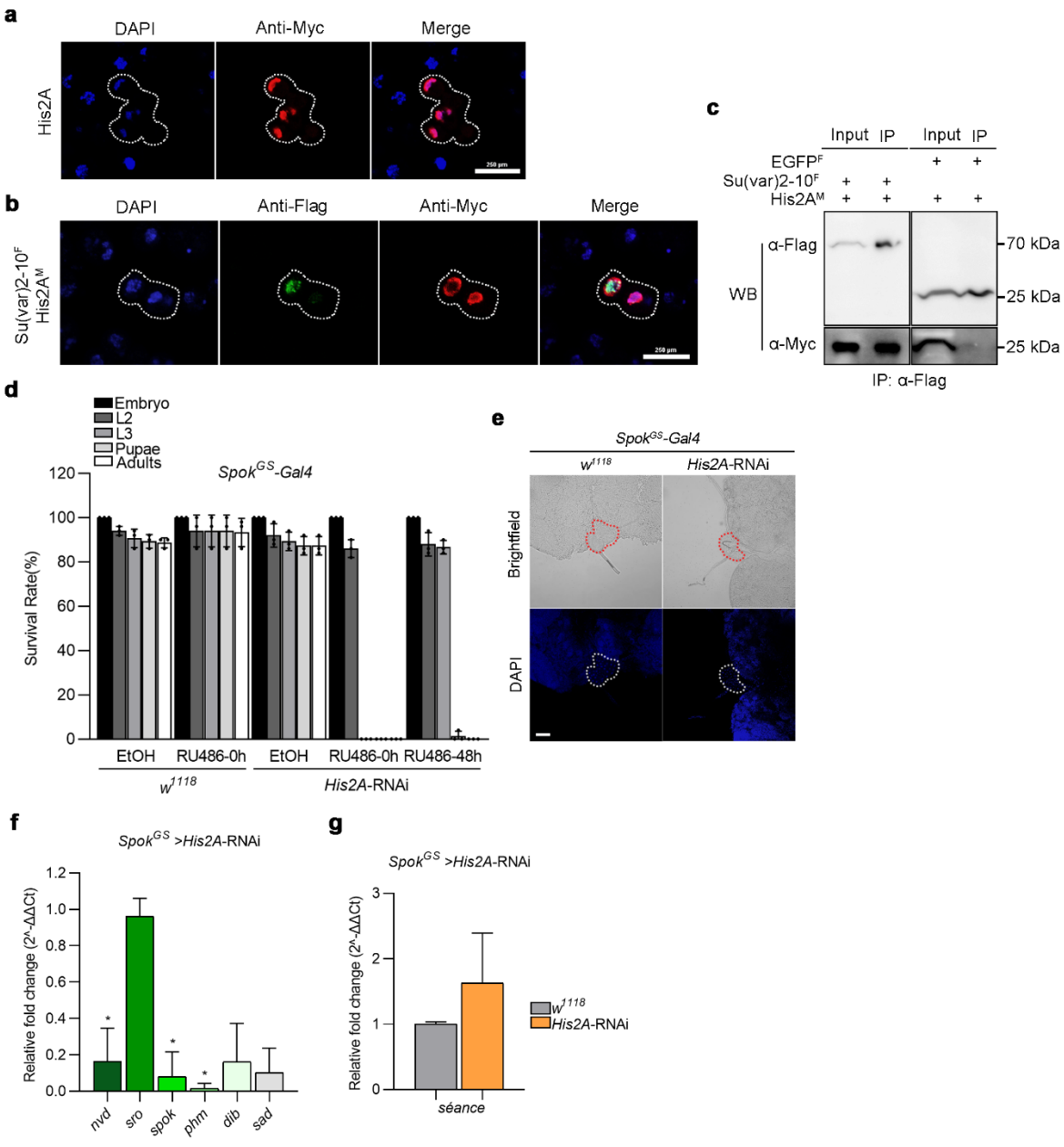

Figure 4.12 His2A is a substrate for Su(var)2-10 in regulating ecdysone biosynthesis.

(a) Transfection of *Drosophila* S2 cells with a plasmid encoding Myc-tagged His2A protein. Scale bar = 250 μm. (b) Co-transfection of S2 cells with plasmids encoding Flag-tagged Su(var)2-10 and Myc-tagged His2A followed by immunostaining and microscopy analysis. Scale bar = 250 μm. (c) Verifying the protein-protein interaction between Su(var)2-10 and His2A using S2 cells. The input

contains 10% total cell lysates. (d) Survival of *Spok*^{GS}>*His2A*-RNAi animals compared to *Spok*^{GS}>*w*^{1118} animals. RU486 (mifepristone) was used in coupled with "GeneSwitch" *Spok-Gal4* to trigger the temporal conditional knockdown of *His2A* in PG cells at the onset of egg deposition (0 h) or early L2 stage (equals to 48 h after egg deposition). (e) Confocal microscopy of dissected ring glands collected from *Spok*^{GS}>*His2A*-RNAi and *Spok*^{GS}>*w*^{1118} 40-42 hours third-instar larvae. Scale bar = 250 μm. (f-g) Measuring mRNA expression levels of ecdysone biosynthetic genes and *séance* in *His2A* conditional loss-of-function brain-ring gland complexes (BRGCs). Error bars represent standard deviation. Asterisk indicates a P-value < 0.05 based on the student's t-test.

4.3.6 Transcriptome analysis of *Su(var)2-10* loss-of-function PG cells via RNA-Seq

My results have demonstrated that Su(var)2-10 is a novel regulator of *neverland* transcription, and therefore indispensable for animal development. To characterize the function of Su(var)2-10 in *Drosophila* in more detail, I conducted an RNA-sequencing (RNA-Seq) experiment for transcriptome-wide analysis of differential gene expression (DGE) using ring glands collected from *phm22>Su(var)2-10*^{IR} third-instar larvae. As next-generation sequencing technologies developed in the past few years, so too has RNA-Seq, which provides far higher coverage and greater resolution of the dynamic nature of the transcriptome, including single-cell gene expression, translation (the translatome) and RNA structure (the structurome) [241, 242]. Since there is not a well-established role of Su(var)2-10, as a SUMO E3 ligase, in the regulation of ecdysone biosynthesis, I included another set of control samples in the RNA-Seq analysis in addition to the *phm22>w*^{1118} control, which was *SUMO* (also named as *smt3* in flies) loss-of-function ring gland samples (*phm22>smt3*-RNAi). *smt3* encodes the only *Drosophila* SUMO family protein required for *Drosophila* metamorphosis at the time of puparium formation [203, 243]. Interestingly, *smt3* knockdown in the PG also completely blocked the larval to pupal transition and caused enlarged ring glands, similar to *Su(var)2-10*-RNAi [203]. The reduced ecdysteroid titers of *smt3*-RNAi PG cells were caused by impaired cholesterol homeostasis. *Drosophila ftz-f1* encodes the only ortholog of the mammalian NR5A2 Liver receptor homolog 1 (LRH-1), which has been shown to play an important role in lipid homeostasis [244]. Smt3 is required for *ftz-f1* expression and Ftz-f1 protein

SUMOylation *in vitro* and *in vivo*. Ftz-f1 is critical for regulating the expression of Sensory neuron membrane protein (Snmp1), which belongs to the *Drosophila* Cluster of Differentiation 36 (CD36) family, for sterol uptake and homeostasis [245]. On the other hand, Su(var)2-10, as the SUMO ligase in the SUMOylation pathway, has been suggested to play an essential role in transcriptional silencing by piRNAs [246]. Specifically, Su(var)2-10 recruits the histone methyltransferase complex SetDB1/Wde through depositing SUMO moieties on chromatin. Given the similar phenotype induced by *Su(var)2-10* and *smt3* loss-of-function in PG cells, *smt3* loss-of-function ring glands would serve as an excellent control for identifying both similar and unique functions of these two tightly related genes.

A total of 1,136 differentially expressed genes (DEGs) were identified in the *Su(var)2-10*-RNAi dataset (SV210:C), while 2,361 genes were differentially expressed in the *smt3*-RNAi dataset (smt3:C), using a cutoff of $p < 0.05$ (Fig. 4.13a). To further refine my results, I quantified the number of DEGs that showed at least 2-fold up- or down-regulation in either of the datasets. As a result, 137 genes were found up-regulated, whereas 125 genes were found down-regulated due to the lack of Su(var)2-10 function in the PG (Fig. 4.13b). On the other hand, losing *smt3* function in PG cells significantly up-regulated expression of 374 genes. Only expression of 84 genes were found down-regulated by lack of *smt3* function in the PG. Since disruption of *smt3* or *Su(var)2-10* function in PG cells causes similar phenotypes (third-instar larval arrest and enlarged ring glands), I wanted to know which genes were transcriptionally regulated by *Su(var)2-10* but not *smt3*, and vice versa. To start with, I sought to identify overlapping genes in both RNA-Seq

data sets. These overlapping genes would be genes which expression showed either up- or down-regulation in both *Su(var)2-10* and *smt3* loss-of-function PG cells. As a result, expression of 29 genes were significantly up-regulated when knocking down either *Su(var)2-10* or *smt3* in the PG, whereas expression of 24 genes were significantly down-regulated in both the datasets (Fig. 4.13c). To examine whether the overlap was identified due to the significance of the difference, or because of random chance, I performed a χ^2 test in which the significance of the difference between the observed numbers and expected numbers when two equally sized lists of *Drosophila* genes were randomly picked was compared (Table 4.4). Since p values examined by χ^2 test were significant, I concluded that the overlapping genes were not identified randomly, but because of a strong correlation between the data sets. To know what are the functions of these overlapping genes, I performed a Gene Ontology (GO) analysis using the DAVID tool [226, 227]. Transcriptional responses of these commonly up- and down-regulated genes are listed in Table 4.5 and Table 4.6, respectively.

The similar phenotype of PG-specific *Su(var)2-10*-RNAi and *smt3*-RNAi animals prompted me to examine which genes are transcriptionally regulated by only *Su(var)2-10*, but not *smt3*, and vice versa. To do so, I subtracted the overlapping genes from the total DEG counts (at least two-fold change) for either of the group to acquire lists of genes that are uniquely regulated by *Su(var)2-10* or *smt3*. Similarly, I conducted a series of GO analysis using these unique DEGs in either of the data set. As a result, I found a strong correlation of up-regulated genes in the Su(var)2-10 data set to biological processes, such as positive regulation of Toll signaling, organic hydroxy compound

biosynthesis, ecdysone biosynthesis (Fig. 4.14a). And down-regulated genes in the Su(var)2-10 data set are associated with GO terms, for example, hydrolases activity, serine-type endopeptidase inhibitor activity (Fig. 4.14b). Meanwhile, GO terms in either up- or down-regulated genes identified in the smt3 data set are shown to strongly correlate with *Drosophila* development. *smt3* loss-of-function would up-regulate expression of genes involved in system development, organ and tissue development, which ultimately affect instar larval or pupal morphogenesis of flies (Fig. 4.15a). On the other hand, down-regulated genes identified in the smt3 dataset are associated with GO terms, such as fatty acid biosynthesis, membrane lipid biosynthesis (Fig. 4.15b), consistent with the role of smt3 in cholesterol metabolism and animal's development. Summary of GO term enrichment for both up- and down-regulated genes identified in the Su(var)2-10 and smt3 data set are shown in Fig. 4.16 and Fig. 4.17, respectively.

Of 101 gene that showed a significant down-regulation when knocking down *Su(var)2-10* in the PG, I found *neverland*, which has been previously shown to be a downstream target of Su(var)2-10. Interestingly, *nvd* transcription showed a significant down-regulation (-3.7-fold, $p<0.001$) in *Su(var)2-10*-RNAi PG cells (Table 4.7), whereas *smt3* knockdown in PG cells did the opposite to up-regulate *nvd* transcription (1.28-fold, $p<0.05$). In great contrast, other ecdysone biosynthetic genes, such as *sro*, *Cyp6t3*, and *dib*, showed significant up-regulation in *Su(var)2-10* loss-of-function PG cells. This result was consistent with my previous qPCR result (Fig. 4.10), where I found only one of the ecdysone biosynthetic genes (*nvd*) was significantly down-regulated, therefore suggesting that Su(var)2-10 is essential for *nvd* transcription, and the up-regulation of

other Halloween genes were most likely induced by a feedback mechanism to compensate decreased ecdysone levels in the PG.

snail (*sna*) was also identified as a differentially expressed gene showing a 10-fold down-regulation in the *Su(var)2-10*-RNAi dataset. In contrast, *sna* transcription was not changed by *smt3* loss-of-function in PG cells (-2-fold, $p>0.05$). Therefore, this result suggested that Su(var)2-10 is required for *sna* expression in PG cells. A previous lab member, Dr. Jie Zeng studied the function of *snail* in regulating the attainment of critical weight (CW), which was defined as the body weight at which *Drosophila* larvae are committed to metamorphosis [247]. She found that *snail* expression showed two peaks that coincided with two waves of endocycle progression in PG cells. The first peak was observed at 17-18 hr in the second-instar larval stage (L2) and the second one around 8-12 hr in the last-instar larval stage (L3). Before the CW is attained, Snail is required for the nutrient-dependent endoreplication in the PG through the TOR signaling [248]. Once the DNA content value (C-value) of PG cells exceeds 16 (C-value ≥16), animals can further develop irrespective of nutritional conditions and are competent to produce a major pulse to trigger metamorphosis. *sna* knockdown in PG cells by *sna*-RNAi induced down-regulation of all six ecdysone biosynthetic genes in an exclusive manner [247], consistent with the idea that *snail* plays an essential role for endoreplication and gene expression. However, it seems unlikely that *snail* plays an indispensable role for *nvd* transcription because if *nvd* transcription were down-regulated by affecting *snail* function in *Su(var)2-10*-depleted PG cells, I would expect to see all the ecdysone biosynthetic genes were down-regulated due to paused endoreplication, similar to what occurred in *snail*-RNAi

PG cells. Consistent with this idea, transcription of genes that are tightly associated with endocycling in PG cells, such as *cdk2*, *cyclin E, dup*, *proliferating cell nuclear antigen 2* (*PCNA2*) and *cullin 4* [238, 247], were not affected by *Su(var)2-10* loss-of-function in PG cells, suggesting that the endoreplication process was not affected by the lack of *Su(var)2-10* function in PG cells. Collectively, I reasoned that Su(var)2-10 has a role to regulate *snail* expression in the late larval stage after the attainment of CW. However, the decreased transcription of *nvd* seemed to be explicitly induced by losing *Su(var)2-10*, but not *sna* function in the PG. And it is still currently unknown whether the transcriptional regulation of Su(var)2-10 to *sna* has a biological function for certain cellular processes in flies.

On the other hand, up-regulated genes identified in either *Su(var)2-10* or *smt3* loss-of-function data sets are most likely genes that are suppressed under normal conditions. As shown in Fig. 4.13c, a total of 345 genes were specifically regulated by *smt3*, whereas 108 genes were specifically regulated by *Su(var)2-10*. Interestingly, five out of eight known heme biosynthetic genes (*I(3)02640*, *Alas, Pbgs, Coprox* and *FeCH*) (Table 4.7) and several genes involved in porphyrin and chlorophyll metabolism (*Ugt37c1*, *Ugt35a*, and *Cox10*) showed a ~1-2-fold up-regulation in *Su(var)2-10* loss-of-function PG cells. Of note, only the transcriptional level of *l(3)02640*, which encodes the third enzyme in the heme biosynthetic pathway, was found differentially expressed in *smt3* loss-of-function PG cells (-1.33-fold, $p<0.05$). A block in any of the last four enzymatic reactions of heme biosynthetic pathway can possibly upregulate the expression of the first four heme biosynthetic genes, ultimately resulting in the porphyria-like phenotype in the *Drosophila*

PG. The finding that *Coprox* and *FeCH* transcription were up-regulated by *Su(var)2-10* explained why we couldn't observe the red autofluorescence in the PG, and consistent with the morphological phenotype of *Su(var)2-10* loss-of-function animals showing only big ring glands, but not red ring glands.

Taken together, the transcriptome analysis of *Su(var)2-10* and *smt3* loss-of-function PG cells identified targets that may show coordinate activity for regulating similar processes. In addition, Su(var)2-10 and smt3 also function in different processes in the *Drosophila* prothoracic gland. However, future work should focus on examining whether biological processes identified from the RNA-Seq analysis play critical roles for ecdysone biosynthesis? And how they coordinate with each other to affect developmental progresses in flies.

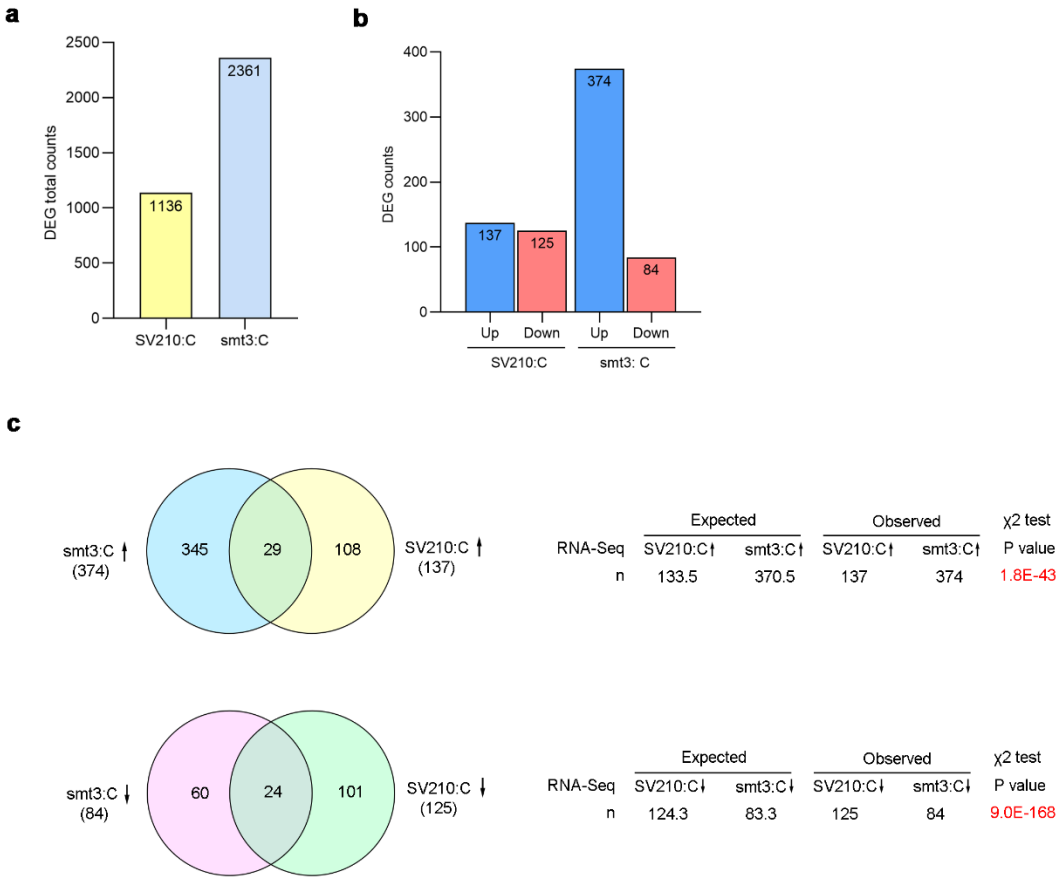

Figure 4.13 Transcriptome analysis of *Su(var)2-10* and *smt3* loss-of-function PG cells.

(a) Total counts of differential expression genes (DEGs) identified in *Su(var)2-10* or *smt3* loss-of-function PG cells, using a cutoff of $p<0.05$. (b) The number of up- and down-regulated genes in both *Su(var)2-10* and *smt3* data sets, using a more restricted cutoff of at least two-fold change and $p<0.05$. (c) Comparing two RNA-Seq data sets to identify overlapping DEGs that can be regulated by both Su(var)2-10 and smt3. The significance of difference between the observed and expected number of genes is determined by χ^2 test.

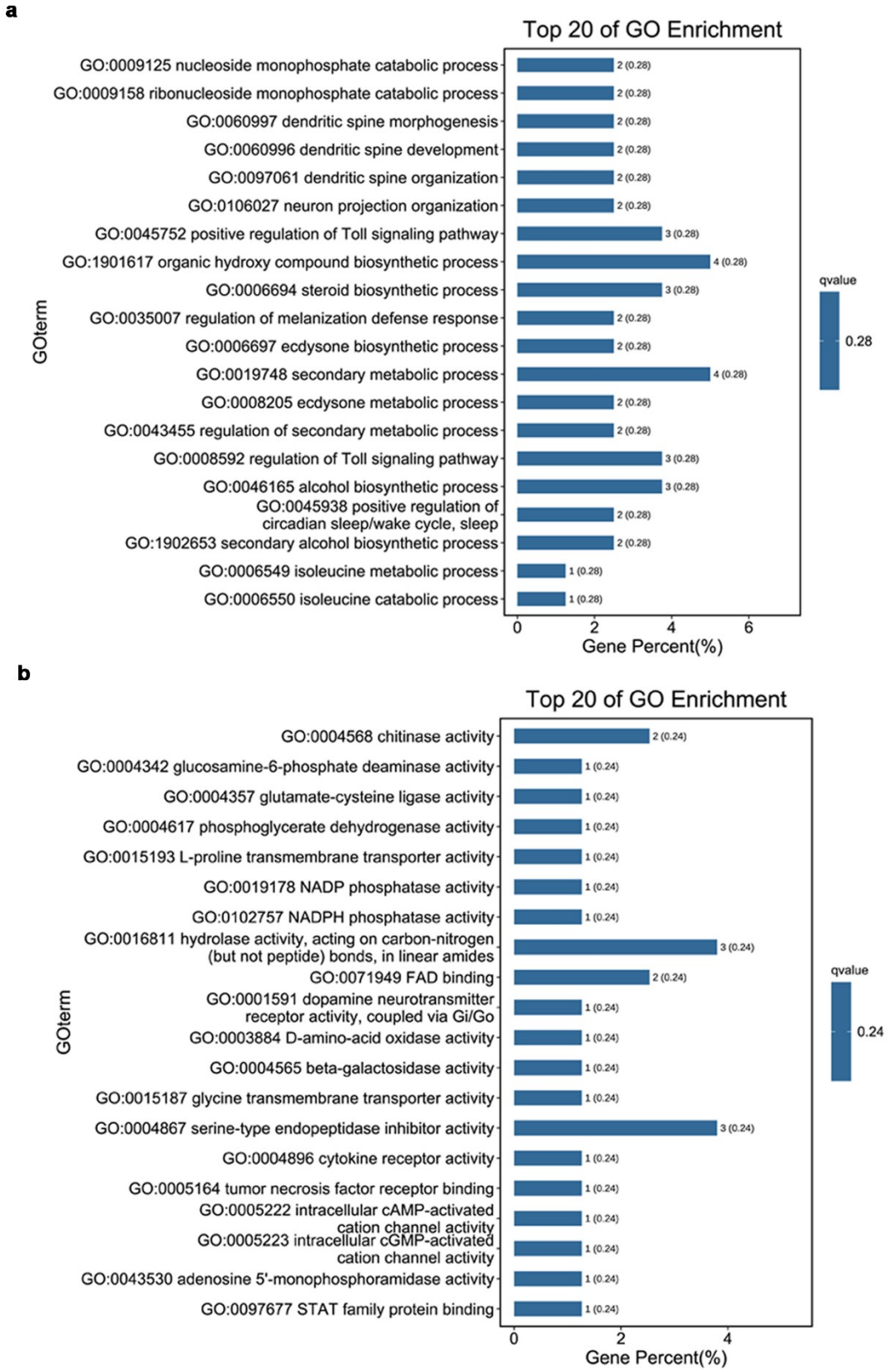
a
Top 20 of GO Enrichment
GO:0009125 nucleoside monophosphate catabolic process
GO:0009158 ribonucleoside monophosphate catabolic process
GO:0060997 dendritic spine morphogenesis
GO:0060996 dendritic spine development
GO:0097061 dendritic spine organization
GO:0106027 neuron projection organization
GO:0045752 positive regulation of Toll signaling pathway
GO:1901617 organic hydroxy compound biosynthetic process
GO:0006694 steroid biosynthetic process
GO:0035007 regulation of melanization defense response
GO:0006697 ecdysone biosynthetic process
GO:0019748 secondary metabolic process
GO:0008205 ecdysone metabolic process
GO:0043455 regulation of secondary metabolic process
GO:0008592 regulation of Toll signaling pathway
GO:0046165 alcohol biosynthetic process
GO:0045938 positive regulation of circadian sleep/wake cycle, sleep
GO:1902653 secondary alcohol biosynthetic process
GO:0006549 isoleucine metabolic process
GO:0006550 isoleucine catabolic process
2 (0.28)
3 (0.28)
4 (0.28)
1 (0.28)
GOterm
0
2
4
6
Gene Percent(%)
qvalue
0.28
b
Top 20 of GO Enrichment
GO:0004568 chitinase activity
GO:0004342 glucosamine-6-phosphate deaminase activity
GO:0004357 glutamate-cysteine ligase activity
GO:0004617 phosphoglycerate dehydrogenase activity
GO:0015193 L-proline transmembrane transporter activity
GO:0019178 NADP phosphatase activity
GO:0102757 NADPH phosphatase activity
GO:0016811 hydrolase activity, acting on carbon-nitrogen (but not peptide) bonds, in linear amides
GO:0071949 FAD binding
GO:0001591 dopamine neurotransmitter receptor activity, coupled via Gi/Go
GO:0003884 D-amino-acid oxidase activity
GO:0004565 beta-galactosidase activity
GO:0015187 glycine transmembrane transporter activity
GO:0004867 serine-type endopeptidase inhibitor activity
GO:0004896 cytokine receptor activity
GO:0005164 tumor necrosis factor receptor binding
GO:0005222 intracellular cAMP-activated cation channel activity
GO:0005223 intracellular cGMP-activated cation channel activity
GO:0043530 adenosine 5'-monophosphoramidase activity
GO:0097677 STAT family protein binding
2 (0.24)
1 (0.24)
3 (0.24)
GOterm
0
2
4
Gene Percent(%)
qvalue
0.24

Figure 4.14 Top 20 of GO enrichment identified for DEGs that respond to *Su(var)2-10* loss-of-function in PG cells.

Top 20 of GO enrichment terms identified from uniquely up- (a) and down-regulated (b) genes in *Su(var)2-10*-RNAi PG cells. q values are adjusted p values based on the False Discovery Rate (FDR). The FDR is the proportion of false positives one would expect to get from a test.

a

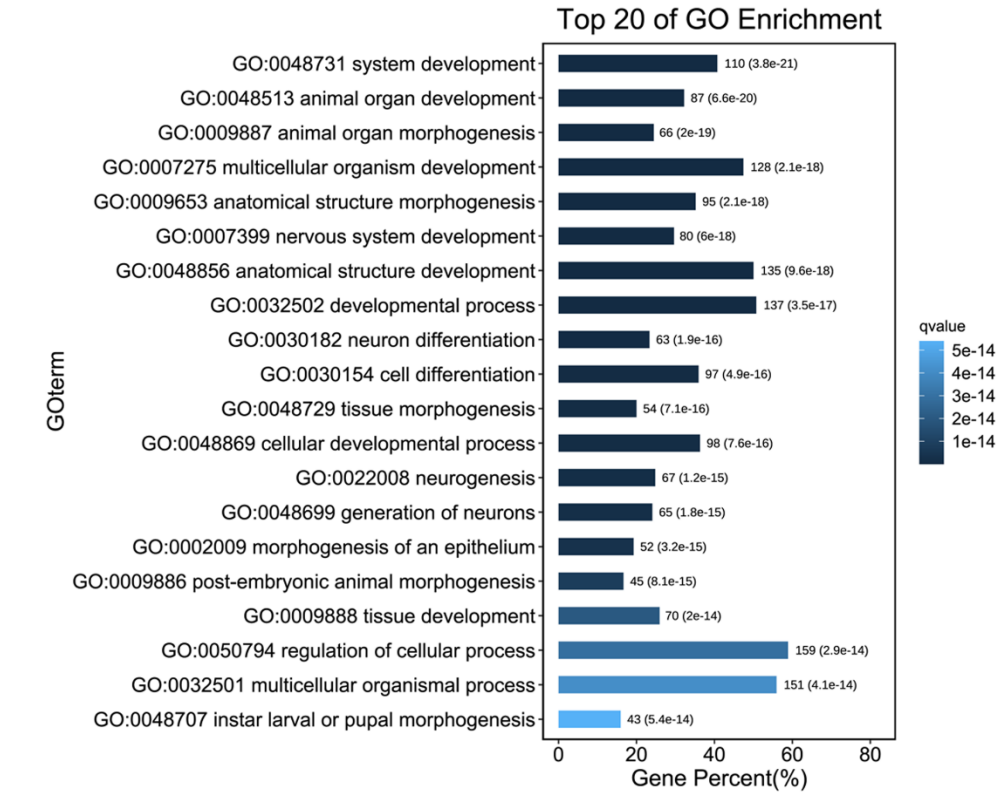
Top 20 of GO Enrichment
GO:0048731 system development
GO:0048513 animal organ development
GO:0009887 animal organ morphogenesis
GO:0007275 multicellular organism development
GO:0009653 anatomical structure morphogenesis
GO:0007399 nervous system development
GO:0048856 anatomical structure development
GO:0032502 developmental process
GO:0030182 neuron differentiation
GO:0030154 cell differentiation
GO:0048729 tissue morphogenesis
GO:0048869 cellular developmental process
GO:0022008 neurogenesis
GO:0048699 generation of neurons
GO:0002009 morphogenesis of an epithelium
GO:0009886 post-embryonic animal morphogenesis
GO:0009888 tissue development
GO:0050794 regulation of cellular process
GO:0032501 multicellular organismal process
GO:0048707 instar larval or pupal morphogenesis
110 (3.8e-21)
87 (6.6e-20)
66 (2e-19)
128 (2.1e-18)
95 (2.1e-18)
80 (6e-18)
135 (9.6e-18)
137 (3.5e-17)
63 (1.9e-16)
97 (4.9e-16)
54 (7.1e-16)
98 (7.6e-16)
67 (1.2e-15)
65 (1.8e-15)
52 (3.2e-15)
45 (8.1e-15)
70 (2e-14)
159 (2.9e-14)
151 (4.1e-14)
43 (5.4e-14)
GOterm
0
20
40
60
80
Gene Percent(%)
qvalue
5e-14
4e-14
3e-14
2e-14
1e-14

b

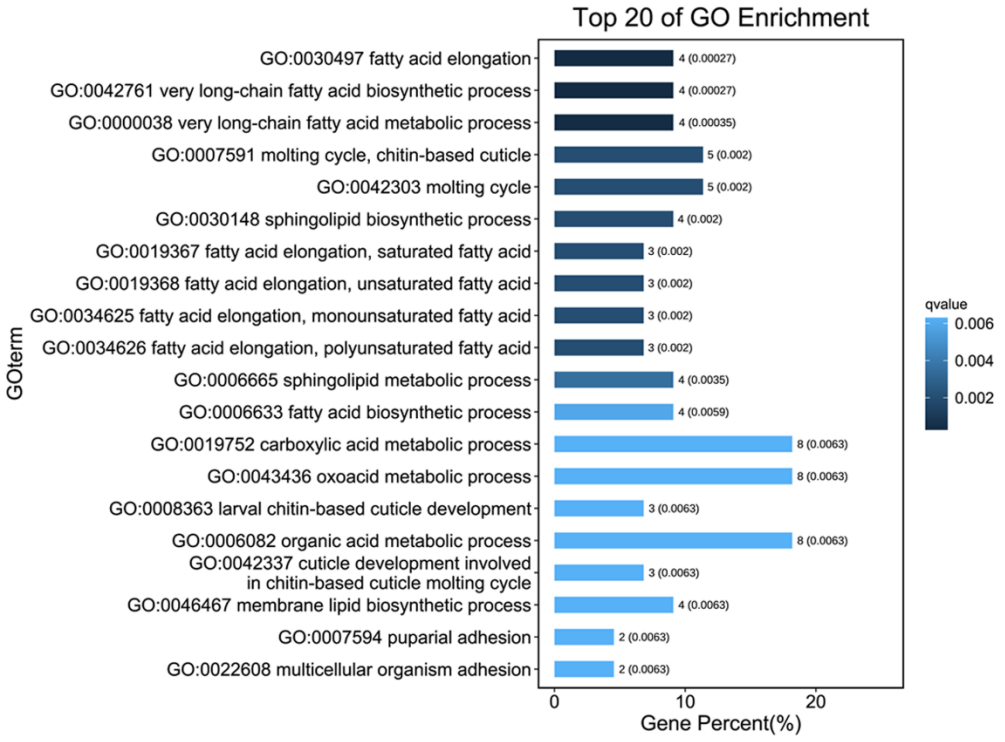
Top 20 of GO Enrichment
GO:0030497 fatty acid elongation
GO:0042761 very long-chain fatty acid biosynthetic process
GO:0000038 very long-chain fatty acid metabolic process
GO:0007591 molting cycle, chitin-based cuticle
GO:0042303 molting cycle
GO:0030148 sphingolipid biosynthetic process
GO:0019367 fatty acid elongation, saturated fatty acid
GO:0019368 fatty acid elongation, unsaturated fatty acid
GO:0034625 fatty acid elongation, monounsaturated fatty acid
GO:0034626 fatty acid elongation, polyunsaturated fatty acid
GO:0006665 sphingolipid metabolic process
GO:0006633 fatty acid biosynthetic process
GO:0019752 carboxylic acid metabolic process
GO:0043436 oxoacid metabolic process
GO:0008363 larval chitin-based cuticle development
GO:0006082 organic acid metabolic process
GO:0042337 cuticle development involved in chitin-based cuticle molting cycle
GO:0046467 membrane lipid biosynthetic process
GO:0007594 puparial adhesion
GO:0022608 multicellular organism adhesion
4 (0.00027)
4 (0.00027)
4 (0.00035)
5 (0.002)
5 (0.002)
4 (0.002)
3 (0.002)
3 (0.002)
3 (0.002)
3 (0.002)
4 (0.0035)
4 (0.0059)
8 (0.0063)
8 (0.0063)
3 (0.0063)
8 (0.0063)
3 (0.0063)
4 (0.0063)
2 (0.0063)
2 (0.0063)
GOterm
0
10
20
Gene Percent(%)
qvalue
0.006
0.004
0.002

Figure 4.15 Top 20 of GO enrichment identified in DEGs that respond to *smt3* loss-of-function in PG cells.

Top 20 of GO enrichment terms identified from uniquely up- (a) and down-regulated (b) genes in *smt3*-RNAi PG cells. q values are adjusted p values based on the False Discovery Rate (FDR). The FDR is the proportion of false positives one would expect to get from a test.

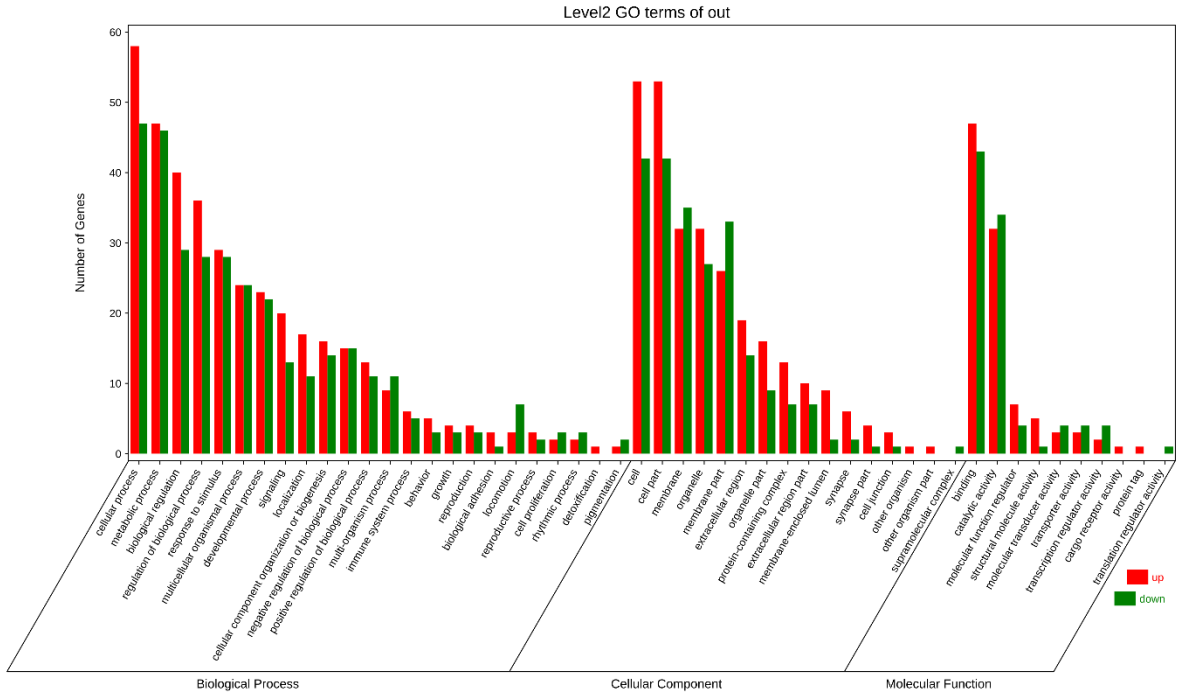

Figure 4.16 A summary of GO term enrichment for transcriptome identified in *Su(var)2-10* loss-of-function PG cells.

Both up- and down-regulated genes (108 and 101) were analyzed for GO terms (Biological Process, Cellular Component, and Molecular Function).

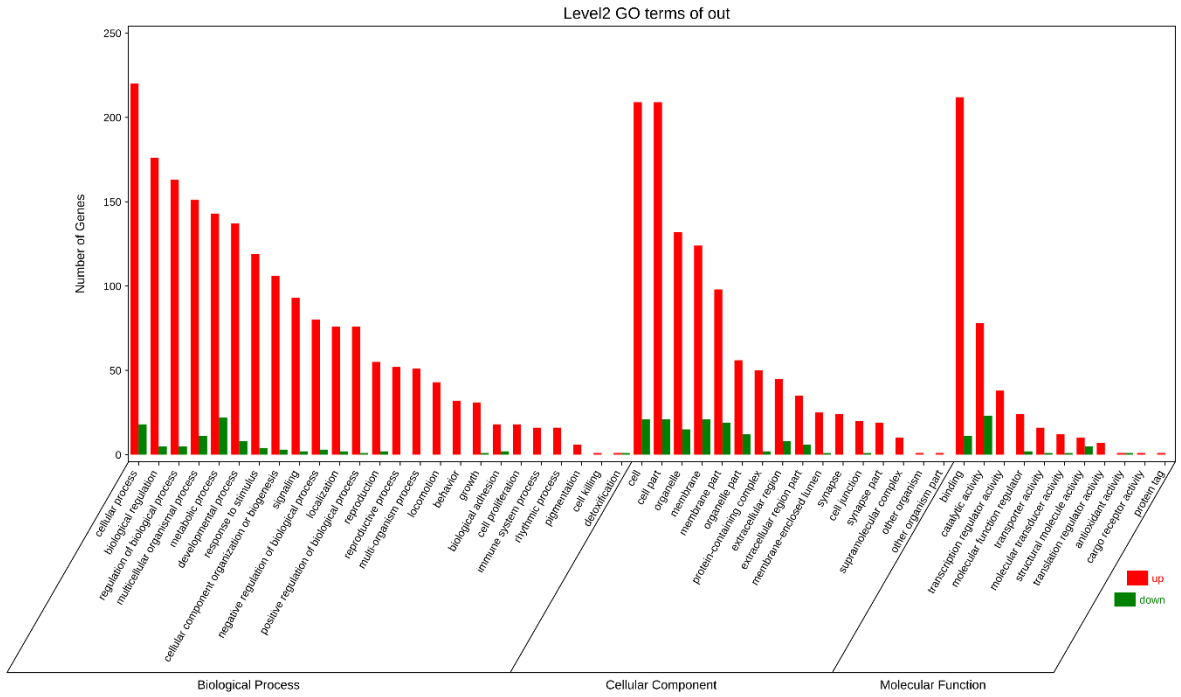

Figure 4.17 A summary of GO term enrichment for transcriptome identified in *smt3* loss-of-function PG cells.

Both up- and down-regulated genes (345 and 60) were analyzed for GO terms (Biological Process, Cellular Component, and Molecular Function).

Table 4.4 *Su(var)2-10* RNA-Seq data compared to *smt3* RNA-seq data

RNA-Seq results (n)		smt3 ↑ (374)		smt3 ↓ (84)	
		n	p value	n	p value
1	Su(var)2-10 ↑ (137)	29	1.8E-43	2	>0.05
2	Su(var)2-10 ↓ (125)	2	>0.05	24	9.0E-168

The RNA-Seq data was acquired by filtering DEGs using a cutoff of >= 2-fold change and $p<0.05$ for both up- and down-regulated gene sets. The number of overlapping genes (n) is shown in each cell and a p value determined by a χ^2 test is shown in the cell next to n. The p values show the significance of the difference between the observed number of genes in the overlap and the expected number of genes on average when two equally sized lists of *Drosophila* genes are randomly picked and compared.

Table 4.5 Transcriptome responses of commonly up-regulated genes (n=29) identified in both RNA-Seq data sets

Gene	FC Su(var)2-10:C	P	FC smt3:C	P	GO[a] molecular function
Hsp70Bb	10.28	4.90E-04	6.89	8.54E-04	ATP hydrolysis
CG5278	8.38	9.58E-05	3.16	2.57E-02	Fatty acid elongation
CR42646	7.63	1.35E-02	5.45	2.32E-02	NA
Hsp70Ab	5.49	4.39E-03	7.84	1.96E-03	Misfold protein binding
fne	5.32	1.99E-02	2.55	4.18E-02	mRNA binding
CG5953	4.76	3.35E-04	4.25	9.59E-04	NA
CG9813	4.71	3.92E-05	2.41	5.82E-03	NA
CG6739	3.48	7.37E-03	3.18	1.36E-02	Low-density lipoprotein particle receptor activity
CG41284	3.32	6.57E-03	2.82	5.57E-04	NA
CG8620	3.26	2.83E-02	4.47	1.25E-02	NA
CG34031	3.16	2.74E-03	2.39	2.21E-03	DNA binding
CG4733	3.09	2.05E-03	2.26	7.30E-03	Calcium ion binding
CG45781	3.08	4.46E-03	2.18	4.13E-04	NA
Cam	3.05	1.39E-03	2.13	2.97E-03	Calcium ion binding
CG9747	2.87	2.92E-03	2.19	8.09E-03	Stearoyl-CoA 9-desaturase activity
CG7616	2.81	2.64E-03	2.19	3.90E-03	NA
ImpE1	2.60	4.07E-02	3.98	2.50E-02	NA
Pzl	2.38	4.48E-03	2.09	9.45E-04	Cation channel activity
CG4456	2.35	5.16E-03	4.99	5.49E-04	NA
CG42402	2.35	2.80E-02	2.05	3.39E-04	Carbohydrate binding

Myo81F	2.34	1.57E-02	2.53	5.80E-04	ATP binding
CR45171	2.31	2.10E-02	2.34	2.15E-02	NA
Cyp317a1	2.17	1.84E-02	2.20	1.47E-02	Oxidoreductase activity
CG17574	2.11	1.94E-02	2.44	5.35E-03	NA
CG45782	2.11	1.37E-02	2.29	1.37E-05	Sucrose: proton symporter activity
Sclp	2.11	1.71E-02	2.56	1.03E-02	NA
Mkp	2.05	1.87E-03	2.61	6.02E-04	Protein tyrosine phosphatase activity
Tg	2.04	2.14E-02	2.44	1.17E-02	Protein-glutamine gamma-glutamyltransferase activity
CG9265	2.02	2.44E-02	2.55	7.99E-03	NAD-retinol dehydrogenase activity

[a] Molecular function of genes were analyzed by the DAVID tool. NA stands for not available.

Table 4.6 Transcriptome responses of commonly down-regulated genes (n=24) identified in both RNA-Seq data sets

Gene	FC Su(var)2-10:C	P	FC smt3:C	P	GO[a] molecular function
CG34140	-7217.52	4.11E-08	-7217.52	4.11E-08	RNA binding
CG6012	-459.09	3.84E-02	-9.23	3.71E-02	Oxidoreductase activity
CG11437	-80.85	1.34E-05	-2.86	6.67E-03	Phosphatidate phosphatase activity
Nox	-7.06	1.80E-06	-2.08	2.43E-03	Calcium ion binding
CG10332	-6.73	7.92E-04	-2.53	3.96E-02	NA
IM18	-6.73	7.92E-04	-2.53	3.96E-02	NA
grass	-6.64	1.27E-03	-2.94	1.04E-02	Serine-type endopeptidase activity
laza	-5.88	6.50E-06	-5.19	5.61E-05	Phosphatidate phosphatase activity
obst-A	-5.16	3.05E-05	-6.70	5.65E-04	Structural constituent of chitin-based cuticle
Dat	-4.79	6.49E-04	-2.14	1.79E-03	NA
CG42331	-4.51	7.31E-06	-3.09	2.84E-02	Heme binding
7B2	-3.93	2.22E-04	-2.86	2.76E-02	Peptidase activator activity
CG17560	-3.50	4.70E-02	-5.06	3.16E-02	Fatty-acyl-CoA reductase (alcohol-forming) activity
Ady43A	-3.48	9.97E-04	-3.63	4.51E-03	Adenosine kinase activity
dop	-3.32	1.28E-03	-3.19	1.44E-03	ATP binding
CG14258	-3.07	4.90E-02	-3.06	3.43E-02	NA
CG4666	-3.01	1.40E-02	-3.52	3.09E-02	NA

CG31388	-2.92	1.28E-03	-2.05	4.81E-02	Zinc ion binding
CG42460	-2.87	5.32E-03	-2.18	6.37E-03	Serine-type endopeptidase inhibitor activity
Mct1	-2.75	3.36E-03	-5.61	4.64E-03	Monocarboxylic acid transmembrane transporter activity
CG5991	-2.64	8.14E-05	-2.58	2.54E-03	Phosphatidylserine decarboxylase activity
CG5196	-2.47	1.60E-04	-2.19	5.75E-03	Protein-cysteine S-palmitoyltransferase activity
CG9541	-2.38	4.10E-04	-5.43	4.27E-04	ATP binding
Pdp	-2.20	1.99E-03	-3.22	2.49E-04	[pyruvate dehydrogenase (lipoamide)] phosphatase activity

[a] Molecular function of genes were analyzed by the DAVID tool. NA stands for not available.

Table 4.7 Transcriptional responses of genes involved in ecdysone biosynthesis and heme synthesis identified by RNA-Seq

Symbol	FC Su(var)2-10:C	P value	FC smt3:C	P value	Pathway
nvd	-3.67	5.3E-04	1.28	2.1E-02	Ecdysone biosynthesis
sro	2.23	1.5E-02	1.27	>0.05	
Cyp6t3	3.94	5.7E-03	-1.15	>0.05	
dib	1.38	8.6E-02	-1.58	2.5E-02	
sad	1.17	>0.05	-1.97	2.2E-02	
phm	-1.39	>0.05	-1.79	3.6E-02	
spok	-1.23	>0.05	1.35	3.6E-02	
alas	1.99	3.1E-03	-1.14	>0.05	Heme biosynthesis
pbgs	1.97	1.8E-02	-1.39	>0.05	
l(3)02640	2.00	1.2E-02	-1.33	4.0E-02	
CG1885	1.27	>0.05	1.09	>0.05	
Updo	1.07	>0.05	-1.13	>0.05	
Coprox	1.51	1.9E-02	-1.08	>0.05	
Ppox	1.24	>0.05	-1.42	>0.05	
FeCH	1.46	4.2E-02	-1.16	>0.05	

4.4 Discussion and future directions

4.4.1 Genome-wide profiling of Su(var)2-10-associated chromatin with CUT&Tag

As previously stated, losing *Su(var)2-10* function in the prothoracic gland significantly down-regulated *séance* transcription, one of the two known transcription factors of *neverland*. In contrast, transcription of *molting defective* remained unchanged in the *Su(var)2-10* loss-of-function BRGCs. Meanwhile, the finding that knocking down *His2A* in PG cells did not affect *Séance* transcription, but down-regulated *nvd* suggested an important role of His2A as a substrate for Su(var)2-10 in regulating *nvd* transcription. There still has not been sufficient evidence showing Su(var)2-10 can bind to the promoter region of *séance* for regulating its transcription. Since Su(var)2-10 is a chromatin-bound protein, one can follow up on this question by adopting an epigenomic profiling strategy such that Su(var)2-10-associated chromatin and chromatin modifications can be characterized.

The mapping of chromatin features has traditionally been performed using Chromatin Immunoprecipitation (ChIP), which was first described 36 years ago [249]. The protocol has not changed much since ChIP was first developed [250, 251]. However, enormous improvements have been made to get high-throughput readouts, including early efforts from Southern blotting to quantitative PCR, to microarrays, and finally to ChIP-Seq. Challenges remain. For example, ChIP requires a large sample size to work and tends to have signal-to-noise ratio issues and artefacts. An alternative chromatin profiling strategy that is becoming increasingly popular is Cleavage Under

Targets & Tagmentation (CUT & Tag), in which chromatin protein is recognized by an antibody that is then used to tether the cut-and-paste transposases Tn5 [252, 253]. Activation of the transposase simultaneously cleaves DNA and adds adapters (a process called “tagmentation”) for paired-end DNA sequencing. This low-cost chromatin profiling method can be performed in a single PCR tube with less than a day of benchwork, from cells to amplified libraries [253]. CUT & Tag has been fully automated for high-throughput applications [254] with a significantly improved signal-to-noise ratio than ChIP. In addition, it is highly efficient not only in a sense that integration by Tn5 is more efficient than enzymatic end-polishing used in traditional library preparation steps, but also because “tagmentation” of targeted Tn5-bound particles is suitable for samples with low cell numbers or even single cell profiling [255].

For CUT & Tag to work for identifying Su(var)2-10-associated chromatin features, such as promoter marks, use of an endogenous GFP-tagged Su(var)2-10 line in which the genomic insertion of the *Su(var)2-10-GFP* cassette is the same as that of the progenitor target insertion (#64795). This line has been previously examined for its expression in the prothoracic gland via anti-GFP antibody staining (Fig. 4.11a), which set a solid foundation for following steps in CUT & Tag. Whole body samples or brain-ring gland complexes (BRGCs) would be used initially as these are relatively easy to collect. Once the workflow and the protocol are confirmed to work well, tissue-specific Su(var)2-10-associated chromatin profiling using ring gland samples will be used.

4.4.2 To characterize novel types of PTMs on Su(var)2-10-binding histone proteins

Since the interaction between Su(var)2-10 and His2A is specific and direct, I reasoned that Su(var)2-10 might exert particular effects on designated chromatin loci in the *Drosophila* genome. The specific Su(var)2-10-histone interactions would be meaningful in the sense that only specific loci on chromatin in the nucleosome could be regulated by post-translational modifications (PTMs). At the same time, the activity of genes in other areas remains unchanged. To this date, there has been a total of 18 types of PTMs described in histone proteins [256]. For the future experiment, "top-down" mass spectrometry can be used to investigate which type of post-translational modification Su(var)2-10 might be involved in the regulation of *neverland* transcription. Top-down mass spectrometry is an emerging technology that preserves the ability to sequence intact proteins since no proteolytic digestion is required. In contrast, the “bottom-up” proteomics is typically carried out by first digesting a protein mixture into short peptides with a protease, then analyzing the peptide mixture by MS [257, 258]. For the same reason, since intact proteins are introduced into the mass spectrometer, important information, especially about combinatorial PTMs, can be retained. This would be especially beneficial for distinguishing positional isomers with the same molecular weight. For example, it could be possible that acetylation occurs on multiple lysine residues. Such PTM isomers can be easily quantified by comparing the ratios of fragment ion abundance produced by two mass analyzers that work dependent on each other in tandem mass spectrometry (also known as MS/MS) [259]. It should also be noted that although there are many

advantages of the top-down MS over the traditional bottom-up assay, extending the approach to whole proteome analysis has been challenging for several reasons. The main obstacle preventing the top-down assay from being more competitive is the requirement for a high-quality proteome fractionation method. Therefore the detection is limited to proteins as large as 229 kDa [260]. In addition, large top-down datasets need to be interpreted using automated software, which is currently in an underdeveloped state.

Overall, the main idea of this assay is to affinity-purify epitope-tagged Su(var)2-10 proteins via antibodies such that histone proteins that are expected to be associated can be enriched at the same time via co-IP. Following this, PTMs identified on Su(var)2-10-binding histones can be compared to PTMs found on control histones for distinguishing PTMs and combinatorial types associated with Su(var)2-10. As mentioned previously, C-terminal EGFP-tagged Su(var)2-10 can only be detected via immunostaining, but not by affinity pull-down assay followed by Western blotting. Therefore, the top-down mass spectrometry assay requires a transgenic UAS-driven tagged line of *Su(var)2-10* that allows for high protein expression in targeted tissues or the whole body.

4.4.3 To examine whether His2A can be SUMOylated

As introduced in section 4.1.6, a SUMOylation site is found at the C-terminal K126 of histone H2A in *S. cerevisiae* by mass spectrometry. However, the substitution of this site did not cause a significant change in H2A SUMOylation levels compared to the wild-type control [216]. Protein

sequence alignment result showed that the SUMOylation site initially identified in yeast (K126) is well-conserved and is located at K119 in the *Drosophila* protein (Fig. 4.18). To see whether SUMOylation can covalently modify His2A at lysine 119, I will perform an *in vitro* SUMOylation assay using purified His2A, SUMO, as well as E1 and E2 enzymes (R&D Systems K715). To begin with, I would generate a series of plasmids encoding critical components required for the SUMOylation assay, including a plasmid encoding Flag-tagged SUMO ($SUMO^{F}$), a plasmid encoding GFP-tagged His2A ($His2A^{EGFP}$), and a plasmid encoding GFP-tagged His2A K119A mutant ($His2A\text{-}K119A^{EGFP}$). *Drosophila* S2 cells will be transfected with these plasmids expressing proteins of interest under the control of the *actin* promoter for a SUMOylation assay following standard protocols [246]. If His2A can be SUMOylated, the Western blotting analysis will show additional higher-molecular-weight bands corresponding to SUMOylated His2A dependent on the presence of the SUMO peptidase inhibitor N-ethylmaleimide (NEM, Sigma 04260-5G-F).

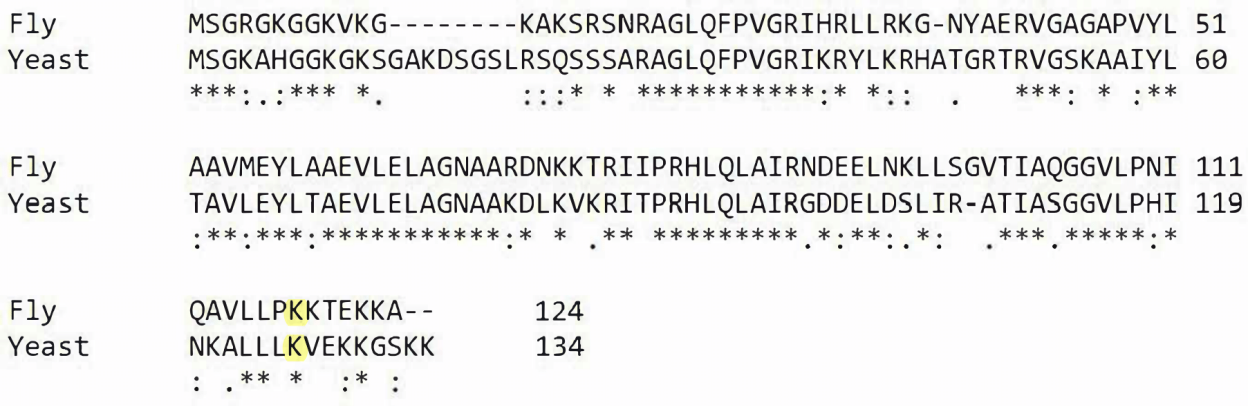

Figure 4.18 Sequence alignment of *Drosophila* and yeast His2A proteins.

Fly His2A protein sequence was compared to counterpart protein in *Saccharomyces cerevisiae* using the "Clustal Omega" web tool. The SUMOylation site initially identified in yeast His2A is well-conserved in *Drosophila* (yellow). An asterisk indicates positions that have a single, fully conserved residue. A colon indicates conservation between groups of strongly similar properties. A period indicates conservation between amino acids of weakly similar properties.

4.4.4 To identify Su(var)2-10-interacting proteins via proximity-based labelling

As a critical component in the SUMO conjugation pathway, Su(var)2-10 (dPIAS) may deliver the SUMO-Ubc9 complex to the target protein via different routes (Fig. 4.4b). The lysine residue on the target protein can directly recognize and bind to Ubc9. Alternatively, the target protein can recruit the SUMO-Ubc9 thioester via the interaction with the SUMO-interacting motif (SIM) located in SUMO. Occasionally, the SUMO E3 ligase positions the SUMO-Ubc9 thioester bond in an orientation that facilitates preferentially binding the lysine residue in the target protein. It should be noted that these modes of recognition are not mutually exclusive, meaning that any of the pathways can catalyze the receptor lysine residue in the substrate. Most of the existing SUMO-enriched proteomes were acquired by a tandem affinity-based approach using SUMO as the bait protein [261, 262]. As introduced earlier in section 4.1.4, both *SUMO* (*smt3*) and *Su(var)2-10* loss-of-function animals showed a blocked larval development, likely due to low ecdysteroid levels. Furthermore, *tonalli* (*tna*) encodes a zinc-finger protein with predicted SUMO transferase activity, similar to Su(var)2-10. Thus, it would be worthwhile to further characterize the role of Su(var)2-10 as a SUMO E3 ligase in the SUMOylation pathway and to distinguish substrate proteins that showed specific protein affinity to Su(var)2-10, but not to other components in the same pathway. One way of solving this question is to conduct an RNA-Seq analysis, as introduced in section 4.3.6, which focuses on the transcription level of gene expression. The other way is to identify endogenous Su(var)2-10-interacting proteins via mass spectrometry assay.

Proximity-based labeling has emerged as a powerful tool to decipher the protein-protein interactions as a complementary approach to the classic affinity purification. Recent innovations have been made to extend the use of biotin-based proximity labeling techniques, such as BioID and APEX, which generate reactive "handle" molecules or "tags" that covalently interact with proximal proteins in live cells [263]. Importantly, these techniques allow for the identification of endogenous protein-protein interactions that most likely occur in the native environment of cells. In addition, given that the use of the biotin tag and the following streptavidin deprivation shows a strong noncovalent binding, proximity labeling can be applied to solubilize, capture and identify proteins that are inaccessible by other affinity-based approaches. There has been a broad range of choices for proximity labeling enzymes [264], such as the bacterial biotin ligase (BirA) and peroxidase-based enzyme (horseradish peroxidase) and ascorbate peroxidase (APEX). Considering that there have been studies applying TurboID to *Drosophila* with high efficiency (short labeling time and wide range of working temperatures) of proximity labeling of endogenous protein-protein interactions[265], I will make a transgenic tag line for Su(var)2-10 that carries the 35 kDa tag for identifying intact interactions *in vivo.* Specifically, TurboID and 3xFlag epitope tags will be inserted in frame with the *Su(var)2-10* cDNA (Fig. 4.19a). This will generate a transgenic line expressing the fusion Su(var)2-10 protein under the regulation of the binary GAL4/UAS system. As a control, a recombinant plasmid encoding GFP protein fused with the same tags will be generated in parallel with the *Su(var)2-10* fusion construct. Followed by embryo injection and standard selection processes, transgenic flies will be crossed with tissue-specific Gal4 drivers, such

as *phm22* (prothoracic gland) and *r4* (fat body), for protein expression in targeted tissues and cells. A workflow showing the optimized TurboID labeling in live *Drosophila* tissues is demonstrated in Fig. 4.19b. The interactome identified by this approach can be cross-compared with established databases via SUMO-trap, which will significantly broaden our current understanding of tissue-specific SUMOylation events explicitly mediated by Su(var)2-10.

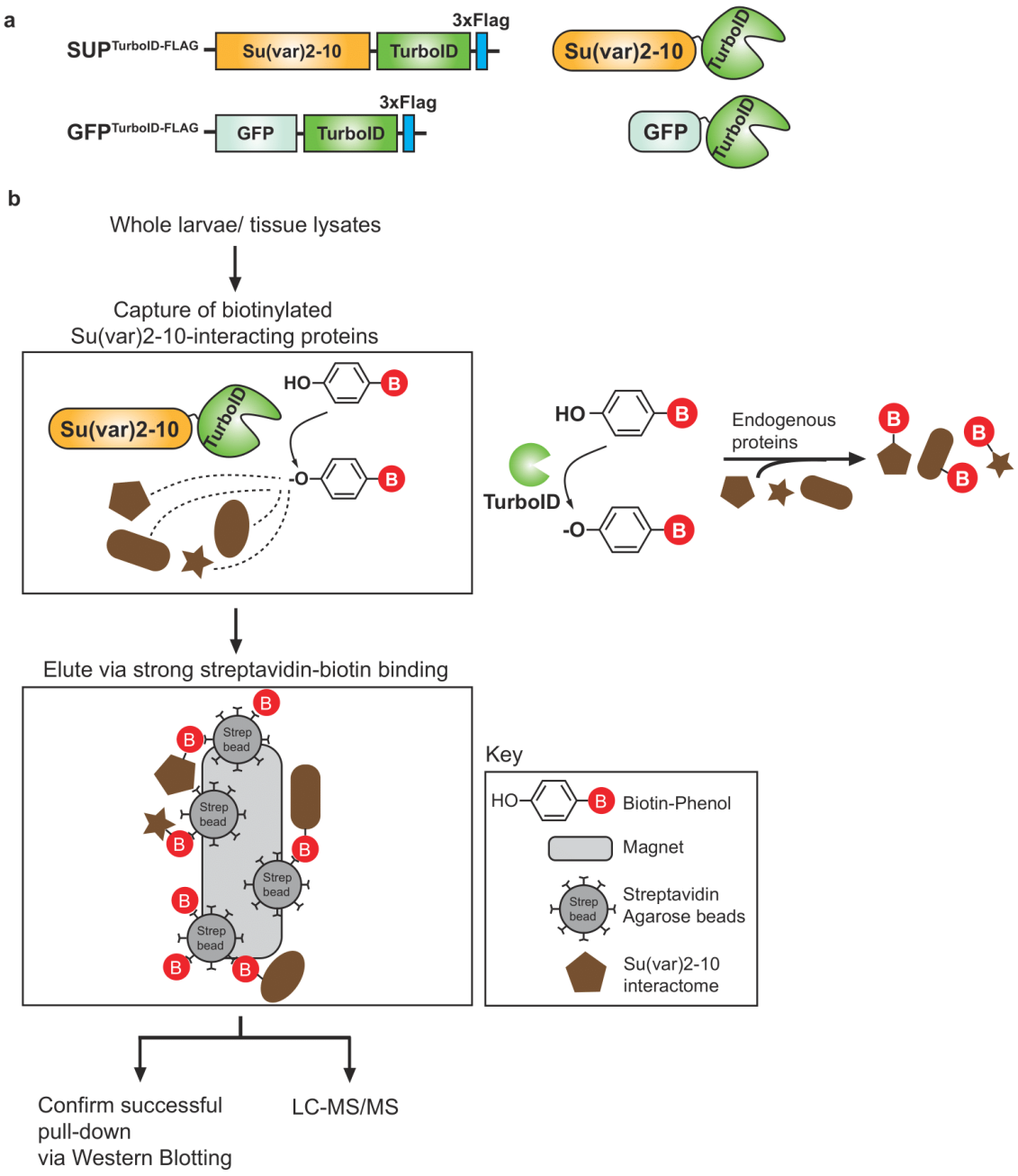

Figure 4.19 Proximity-based labeling of Su(var)2-10 for identification of *in vivo* protein-protein interactions.

(a) A schematic demonstration of recombinant plasmids and corresponding fusion proteins. (b) A workflow of the proximity-based labeling of Su(var)2-10 to its interacting proteins *in vivo*.

Chapter 5 General discussion and perspectives

5.1 Summary of findings

Work in this thesis contributes to our understanding of how IRP1A, the primary cellular iron sensor and regulator in *Drosophila*, is transported into and out of the nucleus through the NPCs. Unlike most nuclear proteins that contain NLS motifs, IRP1A does not have a known NLS and, therefore, cannot be imported into the nucleus via the classical nuclear import pathway mediated by importin-β, a bridge protein that connects the nuclear import complex to the NPC. I reported that the nuclear import of IRP1A in *Drosophila* S2 cells is, instead, through binding to Ran and its nuclear transport factor NTF2. Chickadee was identified as a negative regulator in this process. The replenishment of cytosolic IRP1A is essential for cellular iron homeostasis since the binding of IRP1A to IREs in mRNAs that encode iron metabolism proteins occurs in the cytoplasm. I performed analyses and showed that the binding of *Drosophila* RanBP3 to apo-IRP1A (constitutively RNA-binding) was essential for the nuclear export of IRP1A via the CRM1-mediated nuclear export machinery. Furthermore, I provided molecular evidence showing that RanBP3 may have a role in regulating intracellular iron trafficking via mitoferrin (Chapter 3).

I also characterized the roles of Su(var)2-10 in ecdysone biosynthesis during larval development in *Drosophila melanogaster.* I reported two mechanisms by which Su(var)2-10 regulates transcription of *nvd*, which encodes the enzyme that catalyzes the conversion of cholesterol to 7dC in the prothoracic gland. My initial studies suggested that a post-translational modification, presumably SUMOylation, may modulate *nvd* transcription, which functions irrespective of the transcriptional regulation of *nvd* transcription factors mediated by Séance and

Mld (Chapter 4).

5.2 The complex nature of ecdysone biosynthesis

The synthesis of the primary steroid hormone ecdysone occurs in the larval prothoracic gland by a series of enzymes, including cytochrome P450 enzymes encoded by Halloween genes. Interference of either heme biosynthesis or ISC biogenesis in PG cells causes a block in animals' development, highlighting the importance of using *Drosophila* PG cells to understand the cross-talks of these biological processes. A total of 34 genes identified from previous RNAi screens may have novel roles in heme biosynthesis (Table 3.1). In chapter 3, I demonstrated the novel roles of RanBP3 in ecdysone biosynthesis via regulating cellular iron homeostasis and heme biosynthesis. On the other hand, Su(var)2-10 loss-of-function in PG cells induced only enlarged but not red-autofluorescing ring glands, suggesting that Su(var)2-10 may most likely function differently than RanBP3 to regulate ecdysone biosynthesis and animals' development. Subsequent experiments showed that Su(var)2-10 plays a critical role in regulating *nvd* transcription (chapter 4). Work in this thesis by characterizing functions of two novel genes in ecdysone biosynthesis adds to our current understanding of how heme biosynthesis and cellular iron homeostasis cooperatively regulate ecdysone biosynthesis and *Drosophila* development. Since RanBP3 and Su(var)2-10 are only two representatives, efforts should be made in the future to characterize roles of other genes that displayed abnormal ring gland phenotypes to fulfill our knowledge in *Drosophila* steroidogenesis and development.

5.3 The importance of identifying novel factors that regulate cellular iron homeostasis

Mammalian iron metabolism has been extensively studied, which provided a solid basis for understanding the same processes in *Drosophila* and a chance to use this simpler model organism to model complex human diseases. Despite many similarities, our current understanding suggests that iron metabolism in *Drosophila* is partially conserved to mammals. Many aspects of iron metabolism in *Drosophila* and other insects remain poorly understood. Questions arise mainly because key mammalian players, such as hepcidin, Fpn and TfR1, are lacking in *Drosophila*. However, with new studies in our lab and others exploring different perspectives of iron metabolism in *Drosophila*, we anticipate making great contributions to iron biology in the near future.

One poorly understood topic in *Drosophila* iron biology is how systemic iron metabolism is regulated. *Drosophila* and other insects do not have erythropoiesis. In flies, iron absorbed by intestinal epithelial cells is released into the hemolymph and delivered to target tissues for making iron-containing proteins. In great contrast, mammalian erythropoiesis takes place in the bone marrow, resulting in the highest iron demand for hemoglobin production, far exceeding all other demands for iron [266]. Such a difference in the distribution of iron is also reflected in the regulation of systemic iron homeostasis. Since both the hormone peptide hepcidin and Fpn lack a homologue in *Drosophila*, it is likely that the systemic iron regulation is controlled by different signaling pathways and may have tissue-specific requirements. Insect ferritins are primarily found in the secretory pathway and in the hemolymph, opposite to mammalian ferritins that are

predominantly cytosol. Therefore, ferritin secretion could be one possible explanation for cellular iron export. In addition, *Drosophila* MCO4 [71], a multi-cooper oxidase, may substitute the function of Fpn in flies to mediate iron efflux and high-affinity cellular iron import.

Another layer of complexity of cellular iron absorption comes from the fact that *Drosophila* lacks a TfR1 homologue. In section 3.3.2, I showed that ectopic expression of the *hTfR* allele in the PG complemented the PG-specific *RanBP3*-RNAi phenotype. Both the larval arrest and the porphyria-like phenotype were partially rescued, therefore suggesting that the internalization of Tsf-Fe (III) may most likely highlight the same mechanism as in mammals. Further efforts should be made to identify the transferrin receptor protein that functionally resembles TfR1. We should also consider other pathways to deliver ferric iron into target cells. There has been genetic evidence showing that *Drosophila* ferritin functions as an iron storage protein and is essential for dietary iron absorption and tissue iron detoxification [62]. Since no ferritin receptors have been identified in *Drosophila*, further analysis should focus on characterizing the role of ferritin in circulatory iron trafficking and the mechanism by which iron binds to ferritin followed by internalization into target cells.

The role of *Drosophila* IRP1A in cellular iron regulation has been extensively studied. Only two mRNA transcripts, *SdhB* and *Fer1HCH*, have been reported to possess canonical IREs that enable cellular iron regulation via the IRP1/IRE system. In section 4.3.6, I showed that introducing specific mutations in *IRP1B* cDNA (i.e., $IRP1B^{C447S}$) may result in a conformational change of IRP1B to enable its RNA-binding activity. Future work should focus on identifying non-canonical

(or simply different IRP binding sequences) IREs by bioinformatic tools. Nuclear IRP1A also registers cellular iron homeostasis by transcriptionally regulating gene expression [91]. However, we are at an early stage of understanding the functions of nuclear IRP1A in cellular iron regulation. The interactome for IRP1A indicated interactions with four histone proteins (H2Av, H2A, H2B and H4), consistent with the presence of IRP1A in the nuclei [91]. BPS-mediated iron deprivation induces the translocation of IRP1A from the nucleus to cytosol, and interestingly, a loss of interaction of IRP1A with histone H2Av and H2B in G1, as well as a complete loss of four histone proteins in G2. These results indicate a role of holo-IRP1A in chromatin binding and regulation of gene expression. Histone variants play essential roles in eukaryotic genome organization, cell division, DNA repair, and the control of gene expression [267]. Modulation of gene transcription in eukaryotes is accomplished by covalent modification of the histone tails through PTMs or the replacement of the canonical histones with other variants. *Drosophila* only has one H2A variant (H2Av), orthologous to H2A.Z and H2A.X in eukaryotes. Early studies have shown that H2Av is implicated in heterochromatin formation upstream of H3K9 methylation and HP1 recruitment, two hallmarks of heterochromatin formation and the subsequent transcriptional attenuation [268]. Future work may focus on investigating the nuclear function of IRP1A, for example, if IRP1A regulates gene transcription via H2Av.

5.4 To characterize chromatin-associated protein binding loci in the *Drosophila* genome

Chromatin features, such as epigenetic effects, play critical roles in regulating gene expression.

As stated in section 4.4.1, the revolutionized CUT & Tag approach [252, 253] allows for efficient chromatin profiling performed in a single PCR tube with less than a day of benchwork. It also significantly reduces the sequencing cost compared to traditional approaches, such as ChIP-seq. Therefore, nuclear proteins that show chromatin binding activities can be analyzed in this way to precisely locate their binding sites in the genome using either transgenic tag lines or endogenous knock-in lines, depending on which tool is available for researchers. Of particular relevance to this thesis, there is a need to locate the binding loci of IRP1A and Su(var)2-10 since these two proteins have been shown to interact with histones. More importantly, both proteins regulate ecdysone biosynthetic gene transcription (section 4.3.3 and [91]). The finding of the binding sites of IRP1A in the *Drosophila* genome will provide solid molecular and genetic evidence verifying the novel role of nuclear IRP1A in gene transcription. And the identification of Su(var)2-10-associated binding sites will improve our understanding of SUMOylation in gene regulation.

References

1. Sisk, C.L. and D.L. Foster, *The neural basis of puberty and adolescence.* Nat Neurosci, 2004. **7**(10): p. 1040-7.
2. Brown, G.R. and K.A. Spencer, *Steroid hormones, stress and the adolescent brain: a comparative perspective.* Neuroscience, 2013. **249**: p. 115-28.
3. Robert M. Saplsky, L.M.R., and Allan U. Munck, *How Do Glucocorticoids Influence Stress Responses? Integrating Permissive, Suppressive, Stimulatory, and Preparative Actions.* Endocrine Reviews, 2000.
4. Bouman, A., M.J. Heineman, and M.M. Faas, *Sex hormones and the immune response in humans.* Hum Reprod Update, 2005. **11**(4): p. 411-23.
5. Fujita, T., *Mineralocorticoid receptors, salt-sensitive hypertension, and metabolic syndrome.* Hypertension, 2010. **55**(4): p. 813-8.
6. McCormick, S.D. and D. Bradshaw, *Hormonal control of salt and water balance in vertebrates.* Gen Comp Endocrinol, 2006. **147**(1): p. 3-8.
7. Thummel, C.S., *Molecular Mechanisms of Developmental Timing in C.elegans and Drosophila.* Developmental Cell, 2001.
8. McGinnis, E.B.a.W., *Model Organisms in the Study of Development and Disease.* Epstein's Inborn Errors of Development, 2016.
9. Bier, E., *Drosophila, the golden bug, emerges as a tool for human genetics.* Nat Rev Genet, 2005. **6**(1): p. 9-23.
10. Morgan, T.H., *Sex Limited Inheritance in Drosophila.* Science, 1910.
11. Adams, M.D. and J.J. Sekelsky, *From sequence to phenotype: reverse genetics in Drosophila melanogaster.* Nat Rev Genet, 2002. **3**(3): p. 189-98.
12. Bellen, H.J., et al., *The Drosophila gene disruption project: progress using transposons with distinctive site specificities.* Genetics, 2011. **188**(3): p. 731-43.
13. Bellen, H.J., et al., *The BDGP gene disruption project: single transposon insertions associated with 40% of Drosophila genes.* Genetics, 2004. **167**(2): p. 761-81.
14. Fish, M.P., et al., *Creating transgenic Drosophila by microinjecting the site-specific phiC31 integrase mRNA and a transgene-containing donor plasmid.* Nat Protoc, 2007. **2**(10): p. 2325-31.
15. Amy C. Groth, M.F., Roel Nusse and Michele P, *Construction of Transgenic Drosophila by Using the Site-Specific Integrase From Phage φC31.* Genetics, 2003.
16. Duffy, J.B., *GAL4 system in Drosophila: a fly geneticist's Swiss army knife.* Genesis, 2002. **34**(1-2): p. 1-15.
17. Wilder, E.L., *Ectopic expression in Drosophila.* Methods in Molecular Biology, 2000. **137**: p. 9-14.
18. Gratz, S.J., et al., *Highly specific and efficient CRISPR/Cas9-catalyzed homology-directed*

repair in Drosophila. Genetics, 2014. **196**(4): p. 961-71.
19. Port, F., et al., *Optimized CRISPR/Cas tools for efficient germline and somatic genome engineering in Drosophila.* Proc Natl Acad Sci U S A, 2014. **111**(29): p. E2967-76.
20. Sokolowski, M.B., *Drosophila: genetics meets behaviour.* Nat Rev Genet, 2001. **2**(11): p. 879-90.
21. St Johnston, D., *The art and design of genetic screens: Drosophila melanogaster.* Nat Rev Genet, 2002. **3**(3): p. 176-88.
22. Jennings, B.H., *Drosophila – a versatile model in biology & medicine.* Materials Today, 2011. **14**(5): p. 190-195.
23. Truman, J.W. and L.M. Riddiford, *Physiology of insect rhythms. 3. The temporal organization of the endocrine events underlying pupation of the tobacco hornworm.* J Exp Biol, 1974. **60**(2): p. 371-82.
24. Yamanaka, N., K.F. Rewitz, and M.B. O'Connor, *Ecdysone control of developmental transitions: lessons from Drosophila research.* Annu Rev Entomol, 2013. **58**: p. 497-516.
25. Kawakami, A., et al., *Molecular cloning of the Bombyx mori prothoracicotropic hormone.* Science, 1990. **247**(4948): p. 1333-5.
26. McBrayer, Z., et al., *Prothoracicotropic hormone regulates developmental timing and body size in Drosophila.* Dev Cell, 2007. **13**(6): p. 857-71.
27. Siegmund, T. and G. Korge, *Innervation of the ring gland of Drosophila melanogaster.* J Comp Neurol, 2001. **431**(4): p. 481-91.
28. Qiuxing Ou, K.K.-J., *What Goes Up Must Come Down: Transcription Factors Have Their Say in Making Ecdysone Pulses.* Current Topics in Developmental Biology, 2013. **103**.
29. Helen E. Thomas, H.G.S.A.F.S., *DrosophHa ecdysone receptor with retinoid X receptor and ultraspiracle.* Nature, 1993.
30. Michael R. Koelle, W.S.T., William A. Segraves, Michael T. Bender, Peter Cherbas, and David S. Hogness, *The Drosophila EcR Gene Encodes an Ecdysone Receptor, a New Member of the Steroid Receptor Superfamily.* Cell, 1991.
31. Tso·Pang Yao, B.M.F., Zeyu Jiangi, Lucy Cherbasi, J.·Don Chen, Michael McKeown, Peter Cherbasi, Ronald M. Evans, *Functional ecdysone receptor is the product of EcR and U'traspirac'e genes.* Nature, 1993.
32. Ono, H., et al., *Spook and Spookier code for stage-specific components of the ecdysone biosynthetic pathway in Diptera.* Dev Biol, 2006. **298**(2): p. 555-70.
33. Niwa, R. and Y.S. Niwa, *Enzymes for ecdysteroid biosynthesis: their biological functions in insects and beyond.* Biosci Biotechnol Biochem, 2014. **78**(8): p. 1283-92.
34. Saito, J., et al., *Characterization of candidate intermediates in the Black Box of the ecdysone biosynthetic pathway in Drosophila melanogaster: Evaluation of molting activities on ecdysteroid-defective larvae.* J Insect Physiol, 2016. **93-94**: p. 94-104.
35. Umbreit, J., *Iron Deficiency: A Concise Review.* American Journal of Hematolog, 2005.
36. Robert E. Fleming, M.D., and Prem Ponka, M.D., Ph.D., *Iron Overload in Human Disease.*

The New England Journal of Medicine, 2012.
37. Hentze, M.W., et al., *Two to tango: regulation of Mammalian iron metabolism.* Cell, 2010. **142**(1): p. 24-38.
38. De Domenico, I., D. McVey Ward, and J. Kaplan, *Regulation of iron acquisition and storage: consequences for iron-linked disorders.* Nat Rev Mol Cell Biol, 2008. **9**(1): p. 72-81.
39. Donovan, A., et al., *Positional cloning of zebrafish ferroportin1 identifies a conserved vertebrate iron exporter.* Nature, 2000. **403**(6771): p. 776-81.
40. Vulpe, C.D., et al., *Hephaestin, a ceruloplasmin homologue implicated in intestinal iron transport, is defective in the sla mouse.* Nat Genet, 1999. **21**(2): p. 195-9.
41. Rouault, T.A., *The role of iron regulatory proteins in mammalian iron homeostasis and disease.* Nat Chem Biol, 2006. **2**(8): p. 406-14.
42. Ajioka, R.S. and J.P. Kushner, *Hereditary hemochromatosis.* Semin Hematol, 2002. **39**(4): p. 235-41.
43. Beutler, E., *Hemochromatosis: genetics and pathophysiology.* Annu Rev Med, 2006. **57**: p. 331-47.
44. Camaschella, C., *Understanding iron homeostasis through genetic analysis of hemochromatosis and related disorders.* Blood, 2005. **106**(12): p. 3710-3717.
45. Heeney, M.M. and N.C. Andrews, *Iron homeostasis and inherited iron overload disorders: an overview.* Hematology-Oncology Clinics of North America, 2004. **18**(6): p. 1379-+.
46. Muckenthaler, M.U., et al., *A Red Carpet for Iron Metabolism.* Cell, 2017. **168**(3): p. 344-361.
47. Li, J.Y., et al., *Scara5 Is a Ferritin Receptor Mediating Non-Transferrin Iron Delivery.* Developmental Cell, 2009. **16**(1): p. 35-46.
48. Chen, T.T., et al., *TIM-2 is expressed on B cells and in liver and kidney and is a receptor for H-ferritin endocytosis.* Journal of Experimental Medicine, 2005. **202**(7): p. 955-965.
49. Rajagopal, A., et al., *Haem homeostasis is regulated by the conserved and concerted functions of HRG-1 proteins.* Nature, 2008. **453**(7198): p. 1127-1131.
50. Soares, M.P. and I. Hamza, *Macrophages and Iron Metabolism.* Immunity, 2016. **44**(3): p. 492-504.
51. Arosio, P. and S. Levi, *Cytosolic and mitochondrial ferritins in the regulation of cellular iron homeostasis and oxidative damage.* Biochimica Et Biophysica Acta-General Subjects, 2010. **1800**(8): p. 783-792.
52. Esther G Meyron-Holtz1, M.C.G., Kazuhiro Iwai1,4, Timothy LaVaute1, XavierBrazzolotto1, Urs V Berger3, William Land1,Hayden Ollivierre-Wilson1, Alex Grinberg2, Paul Love2 and Tracey A Rouault1,*, *Genetic ablations of iron regulatory proteins 1 and 2 reveal why iron regulatory protein 2 dominates iron homeostasis.* The EMBO Journal, 2004.
53. Muckenthaler, M.U., B. Galy, and M.W. Hentze, *Systemic iron homeostasis and the iron-*

responsive element/iron-regulatory protein (IRE/IRP) regulatory network. Annu Rev Nutr, 2008. **28**: p. 197-213.
54. Walden, W.E., et al., *Structure of dual function iron regulatory protein 1 complexed with ferritin IRE-RNA.* Science, 2006. **314**(5807): p. 1903-8.
55. Sheftel, A.D. and R. Lill, *The power plant of the cell is also a smithy: The emerging role of mitochondria in cellular iron homeostasis.* Annals of Medicine, 2009. **41**(2): p. 82-99.
56. Anderson, C.P., et al., *Mammalian iron metabolism and its control by iron regulatory proteins.* Biochim Biophys Acta, 2012. **1823**(9): p. 1468-83.
57. Des R. Richardsona, Darius J. R. Lanea, Erika M. Beckera, Michael L.-H. Huanga, Megan Whitnalla, Yohan Suryo Rahmantoa, Alex D. Sheftelb, and Prem Ponkac,d,1, *Mitochondrial iron trafficking and the integration of iron metabolism between the mitochondrion and cytosol.* PNAS, 2010.
58. Tang, X. and B. Zhou, *Iron homeostasis in insects: Insights from Drosophila studies.* IUBMB Life, 2013. **65**(10): p. 863-72.
59. Latunde-Dada, G.O., et al., *Molecular and functional roles of duodenal cytochrome B (Dcytb) in iron metabolism.* Blood Cells Mol Dis, 2002. **29**(3): p. 356-60.
60. Folwell, J.L., C.H. Barton, and D. Shepherd, *Immunolocalisation of the D. melanogaster Nramp homologue Malvolio to gut and Malpighian tubules provides evidence that Malvolio and Nramp2 are orthologous.* J Exp Biol, 2006. **209**(Pt 10): p. 1988-95.
61. Bettedi, L., et al., *Iron depletion in the intestines of Malvolio mutant flies does not occur in the absence of a multicopper oxidase.* J Exp Biol, 2011. **214**(Pt 6): p. 971-8.
62. Tang, X. and B. Zhou, *Ferritin is the key to dietary iron absorption and tissue iron detoxification in Drosophila melanogaster.* FASEB J, 2013. **27**(1): p. 288-98.
63. Mandilaras, K., T. Pathmanathan, and F. Missirlis, *Iron absorption in Drosophila melanogaster.* Nutrients, 2013. **5**(5): p. 1622-47.
64. Nikolai G Kamyshev, K.G.I., Julia V Bragina, Elena A Kamysheva, Elena V Tokmatcheva, Thomas Preat and Elena V Savvateeva-Popova, *Novel memory mutants in Drosophila: Behavioral characteristics of the mutant nemyP153.* BMC Neurosci, 2002.
65. Ward, D.M. and J. Kaplan, *Ferroportin-mediated iron transport: expression and regulation.* Biochim Biophys Acta, 2012. **1823**(9): p. 1426-33.
66. Fraenkel, P.G., et al., *Ferroportin1 is required for normal iron cycling in zebrafish.* J Clin Invest, 2005. **115**(6): p. 1532-41.
67. Irene E. Zohn, I.D.D., 2 Andrew Pollock,1 Diane McVeyWard,2 Jessica F. Goodman,1 Xiayun Liang,3 Amaru J. Sanchez,1 Lee Niswander,1 and Jerry Kaplan2, *The flatiron mutation in mouse ferroportin acts as a dominant negative to cause ferroportin disease.* Blood, 2007.
68. Mao, J., et al., *The iron exporter ferroportin 1 is essential for development of the mouse embryo, forebrain patterning and neural tube closure.* Development, 2010. **137**(18): p. 3079-88.

69. Lang, M., et al., *Multicopper oxidase-1 is a ferroxidase essential for iron homeostasis in Drosophila melanogaster.* Proc Natl Acad Sci U S A, 2012. **109**(33): p. 13337-42.
70. Wang, X., et al., *Drosophila multicopper oxidase 3 is a potential ferroxidase involved in iron homeostasis.* Biochim Biophys Acta Gen Subj, 2018. **1862**(8): p. 1826-1834.
71. De Silva, D.M., et al., *The FET3 gene product required for high affinity iron transport in yeast is a cell surface ferroxidase.* J Biol Chem, 1995. **270**(3): p. 1098-101.
72. Kawabata, H., *Transferrin and transferrin receptors update.* Free Radic Biol Med, 2019. **133**: p. 46-54.
73. Rouault, T.A., *How Mammals Acquire and Distribute Iron Needed for Oxygen-Based Metabolism.* PLOS Biology, 2003. **1**(3): p. e79.
74. Anderson, G.J. and C.D. Vulpe, *Mammalian iron transport.* Cell Mol Life Sci, 2009. **66**(20): p. 3241-61.
75. Randy L. Hamill, J.C.W., and Bruce A. Cook, *Congenital Atransferrinemia.* Clinical Chemistry, 1990.
76. Geiser, D.L. and J.J. Winzerling, *Insect transferrins: multifunctional proteins.* Biochim Biophys Acta, 2012. **1820**(3): p. 437-51.
77. Locke, H.N.a.M., *The localization of ferritin in insects.* Tissue & Cell, 1990.
78. Arosio, P., R. Ingrassia, and P. Cavadini, *Ferritins: a family of molecules for iron storage, antioxidation and more.* Biochim Biophys Acta, 2009. **1790**(7): p. 589-99.
79. Missirlis, F., et al., *Characterization of mitochondrial ferritin in Drosophila.* Proc Natl Acad Sci U S A, 2006. **103**(15): p. 5893-8.
80. Dunkov, B.C. and T. Georgieva, *Organization of the ferritin genes in Drosophila melanogaster.* DNA Cell Biol, 1999. **18**(12): p. 937-44.
81. Pham, D.Q. and J.J. Winzerling, *Insect ferritins: Typical or atypical?* Biochim Biophys Acta, 2010. **1800**(8): p. 824-33.
82. Locke, M., *Surface membranes, Golgi complexes, and vacuolar systems.* Annu Rev Entomol, 2003. **48**: p. 1-27.
83. Leung, M.L.a.H., *The Induction and Distribution of An Insect Ferritin-A New Function For The Endoplasmic Reticulum.* Tissue & Cell, 1984.
84. Arosio, P. and S. Levi, *Cytosolic and mitochondrial ferritins in the regulation of cellular iron homeostasis and oxidative damage.* Biochim Biophys Acta, 2010. **1800**(8): p. 783-92.
85. Lind, M.I., et al., *Of two cytosolic aconitases expressed in Drosophila, only one functions as an iron-regulatory protein.* J Biol Chem, 2006. **281**(27): p. 18707-14.
86. Melefors, Ö., *Translational Regulation in Vivo of the Drosophila Melanogaster mRNA Encoding Succinate Dehydrogenase Iron Protein via Iron Responsive Elements.* Biochemical And Biophysical Research Communications, 1996.
87. Kohler, S.A., B.R. Henderson, and L.C. Kuhn, *Succinate dehydrogenase b mRNA of Drosophila melanogaster has a functional iron-responsive element in its 5'-untranslated region.* J Biol Chem, 1995. **270**(51): p. 30781-6.

88. Nicola K. Gray, K.P., Thomas Dandekar, Brian A.C. Ackerell, and Matthias W. Hentze, *Translational regulation of mammalian and Drosophila citric acid cycle enzymes via iron-responsive elements.* Proc. Natl. Acad. Sci. USA, 1996.
89. Mehta, A., et al., *Ferritin accumulation under iron scarcity in Drosophila iron cells.* Biochimie, 2009. **91**(10): p. 1331-4.
90. Missirlis, F., et al., *Homeostatic mechanisms for iron storage revealed by genetic manipulations and live imaging of Drosophila ferritin.* Genetics, 2007. **177**(1): p. 89-100.
91. Huynh, N., et al., *Glycogen branching enzyme controls cellular iron homeostasis via Iron Regulatory Protein 1 and mitoNEET.* Nat Commun, 2019. **10**(1): p. 5463.
92. Bhavasar, R., G. Santoshkumar, and B.R. Prakash, *Erythrodontia in congenital erythropoietic porphyria.* J Oral Maxillofac Pathol, 2011. **15**(1): p. 69-73.
93. Cappellini, M.D., et al., *Porphyrias at a glance: diagnosis and treatment.* Intern Emerg Med, 2010. **5 Suppl 1**: p. S73-80.
94. Ciftci, V., et al., *Congenital erythropoietic porphyria with erythrodontia: A case report.* Int J Paediatr Dent, 2019. **29**(4): p. 542-548.
95. Lange, H., et al., *The heme synthesis defect of mutants impaired in mitochondrial iron-sulfur protein biogenesis is caused by reversible inhibition of ferrochelatase.* J Biol Chem, 2004. **279**(28): p. 29101-8.
96. Liu, G., et al., *Heme biosynthesis depends on previously unrecognized acquisition of iron-sulfur cofactors in human amino-levulinic acid dehydratase.* Nat Commun, 2020. **11**(1): p. 6310.
97. Kelley, J.B. and B.M. Paschal, *Fluorescence-based quantification of nucleocytoplasmic transport.* Methods, 2019. **157**: p. 106-114.
98. Danielsen, E.T., et al., *A Drosophila Genome-Wide Screen Identifies Regulators of Steroid Hormone Production and Developmental Timing.* Dev Cell, 2016. **37**(6): p. 558-70.
99. Knockenhauer, K.E. and T.U. Schwartz, *The Nuclear Pore Complex as a Flexible and Dynamic Gate.* Cell, 2016. **164**(6): p. 1162-1171.
100. Dasso, Y.A.a.M., *The role of Ran in nuclear function.* Current Opinion in Cell Biology, 2000.
101. Ohno, M.F., M. Mattaj, I. W., *Nucleocytoplasmic transport: the last 200 nanometers.* Cell, 1998. **92**(3): p. 327-36.
102. Scott Kuersten, M.O.a.I.W.M., *Nucleocytoplasmic transport: Ran,beta and beyond.* Trends in Cell Biology, 2001.
103. Stewart, M., *Molecular mechanism of the nuclear protein import cycle.* Nat Rev Mol Cell Biol, 2007. **8**(3): p. 195-208.
104. Motoaki Ohtsubo, H.O., * and Takeharu Nishimoto, *The RCC1 Protein, a Regulator for the Onset of Chromosome Condensation Locates in the Nucleus and Binds to DNA.* The Journal of Cell Biology, 1989.
105. Michael E. Nemergut, 2*† Craig A. Mizzen,4 Todd Stukenberg,4 C. David Allis,4 Ian G.

Macara, *Chromatin Docking and Exchange Activity Enhancement of RCC1 by Histones H2A and H2B.* Science, 2001.
106. Macara, I.G., *Transport into and out of the nucleus.* Microbiol Mol Biol Rev, 2001. **65**(4): p. 570-94, table of contents.
107. Lange, A., et al., *Classical nuclear localization signals: definition, function, and interaction with importin alpha.* J Biol Chem, 2007. **282**(8): p. 5101-5.
108. Kosugi, S., et al., *Six classes of nuclear localization signals specific to different binding grooves of importin alpha.* J Biol Chem, 2009. **284**(1): p. 478-85.
109. W. David Clarkson1, A.H.C., 3, Bryce M. Paschal4 Helen M. Kent1, Airlie J. McCoy1, Larry Gerace5, Pamela A. Silver2 and Murray Stewart1, *Nuclear protein import is decresased by engineered mutants of nuclear transport factor 2 (NTF2) thtat do not bind GDP-Ran.* JMB, 1997.
110. Quimby, B.B., et al., *Functional analysis of the hydrophobic patch on nuclear transport factor 2 involved in interactions with the nuclear pore in vivo.* J Biol Chem, 2001. **276**(42): p. 38820-9.
111. Monika Grote*, U.K., Rudolf Reichelt and Reiner Peters, *Mapping of nucleoporins to the center of the nuclear pore complex by post-embedding immunogold electron microscopy.* Journal of Cell Science, 1995.
112. Steward, A.B.R., *The Drosophila homolog of NTF-2, the nuclear transport factor-2, is essential for immune response.* EMBO rep, 2002.
113. Minakhina, S., et al., *Crosstalk between the actin cytoskeleton and Ran-mediated nuclear transport.* BMC Cell Biol, 2005. **6**: p. 32.
114. Lynn Cooley, E.V., and Kathleen Ayers, *chickadee Encodes a Profilin Required for Intercellular Cytoplasm Transport during Drosophila Oogenesis.* Cell, 1992.
115. Turner, J.G., J. Dawson, and D.M. Sullivan, *Nuclear export of proteins and drug resistance in cancer.* Biochem Pharmacol, 2012. **83**(8): p. 1021-32.
116. Kau, T.R., J.C. Way, and P.A. Silver, *Nuclear transport and cancer: from mechanism to intervention.* Nat Rev Cancer, 2004. **4**(2): p. 106-17.
117. Kutay, U. and S. Guttinger, *Leucine-rich nuclear-export signals: born to be weak.* Trends Cell Biol, 2005. **15**(3): p. 121-4.
118. Joel G. Turner, R.E., Jennifer A. Derderian, Richard Jove and Daniel M. Sullivan, *Human topoisomerase IIa nuclear export is mediated by two CRM-1-dependent nuclear export signals.* Journal of Cell Science, 2004.
119. Matsuyama, A., et al., *ORFeome cloning and global analysis of protein localization in the fission yeast Schizosaccharomyces pombe.* Nat Biotechnol, 2006. **24**(7): p. 841-7.
120. Mueller, L., et al., *Human RanBP3, a group of nuclear RanGTP binding proteins.* FEBS Lett, 1998. **427**(3): p. 330-6.
121. Englmeier, L., et al., *RanBP3 influences interactions between CRM1 and its nuclear protein export substrates.* EMBO Rep, 2001. **2**(10): p. 926-32.

122. Hendriksen, J., et al., *RanBP3 enhances nuclear export of active (beta)-catenin independently of CRM1.* J Cell Biol, 2005. **171**(5): p. 785-97.
123. Dai, F., et al., *Nuclear export of Smad2 and Smad3 by RanBP3 facilitates termination of TGF-beta signaling.* Dev Cell, 2009. **16**(3): p. 345-57.
124. Zheng, H.-Y.L.a.Y., *Phosphorylation of RCC1 in mitosis is essential for producing a high RanGTP concentration on chromosomes and for spindle assembly in mammalian cells.* Genes Dev, 2004. **18**(5): p. 512-27.
125. Yoon, S.O., et al., *Ran-binding protein 3 phosphorylation links the Ras and PI3-kinase pathways to nucleocytoplasmic transport.* Mol Cell, 2008. **29**(3): p. 362-75.
126. Atkinson, C.E., et al., *Effect of FG Motifs on Ordering Proteins within the Nuclear Pore Complex.* Biophysical Journal, 2012. **102**(3): p. 525a.
127. Isgro, T.A. and K. Schulten, *Association of nuclear pore FG-repeat domains to NTF2 import and export complexes.* J Mol Biol, 2007. **366**(1): p. 330-45.
128. Alex D. Sheftel, A.-S.Z., 2 Claire Brown,3 Orian S. Shirihai,4 and Prem Ponka, *Direct interorganellar transfer of iron from endosome to mitochondrion.* Blood, 2007.
129. Jacobs, A., *Low molecular weight intracellular iron transport compounds.* Blood, 1977. **50**(3).
130. Jacobs, A., *An intracellular transit iron pool. In: Iron Metabolism.* Ciba Found Symp 5, 1977: p. 91-106.
131. Lawen, A. and D.J. Lane, *Mammalian iron homeostasis in health and disease: uptake, storage, transport, and molecular mechanisms of action.* Antioxid Redox Signal, 2013. **18**(18): p. 2473-507.
132. Foury, F. and T. Roganti, *Deletion of the Mitochondrial Carrier Genes MRS3 andMRS4 Suppresses Mitochondrial Iron Accumulation in a Yeast Frataxin-deficient Strain.* Journal of Biological Chemistry, 2002. **277**(27): p. 24475-24483.
133. Brazzolotto, X., F. Pierrel, and L. Pelosi, *Three conserved histidine residues contribute to mitochondrial iron transport through mitoferrins.* Biochem J, 2014. **460**(1): p. 79-89.
134. Shaw, G.C., et al., *Mitoferrin is essential for erythroid iron assimilation.* Nature, 2006. **440**(7080): p. 96-100.
135. Paradkar, P.N., et al., *Regulation of mitochondrial iron import through differential turnover of mitoferrin 1 and mitoferrin 2.* Mol Cell Biol, 2009. **29**(4): p. 1007-16.
136. Metzendorf, C., W. Wu, and M.I. Lind, *Overexpression of Drosophila mitoferrin in l(2)mbn cells results in dysregulation of Fer1HCH expression.* Biochem J, 2009. **421**(3): p. 463-71.
137. Lind, C.M.a.M.I., *Drosophila mitoferrin is essential for male fertility: evidence for a role of mitochondrial iron metabolism during spermatogenesis.* BMC, 2010.
138. Navarro, J.A., et al., *Mitoferrin modulates iron toxicity in a Drosophila model of Friedreich's ataxia.* Free Radic Biol Med, 2015. **85**: p. 71-82.
139. Llorens, J.V., et al., *Mitochondrial iron supply is required for the developmental pulse of ecdysone biosynthesis that initiates metamorphosis in Drosophila melanogaster.* J Biol

Inorg Chem, 2015. **20**(8): p. 1229-38.
140. Elbaz, Y. and M. Schuldiner, *Staying in touch: the molecular era of organelle contact sites.* Trends Biochem Sci, 2011. **36**(11): p. 616-23.
141. Friedman, J.R. and G.K. Voeltz, *The ER in 3D: a multifunctional dynamic membrane network.* Trends Cell Biol, 2011. **21**(12): p. 709-17.
142. Benoît Kornmann, E.C., Sean R. Collins, Maya Schuldiner, Jodi Nunnari,Jonathan S. Weissman, Peter Walter, *An ER-Mitochondria Tethering Complex Revealed by a Synthetic Biology Screen.* Science, 2009.
143. Xue, Y., et al., *Endoplasmic reticulum-mitochondria junction is required for iron homeostasis.* J Biol Chem, 2017. **292**(32): p. 13197-13204.
144. Nicolas Gompel, E.A.S., *Drosophila germline transformation.* Gompel lab, 2015.
145. Xiao, G., et al., *Transferrin 1 Functions in Iron Trafficking and Genetically Interacts with Ferritin in Drosophila melanogaster.* Cell Rep, 2019. **26**(3): p. 748-758 e5.
146. Rogers, S.L. and G.C. Rogers, *Culture of Drosophila S2 cells and their use for RNAi-mediated loss-of-function studies and immunofluorescence microscopy.* Nat Protoc, 2008. **3**(4): p. 606-11.
147. Yang, J. and M. Reth, *Drosophila S2 Schneider cells: a useful tool for rebuilding and redesigning approaches in synthetic biology.* Methods Mol Biol, 2012. **813**: p. 331-41.
148. Katie Welch, J.F., Matthias Kohler, and Ian G. Macara, *RanBP3 Contains an Unusual Nuclear Localization Signal That Is Imported Preferentially by Importin- 3.* Molecular And Cellular Biology, 1999.
149. Wilkinson, N. and K. Pantopoulos, *The IRP/IRE system in vivo: insights from mouse models.* Front Pharmacol, 2014. **5**: p. 176.
150. Christova, T. and D.M. Templeton, *Effect of hypoxia on the binding and subcellular distribution of iron regulatory proteins.* Mol Cell Biochem, 2007. **301**(1-2): p. 21-32.
151. Patton, S.M., et al., *Subcellular localization of iron regulatory proteins to Golgi and ER membranes.* J Cell Sci, 2005. **118**(Pt 19): p. 4365-73.
152. Alicia Smith, A.B.a.I.G.M., *Nuclear import of Ran is mediated by the transport factor NTF2.* Current Biology, 1998.
153. Sara Luscieti, 2 Bruno Galy,3 Lucia Gutierrez,4 Michael Reinke,5 Jorge Couso,1,2 Maya Shvartsman,1 Antonio Di Pascale,6 Walter Witke,5 Matthias W. Hentze,7 Pietro Pilo Boyl,5 and Mayka Sanchez, *The actin-binding protein profilin 2 is a novel regulator of iron homeostasis.* Blood, 2017.
154. Nemergut, M.E., et al., *Ran-binding protein 3 links Crm1 to the Ran guanine nucleotide exchange factor.* J Biol Chem, 2002. **277**(20): p. 17385-8.
155. Jacky Chung, C.C., Barry H Paw, *Heme metabolism and erythropoiesis.* Curr Opin Hematol, 2012. **19**(3): p. 156-62.
156. Troadec, M.B., et al., *Targeted deletion of the mouse Mitoferrin1 gene: from anemia to protoporphyria.* Blood, 2011. **117**(20): p. 5494-502.

157. Chung, J., et al., *Iron regulatory protein-1 protects against mitoferrin-1-deficient porphyria.* J Biol Chem, 2014. **289**(11): p. 7835-43.
158. Maynard, J.C., et al., *Gp93, the Drosophila GRP94 ortholog, is required for gut epithelial homeostasis and nutrient assimilation-coupled growth control.* Dev Biol, 2010. **339**(2): p. 295-306.
159. Gaudet, P., et al., *Phylogenetic-based propagation of functional annotations within the Gene Ontology consortium.* Brief Bioinform, 2011. **12**(5): p. 449-62.
160. Walker, M.J., et al., *Proteomic identification of Drosophila melanogaster male accessory gland proteins, including a pro-cathepsin and a soluble gamma-glutamyl transpeptidase.* Proteome Sci, 2006. **4**: p. 9.
161. Wang, Y., et al., *Abnormal mitoferrin-1 expression in patients with erythropoietic protoporphyria.* Exp Hematol, 2011. **39**(7): p. 784-94.
162. Lund, P.A., *Microbial molecular chaperones.* Adv Microb Physiol, 2001. **44**: p. 93-140.
163. Guruharsha, K.G., et al., *A protein complex network of Drosophila melanogaster.* Cell, 2011. **147**(3): p. 690-703.
164. Guo, B., et al., *Characterization and expression of iron regulatory protein 2 (IRP2). Presence of multiple IRP2 transcripts regulated by intracellular iron levels.* J Biol Chem, 1995. **270**(28): p. 16529-35.
165. Pantopoulos, K., N.K. Gray, and M.W. Hentze, *Differential regulation of two related RNA-binding proteins, iron regulatory protein (IRP) and IRPB.* RNA, 1995. **1**(2): p. 155-63.
166. Samaniego, F., et al., *Molecular characterization of a second iron-responsive element binding protein, iron regulatory protein 2. Structure, function, and post-translational regulation.* J Biol Chem, 1994. **269**(49): p. 30904-10.
167. Martina Muckenthaler, N.G., Dmitrij Frishman, Anna Cryklaff, Pavel Tomancak and Matthias W. Hentze, *Iron-regulatory protein-1 (IRP-1) is highly conserved in two invertebrate species; Characterization of IRP-1 homologues in Drosophila melanogaster and Caenorhabditis elegans.* Eur. J. Biochem, 1998.
168. Kumar L. Hari, K.R.C., 1,4 and Gary H. Karpen, *The Drosophila Su(var)2-10 locus regulates chromosome structure and function and encodes a member of the PIAS protein family.* Genes and Development, 2001.
169. Baker, W.K., *Position-effect variegation.* Adv Genet, 1968. **14**: p. 133-69.
170. Henikoff, S., *Position-effect variegation after 60 years.* Trends Genet, 1990. **6**(12): p. 422-6.
171. Spofford, J.B., *Single-locus modification of position-effect variegation in Drosophila melanogaster. I. White variegation.* Genetics, 1967. **57**(4): p. 751-66.
172. Elgin, L.L.W.a.S.C.R., *Position effect variegation in Drosophila is associated with an altered chromatin structure.* Cold Spring Harb Protoc, 1995.
173. Elgin, S.C. and G. Reuter, *Position-effect variegation, heterochromatin formation, and gene silencing in Drosophila.* Cold Spring Harb Perspect Biol, 2013. **5**(8): p. a017780.

174. Donaldson, K.M., A. Lui, and G.H. Karpen, *Modifiers of terminal deficiency-associated position effect variegation in Drosophila.* Genetics, 2002. **160**(3): p. 995-1009.
175. Fodor, B.D., et al., *Mammalian Su(var) genes in chromatin control.* Annu Rev Cell Dev Biol, 2010. **26**: p. 471-501.
176. S.E. Mohr, R.E.B., *Zimp encodes a homologue of mouse Miz1 and PIAS3 and is an essential gene in Drosophila melanogaster.* Gene, 1999.
177. Joel P, M.a.M.C., *Zinc fingers are sticking together.* Trends Biochem. Sci., 1998.
178. Klug, A., *Zinc Finger Peptides for the Regulation of Gene Expression.* JMB, 1999.
179. Weissman, C.A.P.J.a.A.M., *RING Finger Proteins: Mediators of Ubiquitin Ligase Activity.* Cell, 2000.
180. John H Laity, B.M.L.a.P.E.W., *Zinc finger proteins: new insights into structural and functional diversity.* Current Opinion in Structural Biology, 2001.
181. Sunde, J.M.M.a.M., *Zinc Fingers—Folds for Many Occasions.* IUBMB Life, 2002.
182. Brown, R.S., *Zinc finger proteins: getting a grip on RNA.* Curr Opin Struct Biol, 2005. **15**(1): p. 94-8.
183. Sonnhammer, E.L.L., et al., *Pfam: multiple sequence alignments and HMM-profiles of protein domains.* Nucleic Acids Research, 1998. **26**(1): p. 320-322.
184. S. Sri Krishna1, I.M.a.N.V.G., *Structural classication of zinc fingers.* Nucleic Acids Research, 2003.
185. Kotaja, N., et al., *PIAS Proteins Modulate Transcription Factors by Functioning as SUMO-1 Ligases.* Molecular and Cellular Biology, 2002. **22**(14): p. 5222-5234.
186. Jr., J.E.D., *STATs and Gene Regulation.* Science, 1997.
187. James Herrington, L.S.S., Jessica Schwartz, Christin Carter-Su, *The roles of STAT proteins in growth hormone signaling.* Oncogene, 2000.
188. T. Kisseleva, S.B., J. Braunstein, C.W. Schindler, *Signaling through the JAK/STAT pathway, recent advances and future challenges.* Gene, 2002.
189. Hombria, J.C., et al., *Characterisation of Upd2, a Drosophila JAK/STAT pathway ligand.* Dev Biol, 2005. **288**(2): p. 420-33.
190. H.L.a.C.R.D., *The JAK/STAT pathway and Drosophila development.* Bioessays, 2001.
191. Arbouzova, N.I. and M.P. Zeidler, *JAK/STAT signalling in Drosophila: insights into conserved regulatory and cellular functions.* Development, 2006. **133**(14): p. 2605-16.
192. Darnell, J.E., Jr., *STATs and gene regulation.* Science, 1997. **277**(5332): p. 1630-5.
193. Hong Luo, P.R., Dwayne Barber, William P. Hanratty, Sue Lee, Thomas M. Roberts, Alan D. D' andrea, and Charles R. Dearolf, *Mutation in the Jak Kinase JH2 Domain Hyperactivates Drosophila and Mammalian Jak-Stat Pathways.* Molecular and Cellular Biology, 1997.
194. Riqiang Yan, S.S., Claude Desplan, Charles R. Dearolf, and James E. Darnell, Jr., *Identification of a Stat Gene That Functions in Drosophila Development.* Cell, 1996.
195. Melissa A. Henriksen, A.B., 1 Marc V. Fuccillo,and James E. Darnell, Jr., *Negative*

regulation of STAT92E by an N-terminally truncated STAT protein derived from an alternative promoter site. Genes and Development, 2002.

196. Martin P. Zeidler, E.A.B.a.N.P., *The roles of the Drosophila JAK/STAT pathway.* Oncogene, 2000.
197. Aurel Betz, N.L., Sebastian Martinek, Michael W. Young, and James E. Darnell, Jr, *A Drosophila PIAS homologue negatively regulates Stat92E.* PNAS, 2001.
198. Gronholm, J., et al., *Sumoylation of Drosophila transcription factor STAT92E.* J Innate Immun, 2010. **2**(6): p. 618-24.
199. Cubenas-Potts, C. and M.J. Matunis, *SUMO: a multifaceted modifier of chromatin structure and function.* Dev Cell, 2013. **24**(1): p. 1-12.
200. Flotho, A. and F. Melchior, *Sumoylation: a regulatory protein modification in health and disease.* Annu Rev Biochem, 2013. **82**: p. 357-85.
201. Gareau, J.R. and C.D. Lima, *The SUMO pathway: emerging mechanisms that shape specificity, conjugation and recognition.* Nat Rev Mol Cell Biol, 2010. **11**(12): p. 861-71.
202. Desterro, J.M., et al., *Identification of the enzyme required for activation of the small ubiquitin-like protein SUMO-1.* J Biol Chem, 1999. **274**(15): p. 10618-24.
203. Talamillo, A., et al., *Smt3 is required for Drosophila melanogaster metamorphosis.* Development, 2008. **135**(9): p. 1659-68.
204. Talamillo, A., J. Sanchez, and R. Barrio, *Functional analysis of the SUMOylation pathway in Drosophila.* Biochem Soc Trans, 2008. **36**(Pt 5): p. 868-73.
205. Gutierrez, L., et al., *The Drosophila trithorax group gene tonalli (tna) interacts genetically with the Brahma remodeling complex and encodes an SP-RING finger protein.* Development, 2003. **130**(2): p. 343-54.
206. Juan Monribot-Villanueva, R.A.J.r.-U., Zoraya Palomera-Sa´nchez, Lucı´a Gutie´ rrezAguiar, Mario Zurita, James A. Kennison, Martha Va´zquez, *TnaA, an SP-RING Protein, Interacts with Osa, a Subunit of the Chromatin Remodeling Complex BRAHMA and with the SUMOylation Pathway in Drosophila melanogaster.* Plos One, 2013.
207. Ungureanu, D., et al., *PIAS proteins promote SUMO-1 conjugation to STAT1.* Blood, 2003. **102**(9): p. 3311-3.
208. Shigenobu, S., et al., *Molecular characterization of embryonic gonads by gene expression profiling in Drosophila melanogaster.* Proc Natl Acad Sci U S A, 2006. **103**(37): p. 13728-33.
209. Mukai, M., et al., *Expression of meiotic genes in the germline progenitors of Drosophila embryos.* Gene Expr Patterns, 2006. **6**(3): p. 256-66.
210. Yoshiyama, T., et al., *Neverland is an evolutionally conserved Rieske-domain protein that is essential for ecdysone synthesis and insect growth.* Development, 2006. **133**(13): p. 2565-74.
211. Uryu, O., et al., *Cooperative Control of Ecdysone Biosynthesis in Drosophila by Transcription Factors Seance, Ouija Board, and Molting Defective.* Genetics, 2018. **208**(2):

p. 605-622.
212. Timms, R.T., I.A. Tchasovnikarova, and P.J. Lehner, *Position-effect variegation revisited: HUSHing up heterochromatin in human cells.* Bioessays, 2016. **38**(4): p. 333-43.
213. Khorasanizadeh*, S., *The Nucleosome: From Genomic Organization to Genomic Regulation.* Cell, 2004.
214. Zentner, G.E. and S. Henikoff, *Regulation of nucleosome dynamics by histone modifications.* Nat Struct Mol Biol, 2013. **20**(3): p. 259-66.
215. Kouzarides, T., *Chromatin modifications and their function.* Cell, 2007. **128**(4): p. 693-705.
216. Nathan, D., et al., *Histone sumoylation is a negative regulator in Saccharomyces cerevisiae and shows dynamic interplay with positive-acting histone modifications.* Genes Dev, 2006. **20**(8): p. 966-76.
217. Shiio, Y. and R.N. Eisenman, *Histone sumoylation is associated with transcriptional repression.* Proc Natl Acad Sci U S A, 2003. **100**(23): p. 13225-30.
218. Tan, M., et al., *Identification of 67 histone marks and histone lysine crotonylation as a new type of histone modification.* Cell, 2011. **146**(6): p. 1016-28.
219. Zhang, T., S. Cooper, and N. Brockdorff, *The interplay of histone modifications - writers that read.* EMBO Rep, 2015. **16**(11): p. 1467-81.
220. Vakoc, C.R., et al., *Histone H3 lysine 9 methylation and HP1gamma are associated with transcription elongation through mammalian chromatin.* Mol Cell, 2005. **19**(3): p. 381-91.
221. Verger, A., J. Perdomo, and M. Crossley, *Modification with SUMO. A role in transcriptional regulation.* EMBO Rep, 2003. **4**(2): p. 137-42.
222. Johnson, E.S., *Protein modification by SUMO.* Annu Rev Biochem, 2004. **73**: p. 355-82.
223. Geiss-Friedlander, R. and F. Melchior, *Concepts in sumoylation: a decade on.* Nat Rev Mol Cell Biol, 2007. **8**(12): p. 947-56.
224. Oshlack, A. and M.J. Wakefield, *Transcript length bias in RNA-seq data confounds systems biology.* Biol Direct, 2009. **4**: p. 14.
225. Roberts, A., et al., *Improving RNA-Seq expression estimates by correcting for fragment bias.* Genome Biol, 2011. **12**(3): p. R22.
226. Huang da, W., B.T. Sherman, and R.A. Lempicki, *Systematic and integrative analysis of large gene lists using DAVID bioinformatics resources.* Nat Protoc, 2009. **4**(1): p. 44-57.
227. Glynn Dennis Jr*, B.T.S., Douglas A Hosack*, Jun Yang*, Wei Gao*, H Clifford Lane† and Richard A Lempicki*, *DAVID: Database for Annotation, Visualization, and Integrated Discovery.* Genome Biology, 2003.
228. Amoyel, M., A.M. Anderson, and E.A. Bach, *JAK/STAT pathway dysregulation in tumors: a Drosophila perspective.* Semin Cell Dev Biol, 2014. **28**: p. 96-103.
229. Dearolf, H.L.a.C.R., *The JAK/STAT pathway and Drosophila development.* Bioessays, 2001.
230. Bina, S., et al., *Transcriptional targets of Drosophila JAK/STAT pathway signalling as effectors of haematopoietic tumour formation.* EMBO Rep, 2010. **11**(3): p. 201-7.
231. Takashi Koyama, M.A.R., Alexander W Shingleton, Christen K Mirth, Alekos Athanasiadis,

Nutritional control of body size through FoxO-Ultraspiracle mediated ecdysone biosynthesis. Elife, 2014.
232. Kenneth C. Burtis, C.S.T., C. Weldon Jones, Felix D. Karim, *The Drosophila 74EF Early Puff Contains E74, a Complex Ecdysone-lnducible Gene That Encodes Two ets-Related Proteins.* Cell, 1990.
233. G.Feigl, M.G.a.O.P., *A member of the steroid hormone receptor gene family is expressed in the 20-OH-ecdysone inducible puff 75B in Drosophila melanogaster.* Nucleic Acids Research, 1989.
234. Thummel, E.H.B.a.C.S., *The Drosophila E93 Gene from the 93F Early Puff Displays Stage- and Tissue-Specific Regulation by 20-Hydroxyecdysone.* Development, 1995.
235. Xiang, Y., Z. Liu, and X. Huang, *br regulates the expression of the ecdysone biosynthesis gene npc1.* Dev Biol, 2010. **344**(2): p. 800-8.
236. Warren, J.T., M.B. O'Connor, and L.I. Gilbert, *Studies on the Black Box: incorporation of 3-oxo-7-dehydrocholesterol into ecdysteroids by Drosophila melanogaster and Manduca sexta.* Insect Biochem Mol Biol, 2009. **39**(10): p. 677-87.
237. Fox, D.T. and R.J. Duronio, *Endoreplication and polyploidy: insights into development and disease.* Development, 2013. **140**(1): p. 3-12.
238. Ohhara, Y., S. Kobayashi, and N. Yamanaka, *Nutrient-Dependent Endocycling in Steroidogenic Tissue Dictates Timing of Metamorphosis in Drosophila melanogaster.* PLoS Genet, 2017. **13**(1): p. e1006583.
239. Yoshiyama-Yanagawa, T., et al., *The conserved Rieske oxygenase DAF-36/Neverland is a novel cholesterol-metabolizing enzyme.* J Biol Chem, 2011. **286**(29): p. 25756-62.
240. Osterwalder, T., et al., *A conditional tissue-specific transgene expression system using inducible GAL4.* Proc Natl Acad Sci U S A, 2001. **98**(22): p. 12596-601.
241. Kukurba, K.R. and S.B. Montgomery, *RNA Sequencing and Analysis.* Cold Spring Harb Protoc, 2015. **2015**(11): p. 951-69.
242. Stark, R., M. Grzelak, and J. Hadfield, *RNA sequencing: the teenage years.* Nat Rev Genet, 2019. **20**(11): p. 631-656.
243. Talamillo, A., et al., *Scavenger receptors mediate the role of SUMO and Ftz-f1 in Drosophila steroidogenesis.* PLoS Genet, 2013. **9**(4): p. e1003473.
244. Mataki, C., et al., *Compromised intestinal lipid absorption in mice with a liver-specific deficiency of liver receptor homolog 1.* Mol Cell Biol, 2007. **27**(23): p. 8330-9.
245. Cao, G., et al., *Structure and localization of the human gene encoding SR-BI/CLA-1. Evidence for transcriptional control by steroidogenic factor 1.* J Biol Chem, 1997. **272**(52): p. 33068-76.
246. Ninova, M., et al., *Su(var)2-10 and the SUMO Pathway Link piRNA-Guided Target Recognition to Chromatin Silencing.* Mol Cell, 2020. **77**(3): p. 556-570 e6.
247. Zeng, J., et al., *Snail synchronizes endocycling in a TOR-dependent manner to coordinate entry and escape from endoreplication pausing during the Drosophila critical weight*

checkpoint. PLoS Biol, 2020. **18**(2): p. e3000609.
248. Layalle, S., N. Arquier, and P. Leopold, *The TOR pathway couples nutrition and developmental timing in Drosophila.* Dev Cell, 2008. **15**(4): p. 568-77.
249. Solomon, M.J. and A. Varshavsky, *Formaldehyde-mediated DNA-protein crosslinking: a probe for in vivo chromatin structures.* Proc Natl Acad Sci U S A, 1985. **82**(19): p. 6470-4.
250. Nelson, J.D., O. Denisenko, and K. Bomsztyk, *Protocol for the fast chromatin immunoprecipitation (ChIP) method.* Nat Protoc, 2006. **1**(1): p. 179-85.
251. Carey, M.F., C.L. Peterson, and S.T. Smale, *Chromatin immunoprecipitation (ChIP).* Cold Spring Harb Protoc, 2009. **2009**(9): p. pdb prot5279.
252. Kaya-Okur, H.S., et al., *CUT&Tag for efficient epigenomic profiling of small samples and single cells.* Nat Commun, 2019. **10**(1): p. 1930.
253. Kaya-Okur, H.S., et al., *Efficient low-cost chromatin profiling with CUT&Tag.* Nat Protoc, 2020. **15**(10): p. 3264-3283.
254. Janssens, D.H., et al., *Automated in situ chromatin profiling efficiently resolves cell types and gene regulatory programs.* Epigenetics Chromatin, 2018. **11**(1): p. 74.
255. Skene, P.J., J.G. Henikoff, and S. Henikoff, *Targeted in situ genome-wide profiling with high efficiency for low cell numbers.* Nat Protoc, 2018. **13**(5): p. 1006-1019.
256. Li, X., et al., *Regulation of chromatin and gene expression by metabolic enzymes and metabolites.* Nat Rev Mol Cell Biol, 2018. **19**(9): p. 563-578.
257. Doerr, A., *Top-down mass spectrometry.* NATURE METHODS, 2008.
258. Siuti, N. and N.L. Kelleher, *Decoding protein modifications using top-down mass spectrometry.* Nat Methods, 2007. **4**(10): p. 817-21.
259. James J. Pesavento, C.A.M., and Neil L. Kelleher,, *Quantitative Analysis of Modified Proteins and Their Positional Isomers by Tandem Mass Spectrometry: Human Histone H4.* Analytical Chemistry, 2006.
260. Xuemei Han, M.J., Kathrin Breuker, Fred W. McLafferty, *Extending Top-Down Mass Spectrometry to Proteins with Masses Greater Than 200 Kilodaltons.* Science, 2006.
261. Xiao, Y., et al., *Can your protein be sumoylated? A quick summary and important tips to study SUMO-modified proteins.* Analytical Biochemistry, 2015. **477**: p. 95-97.
262. Mithila Handu, B.K., Ramya Ravindranathan, Amarendranath Soory, Ritika Giri,Vijay Barathi Elango, Harsha Gowda, and Girish S. Ratnaparkhi, *SUMO-Enriched Proteome for Drosophila Innate Immune Response.* G3, 2015.
263. Mannix, K.M., et al., *Proximity labeling reveals novel interactomes in live Drosophila tissue.* Development, 2019. **146**(14).
264. Trinkle-Mulcahy, L., *Recent advances in proximity-based labeling methods for interactome mapping.* F1000Res, 2019. **8**.
265. Branon, T.C., et al., *Efficient proximity labeling in living cells and organisms with TurboID.* Nat Biotechnol, 2018. **36**(9): p. 880-887.
266. Hentze, M.W., M.U. Muckenthaler, and N.C. Andrews, *Balancing acts: Molecular control*

of mammalian iron metabolism. Cell, 2004. **117**(3): p. 285-297.
267. Baldi, S. and P.B. Becker, *The variant histone H2A.V of Drosophila--three roles, two guises.* Chromosoma, 2013. **122**(4): p. 245-58.
268. Jyothishmathi Swaminathan, E.M.B., and Victor G. Corces, *The role of histone H2Av variant replacement and histone H4 acetylation in the establishment of Drosophila heterochromatin.* Genes and Development, 2005.

Appendices

Appendix A1 Candidate protein scores identified from transgenic IRP1A allele MS

Diet type[a]	**Normal fly diet**			**BPS-G1**	**BPS-G2**
Allele[b] / Candidate[c]	*IRP1A*^{WT}	*IRP1A*^{C450S}	*IRP1A*^{3R3Q}	*IRP1A*^{WT}	*IRP1A*^{WT}
Ran	11.73	14.10	NA	5.29	NA
NTF2	NA	NA	NA	6.03	NA
Chickadee	32.85	9.97	24.37	50.56	5.52

[a]Normal fly diet refers to Nutrifly food. Bathophenanthroline sulfate (BPS) is an iron chelator to deprive iron content in transgenic *IRP1A*^{WT} animals for two consecutive generations (G).

[b]Transgenic *IRP1A* alleles carry N-terminal Flag tag. *IRP1A*^{C450S} encodes the constitutively RNA-binding apoprotein, whereas *IRP1A*^{3R3Q} encodes holo-IRP1A in which the RNA-binding sites are abolished by mutation.

[c]Only scores of three candidates that involve in the nuclear import of IRP1A are shown. Results were cross-compared with *w*^{1118} control.

Appendix A2. RNA-Seq library cycle numbers

Library name	Technical replicate	Ct value		
		Dilution 1:1000	Dilution 1:10,000	Dilution 1:100,000
Standard 1[a]	1	8.455		
	2	8.536		
	3	8.604		
Standard 2 [a]	1	12.765		
	2	12.852		
	3	12.917		
Standard 3 [a]	1	16.200		
	2	15.991		
	3	15.919		
Standard 4 [a]	1	19.032		
	2	18.877		
	3	18.932		
No template control [b] (NTC)	1	27.567		
	2	27.415		
	3	27.451		
w^{1118} (R1) [c]	1	8.878	12.490	15.682
	2	8.993	12.517	15.799
	3	9.008	12.525	15.917
w^{1118} (R2) [c]	1	8.755	12.173	15.513
	2	8.903	12.303	15.611
	3	8.895	12.442	15.749
w^{1118} (R3) [c]	1	8.823	12.240	22.965
	2	8.767	12.237	15.527
	3	8.879	12.185	15.743
Su(var)2-10^{IR} (R1) [c]	1	9.146	12.626	15.935
	2	9.339	12.774	16.187
	3	9.318	12.771	16.255
Su(var)2-10^{IR} (R2) [c]	1	8.486	12.036	15.536
	2	8.697	12.201	15.647
	3	8.891	12.266	15.862
Su(var)2-10^{IR} (R3) [c]	1	8.576	11.948	15.303
	2	8.770	12.177	15.391
	3	8.774	12.405	15.704

SUMO^{IR} (R1) [c]	1	8.659	12.120	15.576
	2	8.789	12.294	15.578
	3	8.780	12.418	15.643
SUMO^{IR} (R2) [c]	1	8.523	11.975	15.433
	2	8.747	12.112	15.491
	3	8.703	12.167	15.636
SUMO^{IR} (R3) [c]	1	7.958[d]	11.568	14.914
	2	8.144[d]	11.647	14.973
	3	8.200[d]	11.678	15.051

[a] The range of DNA standard concentrations in the NEBNext Library Quant Kit is 10–0.01 pM.

[b] The Ct from the NTC was not used in quantitation analysis, but serves as a valuable control reaction to ensure performance of the kit and absence of sample contamination. Ct value for NTC should be far enough away from the dynamic range of the DNA standards.

[c] Samples were collected from 40-42 hours third-instar larvae ring glands with genotypes listed below: *phm22* > w^{1118}; *phm22* > *Su(var)2-10*-RNAi (v100813); *phm22* > *SUMO*-RNAi (v105980).

[d] qPCR traces for the diluted samples fell outside of the range of the standards (8.45-19.03), hence discarded in the quantification of library concentrations.

Appendix A3. RNA-Seq library concentrations

Library name	Concentrations (nM)[a]
w^{1118} (R1)	9.66
w^{1118} (R2)	10.77
w^{1118} (R3)	10.86
Su(var)2-10^{IR} (R1)	7.99
Su(var)2-10^{IR} (R2)	11.35
Su(var)2-10^{IR} (R3)	11.86
SUMO^{IR} (R1)	11.16
SUMO^{IR} (R2)	12.08
SUMO^{IR} (R3)	16.95

[a] Library concentrations were calculated using Ct values acquired from qPCR traces in coupled with the online NEBioCalculator tool (https://nebiocalculator.neb.com/#!/qPCRlibQnt).